UNIVERSITAT POLITÈCNICA DE CATALUNYA BARCELONATECH

Assessment of corrosion-induced damage in the mechanical contact response of cemented carbides at different length scales

Yafeng Zheng

UNIVERSITAT POLITÈCNICA DE CATALUNYA
BARCELONATECH
Departament de Ciència i Enginyeria de Materials

Assessment of corrosion-induced damage in the mechanical contact response of cemented carbides at different length scales

A dissertation submitted to partial fulfilment of the requirements for the degree of

Doctor of Philosophy by

Yafeng Zheng

Advisors:

Luis Miguel Llanes Pitarch

Gemma Fargas Ribas

Center of Structural Integrity, Micromechanics and Reliability of Materials

Department of Materials Science and Engineering

Universitat Politècnica de Catalunya – Barcelona Tech

Barcelona, Spain

October 2020

Abstract

Cemented carbides, also referred to as hardmetals, have been the subject of intensive research and technological applications for past few decades, especially for metal cutting, mining and earth drilling industries. They are composite materials consisting of two interpenetrating networks of a hard and brittle ceramic phase (generally WC) embedded into a ductile metallic matrix. Such microstructure leads to an outstanding combination of hardness, wear resistance and toughness. As a result, they have consolidated as first choice materials for tools and components to be used in highly demanding applications, e.g. cutting or forming of metallic alloys, as well as mining operations.

Several of the above applications also include exposure to chemically aggressive media, such as lubricants, chemical products, petrochemical and mine slurries, and seawater. Under these conditions, it has been shown that failure induced under applied load is accelerated, and corresponding service life may be significantly shortened. In this regard, several works have attempted to replicate – at the laboratory level – similar service-like conditions. Among them, the detrimental corrosion-related effects on tribological response and effective wear resistance of cemented carbides have aroused the greatest concern. However, investigations addressing similar information linking corrosion-induced damage and mechanical contact response at different length scales

are quite limited.

Within the above framework, the first part of this thesis was devoted to carry out a systematic and comprehensive study about corrosion-induced damage and residual strength (damage tolerance) for four microstructurally different cemented carbides exposed to acidic, neutral and alkaline solutions. It is found that acidic medium led to higher corrosion rates and more significant strength degradation than those where neutral and basic ones were involved. Regarding corrosion mechanisms, it is evidenced that corrosion starts at binder pool centers and evolves towards binder/WC interfaces when exposed to acid solution. Meanwhile, corrosion is initially located at binder/WC interfaces and subsequently expands into the ceramic particles, when the material is immersed in a basic medium.

The subsequent sections were focused on assessing the corrosion-induced changes on the mechanical contact response of cemented carbides through a wide range of length scales (increasing from 100s nanometers to 1000s microns). First, nanoindentation and nanoscratch techniques were employed to assess the influence of corrosion on the mechanical integrity of hardmetals. Changes in nanoindentation and nanoscratch response and damage scenario are discussed taking into consideration the effective microstructural assemblage remnant after corrosion action. It is concluded that dissolution of metallic phase becomes critical as it yields a mechanically unsupported, contiguous and binderless/porous, carbide network. Consequently, cracking,

fragmentation and easy removal of WC grains under contact loading is evidenced; and thus, mechanical integrity is effectively lessened.

A similar investigation was then extended to a higher length scale range (from 10s to 100s of microns in depth), combining relatively long corrosion times with pyramidal indentation and sliding contact (microscratch) experiments, in order to evaluate corrosion-induced changes on both load-bearing capability and damage scenario of a WC-Co hardmetal grade. The results reveal that mechanical contact strength and resistance to crack extension of the hardmetal grade studied are significantly reduced after exposure to corrosive media. Such lessening effects are found to be dependent on the ratio between indentation and/or scratch depth and thickness of the corroded layer. Alike pronounced corrosion influence is evidenced in surface and subsurface damage scenario. Here, a transition from well-defined cracking systems into a scenario consisting of multiple, branched and less shallow fissures is evidenced when comparing pristine and corroded specimens respectively.

Finally, an even higher length scale (up to 1000s microns) was introduced in the study by combining Hertzian indentation technique and variable (but still relatively long) corrosion times. Corrosion effects on corresponding mechanical response and damage were assessed for three cemented carbides with metallic binders of different chemical nature. Results point out quite significant corrosion-induced changes on indentation stress-strain response and contact damage scenario. Such detrimental influence is found

to be dependent on both the ratio between indentation depth and thickness of the corroded layer as well as chemical nature of the binder. In this regard, critical loads for emergence and evolution of specific damage events - ring and radial cracks, and even specimen failure - are proposed as figures of merit for material selection under the combined action of corrosion and contact loading. Within this context, the hardmetal grade with Co-base binder and addition of Cr is found to be the best option, among the three cemented carbides considered in this part of the investigation. It points out the consideration of the synergic interaction between corrosion resistance and hardness/toughness correlation for microstructural design optimization of hardmetals under service-like conditions.

Acknowledgements

Although I still feel that my PhD experience has not been completed, the three years devoted to achieve this degree have passed quickly. At this moment, I am filled with excitement and gratitude. Looking back on the past three years, I may remember many unforgettable moments: the excitement of setting foot on foreign land for the first time, the anxiety at the beginning of my research work, the joy of playing and talking with nice colleagues, the feeling before giving a speech at the first international conference I participated, etc., as if everything had occurred just yesterday. I don't know what to say except to be grateful. I sincerely thank all the people and things that have helped me with my research work and daily life in the past three years. You are the creators of these unforgettable moments and will be remembered forever with them. Especially, I would like to sincerely thank:

Luis Llanes and **Gemma Fargas**, my supervisors, without whom I would not have been able to complete this thesis, for their continuous support, trust, patience, as well as each great idea in every meeting and conversation. Meanwhile, I have been influenced and taught by many aspects of them, such as their high sense of responsibility to student, immense knowledge and passion for material research, wise and rigorous way of thinking, acute academic insights, etc. All these will constantly urge me to become an excellent teaching and research worker like you.

Olivier Lavigne, for providing me with the research materials, and always willing to discuss about them, and for every suggestion he did when reviewing my papers.

Elaine Armelin, for her continuous patience and kind assistance in electrochemical corrosion tests.

Joan Josep Roa and **Hossein Besharatloo**, for their great help in nanoindentation testing.

Fernando García, for his always active and efficient help on the use of laser scanning confocal microscopy, servo-hydraulic universal testing machine and confocal Raman microscopy.

Marc Serra Fanals, **Josep Maria Pons Portella**, **Albert Marcé Pous** and **Laia Ortiz Membrado**, for their great help to my experiments, and particularly for polishing my Spanish.

Trifon Trifnov, for his immeasurable support with the SEM and FIB equipment.

My colleagues for all the good moments and discussions that we shared during the last years. Special attention is given to Ana, Joaquim, Mona, Junhui, Jing, Shiqi, Chenyang, Yufen, Mingyue, Sergio, Idriss, Marcel, Hossein, Marc, María, Sandra, Daniela(s), Erica and Miquel.

My family and **friends**, for their continuous support and love.

This work was financially supported by the collaborative Industry-University program between Hyperion Materials & Technologies and Universitat Politècnica de Catalunya, and partly funded by the Spanish Ministerio de Economía y Competitividad, and Ciencia e Innovación, through Grants MAT2015-70780-C4-3-P (MINECO/FEDER) and PID2019-106631GB-C41, respectively. I would like to acknowledge the Ph.D. scholarship received from China Scholarship Council (No. 201706890018, Beijing, China).

Preface

This thesis is a collection of results from my doctoral studies in the Department of Materials Science and Engineering at the Universitat Politècnica de Catalunya – Barcelona Tech (UPC) during the period from February 2018 to October 2020, with the support of a scholarship by China Scholarship Council (No. 201706890018, Beijing, China). Work was carried out under the supervision of Prof. Luis Llanes and Prof. Gemma Fargas at the Centre d'Integritat Estructural, Micromecànica i Fiabilitat dels Materials (CIEFMA), a UPC's research group. It was supported by a collaborative Industry-University program between Hyperion Materials & Technologies and UPC, and partly funded by the Spanish Ministerios de Economía y Competitividad, and de Ciencia e Innovación, through Grants MAT2015-70780-C4-3-P (MINECO/FEDER) and PID2019-106631GB-C41, respectively. The content of the thesis is the product of original work, unless otherwise stated in the acknowledgments, footnotes or detailed references.

List of publications

This Ph.D. thesis consists of a compendium of the articles listed below:

Article I

Y.F. Zheng, G. Fargas, E. Armelin, O. Lavigne, L. Llanes. *Corrosion-induced damage and residual strength of WC-Co,Ni cemented carbides: influence of microstructure and corrosion medium.* Metals 9 (2019) 1018. **IF**: 2.117. Q1 (18/79) in the category: "Metallurgy and Metallurgical Engineering", and Q3 (185/314) in the category: "Materials Science, Multidisciplinary".

Article II

Y.F. Zheng, G. Fargas, H. Besharatloo, M. Serra, J.J. Roa, E. Armelin, O. Lavigne, L. Llanes. *Assessment of corrosion-induced changes on the mechanical integrity of cemented carbides at small length scales*. Int. J. Refract. Met. Hard Mater. 84 (2019) 105033. **IF**: 3.407. Q1 (11/79) in the category: "Metallurgy and Metallurgical Engineering", and Q2 (116/314) in the category: "Materials Science, Multidisciplinary".

Article III

Y.F. Zheng, G. Fargas, O. Lavigne, L. Llanes. *Indentation and scratch testing of medium-grained WC-6%wtCo: corrosion effects on load-bearing capability and induced damage.* Ceram. Int. 46 (2020) 17591-17598. **IF**: 3.83. Q1 (2/28) in the category: "Materials Science, Ceramics".

Article IV

Y.F. Zheng, G. Fargas, O. Lavigne, E. Roitero, L. Llanes. *Corrosion-induced changes on Hertzian contact damage in cemented carbides*. Int. J. Refract. Met. Hard Mater. 92 (2020) 105334. **IF**: 3.407. Q1 (11/79) in the category: "Metallurgy and Metallurgical Engineering", and Q2 (116/314) in the category: "Materials Science, Multidisciplinary".

Other contributions

Oral and poster presentations

M. Serra, **Y.F. Zheng**, G. Fargas, H. Besharatloo, J.J. Roa, E. Armelin, O. Lavigne, L. Llanes. *Quantification of corrosion-induced damage on cemented carbides by nanoindentation.* Workshop on Micromechanical Properties of Hard Materials. Poster presentation. Barcelona, Spain, 27-29 June 2018.

Y.F. Zheng, G. Fargas, E. Armelin, O. Lavigne, L. Llanes. *Effect of corrosion-induced damage on microstructure and residual strength of WC-Co,Ni cemented carbides.* Euro PM2018 Congress & Exhibition. Oral presentation. Bilbao, Spain, 14-18 October 2018.

Y.F. Zheng, G. Fargas, H. Besharatloo, M. Serra, J.J. Roa, E. Armelin, O. Lavigne, L. Llanes. *Quantification of corrosion-induced damage on cemented carbides by nanoindentation.* 11th International Conference on the Science of Hard Materials. Poster presentation. Khao Lak, Thailand, 25-29 March 2019.

Y.F. Zheng, G. Fargas, H. Besharatloo, J.J. Roa, E. Armelin, O. Lavigne, L. Llanes. *Evaluation of corrosion-induced damage in hardmetals at micrometric length scale.* VII Congreso Español de Pulvimetalurgia y II Congreso Iberoamericano de Pulvimetalurgia. Oral presentation. Madrid, Spain, 24-26 June 2019.

Y.F. Zheng, G. Fargas, H. Besharatloo, J.J. Roa, E. Armelin, O. Lavigne, L. Llanes. *Small-scale assessment of corrosion-induced damage in hardmetals.* Euro PM2019 Congress & Exhibition. Oral presentation. Maastricht, Netherlands, 13-16 October 2019.

Y.F. Zheng, G. Fargas, O. Lavigne, E. Roitero, L. Llanes. *Corrosion effects on contact damage of a WC-Ni cemented carbide.* Euro PM2020 Congress & Exhibition. Oral presentation. Virtual Congress, 4-7 October 2020.

Contents

Glossary of symbols and abbreviations

Glossary of symbols

a_c Mean radial crack length

a Hertzian contact radius

A_0 Projected nanoindentation contact area at peak load

C_{WC} Contiguity of the carbide phase

d_{WC} Carbide mean grain size

d_{hkl} Spacing between a set of planes with (*hkl*) Miller indices

d_0 Hertzian indentation depth

E Young's modulus of specimen

E' Young's modules of indenter

E_{corr} Corrosion potential in electrochemical measurements

E_r Reduced elastic modulus for the specimen/indenter system

F_{max} Peak load in the nanoindentation loading process

F_N Applied scratch load

H_S Scratch hardness

H Vickers hardness

h_c Nanoindentation contact depth

h_{max} Measured maximum depth of nanoindentation

h_s Elastic deflection of the surface at a specific contact perimeter

i_{corr} Corrosion current density in electrochemical measurements

i_c Critical current density in electrochemical measurements

$i_{p\text{-}min}$ Minimum blunt current density in electrochemical measurements

K_{Ic} Indentation fracture toughness

k Dimensionless constant

k_t Geometric constant of nanoindentation tip

k_0 Numerical constant which equals $8/\pi$ for styli having conical, spherical or parabolic tips

n Integral multiple

P Vickers indentation load

P_m Mean Hertzian contact pressure

p_0 Hertzian indentation stress

R Indenter radius

S Measured contact stiffness

W Crack resistance

w Measured scratch width

β Best fit of constant for calculating indentation fracture toughness

β_0 Constant depending on the tip geometry

ε Geometric constant of indenter

ε_0 Hertzian indentation strain

θ Angle of incidence at which a diffraction peak is measured

λ Wavelength of x-rays

λ_{binder} Binder mean free path

υ Poisson's ratio of specimen

υ' Poisson's ratio of indenter

Glossary of abbreviations

ASTM American society for testing and materials

BIT Bonded-interface technique

FIB Focused ion beam

FESEM Field emission scanning electron microscopy

fcc Face centered cubic

HV Vickers hardness

HK Knoop hardness

hcp Hexagonal close-packed

ISO International organization for standardization

LSCM Laser scanning confocal microscopy

OCP Open circuit potential

SEM Scanning electron microscopy

TRS Transverse rupture strength

TEM Transmission electron microscopy

XRD X-ray diffraction

1 Introduction

Cemented carbides, commonly referred to as hardmetals, are a group of powder metallurgical liquid-phase sintered composite materials. They are constituted by hard/brittle refractory carbides (e.g. WC) embedded in a soft/ductile metallic matrix (e.g. Co, Ni and/or Fe) [1]. The intrinsic composite nature of these materials permits to tailor unique combinations of mechanical properties by proper selection of carbide grain size and metallic binder content [1,2]. As a result, they have consolidated as first choice materials for tools and components to be used in highly demanding applications, such as cutting of metals and wood, forming of metallic alloys, rock drilling and mining, mechanical seals, structural components and wear parts [3].

Many of the above applications often imply exposure of cemented carbide tools and components to various aqueous environments. Metal cutting commonly involves the use of coolants and lubricants, whereas wood cutting implies much more aggressive conditions (i.e. acid media) [4,5]. Lubricants are also required for many metal forming operations, such as wet wire drawing [6]. Drilling operations for oil and gas extraction place the downhole components into neutral or alkaline chloride environments, such as sea-water and sand-bearing liquids [7,8]. Under all these conditions, it has been shown that failure induced under applied load is accelerated, and corresponding service life may be significantly shortened.

From the viewpoint of the material itself, extensive research has proven that corrosion significantly affects microstructural and mechanical/tribological characteristics of cemented carbides [4,5,9–19]. However, critical review of open literature points out that observed detrimental corrosion-related effects are usually discussed in terms of the direct correlation existing between microstructure and macroscopic property/response exclusively. Furthermore, it should be considered that many applications of hardmetal tools and components frequently involve, besides corrosion, contact loads, repetitive impacts, abrasion and/or erosion too [3]. In this regard, there exist some investigations addressing the interaction between corrosion degradation and damage induced by mechanical contact, though their number is rather limited [4,9,16]. They have documented interesting and useful information from a material selection viewpoint, but it is clear that much deeper information is required if optimization of microstructural design against corrosion is aimed. This is particularly true concerning the changes that may be induced by corrosion on damage scenario and/or active micromechanisms, at both surface and subsurface levels, under applied load. Hence, it is the main objective of this doctoral thesis to assess and understand the influence of corrosion-induced changes on both load-bearing capability and damage scenario of cemented carbides, over a wide range of length scales (i.e. from 1s to 1000s of microns in width and depth). Within this context, two baseline aspects are proposed for defining microstructural design criteria towards optimization of the performance of cemented carbides under service-like conditions. First, the synergic consideration of basic mechanical properties (i.e. hardness and toughness) and corrosion resistance by means of analysis and

discussion of the combined interaction among them through concepts like damage tolerance. Second, the effective use of a wide spectrum of testing techniques: sharp and spherical indentation together with scratch, at macro-, micro- and nanometric levels. In order to achieve it successfully, additional specific objectives are pursued throughout the work, as follows:

- To investigate the corrosion-induced damage and the corresponding residual strength of a set of microstructurally different cemented carbides exposed to three distinct corrosion media;
- To assess and analyze surface/subsurface and mechanical integrity changes induced by exposure to corrosive media of a hardmetal grade, by means of nanoindentation and nanoscratch techniques.
- To study the corrosion effects on both load-bearing capability and damage scenario of a hardmetal grade, using pyramidal indentation and sliding contact (microscratch) techniques.
- To determine and analyze the corrosion-induced changes on the indentation stress-strain response as well as in surface/subsurface damage scenarios of hardmetals, through implementation of spherical (Hertzian) indentation techniques.

The thesis layout is schematically illustrated in **Fig. 1.1**. Following this introductory **Chapter 1**, a brief description of the cemented carbides is given in **Chapter 2**. It includes history and current status, microstructure, basic mechanical properties and

applications for these materials. The mechanical contact response and the corrosion behavior of hardmetals are presented and reviewed, as separate and independent subjects, in **Chapters 3** and **4** respectively. In **Chapter 5** the details of the research scope and objectives are given. Experimental details are described in **Chapter 6**, including microstructural and mechanical characterization of the investigated hardmetal grades, corrosion tests, techniques used for inducing contact damage at different length scales, as well as methodologies for inspecting and assessing damage scenarios at both surface and subsurface levels. Publications resulting as direct outcomes of this doctoral thesis are presented in **Chapter 7**. Main results and conclusions obtained in this investigation, as well as suggestions for future work are summarized in **Chapter 8**.

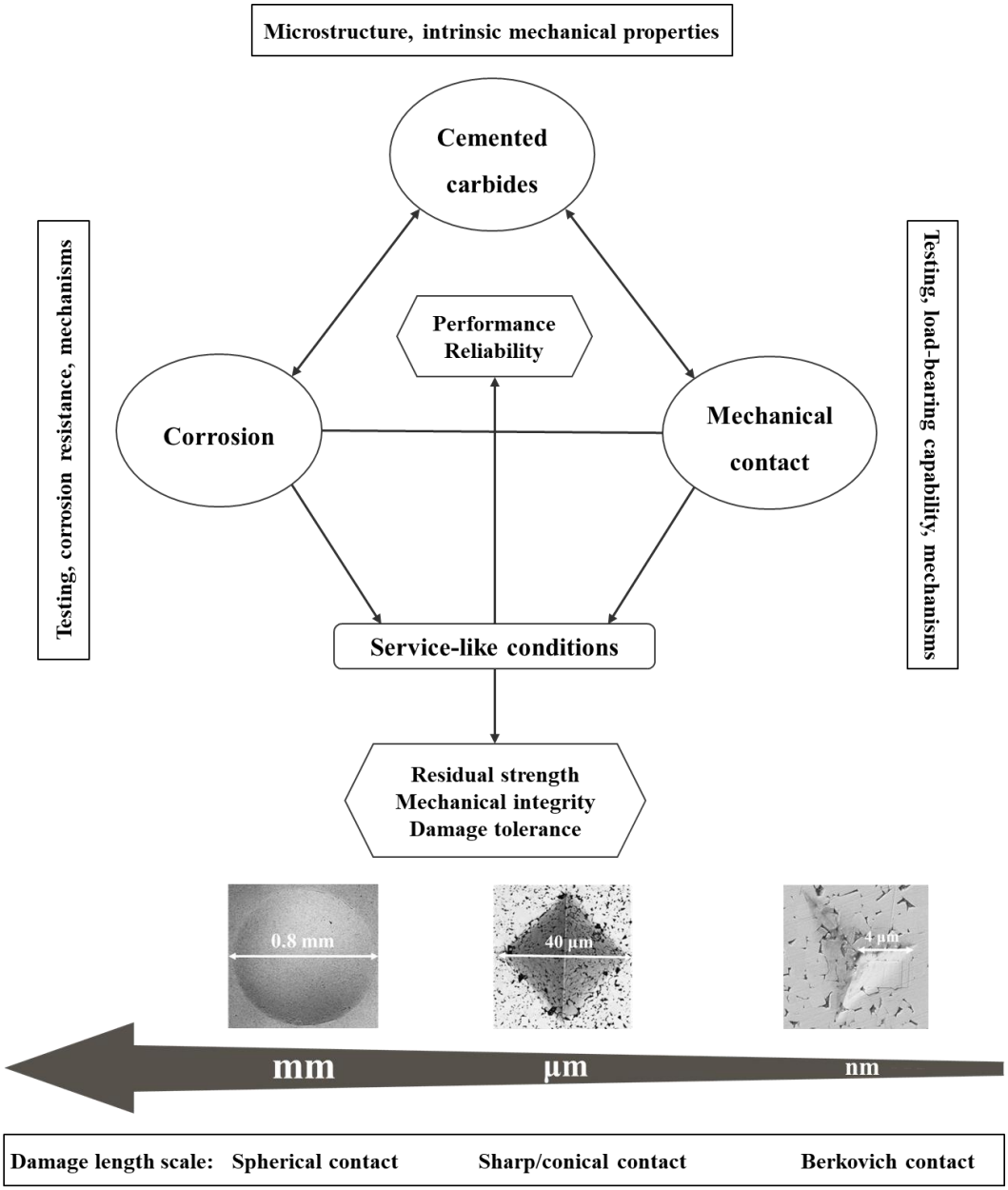

Fig. 1.1. Scheme illustrating the thesis layout.

2 Cemented carbides: general description and basic mechanical properties

2.1 Description and brief history overview

Cemented carbides, often simply termed as hardmetals, belong to a group of ceramic-metal composite materials that exhibit an extraordinary combination of hardness, strength, toughness and wear resistance [1,2,20]. **Fig. 2.1** schematically shows an optimal combination of hardness (wear resistance) and toughness (strength) of hardmetals used in cutting tool classes [3]. Furthermore, this attractive feature makes cemented carbides forefront materials in many engineering and tooling applications, e.g. forming of metallic alloys, rock drilling, mining and tunneling industries [3].

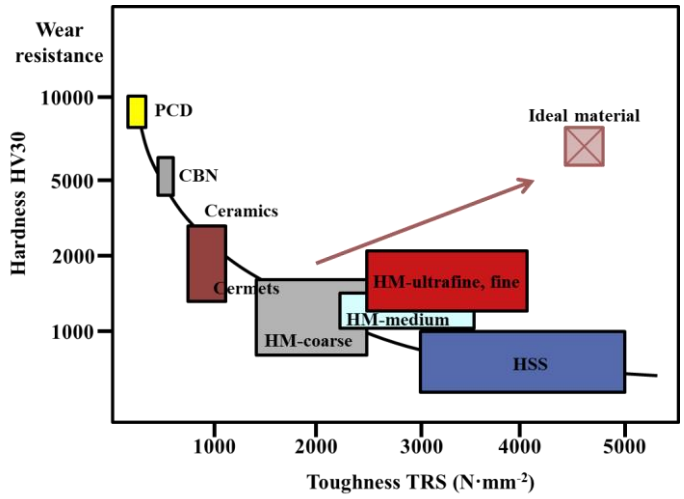

Fig. 2.1. Schematic hardness (wear resistance)–toughness (TRS) relationship for cutting tool material classes [3].

Cemented carbides are conventionally synthesized by powder metallurgy routes. Among them, the ones involving liquid phase sintering are the methods most commonly used. In this regard, the blended powder mixture of tungsten carbide and binder is sintered in a vacuum furnace at temperatures ranging between 1350 and 1500 ℃ [21]. During the sintering process, liquid phase of the binder will cause some carbide particles to dissolve. As the mixture cools, tungsten carbide will precipitate out due to its low solubility, forming a heterogeneous material with significant phase separation, as shown in **Fig. 2.2**.

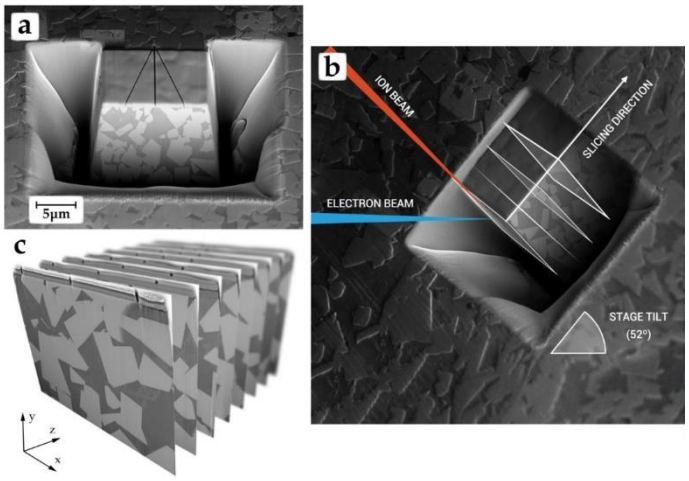

Fig. 2.2. Images showing typical microstructure of cemented carbide by means of 3D FIB/FESEM serial sectioning and imaging. Here, lighter grain-like features are tungsten carbide (WC) and darker regions are the cobalt (Co) binder phase [20].

The development of cemented carbides began due to the search for suitable materials to replace very expensive diamond tools as wire drawing dies after the First World War [22]. They proved to be suitable for production of drawing dies, once the combination of WC and Co was developed. As a consequence, the first related patent was born in

1923 [23]. Three years later (in 1926), this new material was commercialized under the name “WIDIA”. Afterwards, cemented carbides started to replace high speed steels in cutting tools due to their improvement in wear resistance at high temperature [22].

After the Second World War, a huge market opened in the growing economies. Cemented carbides contributed as tool materials and construction parts to their industrial development, resulting in a significant rise in the global consumption of hardmetals. This growth trend has continued until now, as shown in **Fig. 2.3** [24,25]. In such a graph, it is interesting to highlight a slowdown trend in annual output growth between 2007 and 2009, linked to the global economic crisis that took place during those years. It is estimated that the global cemented carbide output in 2015 was about 70,000 tons, a year-on-year increase of 2% [25]. Such rise has been led by China, the country with the largest cemented carbide production in the world in recent years. In 2018, China’s cemented carbide output was 38,500 tons, a year-on-year increase of about 11-12%, accounting for 38% of the global production [25].

With respect to the global consumption of cemented carbides, it has followed a defined trend since many years ago. Considering data of 2008, as an example, it was reported that about 50,000 tons of tungsten (W content) were consumed by cemented carbides worldwide that year, accounting for about 60% of the world’s tungsten consumption (including recycled materials) [26]. **Fig. 2.4** shows the distribution of general application

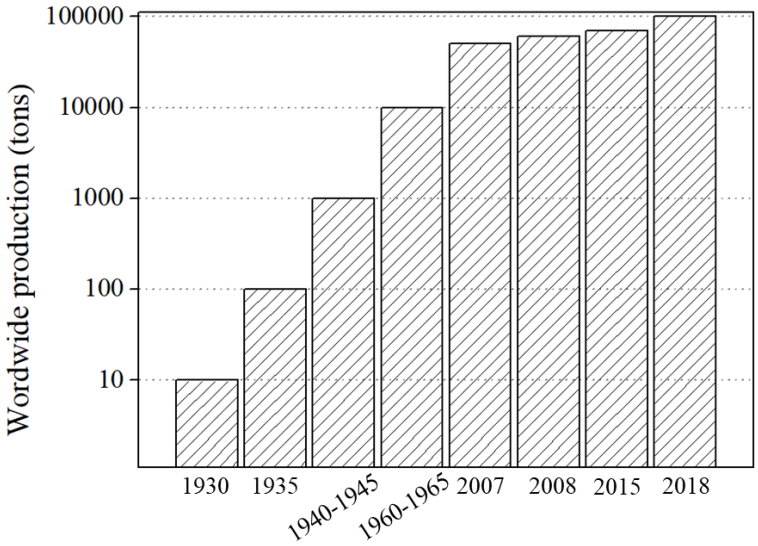

Fig. 2.3. Estimated worldwide production of hardmetals in the years from 1930 to 2018 [24,25].

areas of cemented carbides [27]. In terms of tonnage, general wear parts account for the largest application areas (36%), followed by oil and gas industries (14%), automotive (13%), aerospace and defense (13%), mining construction (10%) and electronics (7%).

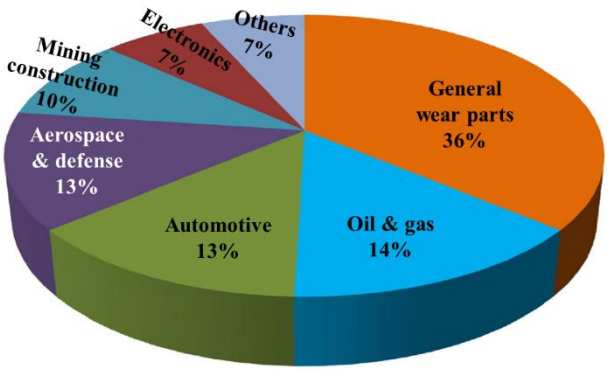

Fig. 2.4. Distribution of application areas of cemented carbides [27].

WC-Co system is by far the most preferred choice for cemented carbide tools and components, due to the outstanding wetting and adhesion between the Co-base solid solution phase and WC during sintering [1,28]. In this regard, the hard and brittle WC particles are the main constituents of cemented carbides, which are the major contributor for their excellent hardness, strength and wear resistance. According to statistics, more than 98% of carbide grades contain WC, of which tungsten monocarbide WC accounts for the most important position of all hard phases in these materials [1].

WC particles in hardmetals can have different sizes, from ultrafine up to extra coarse carbides (**Table 2.1**). The average grain size and distribution of the carbides are closely related to the properties of hardmetals, which may further determine their application fields [3]. For example, grades with grain size less than 1 μm are often chosen for light to medium-heavy roughing cuts due to their high hardness. Medium- and coarse-grained cemented carbides provide a tradeoff between hardness and toughness, which may be used for heavier rough cutting. Finally, extra coarse-grained cemented carbides (over 6 μm) are often applied for making molds instead of cutting because of their relatively high toughness.

Table 2.1. Grain size classification of cemented carbides [3].

Grain size (μm)	Designation
< 0.2	Nano
0.2-0.5	Ultrafine
0.5-0.8	Submicron
0.8-1.3	Fine
1.3-2.5	Medium
2.5-6	Coarse
> 6	Extra coarse

On the other hand, binder phase also plays a vital role in contributing to the excellent properties of cemented carbides, particularly in terms of toughness and impact resistance. In this regard, Co metal currently dominates the market as a binder because some unique properties, such as its favorable chemical bonding with tungsten carbide which results in a very low interfacial energy, nearly perfect wetting and very good adhesion in the solid state [29]. However, Co always undergoes a wavy and rising price, besides negative issues in terms of pollution and health. It yields continuous consideration of other iron group metals as potential substitutes for cobalt as metallic binder. Within this context, Fe and Ni are commonly proposed as ideal alternatives due to their low price, low pollution, and relatively good wettability with WC. It was reported that some of the properties of cemented carbides may be significantly improved by replacing Co-base binders by Ni ones, such as corrosion and oxidation

resistance [29,30]. Meanwhile, cemented carbides with Fe-rich binders have also shown improved properties such as higher hardness, abrasive wear resistance, toughness, and strength compared to Co-bonded hardmetals [31].

2.2 Intrinsic mechanical properties of cemented carbides

2.2.1 Hardness

Hardness may be defined as the resistance of a material to exhibit plastic deformation when subjected to either mechanical indentation or abrasion. It is well known that hardness is one of the key parameters for most applications involving cemented carbides, e.g. machining tools, mining and drilling equipment, and components of valves designed to handle erosive slurries. In such applications, the in-service critical parameter, i.e. wear resistance, is directly related to hardness. As it is shown in **Fig. 2.5**, the abrasive wear resistance of different hardmetals shows varying degrees of improvement as their hardness values increase [32,33]. From a microstructural perspective, the hardness of cemented carbides generally rises as the volume fraction of the carbide phase increases and/or the mean carbide grain size decreases. In this regard, Lee and Gurland [34,35] pointed out that application of reciprocal rule of mixtures describes much better than the direct one, the influence of volume fraction of the carbide phase on the hardness of hardmetals (**Fig. 2.6**). They related it to the physical significance of the contiguity (a two-phase microstructural parameter) of the

hard phase for defining the effective hardness on composites with interpenetrated and continuous phase networks, as it is the case of hardmetals.

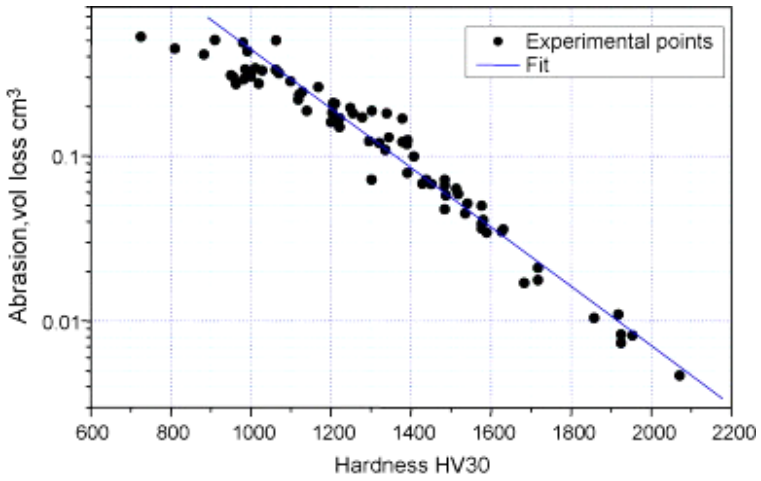

Fig. 2.5. Variation of wear volume with hardness for ASTM B611 tests on range of hardmetals [33].

Regarding the hardness measurement of cemented carbides, the method most commonly used is the Vickers hardness (HV) test (ISO 3878). Nevertheless, Rockwell hardness of scale A test (ISO 3738, ASTM B294) is extensively used in industrial practice too. Knoop hardness (HK) test (ISO 22394) is also employed when the anisotropy of material is of interest, as it is the case in WC crystals [1,36]. For assessment of Vickers hardness, various load weights (e.g. 1, 10, 15, 20, 30, and 50 kgf) can be used, although the most common value is 30 kgf, corresponding value being expressed as HV30. The measured HV value typically ranges from 7 to 22 GPa, and in some cases (e.g. binderless WC, nano-grained hardmetal grades) it can even reach up to about 24 GPa [37–43]. Meanwhile, in order to determine the hardness of the

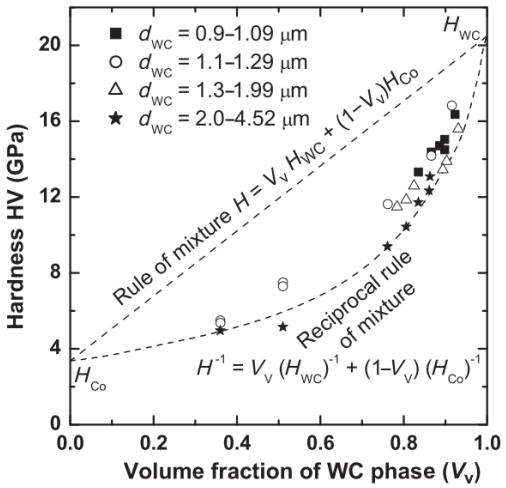

Fig. 2.6. Vickers hardness vs. carbide volume fraction in WC-Co for a wide range of the carbide grain size 0.9-4.52 mm [34].

constituent phases in a local range, nanoindentation testing has been frequently used in the past few decades [40,44,45].

2.2.2 Toughness

Fracture toughness is also one of the major material characteristics to design applications and performance assessment of cemented carbides. It has been extensively reported that this property is affected by many factors, such as binder content, binder mean free path, mean carbide grain size, and macroscopic residual stress, among others [46–49]. Different from hardness, this parameter has been one of the most difficult to define because it largely depends on the history of materials testing. Consequently, a number of distinct testing methods have been introduced to assess the toughness of cemented carbides, e.g. Palmqvist indentation method, impact strength test on plane or notched bars, fracture mechanics protocols using either notched (Chevron or V-notch)

or pre-cracked specimens [50–55]. From all of these, Palmqvist indentation is the most time-saving and efficient test method, after consideration of the time needed for sample preparation and notch geometry control in the other testing protocols [56]. In this regard, Palmqvist initiated and developed the idea of assessing a toughness-like parameter by measuring the lengths of the fissures emanating from each of the four corners of a Vickers imprint [52]. Afterwards, Exner [57] defined a crack resistance parameter, W, based on the observed linear relationship between indentation load (P) and the sum of the radial (also called Palmqvist) cracks length at the corners of the Vickers impression:

$$W = \frac{P}{4a_c} \tag{2.1}$$

where P is the indentation load in N; and a_c is the mean radial crack length in μm.

Fig. 2.7 shows a typical linear relationship determined between mean radial crack length and applied indentation load for a WC-7.6%Co cemented carbide [52]. On the basis of the obtained Palmqvist toughness, Shetty *et al.* [52] further analyzed the resulting crack length-indentation load data in terms of relations characteristic of radial and fully developed radial/median (half-penny) crack geometries. As a result, these investigators proposed a simple correlation among indentation fracture toughness, length of the cracks emanating from imprints, and hardness for a wide range of WC-Co grades, according to:

$$K_{Ic} = \beta\sqrt{HW} \tag{2.2}$$

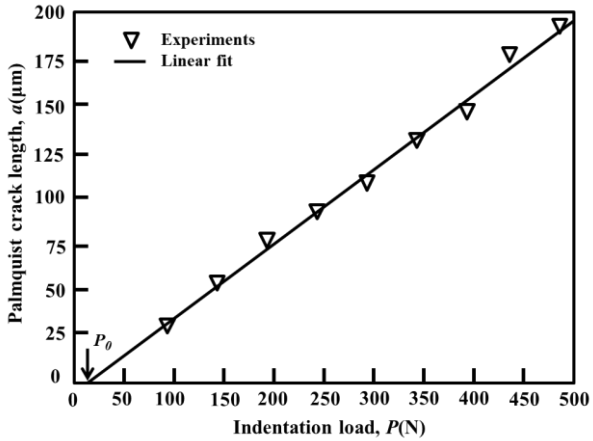

Fig. 2.7. Relationship between mean radial crack length and applied indentation load for a WC-7.6%Co hardmetal grade [52].

where H is the hardness (N/mm^2), β is a best-fit constant with value of 0.0889, and K_{Ic} is indentation fracture toughness (MPa*m$^{1/2}$).

As reported in the literature [58–60], the exceptional fracture toughness levels of hardmetals are mainly attributed to plastic stretching of crack-bridging ductile enclaves. When the indentation load reaches a critical value, cracks are induced and a multiligament zone develops at the crack wake, i.e. behind the crack tip [53,61,62]. It has been shown that this zone extends over a distance about five times the length scale of the microstructure (carbide grain size), and contains 2 to 4 ligaments in the direction of crack propagation [53,62]. Furthermore, the development of a multiligament zone means that there is an increasing crack propagation resistance (R-curve) behavior in hardmetals [63–66], whose size depends on the width and strength of the ligaments [63,67]. During subcritical crack extension, plastic deformation of these reinforcing ligaments is restricted to the binder regions that intersect the crack plane, and proceeds

through nucleation, growth, and coalescence of microcavities [53,59–62,66,68]. As the crack extends, a steady-state zone is formed, in which the ligaments bridging the crack pass through all stretching-up stages until the complete failure of the specimen (**Fig. 2.8**) [66].

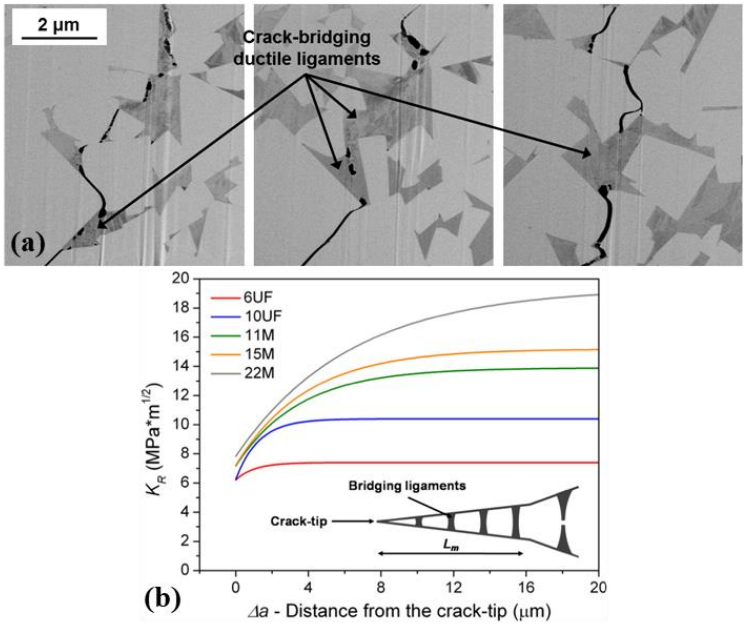

Fig. 2.8. (a) FESEM micrographs illustrating crack-microstructure interactions at the crack wake of a stably propagated crack under monotonic loads and (b) estimated R-curves for several microstructurally different WC-Co cemented carbides [66].

Toughness together with processing- or service-induced defects define another relevant, but this time extrinsic, mechanical property: strength. This is defined as the stress at which a hardmetal specimen results in unstable propagation of a crack, i.e. failure [69]. In general, it is referred to as transverse rupture strength (TRS), because it is commonly measured under bending [69]. It is not intrinsically linked to microstructure because it is very sensitive to flaws inherited from processing like pores, impurity inclusions,

lakes of binder, and abnormally large carbides or binderless agglomerates [70–73]. Moreover, sample preparation (e.g. cutting, grinding, polishing, edge chamfering, etc.) also significantly affects the measured TRS value, as it may result in different surface integrity scenarios, i.e. surface residual stresses, scratches, roughness or surface texture [37,57,71,73–75]. Furthermore, cracks (damage) induced during service will also exert a relevant influence on the measured TRS values. Mechanical testing of cemented carbides implies load bearing and deformation compatibility shared between the two constitutive phases. It yields complex scenarios, in terms of deformation and fracture micromechanisms, at micro- and nanometric length scales for both carbide and binder phases. These include plastic deformation (i.e. dislocations slip and pile-ups), binder phase transformation (from fcc to hcp), microcracking along carbide grain boundaries and through the carbide grains, and all of them may contribute and lead to the failure of hardmetals [34,37,76–79].

3 Contact response of cemented carbides

The exceptional combination of hardness and toughness in cemented carbides is the intrinsic reason for their wide use in various engineering applications (e.g. cutting tools, forming dies, bearings, mining bits, etc.). Failure in such applications may be triggered by a number of mechanisms such as plastic deformation, brittle facture, fatigue and abrasion, which may be assisted to various degrees by corrosion, oxidation and other environmentally-related phenomena [80]. In such cases, contact loading plays a significant role on defining the critical design parameters for optimal material selection, e.g. wear resistance in the oil and gas extraction industry, or continuous solid particle impact (monotonic/cyclic loading) endured in underground and surface mining and rock drilling [81,82]. Contact loading may produce small fissures or microcracks that reduce the strength of brittle-like materials, or even directly lead to catastrophic failure (especially if overloading, impact, or cyclic loading are involved) [83,84]. It is therefore of crucial importance to understand the mechanics and mechanisms linked to contact loading in hard materials. Such knowledge will be relevant for analyzing and rationalizing first the process of introduction and evolution of extrinsic damage, induced during service-like conditions; and subsequently, its consequences on reliability and performance of hardmetal tools and components.

3.1 Spherical indentation

Following the experimental methodology and analysis procedure introduced and extensively developed by Lawn's group for studying ceramic materials using spherical indentation [85], the use of testing protocols based on Hertzian theory has proven to be quite successful on the assessment of mechanical response and induced damage under contact loading in both nude and coated cemented carbides [86–96]. In these studies, indentation has been conducted using spheres with curvature radii in the millimeter length scale. Thus, concentrated stresses are delivered such that: typical ‘‘blunt" in-service conditions are simulated, indentation stress-strain curves may be attained; and damage evolution associated with increasing load or number of cycles can be examined. For hardmetals deformation and damage scenario involved on the surface of a monotonically indented specimen generally includes the following three different types: (1) irreversible "sink in" phenomenon at relatively low load level; (2) partial/full ring cracks formed around the contact area, when the indentation load exceeds a certain value; and (3) radial cracks, which tend to appear under a much higher load level than the former two cases. In this sense, the formation of incipient cracks is known as "quasi-plasticity" and is related with the strain-hardening behavior in cemented carbides, involving thus flow of the binder and accommodation of plastic deformation in WC grains [88]. On the other hand, ring cracks are promoted by the tensile radial stresses and strains existing in the vicinity of residual imprints, while radial fissures are the result of positive hoop (circumferential) stresses [97,98]. In general, for hard and brittle-like materials, the formation of radial cracks heralds the end of the service life of

engineering components [88].

As the indentation load increases, the introduced irreversible damage from deformation to fracture may be divided into three stages: initial elastic, elastic-plastic and fully plastic, as shown in **Fig. 3.1** [88]. In this regard, the first stage is often predicted from Hertz relation. The oblique dashed line passing through the origin is the perfect elastic response calculated using the Hertz relationship, as expressed by the following equation [99]:

$$P_m = \frac{3Ea}{4\pi kR} \tag{3.1}$$

where P_m is the mean contact pressure, E is Young's modulus, a is the contact radius, R is the indenter radius, and k is a dimensionless constant given by:

$$k = \frac{9}{16}\left[\left(1-\nu^2\right)+\left(1-\nu'^2\right)\frac{E}{E'}\right] \tag{3.2}$$

where υ and υ' are Poisson's ratios, and E and E' are Young's moduli of the specimen and indenter respectively.

As it is shown in **Fig. 3.1**, the indentation stress increases linearly versus indentation strain at the beginning of the deformation. Considering that the contact damage in the case of cemented carbides does not recover upon unloading, the Hertzian elastic behavior should be here called as pseudo-elasticity in the strict sense [88]. Regarding the elastic-plastic stage, it shows an obvious deviation of indentation stress-strain curve from the Hertzian elastic relation. Meanwhile, the hardmetal specimen experiences

quasi-plastic yielding and apparent strain hardening. In this sense, WC particles and binder phases successively undergo plastic deformation and even microcracks are formed to accommodate the continuous deformation (**Fig. 3.2**) [88]. In the last stage, even though the strain continues to rise, the indentation stress levels off. The damage scenario involved includes the break-up of WC grains and the formation of microcracks. As the applied load further increases, macro-ring crack and radial crack develop in the specimen at the end of the plastic deformation [88].

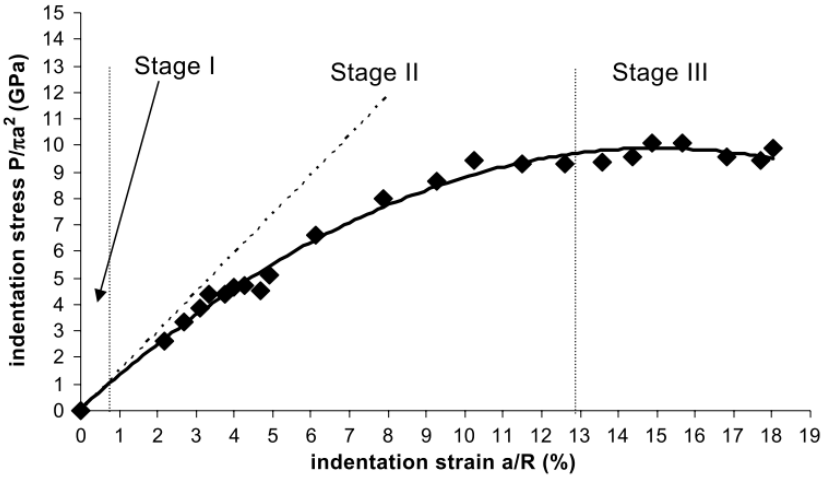

Fig. 3.1. Hertzian indentation stress-strain curve of WC-10 wt%Co, using a polycrystalline diamond indenter of 5 mm in radius. Note three deformation regimes: initial elasticity, elastic-plastic and fully plastic deformation [88].

The analysis of subsurface damage induced by Hertzian indentation test in cemented carbides is important to understand the deformation and damage mechanisms. In this regard, the bonded-interface technique (BIT) has proved to be quite successful in facilitating the analysis of subsurface damage by a number of research groups [85,89,92,94,100–104], as schematically outlined in **Fig. 3.3**. Typically, the damage

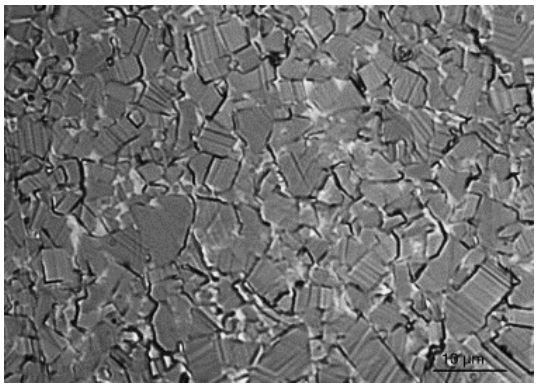

Fig. 3.2. Subsurface damage scenario in heavily damaged area related to the quasi-plastic stage [88].

scenario discerned from the cross-section of an indented hardmetal specimen may involve the appearance of cone crack coming from the curved surface, as shown in **Fig. 3.4**. The corresponding high magnification observation in the heavily deformed zone may include deformation of binder phases and WC grains, as well as the occurrence of microcracks propagating along WC/WC boundaries or WC/Co interfaces (**Fig. 3.2**) [88]. In general, the deformation and fracture scenarios obtained from BIT methodology are more severe than that from integral specimens regarding emergence

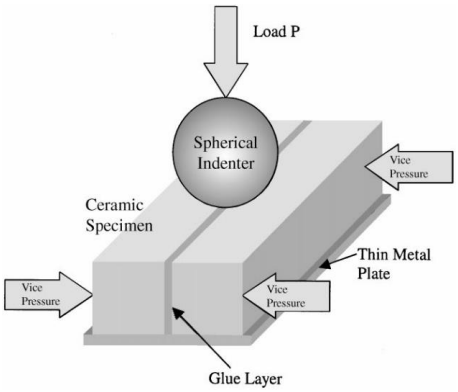

Fig. 3.3. Schematic illustration of bonded-interface technique [103].

and propagation of microcracks at each specific loading condition [87,92,103,105]. The reason behind it is that the centerline of the indenter is over the gap between two halves in the bonded-interface condition, which cannot support the indenter adequately, and thus, the interface edges are more prone to collapse, leading to a corresponding shift of the maximum stress field away from the bonded-interface [103]. Since the interface edge is unsupported by the gap over its whole length, the weaker grain boundaries and friction would have a more pronounced effect than within the bulk of the material [103].

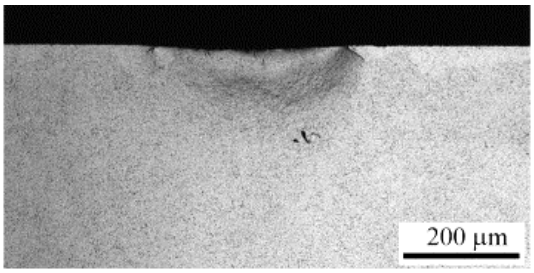

Fig. 3.4. Nomarski optical micrograph showing (cross-section view) contact damage features for a WC-10%Co hardmetal (clamped-interface) specimen under an applied load of 2000 N [92].

Considering that irreversible damage may be induced under contact loading conditions from both surface and subsurface levels, the useful lifetime of hardmetal tools and components involved must be affected, from the perspective of structural integrity. Within this context, Lawn and coworkers [83,106–111] have systematically and extensively investigated the structural integrity changes (e.g. strength lessening) resulting from Hertzian tests using spherical indenters. In these studies, the residual strength of the indented material is found to depend on the nature of the induced contact

damage regarding both brittleness and toughness of the materials under consideration. The more brittle the material is, the more abrupt are the strength losses, once the critical load for cone crack initiation is reached. On the other hand, the tougher the materials are, the more gradual and continuous is the strength decrease, as microcracking associated with a quasi-plastic response develops. However, to the author's knowledge, only two studies have been addressed to correlate strength reduction and contact damage in cemented carbides [86,92]. In these works, it is found that strength retention is improved as contact damage mode goes from brittle to quasi-plastic, and this transition directly depends on microstructure [92]. This provides useful guidelines for microstructural design seeking for higher damage tolerance (i.e. deformation prevailing over fracture as damage mode) in the industrial applications of hardmetals.

3.2 Wear

In addition to the fact that hardmetal tools and components may be exposed to the above-mentioned contact loading conditions, tribological aspects also play an important role from a design viewpoint. Main types of wear of cemented carbides, linked to some contact-like actions in service, are schematically shown in **Fig. 3.5**, and they may be classified in the following three categories: abrasion, sliding and erosion wear. Among them, abrasive wear usually takes place when the hard particles from the processed material (i.e. rock, metal, ceramic) are pulled across the surface of the tool or wear parts

(**Fig. 3.5a** and **b)** [112]. The resulting damage scenario may range from fine scratching to deep gouges. In this regard, the abrasion behavior shows a strong dependence on hardness of the cemented carbides (**Fig. 3.6**) [113]. In addition, size, shape and chemical nature of the abrasive significantly affect the magnitude of wear [112]. Concerning sliding wear, it normally involves two solid surfaces sliding over each other (**Fig. 3.5c** and **d**), with or without lubricant. It occurs in applications such as face seals and forging tools. In the case of erosion wear (**Fig. 3.5e** and **f**), damage scenario involves

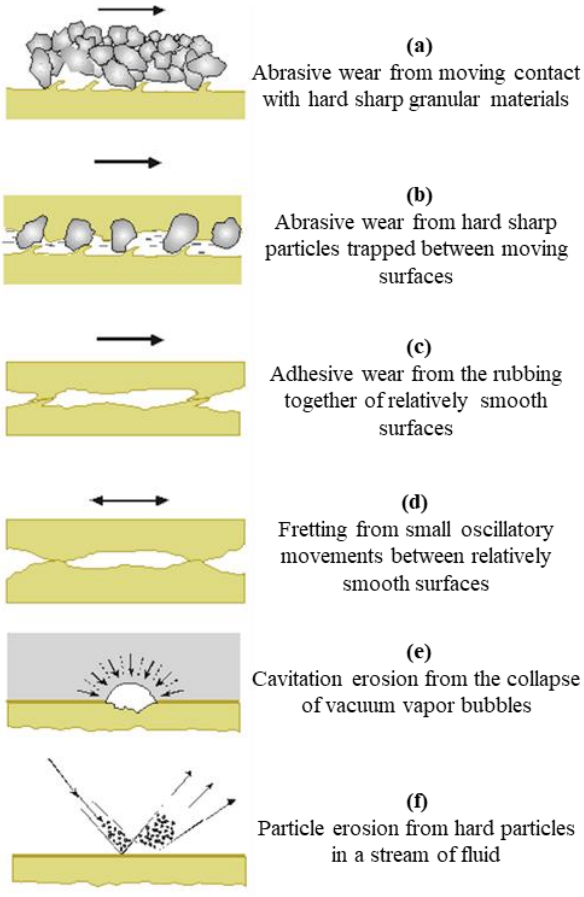

Fig. 3.5. Main types of wear discerned for hardmetals tools and components under common service-like conditions [112].

the removal of material from the surface of hardmetal tools and components by the high-speed impact of either a liquid or a stream of hard particles carried in a fluid flow [112].

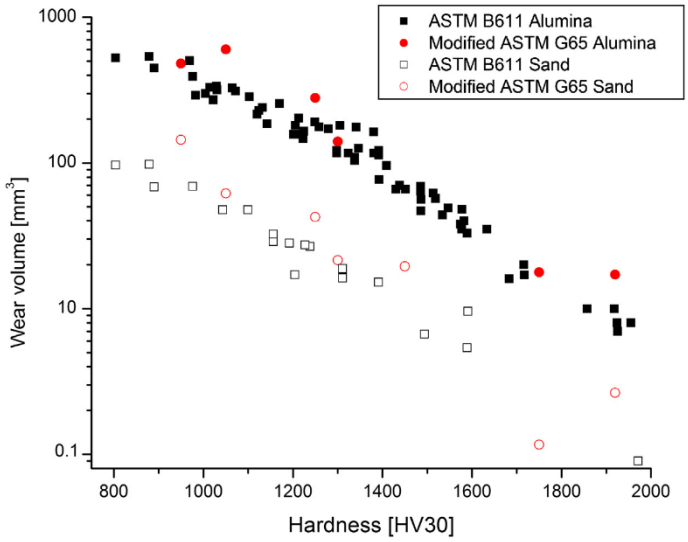

Fig. 3.6. Abrasion volume loss as a function of hardness for a range of WC-Co hardmetal grades [113].

In the past few decades, numerous laboratory studies have been conducted attempting to simulate the above-mentioned tribological conditions. In these works, the correlation between microstructural features and tribological response of cemented carbides has drawn the most attention [114–122]. Microstructural parameters such as WC grain size, binder content and width of WC grain size distribution were considered. In general, the influence of these parameters on the wear resistance has been rationalized on the basis of the effective hardness of the studied hardmetal grades. Wear mechanisms of cemented carbides have also been identified and discussed. Depending on the applied load, a series of different deformation and damage micromechanisms may be involved:

removal of binder phase, plastic deformation and damage within the remaining binder phase, accumulation of plastic strain in WC grains, fracture and fragmentation of individual WC grains, re-embedment of WC fragments in a Co-rich surface layer, cracking between WC grains, and the breakaway of unsupported WC grains. The damage scenario induced during a scratch test, from both top and cross-sectional views, in a hardmetal specimen is schematically described in **Fig. 3.7** [123]. There, an obvious scratch groove and material pile-up are discerned, in which ploughing of the binder phase and fragmentation of carbides may be present [124]. The subsurface cracks induced by grooving (similar to the indentation of a brittle system) develop by forming lateral and median cracks underneath the plastic zone [52,123]. It should be noticed that investigations reviewed in this chapter are only the ones conducted under dry conditions.

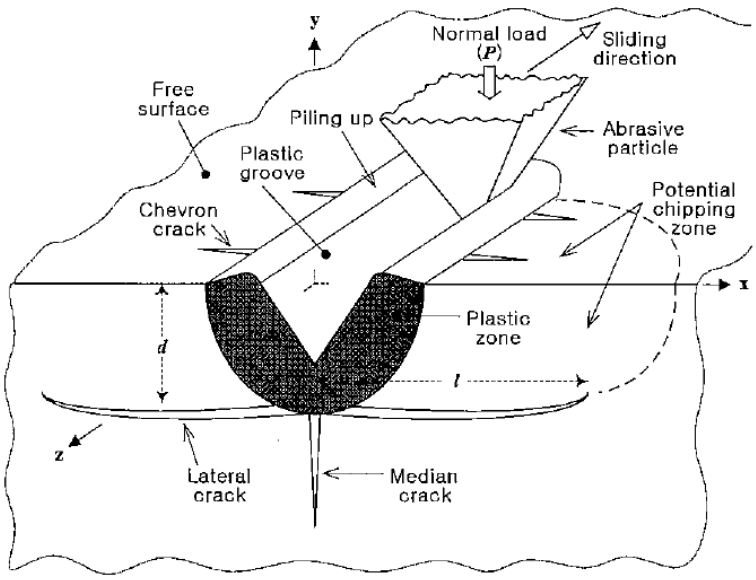

Fig. 3. 7. Schematic view of material removal in cemented carbide as a consequence of abrasive wear [123].

4 Corrosion of cemented carbides

WC-Co composites often suffer from different degradation phenomena that seriously affect the performance and service-life of engineering structural parts. In this regard, many hardmetal applications involve exposure to chemically aggressive media, including a wide variety of corrosive environments such as lubricants, chemical and petrochemical products, and mine and sea waters [6,10,125–127]. Therefore, it is of crucial importance to have a comprehensive understanding of the corrosion behavior and corresponding mechanisms of cemented carbides, from the two-fold perspective of microstructural optimization for material selection and prevention of premature failure of tools and components.

4.1 Characterization methods

Immersion test and electrochemical measurement are the two most commonly used testing techniques for determining the corrosion behavior of cemented carbides. In the former, well-prepared samples (cut, ground and polished) are immersed in corrosive media for given time periods, at a constant temperature. The corrosion behavior of cemented carbides may then be assessed by means of: (1) inspection of the cross-section of corroded samples for determining the depth of the affected zone; (2) calculation of the corrosion rate using the measured weight loss corresponding to different exposure times; and (3) use of atomic absorption techniques to determine the amount of binder

dissolved in the corrosive media [4,16,128]. In the case of electrochemical tests, this technique includes a wide range of methods such as potentiostatic/galvanostatic polarization and cyclic voltammetry. They are used to characterize various aspects of the corrosion process, falling into two categories: corrosion rates and reaction mechanisms [4,6,129–136]. Existing literature related to the corrosion behavior of cemented carbides is mostly based on results obtained by using these two testing techniques.

4.2 Corrosion behavior and mechanisms

It is well known that coupling of two or more metals within a corrosive environment often leads to a galvanic corrosion when the less noble metal shows high dissolution rate, while the more noble metal remains protected [137]. Accordingly, cemented carbides can be considered to be a galvanic couple whose corrosion characteristics depend largely on the corrosion response of its constitutive phases [138]. In many aqueous environments, the electrode potential difference between WC grains (acting as the cathode) and binder phase (acting as the anode) leads to the formation of micro-galvanic couples causing corrosion. In this sense, the dissolution content of W, C and other elements in the binder phase, such Co, is directly proportional to the standard potential value, and inversely proportional to the potential difference of the WC phase [135]. As reported in several studies [10,125,129,136,139–141], the binder phase is

preferentially attacked when exposed to acidic and neutral mediums (pH≤7), whereas it shows passivation behavior in alkaline solutions (pH > 7). This may be predicted by inspection of the Pourbaix diagram of cobalt (**Fig. 4.1**) [142]. Similarly, analysis of the Pourbaix diagram of tungsten indicates that it is unstable in alkaline condition (**Fig. 4.2**). This is also in complete concordance with findings reported in the literature involving

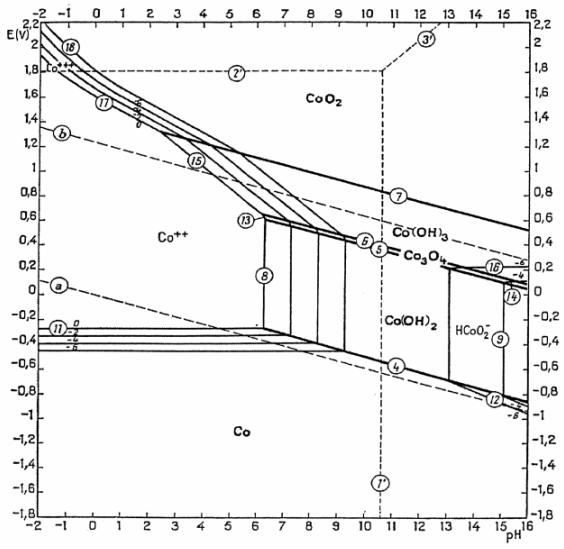

Fig. 4.1. Potential-pH diagram for the cobalt-water system at 25 ℃ [142].

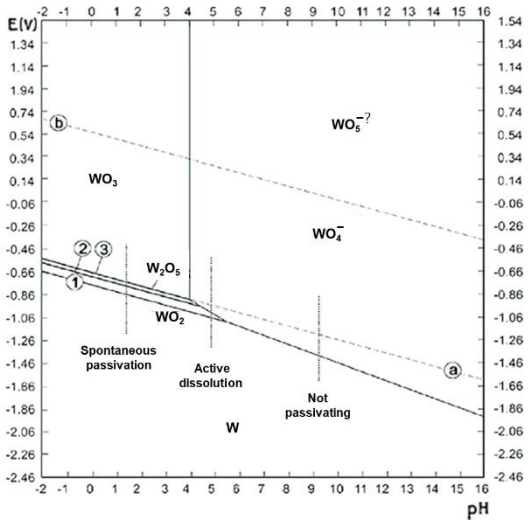

Fig. 4.2. Potential-pH diagram for the tungsten-water system at 25 ℃ [142].

investigations of the corrosion response of WC-based hardmetals when exposed to alkaline environments [11,135,140,141,143–147].

Regarding mechanisms, it is reported that the electrochemical corrosion process of WC-Co hardmetals in acid media is linked to preferential dissolution of a thin Co layer at the WC/Co interface, which is accompanied by the formation Co_3O_4 and $Co(OH)_2$ [135]. As the Co phase gradually dissolves, a slow corrosion reaction occurs to form WO_3. This process is schematically illustrated in **Fig. 4.3a**. Interestingly, in the case of exposure to neutral solutions, the dissolution of metallic binder takes place in the core of binder pools rather than at the binder/carbide interface [16]. However, information on these different responses is quite limited; thus, further research in this subject is needed to corroborate and understand it. Concerning the corrosion process in alkaline solution, as it is shown in **Fig. 4.3b**, the pure Co thin layer and Co phase at the WC/Co

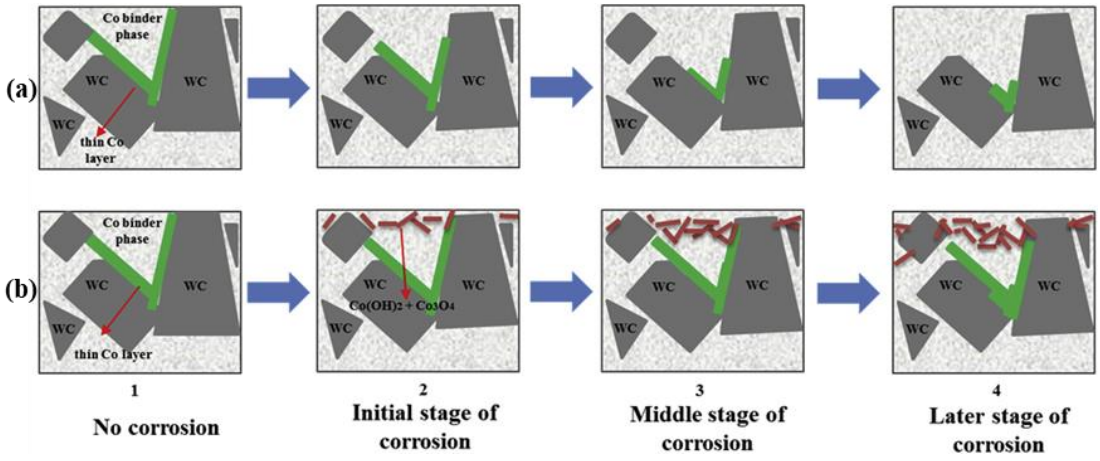

Fig. 4.3. Schematic diagram of WC-Co hardmetal during corrosion process in (a) HCl and (b) NaOH solutions [135].

interface are first oxidized, and then form $Co(OH)_2$. This corrosion product plays an important role in isolating the metallic binder from the corrosive media and impeding its dissolution further [135,148].

4.3 Microstructural effects on the corrosion behavior of cemented carbides

4.3.1 Binder composition

In most instances, corrosion of hardmetals is reflected in the preferential attack of the binder phase, since it has lower electrode potential than the WC phase. It has been demonstrated that addition of alloying elements, such as Ni, V and Cr, into the Co binder phase generally improves the corrosion resistance. In this regard, Wentzel and Allen [149] found that an increase of Ni content yields a positive change of the E_{corr} of the materials, and a sharp decrease of i_c and $i_{p\text{-}min}$. Such beneficial effects of Ni addition are supported by findings extensively reported in the literature [30,134,150–153]. Addition of Cr and V into the binder have also been proven to enhance the corrosion resistance of cemented carbides [139,146,154]. Regarding the former, Cr acts as an alloying element, leading to the formation of a mixed Co-Cr oxide layer which decreases the rate of dissolution of the binder when exposed to acidic and neutral environments. **Fig. 4.4a-d** show the effect of Cr addition on the corrosion mechanism of WC-Co hardmetal [155]. In the latter case, although dissolution of V in the binder

can also improve the corrosion resistance of hardmetals, no thin layer is formed between the binder and the WC grains (**Fig. 4.4e**) [139,154]. Furthermore, other investigations have also reported a positive effect related to Mo, Y, Ti and Ta addition into the binder phase in terms of corrosion resistance of cemented carbides [135,156–158].

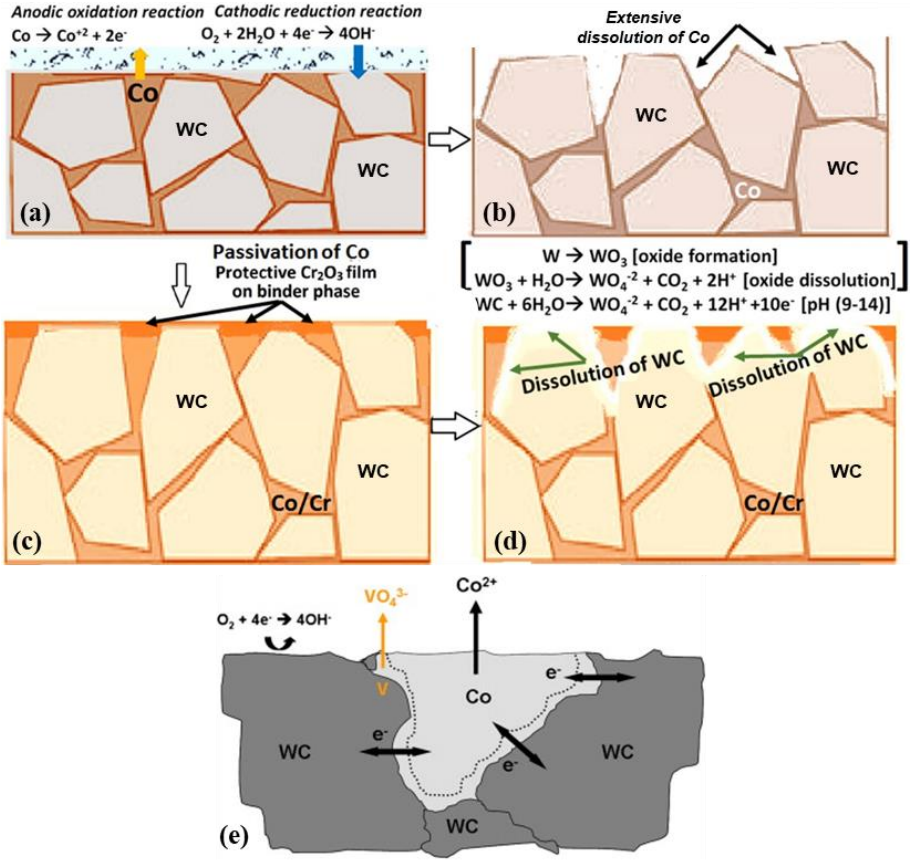

Fig. 4.4. Schematic view of the corrosion mechanisms of Cr-free (a),(b), Cr-containing (c),(d) and V-containing (e) WC-Co hardmetals when exposed to corrosive environment [139,155].

4.3.2 WC grain size

The effect of WC grain size on the electrochemical corrosion resistance of cemented carbides has also drawn a lot of attention [10,140,152,159,160]. **Table 4.1** lists data gathered from a detailed literature survey on the effect of average WC grain size on E_{corr} and $i_{p\text{-}min}$ for WC-Co hardmetals. Tomlinson and Ayerst [159] reported that as the grain size increased from 1.4 to 3.0 μm, the passive current density of straight WC-6Co alloys significantly increased. However, Human and Exner [10,160] found that there was no significant difference among the polarization curves of the studied hardmetal grades with distinct grain sizes in the solution of 0.5 mol/L H_2SO_4. Such a finding is in agreement with the results obtained in the studies of Tomlinson and Linzell [152]. Kellner *et al*. [140] reported that the smaller the grain size, the higher the corrosion resistance. Through XRD analysis, they ascribed the higher corrosion resistance of the small-grained hardmetals to the higher amount of fcc Co, which has a better corrosion behavior than hcp Co due to its higher thermodynamic stability. Thus, there is not any clear picture on the effect of WC grain size on the corrosion behavior of straight WC-Co cemented carbides. Nevertheless, it should be highlighted that neither materials nor electrolytes were the same in all these studies, rising then the uncertainty about this issue.

Table 4.1. Effect of average WC grain size on the E_{corr} and $i_{p\text{-}min}$ of WC-Co alloy.

Sample	Main grain size/μm	E_{corr}/mV	$i_{p\text{-}min}$/(mA/cm^2)	Solution	Reference
WC-6%Co	1.4	-387	0.6	0.01mol/L H_2SO_4+ 0.99mol/L Na_2SO_4	[159]
WC-6%Co	3.0	-378	12.0	pH=2.8	
WC-6%Co	1.4	-430	6.3	0.01 mol/L H_2SO_4 + 0.99 mol/L Na_2SO_4 pH=2.55	[152]
WC-6%Co	4.8	-406	4.9		
WC-11%Co	1.4	-413	14.5		
WC-11%Co	5.1	-430	14.5		
WC-6%Co	4.0	-961	24.8	1 mol/L NaOH	[140]
WC-6.5%Co-Cr_3C_2	1.8	-972	19.8		
WC-6%Co-Cr_3C_2-VC	1.2	-973	12.2		
WC-3.2%Co-1%Ni	0.8	-359	1.48		
WC-6%Co-Cr_3C_2	0.6	-958	7.68		
WC-10%Co	1.0	-330	8.0		[10]
WC-10%Co	2.0	-330	-	0.5 mol/L H_2SO_4	[160]
WC-10%Co	5.0	-321	6.0		[10]
WC-16.5%Co	2.1	-320	-	0.5 mol/L H_2SO_4	[160]
WC-16.5%Co	3.1	-315	-		

5 Objectives

Cemented carbides have consolidated as first choice hard materials for tools and components to be used in highly demanding applications, e.g. cutting or forming of metallic alloys, as well as mining operations [4]. Several of these applications also include exposure to chemically aggressive media, such as lubricants, chemical and petrochemical products, mines and seawater [4,6,127,161]. Under these conditions, it has been shown that failure induced under applied load is accelerated, and corresponding service life may be significantly shortened.

Extensive research has proven that corrosion significantly affects microstructural and mechanical/tribological characteristics of cemented carbides. Regarding fracture behavior, it is of crucial importance to know how transverse rupture strength (TRS), one parameter usually recalled as material selection parameter for hardmetals, is affected by corrosion. There are only a few published reports concerning the correlation between corrosion and strength degradation. Tomlinson and Molyneux [9] found that corrosion in a pH = 1 solution at 20 °C for 24 h had no effects on the mean strength of hardmetals containing 6, 8 and 10% Co with small additions of Cr_3C_2 and VC. Pugsley *et al*. [4] concluded that exposure to a wood cutting environment has a detrimental influence on the strength of cemented carbides containing 6 and 10% Co. They rationalized it on the basis of localized corrosive attack which resulted in the formation

of stress raisers. Gant *et al*. [12] investigated the effect of the corrosive media with different pH values on TRS by immersing the specimens within a relative short time. It was found that a distinct corrosion damage was induced on the sample surface after being corroded in a stronger acidic solution, leading to a significant TRS degradation. In this case, failure was found to preferentially occur from corrosion pits. Similar result was also obtained and documented by Tarragó *et al*. [16]. Recently, Tang *et al*. [17] compared the corrosion and strength degradation behaviors of a binderless WC material with that exhibited by WC-Co grade in alkaline solution. Contrary to the results documented by Gant *et al*. [12], substantial strength degradation was discerned after exposure to alkaline medium. Furthermore, it was reported that TRS gap between the two materials was significantly narrowed for exposure times longer than 28 days. However, most of these studies have focused on either one particular hardmetal grade or a specific corrosive medium. As a consequence, it is quite difficult to derive a general relationship including microstructure and corrosive media. This leads to the first objective of the present study, which is to conduct a systematic and comprehensive investigation about corrosion-induced damage and residual strength (damage tolerance) of four microstructurally different cemented carbides exposed to three distinct corrosion media. In doing so, besides the mechanical response referred, electrochemical parameters are measured and corrosion damage scenario is analyzed. Information gathered is expected to be useful for defining microstructural design guidelines on the basis of damage tolerance, as a function of type of corrosive medium.

Concerning contact-load conditions, numerous efforts have been made to evaluate the combined action of corrosion and wear on hardmetals in the past few decades [12,14,118,119,162–167]. In these studies, testing approaches involving abrasion rigs or sliding contacts are often followed. Regarding the former, a micro-abrasion apparatus, which is modified on the basis of the ASTM G65 abrasion test method, has been employed [165], as schematically illustrated in **Fig. 5.1.** Hence, a series of abrasion-corrosion tests were conducted in the corrosive slurry with different pH values, ranging from 1.1 to 13 [12,163–166]. Several interesting findings have been documented. Under strongly acidic conditions (pH = 1.1), the effective removal of WC particles by binder dissolution appears to be a rate-controlling step to determine volume loss. Meanwhile, under weakly acidic conditions (pH = 2.6 and 6.3), there is more evidence of WC grains fracture and less binder dissolution. Finally, in neutral and alkaline conditions, the overall wear rates are hardly affected. **Fig. 5.2** and **Fig. 5.3** show schematic descriptions of wear-corrosion phenomena during micro-abrasion process

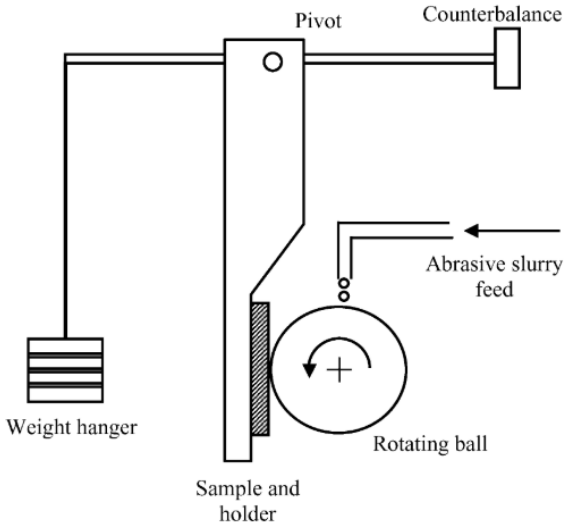

Fig. 5.1. Schematic diagram of the micro-abrasion apparatus [165].

of sintered cemented carbide and sprayed tungsten carbide, respectively. Concerning the combination of corrosion and abrasion (scratch) test, it must be noticed the investigation conducted by Gee and co-workers in the last decade [14,118,119]. In such studies, a special micro-scratch test system was developed, as schematically shown in **Fig. 5.4**. Among the interesting findings reported by this research group, the evidence of structural collapse at the subsurface level together with irregular longitudinal scratch profiles, as a direct consequence of binder leaching, must be highlighted.

Aiming to determine mechanical and tribological properties of cemented carbides at micro- and nanometric length scale, nanoindentation and nanoscratch techniques have been successfully implemented in previous studies. As a result, intrinsic hardness and elastic modulus of individual constituent phases have been measured [40,44,45]; microstructural effects on sliding contact, scratch and wear resistance have been evaluated [168–170]; and deformation, wear and material removal mechanisms have

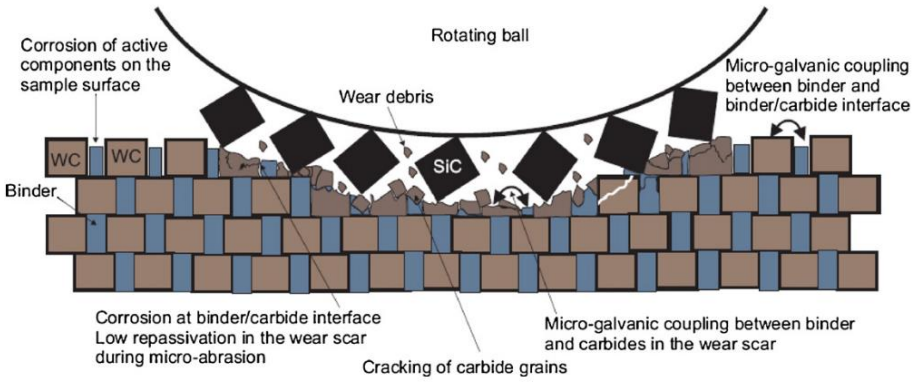

Fig. 5.2. Schematic of wear-corrosion processes occurring in the micro-abrasion system of cemented carbides [166].

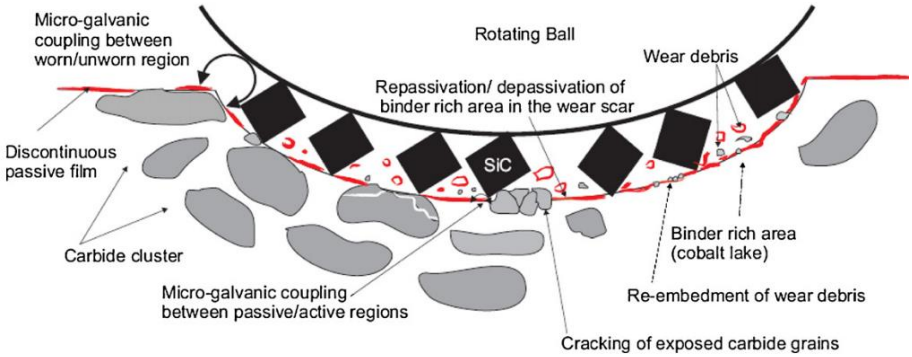

Fig. 5.3. Schematic of wear-corrosion process during micro-abrasion of sprayed hardmetal coating [166].

been documented and analysed [44,45,169,170]. Unfortunately, all the referred works have been conducted on pristine or virgin hardmetals; hence, information on how the limit state – in terms of failure or acceptable/unacceptable criteria from a structural integrity viewpoint – is affected by the damage induced by corrosion is completely missing for cemented carbides. Accordingly, a second objective of this work is to assess and analyse surface/subsurface and mechanical integrity changes induced by exposure to an acidic media of a hardmetal grade, by means of nanoindentation and nanoscratch techniques, i.e. within length scales ranging from 100s to 1000s of nanometers.

Attempting to get closer to service-like conditions, extension of the second goal referred above towards higher length scales, i.e. from 10s to 200 of microns in depth, defines the third objective of this work**.** It consists of carrying out a systematic investigation on corrosion-induced changes on both load-bearing capability and damage scenario of a WC-Co hardmetal grade. In doing so, relatively long corrosion times as well as pyramidal indentation and sliding contact (microscratch) experiments are recalled for

evaluation of microstructure-property-corrosion correlations. The former implies existence of uniform and rather thick corrosion-affected layers, whereas the latter yields damage scenarios whose depth is similar to the length scale of the degraded surface layers. Under these conditions, well-developed cracking systems are induced; and thus, changes on the crack-microstructure interaction as a function of corrosion extension may be studied.

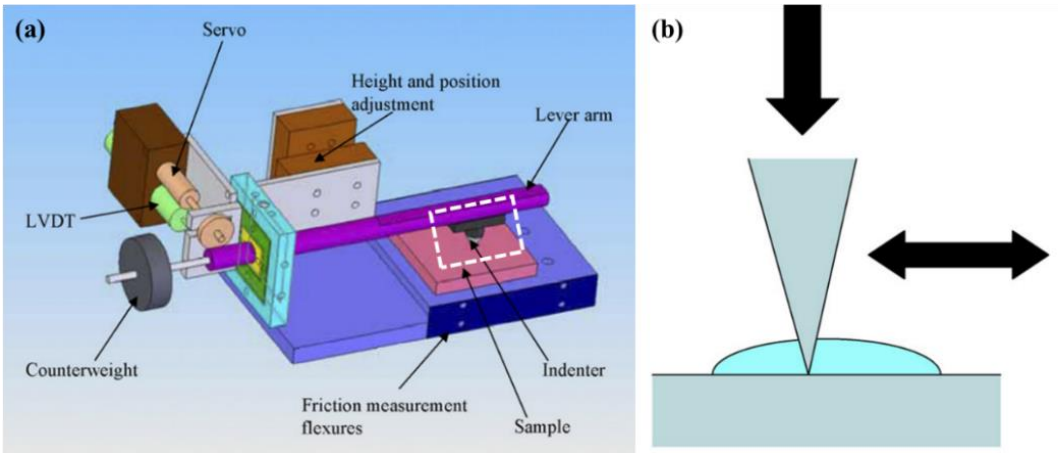

Fig. 5.4. Schematic diagrams of (a) micro-tribology test system [116], and (b) model scratch-corrosion experiment [14,118,119].

As mentioned in section 3.1, the testing protocol based on Hertzian theory has been successfully used for assessing the mechanical response and induced damage under contact loading in nude and coated cemented carbides [86–96]. In such studies, contact damage was introduced using spheres with curvature radii in the millimeter length scale. However, as before for other testing techniques, all these works have also limited their scope to evaluation of pristine or virgin hardmetals. Hence, once again, information addressing simultaneous action of contact loading, using spherical indentation, and

corrosive medium is quite scarce. In this regard, there is only one (and quite recent) study where the combined action of corrosion and repetitive contact loading is considered [171]. Thus, it is the final objective of this thesis to determine and analyse the changes observed in the indentation stress-strain response as well as in surface/subsurface damage scenarios of hardmetals by using Hertzian spherical indentation technique, after exposing them to an acidic medium for different times. Such investigation aims to complement work described above, as it focuses on an even higher length scale, i.e. up to 1000 of microns. In doing so, addition of chromium and/or substitution of cobalt by nickel within the chemical nature of the metallic binder are invoked as experimental variables.

6 Materials and characterization techniques

6.1 Materials

Seven WC-based hardmetal grades with different binders, in terms of both chemical nature and content, and carbide mean grain sizes were studied. All of them corresponded to experimental grades supplied by Hyperion Materials and Technologies. Specimen designation and microstructural characteristics including chemical composition and content (%wt.) of the metallic binder, mean grain size of WC particles (d_{WC}), contiguity of the ceramic phase (C_{WC}), and binder mean free path (λ_{binder}) are listed in **Table 6.1**. Mean grain size was measured following the linear intercept method,

Table 6.1. Designation and microstructural parameters of the hardmetals investigated.

Specimen code	wt.% Co	wt.% Ni	d_{WC} (µm)	C_{WC}	λ_{binder} (µm)
10CoUF	10	--	0.39±0.19	0.46±0.06	0.16±0.06
10CoC	10	--	2.33±1.38	0.31±0.11	0.68±0.48
10CoNiM	8	2	1.44±0.86	0.38±0.08	0.47±0.30
9NiF	--	9	0.83±0.49	0.44±0.08	0.29±0.18
6CoM	6		1.51±0.16	0.48±0.02	0.32±0.03
6CoCrM	6		1.35±0.15	0.48±0.03	0.29±0.05
6NiCrM	0.5	5.5	1.31±0.18	0.47±0.02	0.31±0.04

Indexes UF, F, M and C are used for designing hardmetals with ultrafine, fine, medium and coarse mean grain sizes for the carbide phase, respectively.

using field emission scanning electron microscopy (FESEM) micrographs (**Fig. 6.1**). Meanwhile, carbide contiguity and binder mean free path were estimated from empirical relationships given in the literature [37,172]. A small amount of Cr_3C_2 (< 1%wt.) was added as grain growth inhibitor in 10CoUF, 9NiF, 6CoCrM and 6NiCrM grades.

6.2 Mechanical characterization

Mechanical properties, including hardness (*HV30*) and Palmqvist indentation toughness (K_{Ic}) are listed for the materials studied in **Table 6.2**. Assessment of such properties for 10CoUF, 10CoC, 10CoNiM and 9NiF grades was done and reported in previous works by the research group [172–174]. Similar testing procedures were here implemented to determine such properties for the other three hardmetals under consideration. Hardness was measured using a Vickers diamond pyramidal indenter and applying a load of 294 N. At least ten indentations were carried out in each case, on diamond polished surfaces. Palmqvist indentation toughness was evaluated using Shetty *et al.*'s equation, taking into consideration the length of the cracks emanating from the corners of imprint left after Vickers indentation referred above [52].

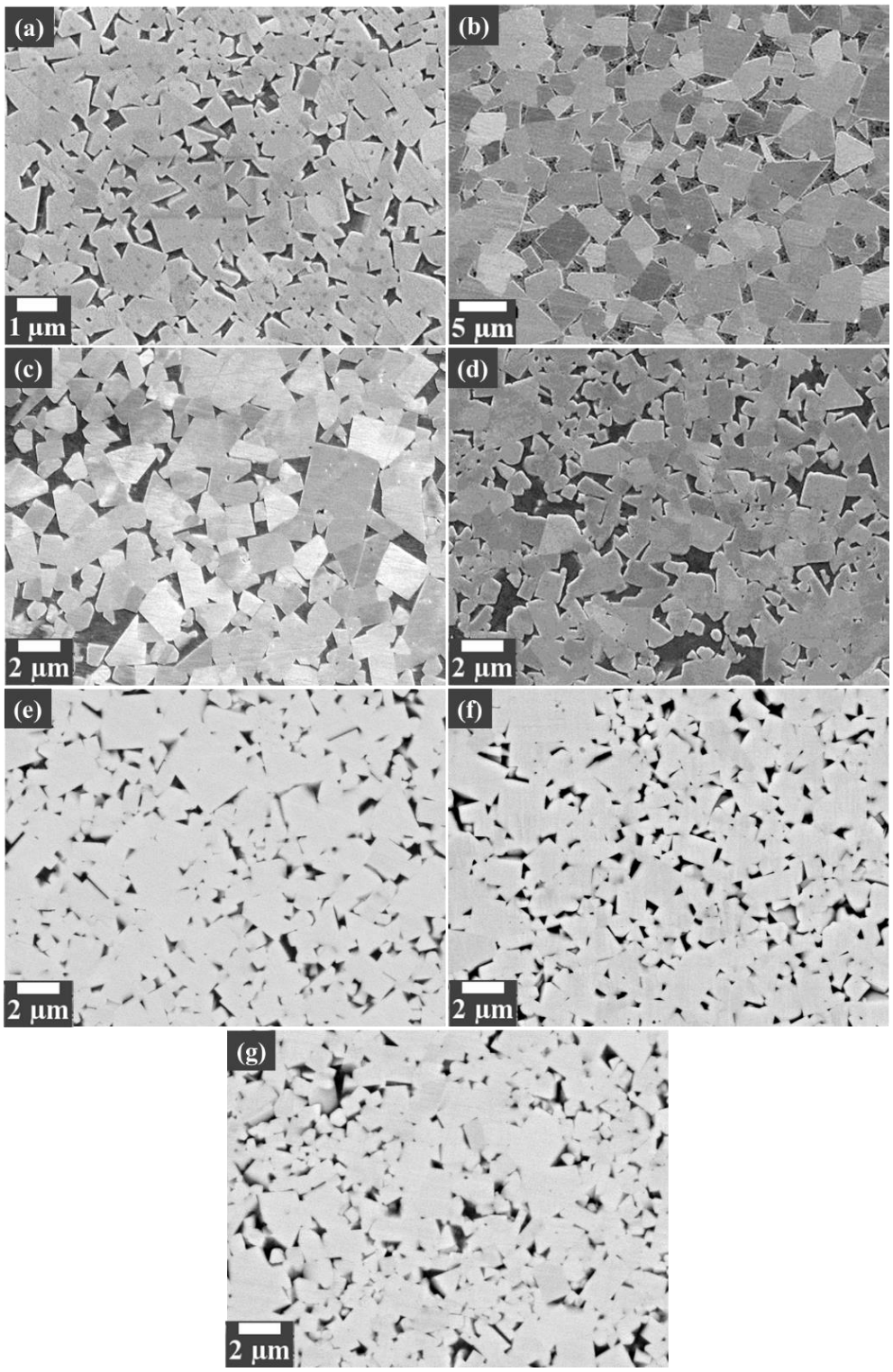

Fig. 6.1. FESEM micrographs of investigated cemented carbide grades: (a) 10CoUF, (b) 10CoC, (c) 10CoNiM, (d) 9NiF, (e) 6CoM, (f) 6CoCrM, and (g) 6NiCrM.

Table 6.2. Basic mechanical parameters for cemented carbides studied.

Specimen code	*HV30* (GPa)	K_{Ic} (MPa$*$m$^{1/2}$)
10CoUF	15.7±0.6	10.4±0.3
10CoC	11.4±0.2	15.8±0.3
10CoNiM	11.6±0.1	15.3±0.3
9NiF	13.2±0.2	11.5±0.2
6CoM	16.0±0.2	11.1±0.2
6CoCrM	15.9±0.1	11.0±0.3
6NiCrM	15.1±0.1	10.0±0.3

6.3 Corrosion behavior

Corrosion behavior was studied by means of immersion test and electrochemical measurements. In the former, well-prepared hardmetal samples (cut, ground and polished) were immersed in a stirred corrosive media during variable periods of time, at a constant temperature. Their corrosion behavior was then determined on the basis of three different approaches [4,16,136]. First, examination of the cross-section of corroded samples aiming to measure the nature and depth of corrosion affected zone. Second, calculation of the corrosion rate using data attained from measurements of weight loss corresponding to different corrosion times. And third, measurement of

amount of dissolved binder by means of atomic absorption techniques. In the latter case, it included potentiostatic/galvanostatic polarization and cyclic voltammetry. In doing so, an electrochemical cell was used to generate voltage and current from chemical reactions or induce chemical reactions by the input of electrochemical signals. The most frequently used electrochemistry system is the three-electrode cell system, and the one employed in this study is shown in **Fig. 6.2**. There, the test specimen is the working electrode, a platinum wire is the counter electrode, and a silver/silver chloride (1M) electrode is used as the reference one.

Fig. 6.2. Three-electrode electrochemical cell system.

In this work, both immersion test and electrochemical measurement were employed with a two-fold purpose: introduction of corrosion damage in a “controlled” way and determination of the corrosion behavior of the hardmetal grades studied. Corrosion rates of the studied materials in different corrosive media (i.e. 0.1M HCl, 0.1M NaCl and 0.1M NaOH solutions) were calculated on the basis of measured weight loss and corrosion front depth as a function of corrosion time. On the other hand, regarding the

potentiodynamic polarization tests, open circuit potential (OCP) was carried out and Tafel extrapolation was used to determine corrosion potential (E_{corr}), current density (i_{corr}), and critical current density (i_c).

6.4 X-ray diffraction

X-ray diffraction (XRD) is a rapid and non-destructive technique in materials science for determining atomic and molecular structure of a material. This is done by irradiating the material sample with incident x-rays, and then measuring the intensity and scattering angle of the x-rays scattered by the material. The intensity of the scattered x-rays is plotted as a function of the scattering angle, and the structure of the material is determined from the analysis of the location, angle, and the intensities of scattered intensity peaks.

Fig. 6.3 schematically shows the radiation-structure interaction taking place when x-ray waves of a specific wavelength (λ) incide upon the atomic plane (hkl) in a crystalline structure with a plane spacing (d_{hkl}). At a certain angle of incidence (θ), the periodic distribution of atoms on planes causes constructive interference of the coherent component of scattered radiation from the individual atoms, which is reflected by the detectable peaks in intensity. In this sense, Bragg's law is well satisfied:

$$n\lambda = 2d_{hkl}\sin\theta \tag{6.1}$$

where n is an integral multiple, λ is the wavelength of the x-rays, d_{hkl} is the spacing between a set of planes with (hkl) Miller indices and θ is the angle of incidence at which a diffraction peak is measured.

In the present study, X-ray diffraction (Philips MRD) using Cu K-α (40 kV and 30 mA) radiation was employed to characterize the phase constitution before and after corrosion tests.

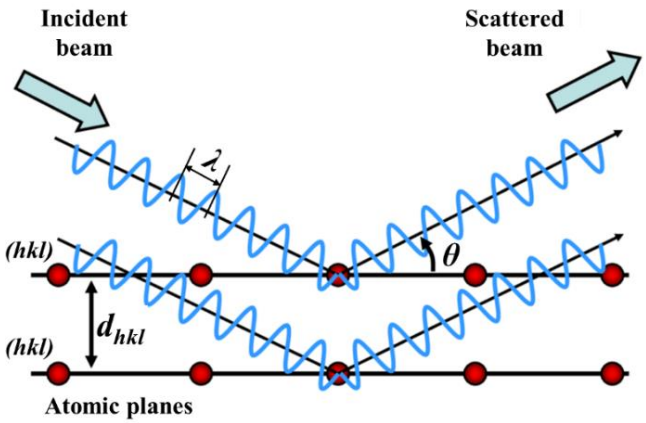

Fig. 6.3. Illustration of Bragg's law.

6.5 Assessment of mechanical contact response

During the last 20 years, several techniques have become popular for measuring the mechanical response of cemented carbides when subjected to contact loading [40,45,86-88,92,115,175,176]. Among them, nanoindentation, nanoscratch, single point scratching and Hertzian indentation are the ones that have received most attention.

6.5.1 Nanoindentation

Nanoindentation is considered a fast and reliable technique for evaluation of local mechanical properties, such as hardness and elastic modulus, in very small volumes of material [177–179]. **Fig. 6.4** schematically illustrates an experimental nanoindenter instrument. During nanoindentation testing, hardness and elastic modulus of the material are determined using the load-displacement data recorded (**Fig. 6.5**). It includes the key parameters for determining the referred properties, i.e. F_{max}, peak indentation load; h_{max}, indenter displacement at peak load; and S, contact stiffness.

In general, hardness (H) is defined as the ratio between the maximum load and the projected contact area (A) at peak load (F_{max}), generated during the indentation testing:

$$H = \frac{F_{\max}}{A} \tag{6.2}$$

where A is given by:

$$A = k_t h_c \tag{6.3}$$

where k_t is geometric constant of the tip, and h_c is the contact depth, which can be

defined as:

$$h_c = h_{\max} - h_s \tag{6.4}$$

where h_{max} can be experimentally measured, and h_s is the elastic deflection of the surface at a specific contact perimeter which depends on the indenter geometry:

$$h_s = \varepsilon\left(\frac{F_{\max}}{S}\right) \tag{6.5}$$

where ε is a geometric constant of indenter [177].

Fig. 6.6 shows a cross section of an indentation, where the parameters used in above analysis can be easily identified.

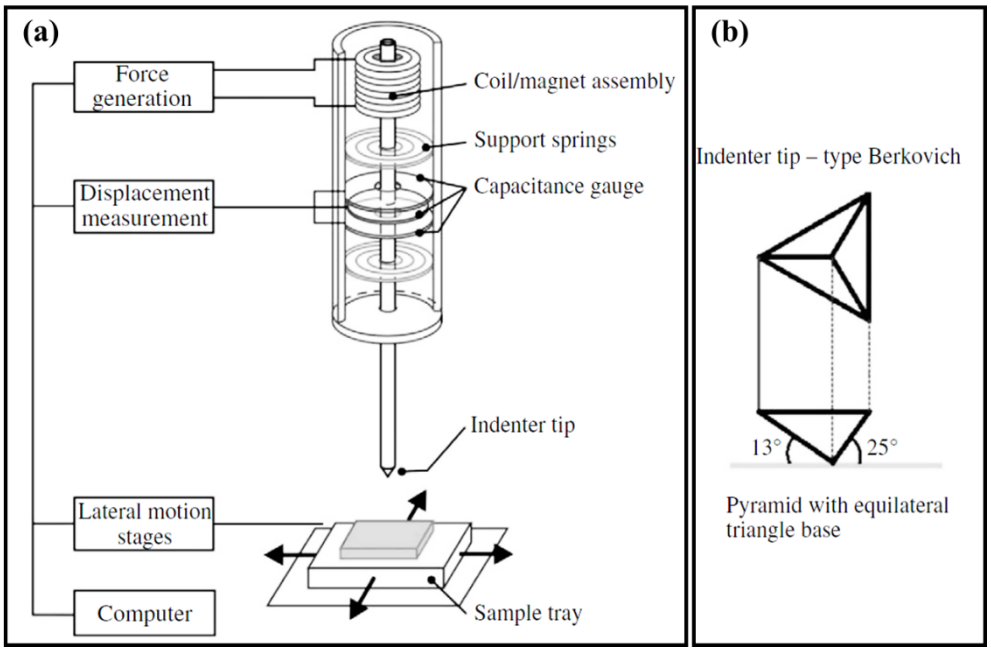

Fig. 6.4. (a) Schematic illustration of the experimental apparatus used to perform a nanoindentation test [178], (b) Berkovich tip: a pyramid with an equilateral triangle as the base area.

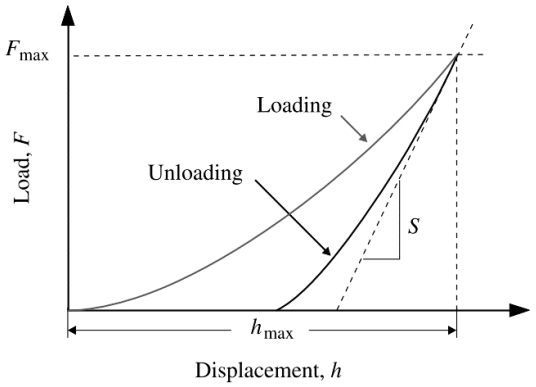

Fig. 6.5. Schematic representation of a load-displacement curve, highlighting key experimental parameters [177].

The reduced elastic modulus, E_r, for the specimen/indenter system can be calculated by the following equation:

$$\frac{1}{E_r} = \frac{\left(1-\nu_s^2\right)}{E_s} + \frac{\left(1-\nu_i^2\right)}{E_i} \tag{6.6}$$

where E_s and E_i are Young's moduli, and ν_s and ν_i are Poisson's ratios, of the tested specimen and the indenter, respectively.

The reduced elastic modulus E_r can also be determined as a function of the experimentally measured contact stiffness (S) and the contact area (A_0), as expressed by:

$$E_r = \frac{S\sqrt{\pi}}{2\beta_0\sqrt{A_0}} \tag{6.7}$$

where β_0 is a constant depending on the tip geometry [177].

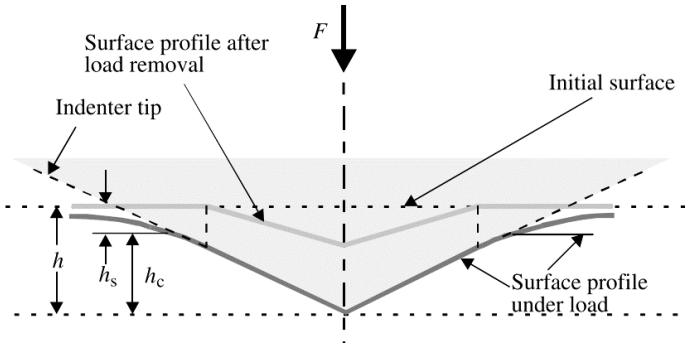

Fig. 6.6. Schematic representation of a section through an indentation [177].

In order to measure the mechanical properties and integrity of very small volumes of cemented carbides, nanoindentation is probably the technique most frequently used, due to the relative easiness in testing. Compared with other techniques involving higher length scales, nanoindentation presents several advantages: measurements are local in the micron range and mechanical properties are depth-sensing. The latter allows to study and analyze evolution of them at different penetration depths, an interesting capability when surface degradation is involved.

In addition to conventional nanoindentation, the equipment may also be used to conduct sliding contact tests. In this process, a series of parameters can be set, such as scratch length, normal load, scratch velocity, etc. In the normal configuration of the test, a diamond (Berkovich) stylus is drawn across the sample surface under an increasing load until some well-defined failure events occur. For the case of hardmetals, such experimental approach has been implemented to evaluate microstructural effects on sliding contact, scratch and wear resistance, as well as to document and analyze deformation, wear and material removal mechanisms [168–170]. Regarding the latter,

scratching has been recalled for emulating individual removal event in abrasive machining, with controllable parameters, such as load and penetration depth. Considering that penetration depth indeed represents the interaction between the diamond tip and the surface of the cemented carbide, changes on this parameter as a function of exposure time to corrosive medium may clearly be used for studying surface and mechanical integrity of corroded hardmetals at very small length scales, corresponding to incipient and/or effectively thin degraded layers.

6.5.2 Pyramid (Vickers) indentation

Vickers (pyramid) indentation is a method commonly used to evaluate hardness and contact damage induced by sharp tips in ceramic-based composites. It involves simultaneous lattice flow and cracking around the imprints generated, even at low loads [52,180–183]. **Fig. 6.7** schematically shows damage scenarios of two different models discerned on the sample surface and underneath the indentation [184]. Vickers hardness of the tested materials can be calculated on the basis of the measured diagonal lengths. On the other hand, fracture toughness of a material may be estimated from the size of the crack emanating out of the corners of the corresponding imprint, assuming the mode of fracture is understood. For sharp indenters, lateral or median vents are formed. In the case of cemented carbides, median vents are formed in the underlying material and they may be classified in two types: Palmqvist and median cracks. Schematic of this indentation-induced crack system is shown in **Fig. 6.7a**. It is defined as a Palmqvist

crack geometry, a necessary condition for assessing fracture toughness through the equation proposed by Shetty and co-workers [52].

In this study, corrosion-induced changes on the load-bearing capability and crack growth resistance of the studied hardmetal grade were assessed by means of Vickers indentation. A range of loads (2–294 N) were chosen to induce relevant irreversible deformation and damage, the latter in terms of defined crack systems as those described above.

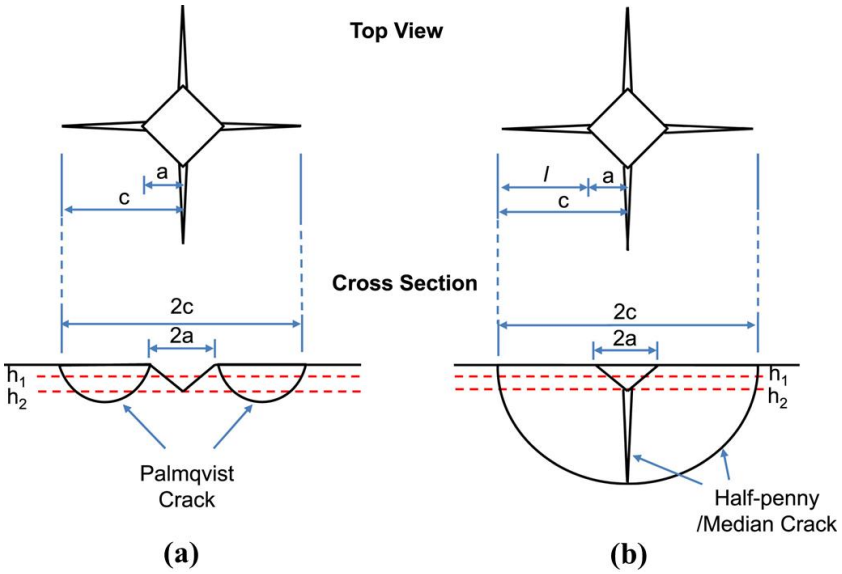

Fig. 6.7. Illustration of top and cross-sectional views of contact damage induced by Vickers indentation: (a) Palmqvist model, and (b) half-penny/median model [184].

6.5.3 Single point scratching

Abrasion is a wear mode that may be described as an accumulation of individual single point abrasion event. Within this context, a number of investigations have attempted to simulate abrasive service-like conditions using single point scratch tests at the laboratory level [33,118,119,185–187]. In doing so, the corresponding deformation and damage scenarios and mechanisms have been well explored and understood. **Fig. 6.8** shows the schematic of the scratch testing and the crack systems developed during such a test [188].

In order to further understand the resistance of a material to experience irreversible deformation under sliding contact conditions, scratch hardness (H_s) value may be recalled [185]. H_s is generally defined as the hardness of a material when it is scratched by a stylus dragged in its surface under a given load. It is expected to be a better correlating parameter than the indentation hardness when assessing the tribological performance of many materials. During the scratch test, the stylus is allowed to plough into the test specimen up to a predetermined distance to form a groove. Then, the scratch hardness can be calculated as [189]:

$$H_s = \frac{k_0 F_N}{w^2} \tag{6.8}$$

where F_N is the applied load, w is the scratch width, and k_0 is a numerical constant which equals $8/\pi$ for styli having conical, spherical or parabolic tips [190].

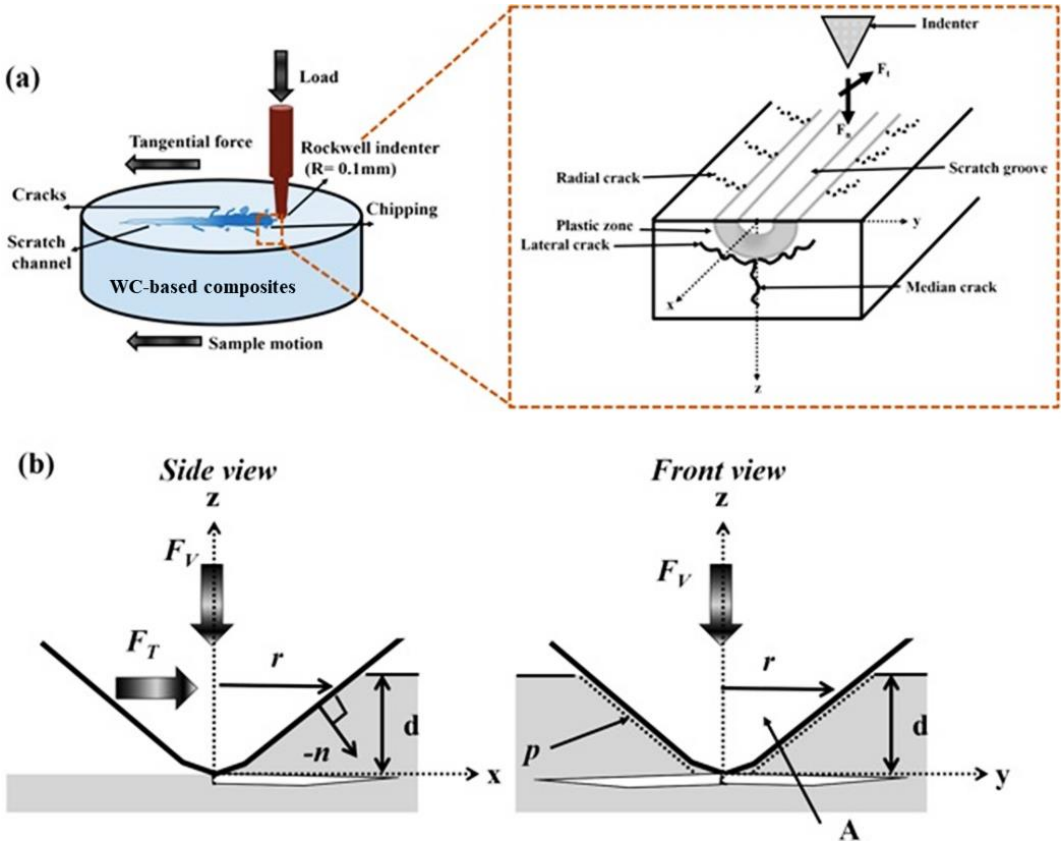

Fig. 6.8. (a) Schematic illustration of the single point scratch process and different crack systems evolving during the process, and (b) side and front view of a symmetric probe used in scratch test [188]. In this figure, x indicates the scratch direction, F_T and F_V are the horizontal and vertical forces respectively, d is the penetration depth of the scratch, n is the outward unit normal to the probe material interface, A is the projected horizontal load bearing contact area, and p is the perimeter.

6.5.4 Hertzian spherical indentation

The experimental setup for Hertzian contact testing consists of indenting a flat surface of a studied specimen with a sphere indenter at a given load. During spherical indentation concentrated stresses are delivered such that typical ‘‘blunt” in-service conditions are simulated. Then, the mechanical integrity of materials may be assessed

on the basis of the damage scenario as a function of increasing applied load or number of cycles. **Fig. 6.9** shows a schematic of the contact between a spherical indenter and deformed specimen as a result of a normal indentation load F. In this regard, the load-bearing capability of the studied materials may be evaluated by measuring the residual depth (d_0) of the indentation as a function of applied load. Data from Hertzian tests are usually presented in terms of contact pressure or indentation stress (p_0) as well as the resulting indentation strain (ε_0), e.g. Refs. [85,191]. Indentation stress is calculated by the equation:

$$p_0 = \frac{F}{\pi a^2} \tag{6.9}$$

where F is the indentation load, and a is the radius of the contact circle.

On the other hand, indentation strain is calculated as:

$$\varepsilon_0 = \frac{a}{R} \tag{6.10}$$

where R is the radius of the indenter.

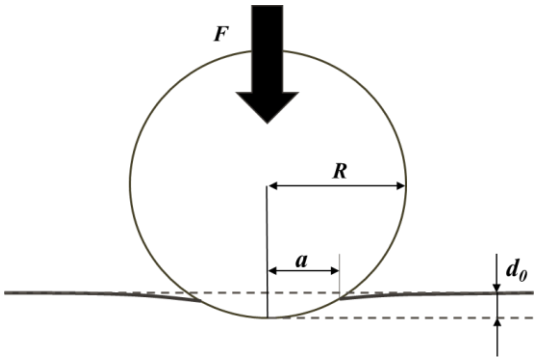

Fig. 6.9. Schematic diagram of the spherical indentation.

Fig. 6.10 presents a typical spherical indentation test on a hardmetal sample, using a servo-hydraulic universal testing machine.

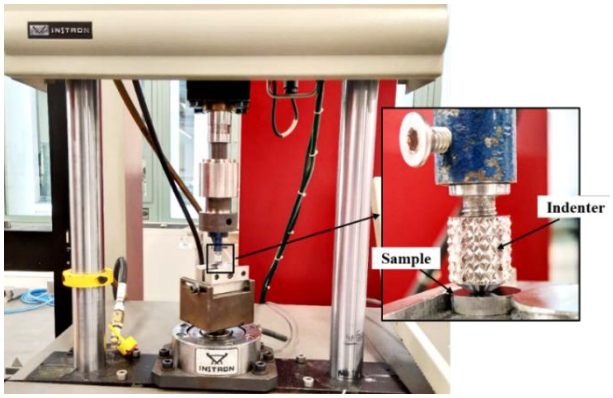

Fig. 6.10. Typical setup of a Hertzian spherical indentation test on a hardmetal sample.

6.6 Microscopy

Microscopy is a broad range technique involving the use of microscopes to determine microstructural characteristics (e.g. metallography, structure and phase constitution), discern and analyze features related to deformation and damage mechanisms, and conduct fractographic analysis. In this thesis, laser scanning confocal microscopy (LSCM) and field emission scanning electron microscopy (FESEM) were extensively used.

6.6.1 Laser scanning confocal microscopy

Laser Scanning Confocal Microscopy (LSCM) became popular and increasingly important in the mid-1980s, due to the need for three-dimensional (3D) information in the plane of focus. **Fig. 6.11** schematically shows the optical principle of LSCM [192]. In such an image, a laser beam is used to supply the excitation, which is emitted as a monochromatic light bundle. The excitation light provided by the laser is uniformly focused on a small spot of the test sample. Then, the fluorescence emitted by the sample is detected by a photomultiplier tube. Moreover, a mirror system is contained to make the laser beam scan across the plane of focus of the specimen (i.e. in x and y directions). The pinhole aperture between the sample and the detector is set for preventing the detection of out of focus fluorescence. With the help of computer data storage and processing, both 2-D and 3-D images can be obtained by using the different scanning types. Regarding the former, it can be done by an x-y scan. In the latter case, a consecutive series of x-y scans at different depths are taken in the specimen. The measurements are achieved by the microscope stage being repeatedly raised or lowered by a small distance (0.25-0.50 μm), and each time a new x-y scan is performed.

In this thesis, the LSCM was extensively employed for determining the deformation and damage scenarios induced by indentation and scratch testing at different length scales. Appropriateness of using such technique was based on the consideration of clarifying the information difference from a three-dimensional view.

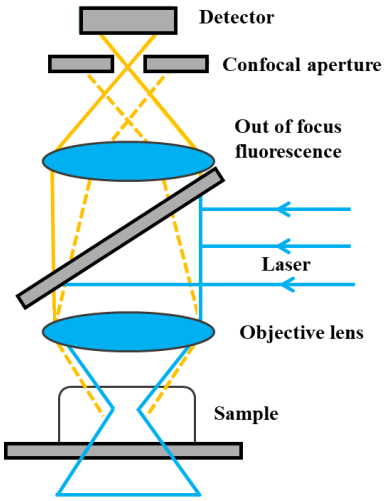

Fig. 6.11. Optical principle of laser scanning confocal microscopy (LSCM) [192].

6.6.2 Field emission scanning electron microscopy

Field emission scanning electron microscopy (FESEM) is a technique which permits the observation of a wide variety of information out of the sample surface, from nanometer to micrometer length scales. **Fig. 6.12** shows the principle of FESEM operation [193]. It works with electrons with negative charge instead of light. These electrons are released by a field emission source and accelerated in a high electrical field gradient. Within the high vacuum column, these so-called primary electrons are focused and deflected by electronic lenses, to produce a narrow scan beam that bombards the specimen. As a result, secondary electrons are emitted from each spot on the specimen, the angle and velocity of which are determined by the surface structure of the test material. Subsequently, the secondary electrons are caught by a detector to produce an electronic signal that is finally amplified and transformed into a monitor or to a digital image.

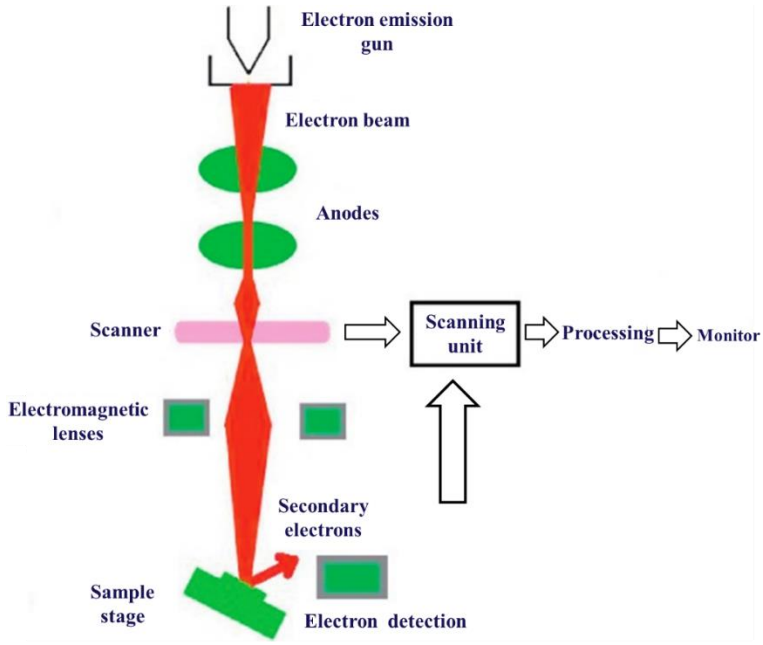

Fig. 6.12. Schematic illustration of principle of FESEM operations [193].

6.7 Focused ion beam

Focused ion beam (FIB) and combined FIB/FESEM dual systems have proved to be invaluable tools for in-situ observation of structural cross-sections, preparation of TEM lamella and atom probe specimens, generation of microstructural data in three dimensions, and nanofabrication of device and protypes [194–196]. **Fig. 6.13** illustrates the operating principle of the FIB/SEM instrument [196]. During FIB milling, the focused ion beam removes material from the sample surface in a precise and controlled manner. With the combined use of FIB instrument and SEM (**Fig. 6.13a**), it can simultaneously monitor the milling process of the electron beam, and more importantly, perform non-destructive imaging of the sample surface compared to ion beam imaging. By accelerating and focusing an ionized gallium atom beam (i.e. with a high current

density) on the sample surface, the FIB system can be used to perform material removal at specific locations. The impinging ions can expel surface layer atoms from their positions by collision. Scanning the ion beam on the sample surface step by step can remove material layer by layer (**Fig. 6.13b**), which is the so-called ion milling process. In addition, the ion beam can also guide the deposition of materials in gas precursors that are released into the microscope cavity through a gas injection system (**Fig. 6.13c**). In this regard, the ion beam is usually generated by a source of liquid metal ions, of which the most popular ion species is gallium (Ga^+) because of its low melting point, volatility, and vapor pressure.

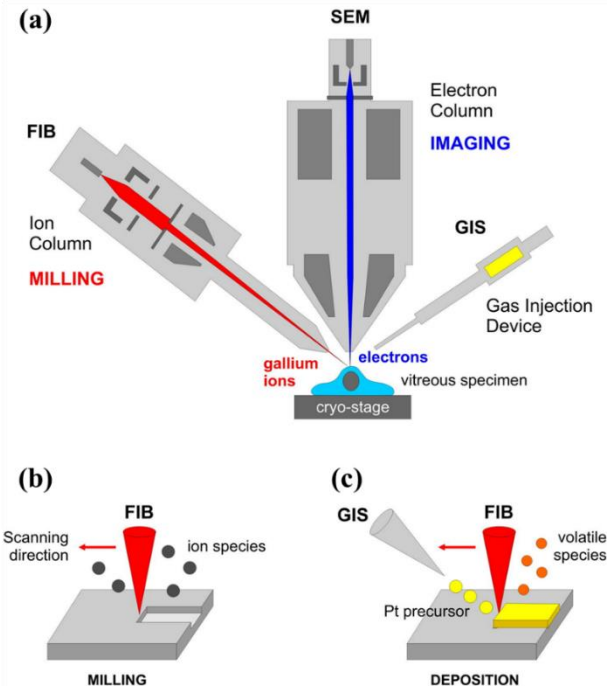

Fig. 6.13. Operating principle of a FIB/SEM microscope: (a) removal of material from the sample surface using a focused gallium ion beam, (b) ion beam milling, and (c) ion beam-assisted deposition [196].

7 Articles presentation

This Ph.D. thesis includes four sections involving: corrosion-induced changes on (1) residual strength, (2) small-scale mechanical integrity, (3) load-bearing capability and (4) Hertzian contact damage in cemented carbides. These sections correspond to **Articles I**, **II**, **III** and **IV**, respectively.

7.1 Article I

Corrosion-induced damage and residual strength of WC-Co,Ni cemented carbides: influence of microstructure and corrosion medium

Yafeng Zheng, Gemma Fargas, Elaine Armelin, Olivier Lavigne, Luis Llanes.

The corrosion behavior of cemented carbides with binders of different chemical nature (Co and Ni) and carbides with distinct mean grain size (ultrafine and coarse) was studied. The investigation also included different corrosion media: acidic and neutral solutions containing chlorides and an alkaline one, as experimental variables. Immersion tests were performed to induce corrosion damage in a controlled way. Electrochemical parameters were measured together with a detailed inspection of the corroded surfaces. Microstructural influence on the tolerance to corrosion damage was evaluated in terms of residual strength. Results pointed out that corrosion rates were lower in the alkaline solution. In contrast, acidic media led to higher corrosion rates, especially for cemented carbides with Co, regardless the influence of carbide mean grain size. Corrosion damage resulted in strength degradation due to the formation of surface corrosion pits in acidic solution. In neutral and alkaline solutions, much less pronounced effects were determined. FIB/FESEM results revealed differences in corrosion-induced damage scenario. In acidic solution, corrosion starts at binder pool centres and evolves towards binder/WC interfaces. Meanwhile, corrosion in alkaline solution is initially located at binder/WC interfaces, and subsequently expands into the ceramic particles.

Article I

Corrosion-induced damage and residual strength of WC-Co,Ni cemented carbides: influence of microstructure and corrosion medium

Y.F. Zheng

G. Fargas

E. Armelin

O. Lavigne

L. Llanes

Metals 9 (2019) 1018

metals

MDPI

Article

Corrosion-Induced Damage and Residual Strength of WC-Co,Ni Cemented Carbides: Influence of Microstructure and Corrosion Medium †

Yafeng Zheng [1,2,*], Gemma Fargas [1,2], Elaine Armelin [2,3], Olivier Lavigne [4] and Luis Llanes [1,2]

1 CIEFMA, Departament de Ciència dels Materials i Enginyeria Metal·lúrgica, EEBE, Universitat Politècnica de Catalunya, 08019 Barcelona, Spain; gemma.fargas@upc.edu (G.F.); luis.miguel.llanes@upc.edu (L.L.)
2 Barcelona Research Center in Multiscale Science and Engineering, Universitat Politècnica de Catalunya, 08019 Barcelona, Spain; elaine.armelin@upc.edu
3 IMEM, Departament d'Enginyeria Química, EEBE, Universitat Politècnica de Catalunya, 08019 Barcelona, Spain
4 Hyperion Materials and Technologies, 08107 Martorelles, Spain; olivier.lavigne@hyperionmt.com
* Correspondence: yafeng.zheng@upc.edu; Tel.: +34-934011083
† This paper is an extended version of our paper published in Euro PM 2018, Bilbao, Spain, 14–18 October 2018.

Received: 30 July 2019; Accepted: 17 September 2019; Published: 19 September 2019

Abstract: The corrosion behavior of cemented carbides with binders of different chemical nature (Co and Ni) and carbides with distinct mean grain size (ultrafine and coarse) was studied. The investigation also included corrosion media (acidic and neutral solutions containing chlorides and an alkaline solution) as experimental variables. Immersion tests were performed to induce corrosion damage in a controlled way. Electrochemical parameters were measured together with a detailed inspection of the corroded surfaces. Microstructural influence on the tolerance to corrosion damage was evaluated in terms of residual strength. Results pointed out that corrosion rates were lower in the alkaline solution. In contrast, acidic media led to higher corrosion rates, especially for cemented carbides with Co regardless the influence of carbide mean grain size. Corrosion damage resulted in strength degradation due to the formation of surface corrosion pits in acidic solution. In neutral and alkaline solutions, much less pronounced effects were determined. Focused Ion Beam (FIB)/ Field Emission Scanning Electron Microscopy (FESEM) results revealed differences in corrosion-induced damage scenario. In acidic solution, corrosion starts at binder pool centers and evolves towards binder/WC interfaces. Meanwhile, corrosion in alkaline solution is initially located at binder/WC interfaces, and subsequently expands into the ceramic particles, developing a microcrack network inside this phase.

Keywords: corrosion; cemented carbides; binder; grain size; damage tolerance

1. Introduction

Cemented carbides, usually referred to as hardmetals, are preeminent material choices for extremely demanding applications, such as cutting and forming tools, mechanical seals, and mining bits. The main reason behind this is the unique combination of hardness, toughness, and wear resistance they exhibit. It results from their two-phase interpenetrated network as well as the intrinsic properties of the ceramic particles and the metallic binder [1–5]. Many of the referred applications often imply exposure of cemented carbides tools and components to chemically aggressive media including a large variety of corrosive environments, such as lubricants, chemical and petrochemical products, as well as mine- and sea-water (e.g., References [6–9]).

Corrosion mechanisms in cemented carbides depend on a large number of factors, such as surface state, corrosive medium, microstructural assemblage, and binder chemical nature. It has been found that nickel, nickel-chromium, and nickel-cobalt binder exhibit higher corrosion resistance compared to plain cobalt one, especially in acidic and neutral media. Under these conditions, metallic binders are preferentially attacked, while ceramic phase is the one corroded in alkaline solution [10,11]. Regarding the influence of grain size, it is difficult to extract clear conclusions from the literature. While some authors report a negligible influence of the grain size on the corrosion behavior in acids [6], others have found a direct correlation between passive current density and grain size in acidic solutions [12]. The fact that neither materials nor the electrolytes were the same in these studies, increases the uncertainty about this issue.

Performance and reliability of engineering components depend on how service-like conditions may affect their properties. Several studies have shown detrimental corrosion effects on the effective wear resistance of cemented carbides, as a result of synergic interactions among different degradation phenomena [13–15]. Similar correlations have been reported regarding residual strength, measured under either monotonic or cyclic loads [16–21]. However, most of these works have focused on either one particular hardmetal grade or a specific corrosive medium. As a consequence, to draw generic relationships including microstructure and corrosive medium aspects is not possible. Following the above ideas, the corrosion-induced damage and the corresponding residual strength (tolerance) behavior of four microstructurally different cemented carbides exposed to three distinct corrosion media are studied here. In doing so, besides the mechanical response referred, electrochemical parameters are measured as well as corrosion damage scenario is documented and analyzed. Information gathered is expected to be useful for defining microstructural design guidelines on the basis of damage tolerance as a function of type of corrosive medium.

2. Materials and Methods

Four hardmetal grades with different binder and carbide mean grain size were studied. All materials were supplied by Hyperion Materials and Technologies. Hardness, fracture toughness and main microstructural characteristics including specimen designations, binder content (%wt.), mean grain size (d_{WC}), contiguity (C_{WC}) and binder mean free path (λ_{binder}) are listed in Table 1. Mean grain size was measured following the linear intercept method, using field emission scanning electron microscopy (FESEM) micrographs. On the other hand, carbide contiguity and binder mean free path were deduced according to empirical relationships given in the literature [2,22]. A small amount of Cr_3C_2 (i.e., <1%wt.) was added in 10CoUF and 9NiF grades as grain growth inhibitor.

Table 1. Microstructural parameters, hardness and fracture toughness for the investigated cemented carbides [20,23,24].

Specimen Code	%wt. Co	%wt. Ni	d_{WC} (μm)	C_{WC}	λ_{binder} (μm)	HV30 (GPa)	K_{Ic} (MPa)
10CoUF	10	-	0.39 ± 0.19	0.46 ± 0.06	0.16 ± 0.06	15.7 ± 0.6	10.4 ± 0.3
10CoC	10	-	2.33 ± 1.38	0.31 ± 0.11	0.68 ± 0.48	11.4 ± 0.2	15.8 ± 0.3
10CoNiM	8	2	1.44 ± 0.86	0.38 ± 0.08	0.47 ± 0.30	11.6 ± 0.1	15.3 ± 0.3
9NiF	-	9	0.83 ± 0.49	0.44 ± 0.08	0.29 ± 0.18	13.2 ± 0.2	11.5 ± 0.2

Corrosion behavior was studied on the basis of the electrochemical response of the studied grades in three different solutions: acidic (0.1M HCl), neutral containing chlorides (0.1M NaCl), and alkaline (0.1M NaOH). The electrochemical tests were carried out using a VersaStat™ II potentiostat-galvanostat (Princeton Applied Research, Oak Ridge, TN, USA.) and a standard three-electrode cell in which the test specimen was the working electrode (area: 1.0 cm^2), a platinum wire was the counter electrode, and a silver/silver chloride electrode was used as the reference electrode. After immersion in the electrolyte, the open circuit potential was stabilized for 30 min. Subsequently, the samples were polarized into the

cathodic region at –500 mV. Then, the potential was increased towards the anodic region with a scan rate of 600 mV/h in the positive direction up to 500 mV.

Immersion tests were performed to induce corrosion damage in a controlled way and to determine the corrosion rates by gravimetric analysis. These tests were done at room temperature in the same three solutions (stirred) as mentioned above. Weight loss was measured after immersion tests performed from 1 to 240 h. Before and after immersion tests, the specimens were hand-cleaned using soapy water, then ultrasonically cleaned for 15 min in ethanol, and subsequently dried in air. In this case, at least five samples were tested for each material and solution. The specimens were weighted using an electronic balance having a resolution of ±0.1 mg, and the corrosion rates were determined using Equation (1):

$$Corrosion(\mathrm{mm/year}) = 87.6(\frac{w}{A\rho t}) \quad (1)$$

where w is the weight loss in mg; A is the surface area of the specimen in cm^2; ρ is the density of the material in g/cm^3; and t is the corrosion time in hours.

After immersion tests, mechanical tests were carried out to assess the tolerance to corrosion-induced damage—measured in terms of residual flexural strength—as a function of microstructure and corrosion medium. Flexural strength (σ_r) was determined according to ASTM Standard C1161-13 by using a fully articulating jig fixture in a four-point bending configuration, with inner and outer spans of 20 and 40 mm respectively [25]. Measurements were done on beam-like specimens (with dimensions of 4 mm × 3 mm × 45 mm) whose longitudinal edges were beveled before testing for avoiding stress rising effects. A minimum of three specimens were tested for each corroded condition. Aiming to define the "baseline" intrinsic flexural strength for each hardmetal grade studied, the same tests were also conducted on uncorroded samples (eight tests per hardmetal grade). The equation used for the strength calculation can be expressed as [25]:

$$\sigma_r = \frac{3PL}{4bd^2} \quad (2)$$

where P is break force in N; L is outer span in mm; b is specimen width in mm; and d is specimen thickness in mm.

The mechanical study was complemented by fractographic inspection by means of optical microscopy and FESEM. For each specimen, fracture initiation sites were identified at low magnification; and then, strength-limiting flaws were further analyzed at higher magnifications. Finally, cross-sectional samples were prepared by Focused Ion Beam (FIB) milling, using a dual bean Workstation. They were used for evaluation of corrosion-induced damage at the subsurface level through FESEM imaging.

3. Results and Discussion

3.1. Corrosion Behavior

In immersion tests, the corrosion rates in acidic solution were higher for all studied cemented carbides grades compared to neutral and alkaline ones, as shown in Figure 1. Table 2 gives the corrosion rate values of investigated cemented carbides after immersion for 168 h in these three different media. Coarse-grained cobalt grade, 10CoC, displayed in each solution the highest values, while 9NiF showed the best corrosion resistance. The presence of small amount of chromium in 10CoUF grade together with the ultrafine microstructure proved to be more effective than the presence of 2%wt. of nickel in a coarse-grained cobalt grade, 10CoNiM. This result is in agreement with previous studies which pointed out that during sintering chromium dissolves into the binder, resulting in a beneficial effect against corrosion [26]. TEM analysis performed by Suttihiruangwong et al. [27] demonstrated the formation of a passivating Co-based chromium oxide layer film at the binder surface, which strongly decreased the rate dissolution of the binder, and hence improved the corrosion resistance of Cr-containing cemented carbides.

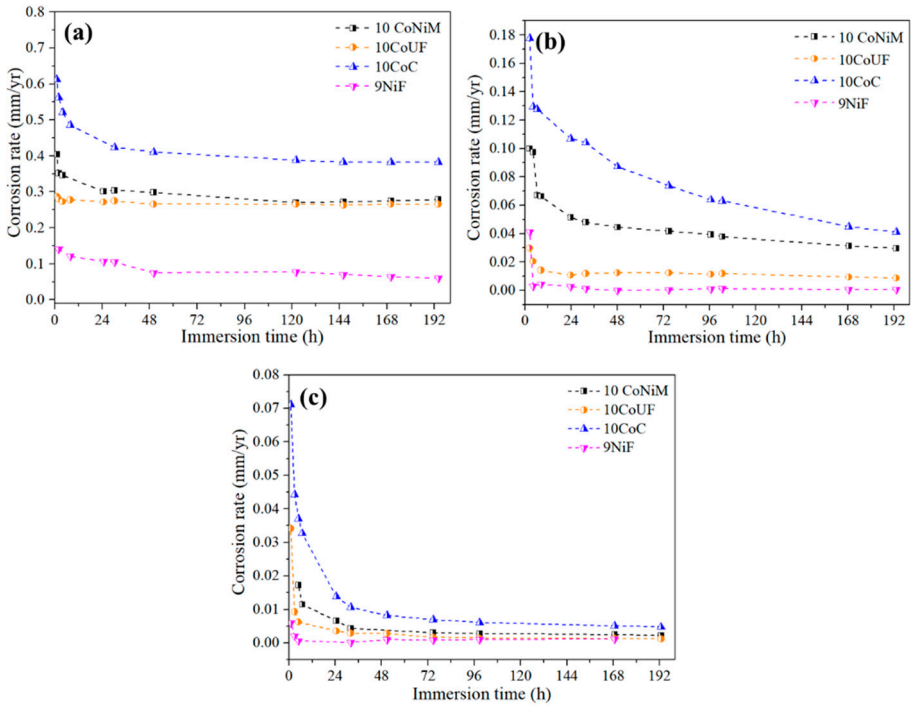

Figure 1. Corrosion rates as a function of immersion time for the studied cemented carbides in different solutions: (**a**) 0.1M HCl, (**b**) 0.1M NaCl and (**c**) 0.1M NaOH.

Table 2. Corrosion rates of investigated cemented carbides after the immersion for 168 h.

Specimen Code	Corrosion Rate (mm/y)		
	0.1M HCl	**0.1M NaCl**	**0.1M NaOH**
10CoNiM	2.8×10^{-1}	2.96×10^{-2}	2.23×10^{-3}
10CoUF	2.7×10^{-1}	8.67×10^{-3}	1.19×10^{-3}
10CoC	3.8×10^{-1}	4.12×10^{-2}	4.77×10^{-3}
9NiF	5.97×10^{-2}	4.76×10^{-4}	1.09×10^{-3}

For all studied grades and solutions, the corrosion rates decreased with increasing immersion time. In acidic and alkaline solutions, the corrosion rates sharply decreased after the first 6–8 h of immersion, remaining constant beyond 24 h. At the beginning of corrosion tests, the higher corrosion rate may be attributed to the relatively large area of the alloy exposed to the corrosive media. As the immersion progresses, the generated corrosion products gradually cover the surface of the alloy, which reduces the contact area between the alloy and the corrosive medium, thereby reducing the corrosion rate. For these two solutions, no layer of corrosion products was observed at the surface. In neutral solution, the reduction of the corrosion rate as a function of immersion time was observed to be more gradual for the coarse-grained cobalt grades, 10CoC and 10CoNiM. In this case, the presence of chloride ions enhances the formation of a corrosion product layer which seems to slow down the dissolution of cobalt. This layer does not protect the material from corrosion, as chromium, but hinders the dissolution process of cobalt.

Figure 2 shows the obtained potentiodynamic polarization curves for the studied grades in the acidic, neutral and alkaline solutions. The electrochemical parameters measured for the studied cemented carbides are listed in Table 3. They include corrosion potential (E_{corr}), corrosion current density (i_{corr}) measured using the Tafel method, and critical current density (i_c), which refers to the current density necessary to reach the passive or pseudo-passive potential. In acidic and neutral solution, the grade with nickel as a binder, 9NiF, clearly displayed the noblest corrosion potential. Meanwhile, coarse-grained cobalt grade, 10CoC, presented the most negative values. For this type of microstructure, the corrosion potential was shifted to more positive values with the presence of

2 wt.% of nickel as a binder, 10CoNiM. It is important to point out that although i_{corr} is higher in acidic solutions for 9NiF, i_c was at least one order of magnitude lower than for the rest of the cobalt grades. The addition of chromium in cobalt grades, 10CoUF, did not contribute to a better corrosion response. As can be seen in Table 3, the E_{corr} is moved in the noble direction. Likely, the apparent transpassive region is shifted to higher potentials and lower i_c, compared to the other grades. However, at about +100 mV, the self-passivating layer underwent pitting corrosion and the surface response became similar to the other cobalt grades. This phenomenon is supposed to be related to the fracture of the protective oxide film referred above. Nevertheless, future works are needed to corroborate it. Regarding the alkaline solution, no significant differences were observed among cobalt grades. In this media, where the ceramic phase is easily corroded [10,11], the nickel grade showed the highest current densities.

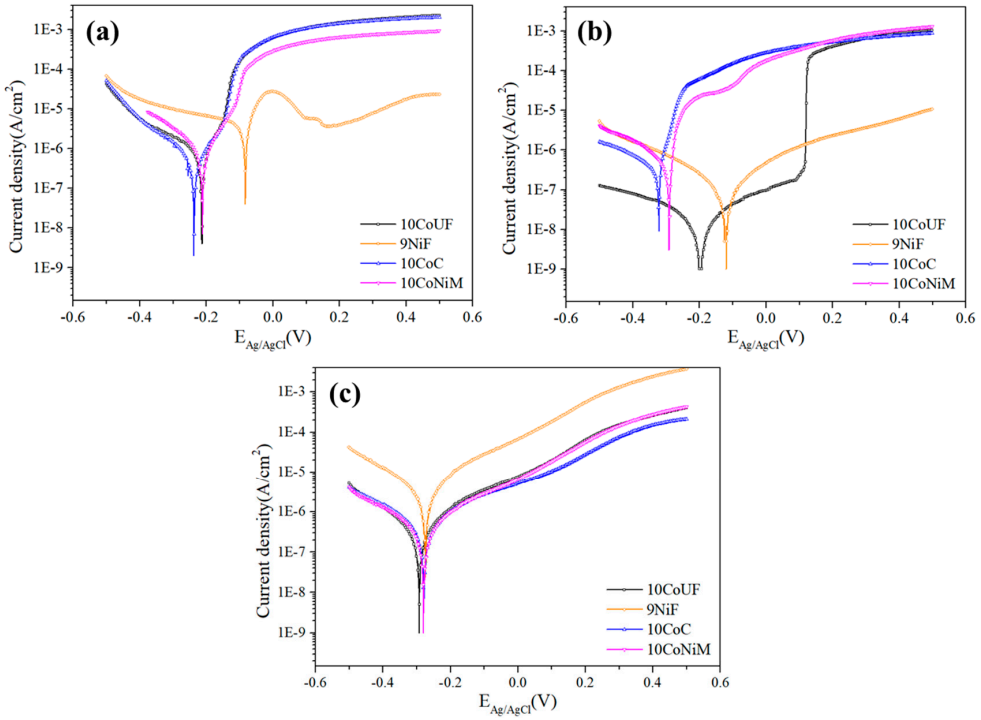

Figure 2. Potentiodynamic polarization curves of studied cemented carbide grades in: (**a**) 0.1M HCl, (**b**) 0.1M NaCl and (**c**) 0.1M NaOH.

Table 3. Electrochemical corrosion parameters of studied cemented carbide grades in acidic, neutral and alkaline solutions.

Corrosive Media	Specimen Code	E_{corr} (V)	i_{corr} (A/cm^2)	i_c (A/cm^2)
0.1M HCl	10CoUF	−0.213	1.05×10^{-6}	1.90×10^{-3}
	10CoC	−0.237	9.27×10^{-7}	1.90×10^{-3}
	10CoNiM	−0.212	1.30×10^{-6}	8.92×10^{-4}
	9NiF	−0.084	1.54×10^{-5}	2.11×10^{-4}
0.1M NaCl	10CoUF	−0.196	7.38×10^{-8}	2.21×10^{-7}
	10CoC	−0.322	5.05×10^{-6}	3.67×10^{-4}
	10CoNiM	−0.291	5.22×10^{-6}	2.07×10^{-4}
	9NiF	−0.124	5.20×10^{-7}	-
0.1M NaOH	10CoUF	−0.292	1.19×10^{-6}	-
	10CoC	−0.278	1.12×10^{-6}	-
	10CoNiM	−0.279	1.02×10^{-6}	-
	9NiF	−0.274	1.20×10^{-5}	-

3.2. Residual Strength of Corroded Hardmetals

Retained strength was measured using samples subjected to immersion tests of 240 h in acidic, neutral and alkaline solutions respectively (Figure 3b). Values are plotted as normalized strength loss, using as reference baseline the strength exhibited by uncorroded specimens (Figure 3a). As it can be observed, each studied corrosive medium induces relatively different strength losses, most likely related to significant differences in the size and geometry of corrosion-induced damage acting as critical flaws for fracture. HCl solution was found to be the most aggressive medium, i.e., flexural strength for all studied grades, including the one with nickel as a binder, was significantly lessened. The highest strength loss, 60% approximately, was observed for 10CoC. Meanwhile, for neutral and alkaline solutions, retained strength was at least 80% in the worst-case scenario.

Aiming to analyze corrosion-induced damage promoting failure, a detailed inspection of fractured surfaces was conducted by means of FESEM. In doing so, Figure 4 shows the fracture initiation sites that were identified at low magnification together with the corresponding high magnification images showing the strength-limiting flaws, in which corrosion pits and binderless carbide agglomerate act as starting locations for subcritical crack growth until they reach a critical size where unstable fracture takes place. Furthermore, the observations revealed clear differences between the corrosion-induced damage as a function of the pH solution. In this sense, the affected depth from the surface for 10CoC in acidic media was about 150 μm, Figure 5a, followed by the corroded zones from neutral and alkaline medias, where the affected depths were close to 30 and 20 μm, respectively, as the maximum value, Figure 5b,c. It reveals that corrosion affected zone act as critical points for starting fracture, and the strength degradation shows a significant dependence on the depth of the corroded zone. A more pronounced deterioration in the flexural strength is discerned as the corroded zone gets deeper.

Regarding carbide grain size in the neutral and alkaline solutions, the ultrafine-sized studied grade was much more affected by corrosion-induced damage than the coarser ones. As reported in previous investigations, sharp corrosion pits are formed in ultrafine-sized cemented carbides as immersion time increases, which have a much more pronounced stress rising effect. Consequently, higher strength loss was expected for ultrafine grades [19,20].

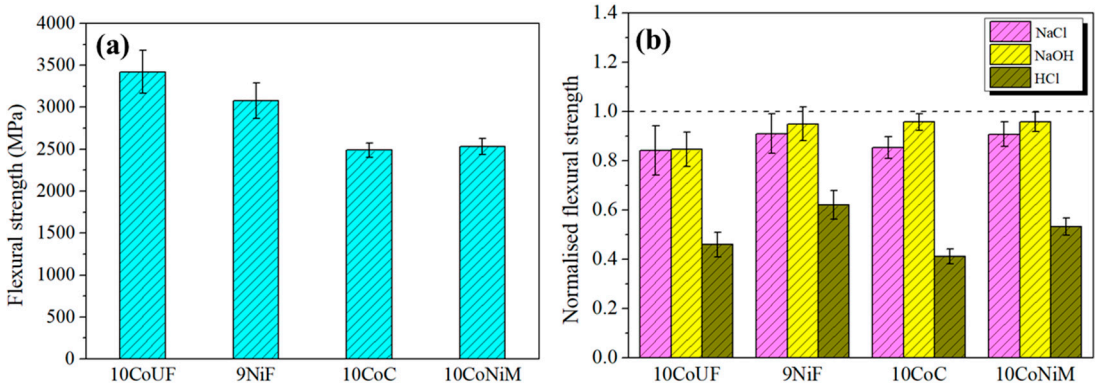

Figure 3. (**a**) Flexural strength of uncorroded specimens, and (**b**) normalized retained strength for the studied materials in different corrosive media where strength of uncorroded specimens is used as reference baseline.

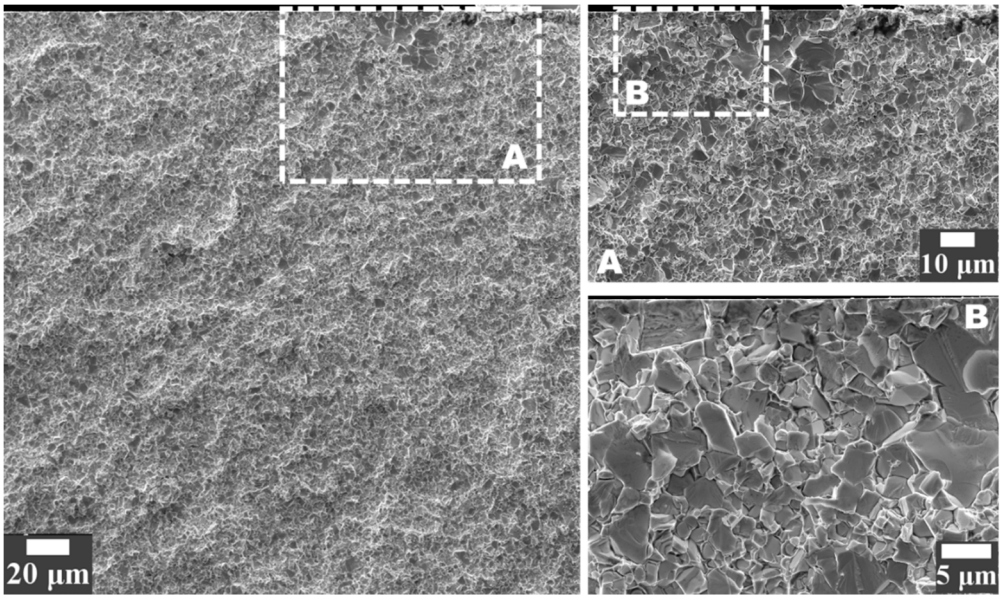

Figure 4. Example of a critical flaw (corrosion pits and binderless carbide agglomerate) that originates fracture in 10CoNiM grade corroded for 240 h.

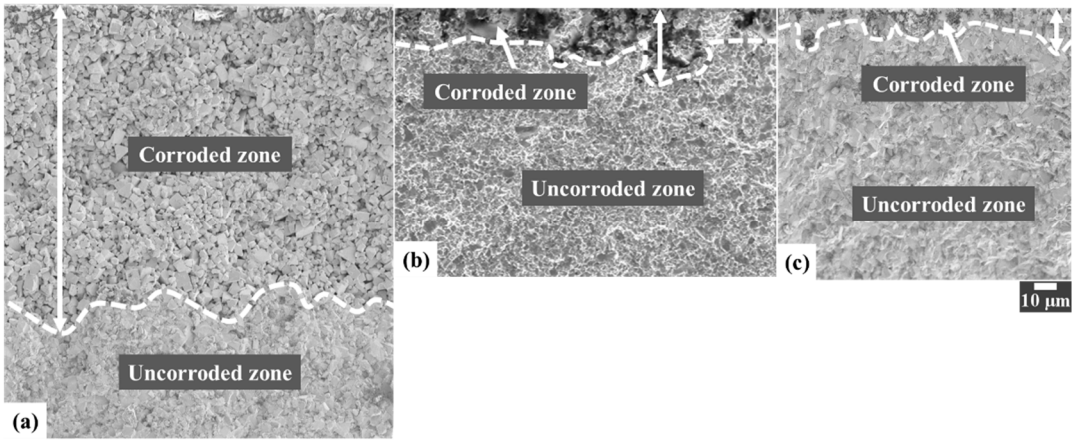

Figure 5. Critical corrosion damage promoting failure in different corrosive solutions for 240 h for studied cemented carbides: (**a**) 10CoC in HCl, (**b**) 10CoC in NaCl, (**c**) 10CoC in NaOH.

3.3. FIB/FESEM Characterization of Corrosion-Induced Damage

A detailed inspection of transversal cut micrographs was conducted for all grades in the studied media. As demonstrated in previous studies by the authors [19,20], the dissolution of metallic binder in neutral solutions takes place in the core of binder pools rather than at the binder/carbide interface. According to Figure 6, such damage emergence and evolution may be directly extrapolated to acidic solutions. Here, the dissolution of metallic binders started from the center towards the carbide/binder interface, independent of binder chemical nature (Co, Ni or CoNi) or grain size (coarse, fine or ultrafine). Within this context, such observations yield further support to the hypothesis that binder dissolution process is related to tensile thermal residual stress (TRS) state. On the other hand, they would discard the hypothesis of Cr-enrichment effects at binder/WC interfaces [26–29]. TRS state emerges during cooling from sintering temperature, due to the large difference on the coefficients of thermal expansion between the carbide and binder phases. Indeed, Co has a coefficient of thermal expansion of about twice that of WC, and consequently the binder phase is in tension while the WC particles are in compression [30,31]. Therefore, the maximum tensile TRS are located in the center of the binder pools, and consequently, stress corrosion effects are to be expected in these areas.

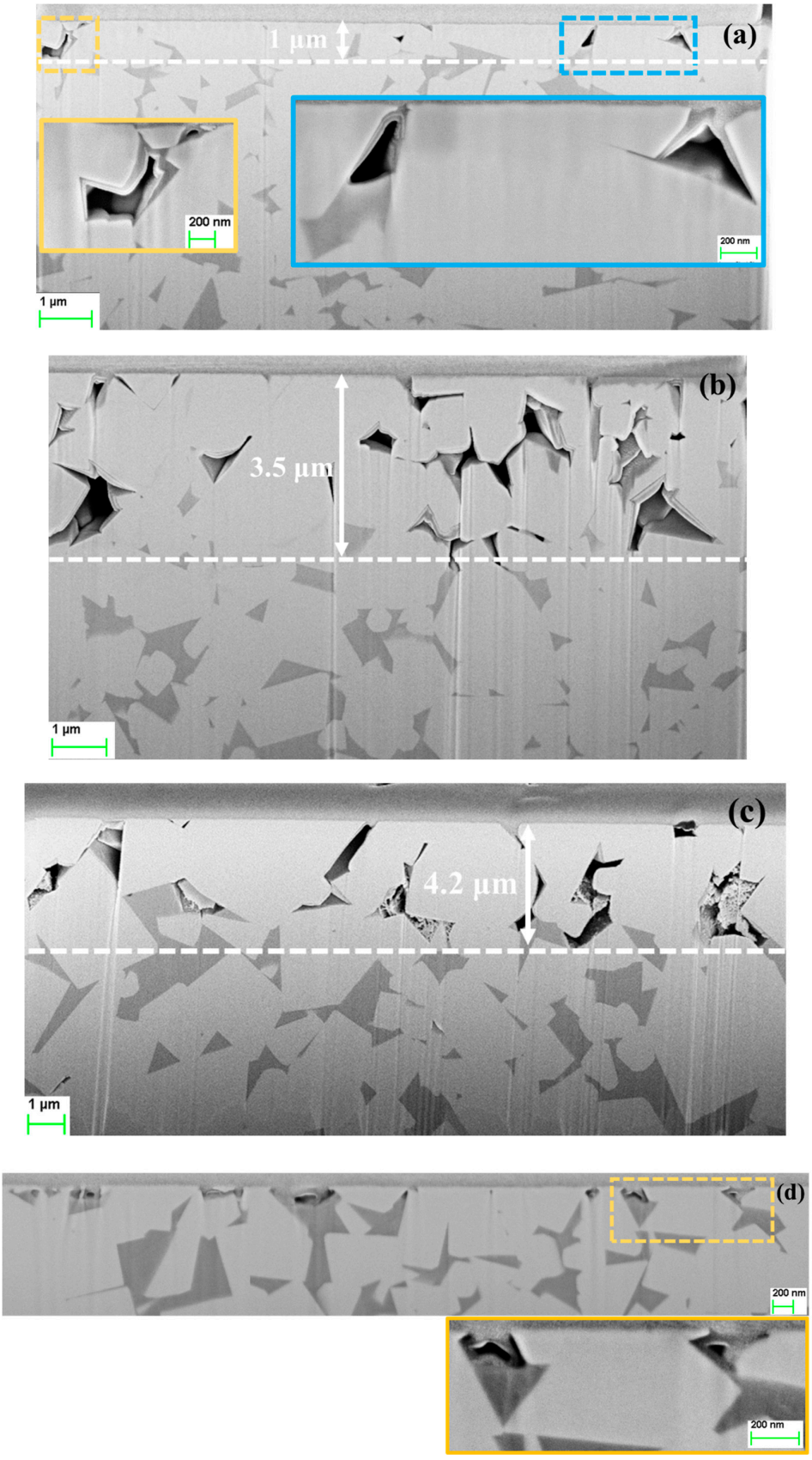

Figure 6. Micrographs showing corrosion damage-microstructure interactions on cross-section for the studied corroded grades in 0.1M HCl solution: (**a**) 9NiF (6 h), (**b**) 10CoNiM (6 h), (**c**) 10CoC (6 h) and (**d**) 10CoUF (5 min).

It is well known that in alkaline solutions WC–Co cemented carbides show a different behavior compared to acidic or neutral solutions. In the former case, corrosion properties are controlled by the corrosion resistance of the WC grains [15,21,32,33]. In this work, exhaustive observations have been carried out in WC grains at increasing immersion time in 0.1 M NaOH. At low time exposures, the degradation of the WC grains has been discerned to start at the binder/WC interface which leaded to the formation of microcracks and their growth inside WC grains at increasing dwell time, Figure 7.

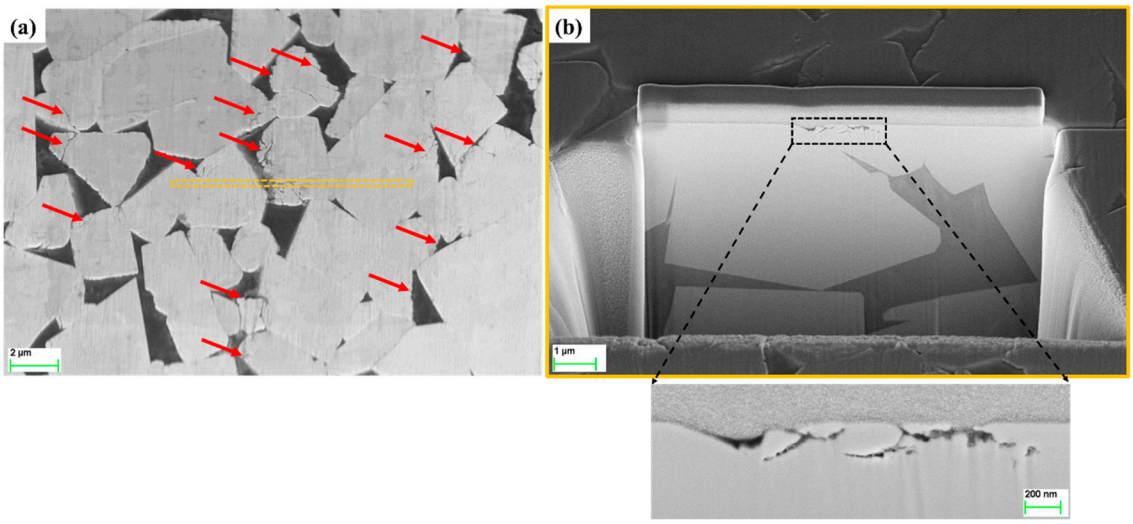

Figure 7. Micrographs showing corrosion damage-microstructure interactions for 10CoC grade corroded in 0.1M NaOH during 240 h.

4. Conclusions

In this study, corrosion behavior was studied together with the effect of the corrosion-induced damage on residual strength of cemented carbides with different binders and carbide grain size by immersing them in acidic, neutral and alkaline solutions. The following conclusions may be drawn:

(1) Electrochemical and immersion tests revealed that nickel binder displays more noble corrosion potential and critical current density compared to cobalt grades in acidic and neutral solutions containing chlorides. In these conditions, the presence of small amounts of chromium improves more the corrosion resistance of the materials than mixing nickel and cobalt as a binder. No significant differences among studied grades were observed in alkaline solution.

(2) Corrosion damage resulted in strength degradation on the basis of stress rising effects associated with the formation of surface corrosion pits in acidic solution for all studied grades. In neutral and alkaline solutions, corrosion effects on residual strength are less pronounced. Under these conditions, the grade more affected by exposure to corrosion medium is the ultrafine one.

(3) In acidic solution, the binder was preferentially attacked. The binder dissolution started from the center of binder pools, independent of binder chemical nature, and spreads to the edges until binder phase was completely consumed. In alkaline solution, corrosion process was initially located at the binder/WC interface. As exposure time increased, degradation evolved into microcracks which propagated inside the WC phase, yielding finally a fragmented-like scenario.

Author Contributions: Y.Z., G.F., E.A., O.L. and L.L. conceived and designed the experiments; Y.Z. performed the experiments; Y.Z. analyzed the data; O.L., E.A. and L.L. contributed reagents/materials/analysis tools; Y.Z., G.F. and L.L. wrote the paper.

Funding: This work was financially supported by the collaborative Industry-University program between Hyperion Materials & Technologies and Universitat Politècnica de Catalunya, and partly funded by the Spanish Ministerio de Economía y Competividad through Grant MAT2015-70780-C4-3-P (MINECO/FEDER).

Acknowledgments: Yafeng Zheng acknowledges the Ph.D. scholarship received from China Scholarship Council.

Conflicts of Interest: The authors declare no conflict of interest.

References

1. Exner, H.E. Physical and chemical nature of cemented carbides. *Int. Met. Rev.* **1979**, *24*, 149–173. [CrossRef]
2. Roebuck, B.; Almond, E.A. Deformation and fracture processes and the physical metallurgy of WC-Co hardmetals. *Int. Mater. Rev.* **1988**, *33*, 90–110. [CrossRef]
3. Upadhyaya, G.S. Materials science of cemented carbides-an overview. *Mater. Des.* **2001**, *22*, 483–489. [CrossRef]
4. Roa, J.J.; Jiménez-Piqué, E.; Verge, C.; Tarragó, J.M.; Mateo, A.; Fair, J.; Llanes, L. Intrinsic hardness of constitutive phases in WC-Co composites: Nanoindentation testing, statistical analysis, WC crystal orientation effects and flow stress for the constrained metallic binder. *J. Eur. Ceram. Soc.* **2015**, *35*, 3419–3425. [CrossRef]
5. Jiménez-Piqué, E.; Turon-Vinas, M.; Chen, H.; Trifonov, T.; Fair, J.; Tarrés, E.; Llanes, L. Focused ion beam tomography of WC-Co cemented carbides. *Int. J. Refract. Met. Hard Mater.* **2017**, *67*, 9–17. [CrossRef]
6. Human, A.M.; Exner, H.E. The relationship between electrochemical behaviour and in-service corrosion of WC based cemented carbides. *Int. J. Refract. Met. Hard Mater.* **1997**, *15*, 65–71. [CrossRef]
7. Bozzini, B.; De Gaudenzi, G.P.; Serra, M.; Fanigliulo, A.; Bogani, F. Corrosion behaviour of WC-Co based hardmetal in neutral chloride and acid sulphate media. *Mater. Corros.* **2002**, *53*, 328–334. [CrossRef]
8. Lu, R.; Minarro, L.; Su, Y.Y.; Shemenski, R.M. Failure mechanism of cemented tungsten carbide dies in wet drawing process of steel cord filament. *Int. J. Refract. Met. Hard Mater.* **2008**, *26*, 589–600. [CrossRef]
9. Bozzini, B.; Busson, B.; De Gaudenzi, G.P.; Humbert, C.; Tadjeddine, A. Corrosion of cemented carbide grades in petrochemical slurries. Part I—Electrochemical adsorption of CN^-, SCN^- and MBT: A study based on in situ SFG. *Int. J. Refract. Met. Hard Mater.* **2016**, *60*, 37–51. [CrossRef]
10. Konadu, D.S.; Van Der Merwe, J.; Potgieter, J.H.; Potgieter-Vermaak, S.; Machio, C.N. The corrosion behaviour of WC-VC-Co hardmetals in acidic media. *Corros. Sci.* **2001**, *52*, 3118–3125. [CrossRef]
11. Kellner, F.J.J.; Hildebrand, H.; Virtanen, S. Effect of WC grain size on the corrosion behaviour of WC-Co based hardmetals in alkaline solutions. *Int. J. Refract. Met. Hard Mater.* **2009**, *27*, 806–812. [CrossRef]
12. Tomlinson, W.J.; Ayerst, N.J. Anodic polarization and corrosion of WC-Co hardmetals containing small amounts of Cr_3C_2 and/or VC. *J. Mater. Sci.* **1989**, *24*, 2348–2354. [CrossRef]
13. Engqvist, H.; Beste, U.; Axén, N. The influence of pH on sliding wear of WC-based materials. *Int. J. Refract. Met. Hard Mater.* **2000**, *18*, 103–109. [CrossRef]
14. Gant, A.J.; Gee, M.G.; May, A.T. The evaluation of tribo-corrosion synergy for WC-Co hardmetals in low stress abrasion. *Wear* **2004**, *256*, 500–516. [CrossRef]
15. Thakare, M.R.; Wharton, J.A.; Wood, R.J.K.; Menger, C. Exposure effects of alkaline drilling fluid on the microscale abrasion-corrosion of WC-based hardmetals. *Wear* **2007**, *263*, 125–136. [CrossRef]
16. Tomlinson, W.J.; Molyneux, I.D. Corrosion, erosion-corrosion, and the flexural strength of WC-Co hardmetals. *J. Mater. Sci.* **1991**, *26*, 1605–1608. [CrossRef]
17. Pugsley, V.A.; Korn, G.; Luyckx, S.; Sockel, H.G.; Heinrich, W.; Wolf, M.; Feld, H.; Schulte, R. The influence of a corrosive wood-cutting environment on the mechanical properties of hardmetal tools. *Int. J. Refract. Met. Hard Mater.* **2001**, *19*, 311–318. [CrossRef]
18. Pugsley, V.A.; Sockel, H.G. Corrosion fatigue of cemented carbide cutting tool materials. *Mater. Sci. Eng. A.* **2004**, *366*, 87–95. [CrossRef]
19. Tarragó, J.M.; Fargas, G.; Jimenez-Piqué, E.; Felip, A.; Isern, L.; Coureaux, D.; Roa, J.J.; Al-Dawery, I.; Fair, J.; Llanes, L. Corrosion damage in WC-Co cemented carbides: Residual strength assessment and 3D FIB-FESEM tomography characterization. *Powder Metall.* **2014**, *57*, 324–330. [CrossRef]
20. Tarragó, J.M.; Fargas, G.; Isern, L.; Dorvlo, S.; Llanes, L. Microstructural influence on tolerance to corrosion-induced damage in hardmetals. *Mater. Des.* **2016**, *111*, 36–43. [CrossRef]
21. Tang, W.; Zhang, L.; Chen, Y.; Zhang, H.; Zhou, L. Corrosion and strength degradation behaviors of binderless WC material and WC-Co hardmetal in alkaline solution: A comparative investigation. *Int. J. Refract. Met. Hard Mater.* **2017**, *68*, 1–8. [CrossRef]

22. Tarragó, J.M.; Coureaux, D.; Torres, Y.; Yu, F.; Al-Dawery, I.; Llanes, L. Implementation of an effective time saving two-stage methodology for microstructural characterization of cemented carbides. *Int. J. Refract. Met. Hard Mater.* **2016**, *55*, 80–86. [CrossRef]
23. Tarragó, J.M.; Dorvlo, S.; Esteve, J.; Llanes, L. Influence of the microstructure on the thermal shock behavior of cemented carbides. *Ceram. Int.* **2016**, *42*, 12701–12708.
24. Tarragó, J.M.; Roa, J.J.; Valle, V.; Marshall, J.M.; Llanes, L. Fracture and fatigue behavior of WC-Co and WC-CoNi cemented carbides. *Int. J. Refract. Met. Hard Mater.* **2015**, *49*, 184–191. [CrossRef]
25. ASTM C1161-13. *Standard Test Method for Flexural Strength of Advanced Ceramics at Ambient Temperature*; ASTM International: West Conshohocken, PA, USA, 2013.
26. Sutthiruangwong, S.; Mori, G.; Kösters, R. Passivity and pseudopassivity of cemented carbides. *Int. J. Refrac. Met. Hard Mater.* **2005**, *23*, 129–136. [CrossRef]
27. Sutthiruangwong, S.; Mori, G. Corrosion properties of Co-based cemented carbides in acidic solutions. *Int. J. Refrac. Met. Hard Mater.* **2003**, *21*, 135–145. [CrossRef]
28. Schnyder, B.; Stössel-Sittig, C.; Kötz, R.; Hochstrasser-Kurz, S.; Virtanen, S.; Jaeggi, C. Investigation of the electrochemical behaviour of WC-Co hardmetal with electrochemical and surface analytical methods. *Surf. Sci.* **2004**, *566*, 1240–1245. [CrossRef]
29. Henjered, A.; Hellsing, M.; Andrén, H.O.; Nordén, H. Quantitative microanalysis of carbide/carbide interfaces in WC-Co-base cemented carbides. *Mater. Sci. Technol.* **1986**, *8*, 847–855. [CrossRef]
30. Krawitz, A.D.; Drake, E.F.; Clausen, B. The role of residual stress in the tension and compression response of WC-Ni. *Mater. Sci. Eng. A.* **2010**, *527*, 3595–3601. [CrossRef]
31. Krawitz, A.; Drake, E. Residual stresses in cemented carbides—An overview. *Int. J. Refract. Met. Hard Mater.* **2015**, *49*, 27–35. [CrossRef]
32. Hochstrasser-Kurz, S.; Reiss, D.; Suter, T.; Latkoczy, C.; Günther, D.; Virtanen, S.; Schmutz, P. ICP-MS, SKPFM, XPS, and microcapillary investigation of the local corrosion mechanisms of WC-Co hardmetal. *J. Electrochem. Soc.* **2008**, *155*, C415–C426. [CrossRef]
33. Lin, N.; He, Y.; Wu, C.; Liu, S.; Xiao, X.; Jiang, Y. Influence of TiC additions on the corrosion behavior of WC-Co hardmetals in alkaline solution. *Int. J. Refract. Met. Hard Mater.* **2014**, *46*, 52–57. [CrossRef]

7.2 Article II

Assessment of corrosion-induced changes on the mechanical integrity of cemented carbides at small length scales

Yafeng Zheng, Gemma Fargas, Hossein Besharatloo, Marc Serra, Joan Josep Roa, Elaine Armelin, Olivier Lavigne, Luis Llanes.

In this work, the effect of corrosion-induced damage on the mechanical response of hardmetals was evaluated at small length-scale by means of nanoindentation and nanoscratch techniques. Damage was introduced in a controlled way through immersion of samples in acidic solution. It was found that surface degradation associated with corrosion leads to strong reduction of elastic modulus and hardness, as compared to non-corroded samples. Similarly, significant differences were observed in nanoscratch response, regarding not only the width and depth of tracks but also the deformation mechanisms developed as contact load is progressively increased. Damage emergence and evolution were evidenced in corroded surfaces at scratching loads significantly lower than for non-corroded specimens. Changes in nanoindentation and nanoscratch response and damage scenario are discussed on the basis of the effective microstructural assemblage remnant after corrosion action. In this regard, dissolution of metallic phase becomes critical as it yields a mechanically unsupported, contiguous and binderless/porous, carbide network. Consequently, cracking, fragmentation and easy removal of WC grains under contact loading is evidenced; and thus, mechanical integrity is effectively lessened.

Article II

Assessment of corrosion-induced changes on the mechanical integrity of cemented carbides at small length scales

Y.F. Zheng

G. Fargas

H. Besharatloo

M. Serra

J. J. Roa

E. Armelin

O. Lavigne

L. Llanes

Int. J. Refract. Met. Hard Mater. 84 (2019) 105033

International Journal of Refractory Metals & Hard Materials 84 (2019) 105033

Contents lists available at ScienceDirect

International Journal of Refractory Metals & Hard Materials

journal homepage: www.elsevier.com/locate/IJRMHM

Assessment of corrosion-induced changes on the mechanical integrity of cemented carbides at small length scales

Y.F. Zheng[a,b,*], G. Fargas[a,b], H. Besharatloo[a,b], M. Serra[a], J.J. Roa[a,b], E. Armelin[b,c], O. Lavigne[d], L. Llanes[a,b]

[a] CIEFMA, Departament de Ciència dels Materials i Enginyeria Metal·lúrgica, EEBE, Universitat Politècnica de Catalunya, Barcelona 08019, Spain
[b] Barcelona Research Center in Multiscale Science and Engineering, Universitat Politècnica de Catalunya, Barcelona 08019, Spain
[c] IMEM, Departament d'Enginyeria Química, EEBE, Universitat Politècnica de Catalunya, Barcelona 08019, Spain
[d] Hyperion Materials & Technologies, 08107 Martorelles, Spain

ARTICLE INFO

Keywords:
Cemented carbide
Corrosion
Nanoindentation
Nanoscratch
Small-scale mechanical integrity

ABSTRACT

In this work, the effect of corrosion-induced damage on the mechanical response of hardmetals was evaluated at small length-scale by means of nanoindentation and nanoscratch techniques. Damage was introduced in a controlled way through immersion of samples in acidic solution. It was found that surface degradation associated with corrosion leads to strong reduction of elastic modulus and hardness, as compared to non-corroded samples. Similarly, significant differences were observed in nanoscratch response, regarding not only the width and depth of tracks but also the deformation mechanisms developed as contact load is progressively increased. Damage emergence and evolution were evidenced in corroded surfaces at scratching loads significantly lower than for non-corroded specimens. Changes in nanoindentation and nanoscratch response and damage scenario are discussed on the basis of the effective microstructural assemblage remnant after corrosion action. In this regard, dissolution of metallic phase becomes critical as it yields as a result a mechanically unsupported, contiguous and binderless/porous, carbide network. Consequently, cracking, fragmentation and easy removal of WC grains under contact loading is evidenced; and thus, mechanical integrity is effectively lessened.

1. Introduction

WC-Co cemented carbides, usually referred to as hardmetals, are found at the forefront of a wide range of engineering products that operate under harsh working conditions. Indeed, cemented carbides are the preferential choice in almost all the applications where the best solution against combined wear, impact and corrosion is sought [1]. The main reason behind it is the exceptional combination of intrinsic mechanical parameters (i.e. hardness and toughness), wear resistance and damage tolerance exhibited by them, as a result of the extremely different properties of their two interpenetrating constitutive phases: hard, brittle carbides and a soft, ductile metallic binder [2–4]. However, despite their outstanding properties, WC-Co alloys suffer from different degradation phenomena that seriously affect the performance and service-life of engineering structural parts. In this regard, many hardmetal applications involve exposure to chemically aggressive media, including a wide variety of corrosive environments such as lubricants, chemical and petrochemical products, and mine and sea waters, among others (e.g. Refs [5–9]).

Resistance to corrosion is not to be considered as a well-defined intrinsic material parameter; as it represents an observed qualitative performance which depends on various internal and external factors. From this perspective, the corrosion behavior of hardmetals has been extensively investigated in recent decades using different testing methodologies and addressing influence of multiple factors, such as surface state, corrosive medium, microstructural assemblage and binder chemical nature [5–22]. In these studies, it has been shown that: (1) corrosive media preferentially attack the binder phase when exposed to acidic and neutral environments; (2) in alkaline solution, the Co binder exhibits a stable passivation, while the WC phase dissolves easily; (3) damage by corrosion induced by acidic media is usually much more pronounced than that of neutral and basic ones; and (4) a greater amount of dissolution of the binder phase in acid solution eventually results in the formation of the oxide layer of W and a region depleted in Co, compared to the exposure in neutral and basic solutions.

Optimal performance of engineering components is based on

* Corresponding author at: CIEFMA, Departament de Ciència dels Materials i Enginyeria Metal·lúrgica, EEBE, Universitat Politècnica de Catalunya, Barcelona 08019, Spain.
E-mail address: yafeng.zheng@upc.edu (Y.F. Zheng).

https://doi.org/10.1016/j.ijrmhm.2019.105033
Received 2 July 2019; Received in revised form 17 July 2019; Accepted 24 July 2019
Available online 25 July 2019
0263-4368/

Table 1
Microstructural parameters for the investigated cemented carbide.

wt% Co	d_{WC} (μm)	C_{WC}	λ_{binder} (μm)
6	1.51 ± 0.16	0.48 ± 0.02	0.32 ± 0.03

laboratory experiments attempting to simulate service-like conditions. Within this context, several studies have shown detrimental changes in the tribological response and effective wear resistance of cemented carbides as a result of the interaction among corrosion and other degradation phenomena such as erosion and abrasion [23–26]. Furthermore, relevant corrosion effects on residual strength, under imposed mechanical loads, have also been reported for hardmetals [27–32]. However, most of the above literature reports mainly address microstructure-medium-performance correlations from a macroscopic perspective, without in-depth analysis of damage micromechanisms involved. Interesting exceptions are the relatively recent works by Gee and coworkers [33–37] where degradation micromechanisms have been studied by implementing model abrasion tests, complemented with the use of advanced microscopic inspection techniques. This study attempts to follow an alike approach by evaluating corrosion effects on small-scale mechanical response of hardmetals. In this regard, nanoindentation and nanoscratch techniques have been successfully implemented for determining mechanical and tribological properties of cemented carbides at micro- and nanometric length scales, as given by: (1) measurement of intrinsic hardness and elastic modulus of individual constituent phases [38–40]; (2) evaluation of microstructural effects on sliding contact, scratch and wear resistance [41–43]; and (3) documentation and analysis of deformation, wear and material removal mechanisms [39,40,42,43]. Unfortunately, all the referred works have been conducted on pristine or virgin hardmetals; hence, information on how the limit state – in terms of failure or acceptable/unacceptable criteria from a structural integrity viewpoint – is affected by the damage induced by corrosion is completely missing for cemented carbides. Within the above framework, it is the aim of this investigation to assess and analyze surface/subsurface and mechanical integrity changes induced by exposure to an acidic media of a hardmetal grade, by means of nanoindentation and nanoscratch testing complemented with combined use of Field Emission Scanning Electron Microscopy (FESEM) and Focused Ion Beam (FIB).

2. Experimental aspects

A plain WC-Co hardmetal grade was chosen for this study. It was supplied by Hyperion Materials and Technologies and is here referred to as 6CoM. Key microstructural parameters of the material investigated, including binder content ($\%_{wt.}$), mean grain size (d_{WC}), contiguity (C_{WC}) and binder mean free path (λ_{binder}), are listed in Table 1. Mean grain size was measured by the linear intercept method (LIM), using FESEM micrographs. Carbide contiguity and binder mean free path were estimated following empirical relationship given in the literature [3,44].

Corrosion damage was induced in a controlled way by immersing the hardmetal specimens in stirred 0.1 M HCl solution at room temperature. A long exposure time (264 h) was selected, in order to obtain significant changes at both surface and subsurface levels. Before and after immersion tests, samples were hand-cleaned using soapy water, then ultrasonically cleaned for 15 min in ethanol, and finally dried in air. Corrosion effects were evaluated in terms of (1) existing phases, before and after immersion tests, by means of X-Ray diffraction (XRD) using Cu Kα (40 kV and 30 mA) radiation; and (2) microstructural changes discerned by cross-sectional inspection using optical microscopy (OM), laser scanning confocal microscopy (LSCM) and FESEM. The latter also allowed assessment of surface and subsurface integrity of corroded specimens.

Corrosion-induced changes on the mechanical properties were evaluated at small-length scale. Nanoindentation and nanoscratch tests were performed on both non-corroded (virgin and polished) and corroded surfaces using a Berkovich diamond indenter. Indentations were performed at a constant strain rate of $0.05\,s^{-1}$, up to the maximum displacement into surface or until reaching the maximum applied load of 650 mN. In these tests, hardness (H) and Young's modulus (E) were evaluated as a function of the penetration depth with a nanoindenter unit, according to Oliver and Pharr's model [45]. A homogeneous array of twenty-five indentations (5 by 5) were made on each sample and the results were averaged. Meanwhile, scratch tests were carried out under constant sliding contact rate (1 μm/s) while the indenter applied increasing loads as it moved along the scratch length. Tests were run until maximum load values of either 60 mN or 500 mN, along scratch lengths of 60 or 200 μm respectively.

Deformation and damage scenarios induced by residual imprints (nanoindentations) and tracks (nanoscratchs) were evaluated by inspecting contact surface and corresponding subsurface regions through a dual beam FESEM/FIB unit. Regarding cross-section examination, prior to milling, a thin protective layer of platinum was deposited on the region of interest to reduce waterfall effects, which affect the quality of the images. Current and acceleration voltage of Ga^+ source was subsequently reduced down to a final polishing stage at 500 pA at 30 kV respectively.

3. Results and discussion

3.1. Microstructural changes induced by corrosion

Fig. 1 shows cross-sectional images obtained from OM and FESEM/FIB for the corroded specimen. They reveal a homogeneously degraded layer of about 450 μm in-depth (Fig. 1a). As evidenced in Fig. 1b, it is mainly the result of a preferential attack of cobalt binder which leads to a network of unsupported carbides throughout the affected layer. Such a finding is consistent with literature reports on the corrosion of WC-based hardmetals exposed to acidic media [15,17]. It is also in complete

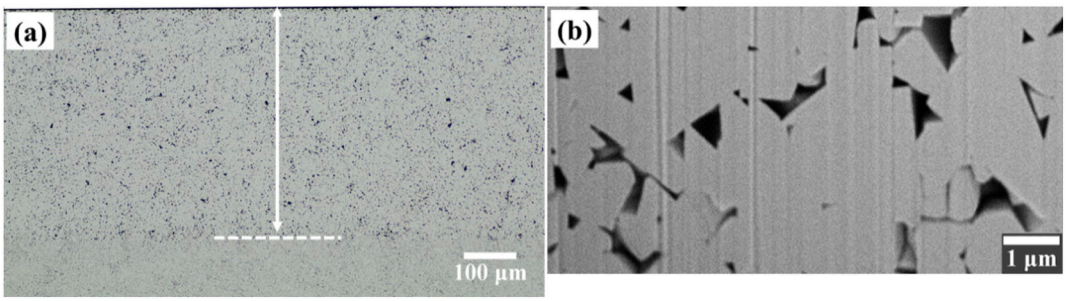

Fig. 1. Cross-section images illustrating **(a)** microscopic aspect and **(b)** microstructural changes of degraded layer, resulting after immersion in 0.1 M HCl solution for 264 h of the hardmetal grade studied.

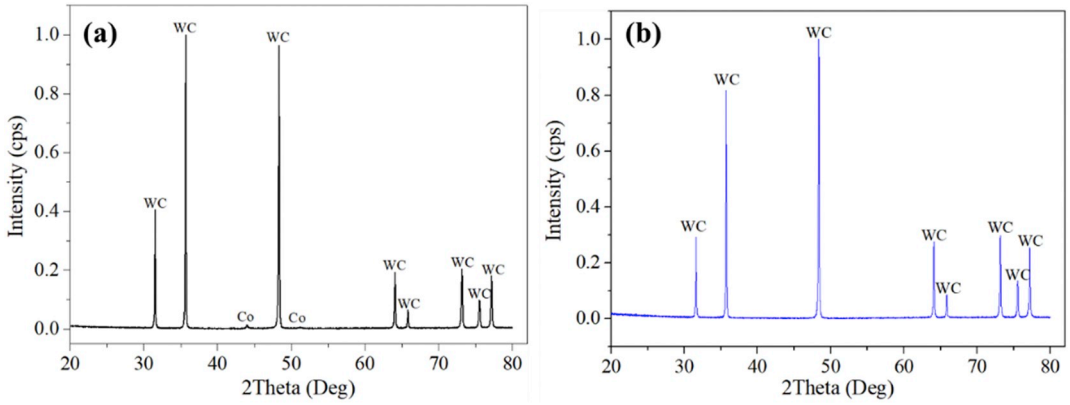

Fig. 2. XRD patterns determined for the alloy studied: **(a)** before, and **(b)** after immersion test.

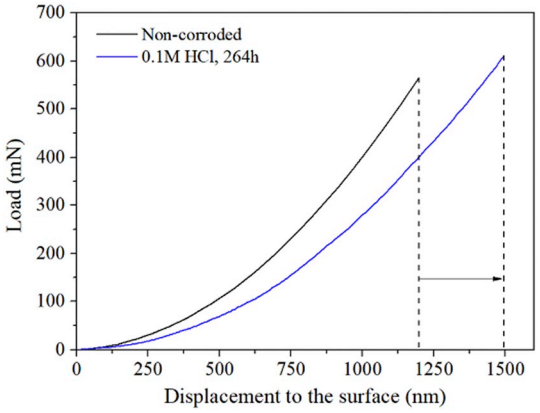

Fig. 3. Representative indentation *P-h* curves from Berkovich indentation for both surface conditions studied.

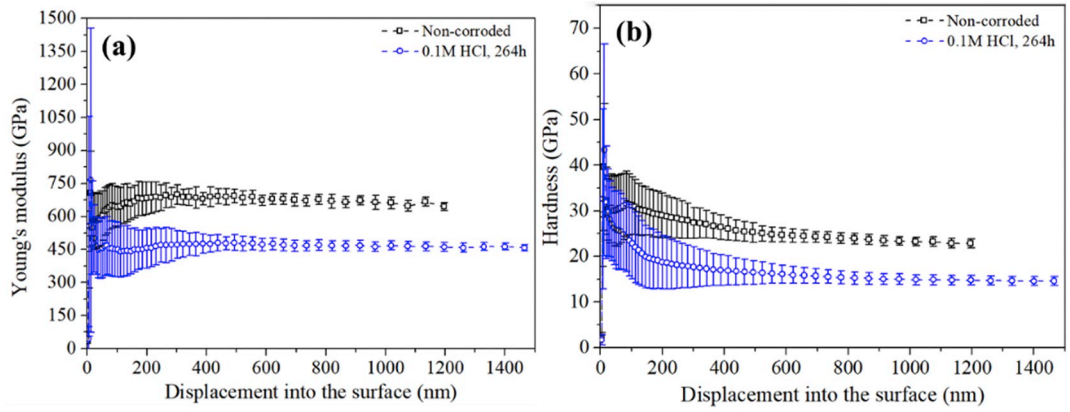

Fig. 4. (a) Young's modulus and **(b)** hardness values as a function of penetration depth for non-corroded (black) and corroded (blue) samples. (For interpretation of the references to colour in this figure legend, the reader is referred to the web version of this article.)

agreement with differences determined, before and after corrosion, in XRD patterns of the material studied. As it is discerned in Fig. 2, cobalt peaks observed in the pristine specimens are absent after corrosion.

3.2. Nanoindentation tests: mechanical response and deformation/damage micromechanisms

Typical load-displacement (*P-h*) curves recorded from Berkovich indentation tests are given in Fig. 3. It is clearly discerned that corrosion-induced damage has a significant effect on P-h behavior for the studied grade. It translates in an obvious increase (about 300 nm) of maximum penetration depth. Fig. 4 shows elastic modulus and hardness values as a function of penetration depth for both non-corroded and corroded surface conditions. Values are stabilised for penetration depths larger than 500 nm. At lower depths, measured values display considerable scatter due to scale effects (e.g. surface defects and roughness). Mechanical properties of the studied grade are pronouncedly degraded due to the corrosion-induced damage. Young's modulus of 679 GPa and hardness of 24 GPa obtained for the virgin condition are in satisfactory agreement with those measured for similar grade at such small length scale. It then validates the much lower values determined for the corroded condition, 464 GPa and 15 GPa respectively, as a

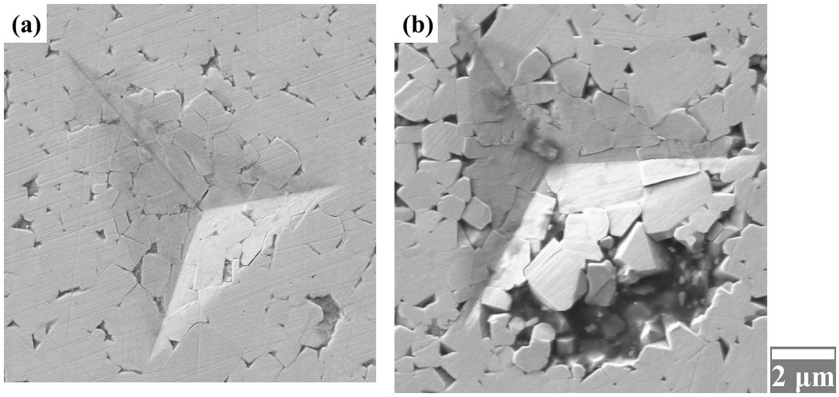

Fig. 5. Residual imprints obtained as a result of nanoindenting (up to maximum displacement into surface of 2000 nm) **(a)** non-corroded and **(b)** corroded surfaces.

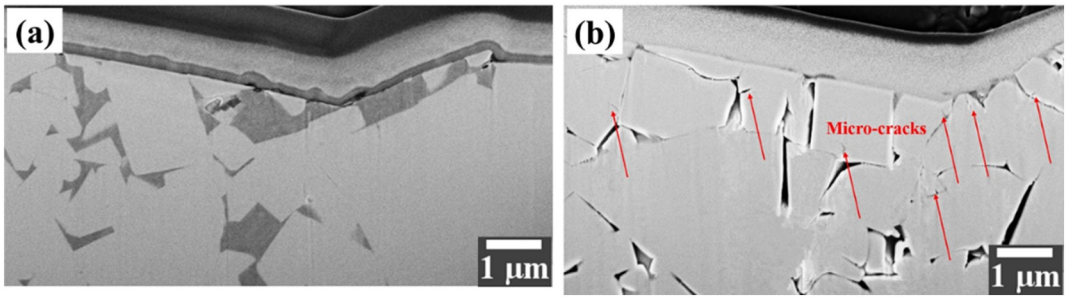

Fig. 6. FIB cross-section of a Berkovich indented surface: **(a)** non-corroded and **(b)** corroded 6CoM.

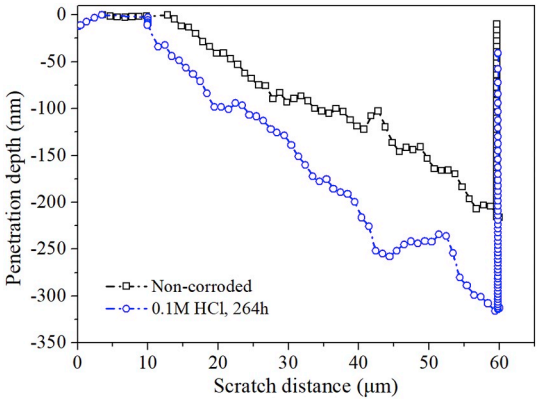

Fig. 7. Typical penetration depth - scratch distance (under increasing applied load condition) curves obtained for uncorroded and corroded specimens.

genuine effect of the corrosion-induced changes.

Deformation and damage scenario is also observed to change dramatically when comparing virgin and corroded specimens, as shown in Fig. 5. For the non-corroded condition, as expected, both hard and soft phases exhibit effective deformation compatibility between them, with very few fracture features (cracks) localized in WC grains (Fig. 5a). When subjected to mechanical loads, relatively high fracture toughness is beneficial for supressing and/or tolerating damage in structural materials. In cemented carbides, the metallic Co-base binder is able to deform by either mechanical twinning, dislocation slip and/or phase transformation [46–48]. Hence, most of the deformation imposed is absorbed for the metallic phase, avoiding then cracking of carbides. For the corroded specimen, the dissolution of the metallic binder reduces significantly load-bearing capability of the remnant microstructure, i.e. a mechanically unsupported carbide skeleton. This translates in easy removal of loose grains, as shown in Fig. 5b.

Above ideas are further supported by FIB/FESEM cross-sectional inspection of residual imprints. As it is shown in Fig. 6, the surface and mechanical integrity are significantly affected by corrosion. Different from the non-corroded specimen, where effective load-sharing between metal and ceramic phases is evidenced, the absence of the former in the corroded sample yields a completely distinct scenario. Here, the brittle carbide phase must accommodate all the irreversible deformation imposed through direct load transfer between neighboring grains. As a result, local collapse of the unsupported (binderless and porous) carbide network and intensified multiple cracking is discerned.

3.3. Nanoscratch tests: mechanical response and deformation/damage micromechanisms

Scratch load-penetration depth curves resulting from nanoscratch testing are presented in Fig. 7. As the load increases, both samples exhibit a rising penetration depth, as expected. Scratching penetration for a given applied load is significantly deeper for the corroded condition. This is consistent with the mechanical response recorded during nanoindentation. Under given nanoscratch condition, deeper penetration inevitably results in a larger damaged area, as it will be described later.

Fig. 8 shows different post-scratch scenarios for both non-corroded and corroded conditions. In general, it is clearly discerned that failure-related events, i.e. spallation, cracking, etc., are much more pronounced in the corroded specimen. Virgin specimen exhibits a higher scratch resistance response, as concluded from the narrower and shallower tracks. This also applies to damage tolerance, as related to spallation and local chipping degree.

For non-corroded condition, a clear groove is discerned, where debris and some crushed particles are found to pile-up at the corresponding edges. This irreversible deformation and damage scenario is extremely more pronounced for the corroded condition, mainly as a result of a higher accumulation of the referred debris features. Thus, track edges are rather ill-defined, although clearly linked to wider and deeper tracks, for a given applied load level.

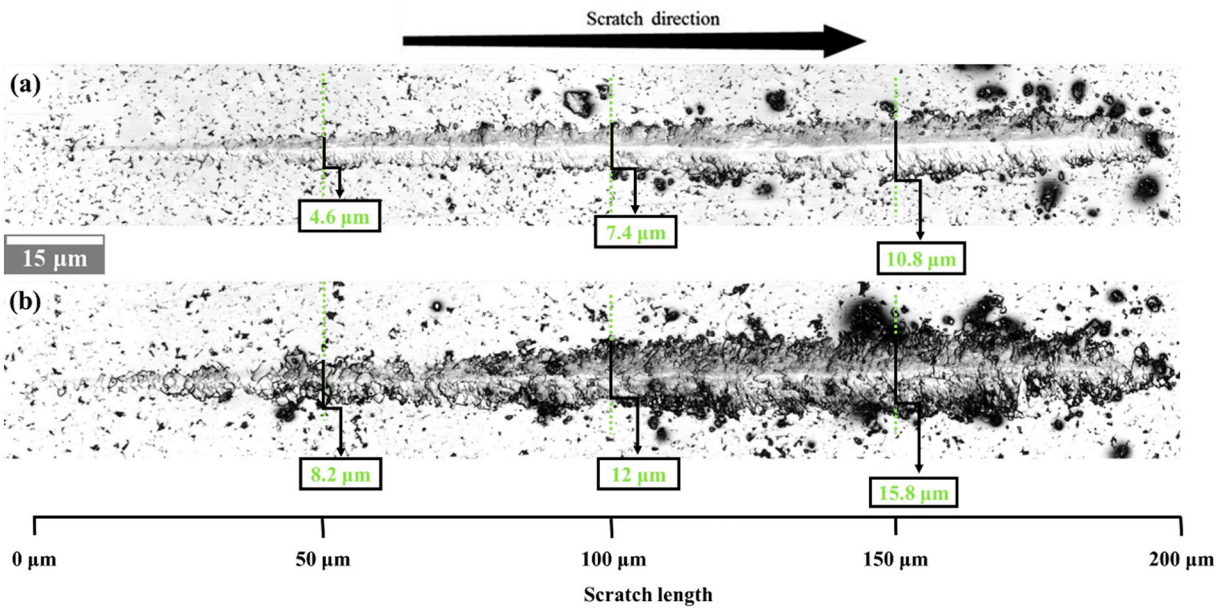

Fig. 8. LSCM micrographs of two scratch tracks performed on **(a)** non-corroded and **(b)** corroded samples.

Deformation and removal mechanisms along the scratch track were inspected in detail by means of FESEM. Fig. 9 illustrates that damage emerges earlier in the corroded specimen, as compared to the non-corroded one and in terms of applied load, i.e. ~50 mN and ~ 65 mN respectively. In the latter, changes are evidenced in terms of compatible plastic deformation between both phases as well as localized microfracture within contiguous carbide grains (Fig. 9a). In this regard, the intrinsic toughening capability of the binder delays the generation of carbide microfracture and avoids potential grain pull-out [35,42]. Similar plastic deformation mechanisms are no longer discerned in scratch tracks for corroded specimens, regarding both metallic and ceramic phases. On the one hand, this finding is obvious as it is directly related to the absence of the metallic binder. On the other hand, it is the consequence of intensified stress at carbide/carbide contacts which then promotes fracture over plasticity within the hard phase. Finally, WC grains get severely fragmented and subsequently removed (Fig. 9b).

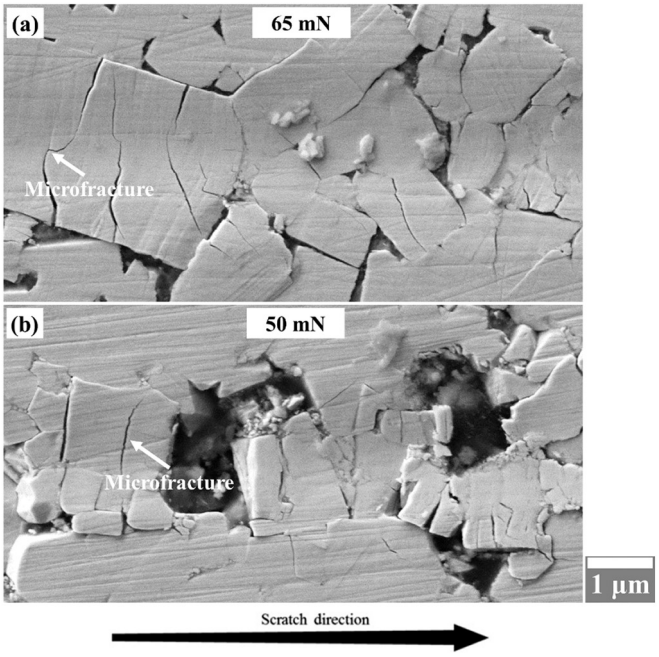

Fig. 9. FESEM images showing early damage features along the scratch track in **(a)** non-corroded and **(b)** corroded samples.

Evolution of damage scenario with increasing imposed load for both non-corroded and corroded specimens is illustrated in Fig. 10. It is seen that multiple and increasingly finer cracking of individual WC grains is also reached in the non-corroded specimen. However, different from the corroded case, WC fragments are then re-embedded into the deformed Co phase (Fig. 10a), in agreement with wear mechanisms described in the literature [33–37,41,42,49,50]. In the corroded specimens, early fragmentation of individual carbide grains directly evolves into grain chipping, delamination and dislodging (Fig. 10b). At larger length scales, as applied load increases a rougher morphology, as well as a larger lump piling up near the groove edge, is also discerned.

In order to further document and understand the correlation between corrosion-induced damage and mechanical response degradation, a detailed cross-sectional inspection of scratch tracks was carried out by means of FIB/FESEM. Fig. 11 shows images corresponding to scratch tracks, at an applied load level of 225 mN, for non-corroded and corroded surfaces. Clearly, two-phase built-up material piled-up can be seen on the edge of the scratch track for the non-corroded surface. In contrast, edge tracks for the corroded specimens are characterized for large clumps of removed (and previously fragmented) carbide grains. As it has been discussed above, after binder dissolution, mechanical integrity of the remaining WC skeleton is significantly decreased; thus, loose grains can be easily removed even by light abrasion.

For the applied load level under consideration (225 mN), thickness of deformed zone discerned for the non-corroded specimen is around 2 µm (Fig. 11a). Within such affected zone, deformation and fracture features are clearly discerned in both phases. When subjected to the compressive stresses induced by sliding contact (scratching), plastic deformation of Co binder first occurs close to interphase boundaries. As imposed stress rises, extrusion, cracking and removal of the binder phase (Figs. 11**a-1** and 11**a-2**) takes place. A further increase of stress induces WC microfracture and potential fragmentation of the individual grains. For the corroded specimens, strain energy associated with sliding contact is absorbed/released by means of two different deformation/fracture micromechanisms. On the one hand, loose WC grains near track edges are removed without further damage (e.g. cracking, chipping), as shown in Fig. 11b, due to lack of mechanical support. On the other hand, multiple cracking and fragmentation of

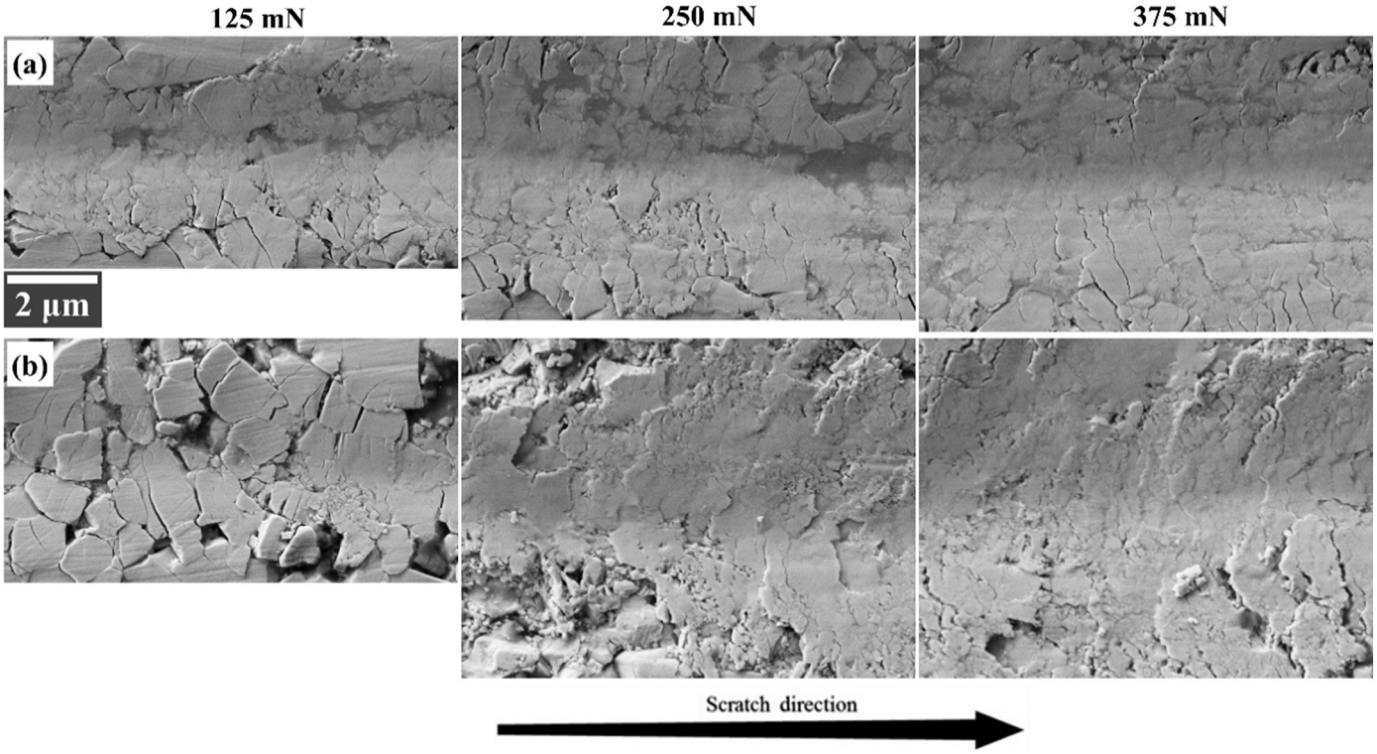

Fig. 10. Scratch track view associated with three different applied load levels: 125 mN, 250 mN and 375 mN, for **(a)** non-corroded and **(b)** corroded surfaces.

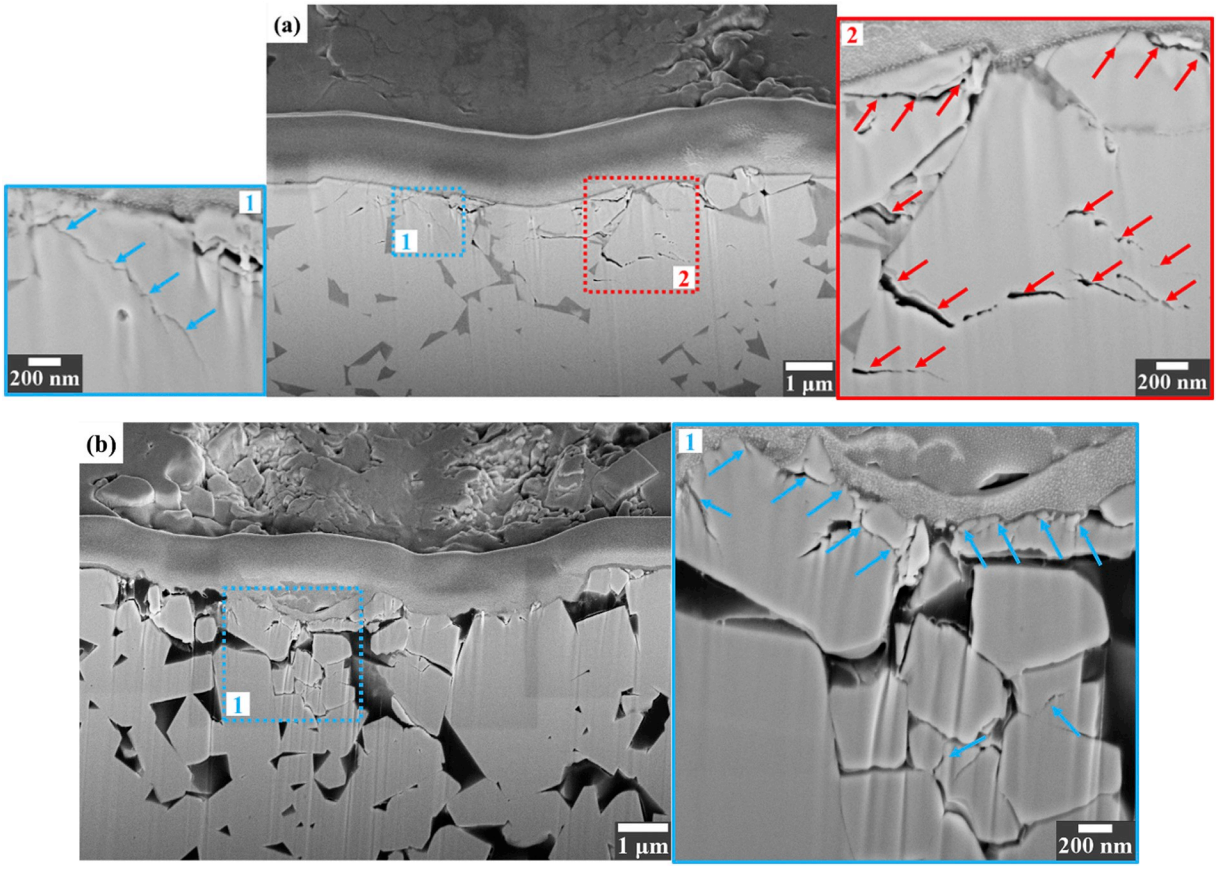

Fig. 11. FIB cross-sections of the scratch track corresponding to a load level of 225 mN in **(a)** non-corroded and **(b)** corroded surfaces.

individual carbides is extensively observed, as a direct consequence of load transfer through a contiguous and binderless (and porous) carbide network. Furthermore, some compaction of the open structure at the subsurface is also discerned by filling out of cavities with fragmented carbides as well as potential rotation and collapse of remnant carbide grains (Fig. 11b-1).

4. Conclusions

Corrosion effects on microstructural assemblage, small-scale mechanical response (under contact loading) and involved deformation/fracture micromechanisms for a plain WC-Co hardmetal grade have been investigated. From the results presented in this study, the following conclusions may be drawn:

(1) Immersion testing in an acidic solution results in a significant degradation of surface/subsurface integrity of cemented carbides. In this regard, effective changes in microstructural assemblage of the material are discerned by FESEM/FIB inspection: from an interpenetrating two-phase network for the non-corroded composite to a contiguous and binderless (i.e. with cavities in regions where binder has been dissolved) carbide skeleton in the corroded material.
(2) Corrosion in acidic media is found to be quite detrimental for the mechanical integrity of the hardmetal alloy studied. Due to the lower load-bearing capability of the referred mechanically unsupported carbide network existing in the corroded cemented carbide, their elastic modulus, hardness and sliding contact (scratch) resistance are significantly degraded, as compared to those exhibited by the non-corroded hardmetal.
(3) Deformation/fracture micromechanisms are also significantly affected by corrosion. As the metallic binder is leached out during exposure to the acidic solution, its well-established toughening capability in non-corroded hardmetals is also completely lost. Consequently, deformation induced by the imposed loads must be exclusively accommodated by the binderless and porous network of carbide phase. It is done through multiple cracking and fragmentation of individual grains. Furthermore, as re-embedment of them into the metallic phase (as it occurs for the non-corroded specimens) is no longer possible, it finally yields easy pull-out and removal of the hard phase in the corroded material.

Acknowledgements

This work was financially supported by the collaborative Industry-University program between Hyperion Materials & Technologies and Universitat Politècnica de Catalunya, and partly funded by the Spanish Ministerio de Economía y Competividad through Grant MAT2015-70780-C4-3-P (MINECO/FEDER). Y. F. Zheng acknowledges the Ph.D. scholarship received from China Scholarship Council. J. J. Roa acknowledges the Serra Húnter programme of the Generalitat de Catalunya.

References

[1] L. Prakash, Fundamentals and general applications of hardmetals, in: V.K. Sarin, D. Mari, L. Llanes (Eds.), Comprehensive Hard Materials, Elsevier, UK, 2014, pp. 29–90, , https://doi.org/10.1016/B978-0-08-096527-7.00002-7.
[2] H. Exner, Physical and chemical nature of cemented carbides, Int. Met. Rev. 24 (1979) 149–173, https://doi.org/10.1179/imtr.1979.24.1.149.
[3] B. Roebuck, E.A. Almond, Deformation and fracture processes and the physical metallurgy of WC-Co hardmetals, Int. Mater. Rev. 33 (1988) 90–110, https://doi.org/10.1179/imr.1988.33.1.90.
[4] E. Jiménez-Piqué, M. Turon-Vinas, H. Chen, T. Trifonov, J. Fair, E. Tarrés, L. Llanes, Focused ion beam tomography of WC-Co cemented carbides, Int. J. Refract. Met. Hard Mater. 67 (2017) 9–17, https://doi.org/10.1016/j.ijrmhm.2017.04.007.
[5] A.M. Human, H.E. Exner, The relationship between electrochemical behaviour and in-service corrosion of WC based cemented carbides, Int. J. Refract. Met. Hard Mater. 15 (1997) 65–71, https://doi.org/10.1016/S0263-4368(96)00014-5.
[6] B. Bozzini, G.P. De Gaudenzi, M. Serra, A. Fanigliulo, F. Bogani, Corrosion behaviour of WC-Co based hardmetal in neutral chloride and acid sulphate media, Mater. Corros. 53 (2002) 328–334, https://doi.org/10.1002/1521-4176(200205)53:5<328::AID-MACO328>3.0.CO;2-G.
[7] R. Lu, L. Minarro, Y.-Y. Su, R.M. Shemenski, Failure mechanism of cemented tungsten carbide dies in wet drawing process of steel cord filament, Int. J. Refract. Met. Hard Mater. 26 (2008) 589–600, https://doi.org/10.1016/j.ijrmhm.2008.01.009.
[8] Q. Zhang, Y. He, W. Wang, N. Lin, N. Li, Corrosion behavior of WC-Co hardmetals in the oil-in-water emulsions containing sulfate reducing Citrobacter sp, Corros. Sci. 94 (2015) 48–60, https://doi.org/10.1016/j.corsci.2015.01.036.
[9] B. Bozzini, B. Busson, G.P. De Gaudenzi, C. Humbert, C. Mele, S. Tedeschi, A. Tadjeddine, Int. J. Refract. Met. Hard Mater. 60 (2016) 37–51, https://doi.org/10.1016/j.ijrmhm.2016.06.010.
[10] W.J. Tomlinson, C.R. Linzell, Anodic polarisation and corrosion of cemented carbides with cobalt and nickel binders, J. Mater. Sci. 23 (1988) 914–918, https://doi.org/10.1007/BF01153988.
[11] S. Sutthiruangwong, G. Mori, Corrosion properties of Co-based cemented carbides in acidic solutions, Int. J. Refract. Met. Hard Mater. 21 (2003) 135–145, https://doi.org/10.1016/S0263-4368(03)00027-1.
[12] B. Schnyder, C. Stössel-Sittig, R. Kötz, S. Hochstrasser-Kurz, H. Siegenthaler, Investigation of the electrochemical behaviour of WC-Co hardmetal with electrochemical and surface analytical methods, Surf. Sci. 566-568 (2004) 1240–1245, https://doi.org/10.1016/j.susc.2004.06.102.
[13] S. Sutthiruangwong, G. Mori, R. Kösters, Passivity and pseudopassivity of cemented carbides, Int. J. Refract. Met. Hard Mater. 23 (2005) 129–136, https://doi.org/10.1016/j.ijrmhm.2004.11.006.
[14] C.F. Barbatti, F. Sket, J. Garcia, A. Pyzalla, Influence of binder metal and surface treatment on the corrosion resistance of (W,Ti)C-based hardmetals, Surf. Coat. Technol. 201 (2006) 3314–3327, https://doi.org/10.1016/j.surfcoat.2006.07.135.
[15] S. Hochstrasser, Y. Mueller, C. Latkoczy, S. Virtanen, P. Schmutz, Analytical characterization of the corrosion mechanisms of WC-Co by electrochemical methods and inductively coupled plasma mass spectroscopy, Corros. Sci. 49 (2007) 2002–2020, https://doi.org/10.1016/j.corsci.2006.08.022.
[16] F.J.J. Kellner, H. Hildebrand, S. Virtanen, Effect of WC grain size on the corrosion behavior of WC-Co based hardmetals in alkaline solutions, Int. J. Refract. Met. Hard Mater. 27 (2009) 806–812, https://doi.org/10.1016/j.ijrmhm.2009.02.004.
[17] D.S. Konadu, J. Van der Merwe, J.H. Potgieter, S. Potgieter-Vermaak, C.N. Machio, The corrosion behaviour of WC-VC-Co hardmetals in acidic media, Corros. Sci. 52 (2010) 3118–3125, https://doi.org/10.1016/j.corsci.2010.05.033.
[18] Q. Zhang, N. Lin, Y. He, Effects of Mo additions on the corrosion behavior of WC-TiC-Ni hardmetals in acidic solutions, Int. J. Refract. Met. Hard Mater. 38 (2013) 15–25, https://doi.org/10.1016/j.ijrmhm.2012.12.003.
[19] N. Lin, Y. He, C. Wu, S. Liu, Y. Jiang, Influence of TiC additions on the corrosion behaviour of WC-Co hardmetals in alkaline solution, Int. J. Refract. Met. Hard Mater. 46 (2014) 52–57, https://doi.org/10.1016/j.ijrmhm.2014.05.009.
[20] L. Zhang, Y. Chen, Q.-L. Wan, T. Liu, W. Tian, Electrochemical corrosion behaviors of straight WC-Co alloys: exclusive variation in grain sizes and aggressive media, Int. J. Refract. Met. Hard Mater. 57 (2016) 70–77, https://doi.org/10.1016/j.ijrmhm.2016.02.009.
[21] A.M. Ferro Rocha, A.C. Bastos, J.P. Cardoso, F. Rodrigues, M.G.S. Ferreira, Corrosion behaviour of WC hardmetals with nickel-based binders, Corros. Sci. 147 (2019) 384–393, https://doi.org/10.1016/j.corsci.2018.11.015.
[22] X. Zhang, J. Zhou, C. Liu, K. Li, N. Lin, Effects of Ni addition on mechanical properties and corrosion behaviors of coarse-grained WC-10(co, Ni) cemented carbides Int, J. Refract. Met. Hard Mater. 80 (2019) 123–129, https://doi.org/10.1016/j.ijrmhm.2019.01.004.
[23] H. Engqvist, U. Beste, N. Axén, The influence of pH on sliding wear of WC-based materials, Int. J. Refract. Met. Hard Mater. 18 (2000) 103–109, https://doi.org/10.1016/S0263-4368(00)00007-X.
[24] A.J. Gant, M.G. Gee, A.T. May, The evaluation of tribo-corrosion synergy for WC-Co hardmetals in low stress abrasion, Wear 256 (2004) 500–516, https://doi.org/10.1016/j.wear.2003.04.001.
[25] M.R. Thakare, J.A. Wharton, R.J.K. Wood, C. Menger, Exposure effects of alkaline drilling fluid on the microscale abrasion-corrosion of WC-based hardmetals, Wear 263 (2007) 125–136, https://doi.org/10.1016/j.wear.2006.12.047.
[26] R.J.K. Wood, S. Herd, M.R. Thakare, A critical review of the tribocorrosion of cemented and thermal sprayed tungsten carbide, Tribol. Int. 119 (2018) 491–509, https://doi.org/10.1016/j.triboint.2017.10.006.
[27] W.J. Tomlinson, I.D. Molyneux, Corrosion, erosion-corrosion, and the flexural strength of WC-Co hardmetals, J. Mater. Sci. 26 (1991) 1605–1608, https://doi.org/10.1007/BF00544670.
[28] V.A. Pugsley, G. Korn, S. Luyckx, H.G. Sockel, W. Heinrich, M. Wolf, H. Feld, R. Schulte, The influence of a corrosive wood-cutting environment on the mechanical properties of hardmetal tools, Int. J. Refract. Met. Hard Mater. 19 (2001) 311–318, https://doi.org/10.1016/S0263-4368(01)00059-2.
[29] V.A. Pugsley, H.-G. Sockel, Corrosion fatigue of cemented carbide cutting tool materials, Mater. Sci. Eng. A 366 (2004) 87–95, https://doi.org/10.1016/j.msea.2003.08.057.
[30] J.M. Tarragó, G. Fargas, E. Jimenez-Piqué, A. Felip, L. Isern, D. Coureaux, J.J. Roa, I. Al-Dawery, J. Fair, L. Llanes, Corrosion damage in WC-Co cemented carbides: residual strength assessment and 3D FIB-FESEM tomography characterisation, Powder Metall. 57 (2014) 324–330, https://doi.org/10.1179/1743290114Y.0000000115.
[31] J.M. Tarragó, G. Fargas, L. Isern, S. Dorvlo, L. Llanes, Microstructural influence on tolerance to corrosion-induced damage in hardmetals, Mater. Design 111 (2016)

36–43, https://doi.org/10.1016/j.matdes.2016.08.066.
[32] W. Tang, L. Zhang, Y. Chen, H. Zhang, L. Zhou, Corrosion and strength degradation behaviors of binderless WC material and WC-Co hardmetal in alkaline solution: a comparative investigation, Int. J. Refract. Met. Hard Mater. 68 (2017) 1–8, https://doi.org/10.1016/j.ijrmhm.2017.06.003.
[33] M.G. Gee, Model scratch corrosion studies for WC/co hardmetals, Wear 268 (2010) 1170–1177, https://doi.org/10.1016/j.wear.2010.01.004.
[34] M.G. Gee, L. Nimishakavi, Model single point abrasion experiments on WC/co hardmetals, Int. J. Refract. Met. Hard Mater. 29 (2011) 1–9, https://doi.org/10.1016/j.ijrmhm.2010.04.009.
[35] J.C.P. Zuñega, M.G. Gee, R.J.K. Wood, J. Walker, Scratch testing of WC/Co hardmetals, Tribol. Int. 54 (2012) 77–86, https://doi.org/10.1016/j.triboint.2012.02.027.
[36] A.J. Gant, M.G. Gee, D.D. Gohil, H.G. Jones, L.P. Orkney, Use of FIB/SEM to assess the tribo-corrosion of WC/co hardmetals in model single point abrasion experiments, Tribol. Int. 68 (2013) 56–66, https://doi.org/10.1016/j.triboint.2012.11.008.
[37] M. Gee, K. Mingard, J. Nunn, B. Roebuck, A. Gant, In situ scratch testing and abrasion simulation of WC/co, Int. J. Refract. Met. Hard Mater. 62 (2017) 192–201, https://doi.org/10.1016/j.ijrmhm.2016.06.004.
[38] M.G. Gee, B. Roebuck, P. Lindahl, H.-O. Andren, Constituent phase nanoindentation of WC/Co and Ti(C,N) hard metals, Mater. Sci. Eng. A209 (1996) 128–136, https://doi.org/10.1016/0921-5093(95)10099-7.
[39] A. Duszová, R. Halgaš, M. Bľanda, P. Hvizdoš, J. Morgiel, Nanoindentation of WC–Co hardmetals, J. Eur. Ceram. Soc. 33 (2013) 2227–2232, https://doi.org/10.1016/j.jeurceramsoc.2012.12.018.
[40] J.J. Roa, E. Jimenez-Pique, C. Verge, J.M. Tarragó, L. Llanes, Intrinsic hardness of constitutive phases in WC–Co composites: Nanoindentation testing, statistical analysis, WC crystal orientation effects and flow stress for the constrained metallic binder, J. Eur. Ceram. Soc. 35 (2015) 3419–3425, https://doi.org/10.1016/j.jeurceramsoc.2015.04.021.
[41] S. Ndlovu, K. Durst, M. Göken, Investigation of the sliding contact properties of WC-Co hard metals using nanoscratch testing, Wear 263 (2007) 1602–1609, https://doi.org/10.1016/j.wear.2006.11.044.
[42] H.Q. Sun, R. Irwan, H. Huang, G.W. Stachowiak, Surface characteristics and removal mechanism of cemented tungsten carbides in nanoscratching, Wear 268 (2010) 1400–1408, https://doi.org/10.1016/j.wear.2010.02.014.
[43] T. Csanádi, M. Novák, A. Naughton-Duszová, J. Dusza, Anisotropic nanoscratch resistance of WC grains in WC–Co composite, Int. J. Refract. Met. Hard Mater. 51 (2015) 188–191, https://doi.org/10.1016/j.ijrmhm.2015.03.005.
[44] J.M. Tarragó, D. Coureaux, Y. Torres, F. Yu, I. Al-Dawery, L. Llanes, Implementation of an effective time-saving two-stage methodology for microstructural characterization of cemented carbides, Int. J. Refract. Met. Hard Mater. 55 (2016) 80–86, https://doi.org/10.1016/j.ijrmhm.2015.10.006.
[45] W.C. Oliver, G.M. Pharr, An improved technique for determining hardness and elastic modulus using load and displacement sensing indentation experiments, J. Mater. Res. 7 (1992) 1564–1583, https://doi.org/10.1557/JMR.1992.1564.
[46] V.K. Sarin, T. Johannesson, On the deformation of WC-Co cemented carbides, Meter. Sci. 9 (1975) 472–476, https://doi.org/10.1179/030634575790444531.
[47] B. Roebuck, E.A. Almond, A.M. Cottenden, The influence of composition, phase transformation and varying the relative F.C.C. and H.C.P. phase contents on the properties of dilute Co-W-C alloys, Mater. Sci. Eng. A 66 (1984) 179–194, https://doi.org/10.1016/0025-5416(84)90179-4.
[48] C.H. Vasel, A.D. Krawitz, E.F. Drake, E.A. Kenik, Binder deformation in WC-(Co,Ni) cemented carbide composites, Metall. Mater. Trans. A 16 (1985) 2309–2317, https://doi.org/10.1007/BF02670431.
[49] M. Gee, A. Gant, B. Roebuck, Wear mechanisms in abrasion and erosion of WC/co and related hardmetals, Wear 263 (2007) 137–148, https://doi.org/10.1016/j.wear.2006.12.046.
[50] J. Heinrichs, M. Olsson, S. Jacobson, Surface degradation of cemented carbides in scratching contact with granite and diamond-the roles of microstructure and composition, Wear 342 (2015) 210–221, https://doi.org/10.1016/j.wear.2015.08.024.

7.3 Article III

Indentation and scratch testing of medium-grained WC-6%wtCo: corrosion effects on load-bearing capability and induced damage

Yafeng Zheng, Gemma Fargas, Olivier Lavigne, Luis Llanes.

In this work, corrosion effects on the indentation and scratch response of a WC-6%Co hardmetal are investigated. Experimental variables include relative long corrosion times as well as indentation and scratch testing conditions, yielding damage scenarios whose depths are similar to length scale of the degraded surface layers. It is found that load-bearing capability and crack extension resistance of the cemented carbide grade studied are significantly reduced after exposure to corrosive media. This is related to relevant changes within the microstructural assemblage of the material, from an effective bulk ceramic-metal composite into a porous layer consisting of a binderless carbide network on top of a pristine-like hardmetal substrate. However, such lessening effects are found to be dependent on the ratio between indentation and/or scratch depth and thickness of the corroded layer. Hence, relative changes decrease as corrosion time increases, and no differences are discerned after seven days of immersion. Similar pronounced corrosion influence is evidenced in surface and subsurface damage scenario resulting after indentation and scratch tests. In this regard, a transition from well-defined cracking systems into a scenario consisting of multiple, branched and less shallow fissures is evidenced when comparing pristine and corroded specimens respectively. The experimental fact that referred cracking features for corroded specimens are confined within the porous-like degraded layers points out that it is the result of small length-scale interaction between cracks and the cavities within the binderless WC skeleton, left after the metallic binder has been leached away.

Article III

Indentation and scratch testing of medium-grained WC-6%wtCo: corrosion effects on load-bearing capability and induced damage

Y.F. Zheng

G. Fargas

O. Lavigne

L. Llanes

Ceram. Int. 46 (2020) 17591-17598

Ceramics International 46 (2020) 17591–17598

Contents lists available at ScienceDirect

Ceramics International

journal homepage: www.elsevier.com/locate/ceramint

Indentation and scratch testing of a WC-6%$_{wt}$Co cemented carbide: Corrosion effects on load-bearing capability and induced damage

Y.F. Zheng[a,b], G. Fargas[a,b], O. Lavigne[c], L. Llanes[a,b,*]

[a] CIEFMA - Department of Materials Science and Engineering, Universitat Politècnica de Catalunya, Campus Diagonal Besòs-EEBE, Barcelona, 08019, Spain
[b] Barcelona Research Center in Multiscale Science and Engineering, Universitat Politècnica de Catalunya, Campus Diagonal Besòs-EEBE, Barcelona, 08019, Spain
[c] Hyperion Materials and Technologies, 08107, Martorelles, Spain

ARTICLE INFO

Keywords:
Corrosion
Load-bearing capability
Damage
Indentation
Scratch
Cemented carbide

ABSTRACT

In this work, corrosion effects on the indentation and scratch response of a WC-6%Co hardmetal are investigated. Experimental variables include relative long corrosion times as well as indentation and scratch testing conditions yielding damage scenarios whose depths are similar to length scale of the degraded surface layers. It is found that load-bearing capability and crack extension resistance of the cemented carbide grade studied are significantly reduced after exposure to corrosive media. This is related to relevant changes within the microstructural assemblage of the material, from an effective bulk ceramic-metal composite into a porous layer consisting of a binderless carbide network on top of a pristine-like hardmetal substrate. However, such lessening effects are found to be dependent on the ratio between indentation and/or scratch depth and thickness of the corroded layer. Hence, relative changes decrease as corrosion time increases, and no differences are discerned after seven days of immersion. Similar pronounced corrosion influence is evidenced in surface and subsurface damage scenario resulting after indentation and scratch tests. In this regard, a transition from well-defined cracking systems into a scenario consisting of multiple, branched and less shallow fissures is evidenced when comparing pristine and corroded specimens respectively. The experimental fact that referred cracking features for corroded specimens are confined within the porous-like degraded layers points out that it is the result of small length-scale interaction between cracks and the cavities within the binderless WC skeleton, left after the metallic binder has been leached away.

1. Introduction

WC-Co cemented carbides, usually referred to as hardmetals, consist of two interpenetrating networks of their metallic and ceramic constitutive phases [1]. The intrinsic composite nature of these materials permits to tailor unique combinations of mechanical properties by proper selection of carbide grain size and metallic binder content [2,3]. As a result, they have consolidated as first choice materials for tools and components to be used in highly demanding applications, e.g. cutting or forming of metallic alloys, as well as mining operations [4].

Several of the above applications also include exposure to chemically aggressive media, such as lubricants, chemical products, petrochemical and mine slurries, and seawater [5–8]. Under these conditions, it has been shown that failure induced under applied load is accelerated, and corresponding service life may be significantly shortened. In this regard, extensive research has proven that corrosion significantly affects microstructural and mechanical/tribological characteristics of cemented carbides. Regarding the former, it is well-known that the original microstructural scenario is changed, through dissolution of different individual phases depending on acidic or basic nature of the media [9–14]. Concerning the latter, it is established that rupture, wear and fatigue resistance of corroded hardmetals decrease [5,10,15–21]. One reason behind it is the pronounced stress rising effect of corrosion pits. Another one is a lower load-bearing capability linked to an unsupported carbide skeleton resulting from removal of the binder phase.

Critical review of most of the above works points out that observed detrimental corrosion-related effects are usually discussed on the basis of the direct correlation existing between microstructure and macroscopic property/response exclusively. Although this knowledge is interesting and useful from a material selection viewpoint, additional information is required if microstructural design against corrosion is

* Corresponding author. CIEFMA - Department of Materials Science and Engineering, Universitat Politècnica de Catalunya, Campus Diagonal Besòs-EEBE, Barcelona, 08019, Spain.
E-mail address: luis.miguel.llanes@upc.edu (L. Llanes).

https://doi.org/10.1016/j.ceramint.2020.04.059
Received 21 March 2020; Accepted 6 April 2020
Available online 10 April 2020

aimed. This is particularly true concerning the changes that may be induced by corrosion on damage scenario and/or active micromechanisms, at both surface and subsurface levels, under applied load. In this regard, an outstanding exception is the investigation conducted by Gee and coworkers in the last decade [18,22,23]. In such studies, they combined model single point abrasion (scratch) experiments and advanced characterization techniques to document and rationalize the influence of corrosion on corresponding damage micromechanisms. Among their interesting observations, the evidence of structural collapse at the subsurface level together with irregular longitudinal scratch profiles, as a direct consequence of binder leaching, must be highlighted. A similar approach has been recently followed by Zheng et al. [24] to assess and analyze surface/subsurface and small-scale mechanical integrity changes induced by exposure to an acidic media of a hardmetal grade. Such study included nanoindentation and nanoscratch testing together with inspection by means of Field Emission Scanning Electron Microscopy (FESEM). Lower mechanical properties were determined for the corroded cemented carbide investigated. This finding was discussed on the basis of the effective microstructural assemblage remnant after corrosion action. In this regard, and in agreement with the findings of Gee and coworkers, dissolution of the metallic phase was found to yield a mechanically unsupported, contiguous and binderless/porous, carbide network. As a final consequence, cracking, fragmentation and easy removal of WC grains under contact loading was observed on the corroded hardmetal.

It is the aim of this study to conduct a systematic investigation on corrosion-induced changes on both load-bearing capability and damage scenario of a WC-Co hardmetal grade. Different from the nanomechanical study referred above, this investigation focusses on a higher length scale (from 10s to 100s of microns in depth) as it includes relatively long corrosion times as well as pyramidal indentation and sliding contact (microscratch) experiments applying loads ranging from 5 to 300 N. The former implies existence of uniform and rather thick corrosion-affected layers, whereas the latter yields damage scenarios whose depth is similar to length scale of the degraded surface layers. Under these conditions, well-developed cracking systems are induced; and thus, changes on the crack-microstructure interaction as a function of corrosion extension may be studied.

2. Material and experimental aspects

The investigated material is a plain WC-Co supplied by Hyperion Materials and Technologies. Binder content is $6_{\%wt}$ and mean value of carbide grain size is about 1.5 μm, as measured by linear interception using FESEM micrographs.

Corrosion damage was induced in a controlled way by immersing the hardmetal specimens in stirred 0.1 M HCl solution at room temperature during variable time periods: one (1D), three (3D), seven (7D) and eleven (11D) days. Weight loss was measured during the immersion tests. Corrosion rate was determined according to the following equation:

$$Corrosion\,(mm/year) = 87.6\left(\frac{w}{A\rho t}\right) \quad (1)$$

where w is the weight loss in mg; A is the surface area of the specimen in cm^2; ρ is the density of the material in g/cm^3; and t is the corrosion time in hours. Phase characterization, before and after corrosion tests, was conducted by means of FESEM and X-Ray diffraction (Philips MRD) using Cu K-α (40 kV and 30 mA) radiation. Microstructural changes induced by corrosion take place at both surface and subsurface levels. In this regard, corrosion effects on surface integrity was evaluated through examination of carefully prepared (cut, ground and polished) transverse sections by means of laser scanning confocal microscopy (LSCM) and FESEM.

Load-bearing capacity was investigated under two different loading conditions: indentation and sliding contact (scratch) using pyramid (Vickers) and conical (Rockwell) diamond indenters, respectively. Range of loads used was different in both cases: 2–294 N in the former and 5–60 N (at a loading rate of 50 N/min) in the latter. They were chosen such to induce relevant irreversible deformation and damage, including radial cracks out of the corners of the indentation imprints as well as cracks and spallation in scratch tracks. At least three tests were performed for each material and loading condition. Load-bearing capability associated with indentation tests was assessed in terms of Vickers hardness by measuring length of diagonals. On the other hand, irreversible deformation resistance under sliding contact conditions was evaluated in terms of an apparent scratch hardness (H_s) value, calculated as [25]:

$$H_s = \frac{8P_s}{\pi w^2} \quad (2)$$

where P_s is the applied scratch load in N; and w is the corresponding scratch width in μm. Scratch testing unit used (CSM Revetest) is equipped with an optical microscope which was set for measuring track width corresponding to a given applied load value.

An extensive and systematic inspection of the damage scenario was carried out. At the surface level, morphologies of residual imprints and scratch tracks were observed using LSCM and FESEM. Regarding pyramidal indentation tests, they yield nucleation and extension of cracks out of the corners of residual imprints. Relative length of induced cracks is related to effective toughness of the microstructural assemblage; and thus, indirectly to their damage tolerance, a key parameter for optimal microstructural design of hardmetals. Hence, corrosion effects on effective toughness were assessed by measuring the length of the induced cracks using optical photographs acquired by LSCM. Crack extension resistance (W) was then calculated using the following equation [26]:

$$W = \frac{P}{4a} \quad (3)$$

where P is the indentation load in N; and a is the mean radial crack length in μm.

Subsurface evolution of indentation and scratch damage with increasing load was examined by conducting specific tests on “clamped-interface” specimens. In doing so, the procedure followed included five sequential stages [27,28]. First, pristine and corroded specimens were transversally cut to obtain different halves corresponding to each specific condition. Second, these two half-surfaces were put into a mold of bakelite, with the original top surfaces facing each other, and the cut section was ground and polished. Third, this mold was mechanically broken and, once more, the two halves were put into another mold of bakelite, with the newly polished surfaces clamped face-to-face. Fourth, uncorroded and corroded surfaces were indented (under applied load of 294 N) and scratched (up to 60 N) near the surface trace of the interface - keeping an equal distance between interface and either indentation imprint or end of scratch track, respectively. Fifth, the two parts were mechanically separated again, and polished cross-sections of corresponding half-surfaces were finally examined using LSCM. Here, special attention was paid to examine subsurface damage introduced by indentation and scratches done on the top surface of the “clamped-interface” specimens.

3. Results and discussion

3.1. Corrosion-induced changes at both surface and subsurface levels

Fig. 1 shows top-view and cross-sectional micrographs from corroded samples. As expected from the relatively long corrosion times investigated, microstructural changes are uniformly distributed at both surface and subsurface regions. In this regard, longer immersion times yield more relevant changes on microstructural assemblage as well as deeper corrosion fronts. Direct measurement of corrosion front depth indicates a linear correlation with time, in agreement with the

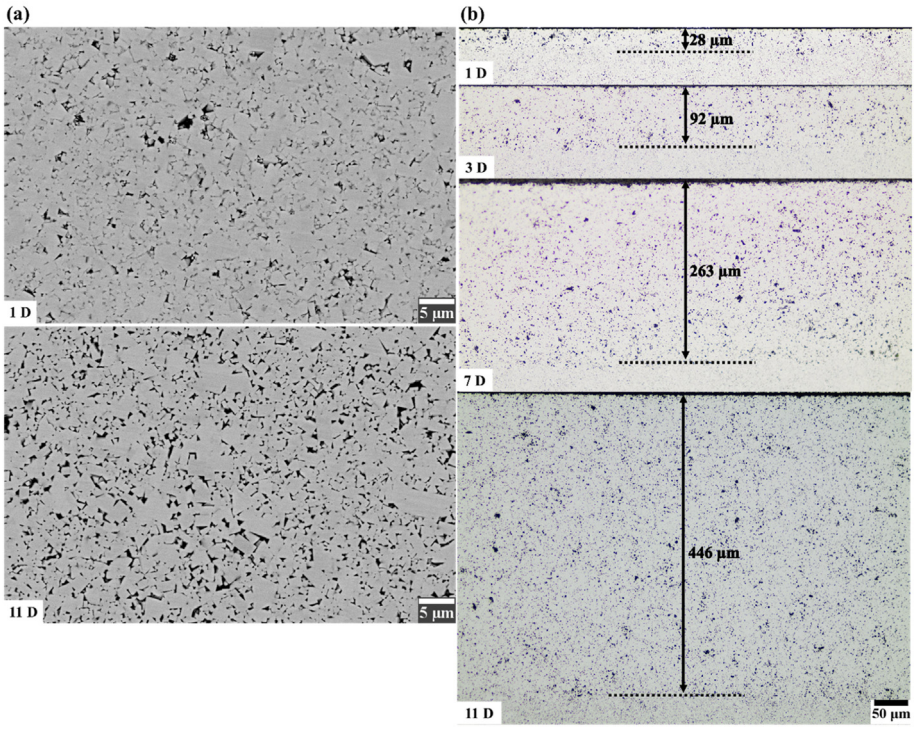

Fig. 1. FESEM top-view (a) and LSCM cross-sectional (b) micrographs of corroded samples: Microstructural aspect at the surface and subsurface of corroded layers for different corrosion times.

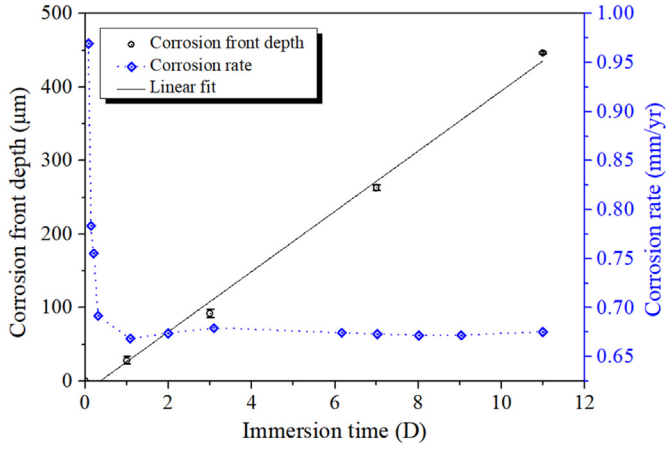

Fig. 2. Average corrosion front depth and corrosion rate as a function of immersion time.

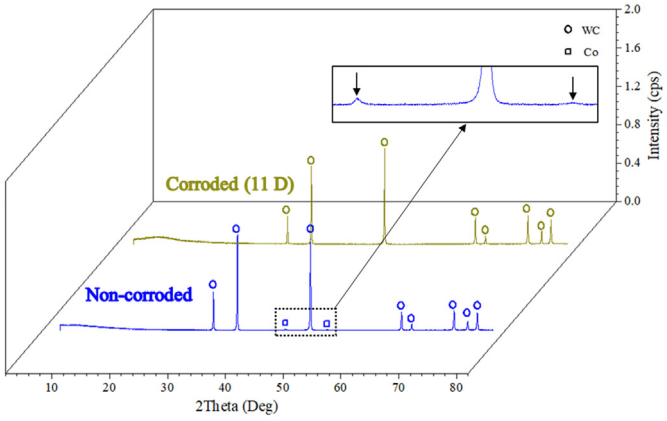

Fig. 3. XRD analysis for non-corroded and corroded (11D) samples.

relatively constant corrosion rates determined (using weight loss data), within the exposure time studied in this work, i.e. between 1 and 11 days (Fig. 2). Detailed microstructural observation and analysis carried out by FESEM and XRD (Fig. 3) pointed out that corrosion mainly affects the metallic binder. This is leached away yielding a simple carbide skeleton as the effective microstructural scenario for the degraded surface layer in the corroded specimens.

3.2. Corrosion effects on load-bearing capability of hardmetals

Pyramidal indentation and scratch tests were performed on the surface of non-corroded and corroded specimens to induce irreversible deformation. Representative images of residual imprints and scratch tracks for pristine and corroded conditions are shown in Figs. 4 and 5. They are less pronounced but better defined in the uncorroded material. On the other hand, discrete failure-related events such as chipping or spallation, are rather discerned for the corroded conditions.

Fig. 6 shows the residual indentation depth as a function of applied load for all the conditions studied. As expected, penetration increases as the applied load gets higher. On the other hand, clear corrosion effects are discerned in terms of a lower load-bearing capability of the exposed material. Similar observations may be done from experimental data collected from sliding contact tests, as shown in Fig. 7. In general, mechanical response lessening increases for longer immersion times. However, relative changes are much less pronounced after 3 days of exposure to corrosive solution, and no differences are discerned after 7 days of immersion.

Similar corrosion effects are found on measured Vickers and apparent (scratch) hardness values, as shown in Fig. 8 and Table 1, respectively. Within the experimental scatter, Vickers hardness decreases from 17 to 18 GPa for the uncorroded material to 11–12 GPa for the 7D and 11D corroded conditions. The latter then represents the effective load-bearing capability of the unsupported WC skeleton. This statement is sustained by the fact that variable and intermediate hardness values

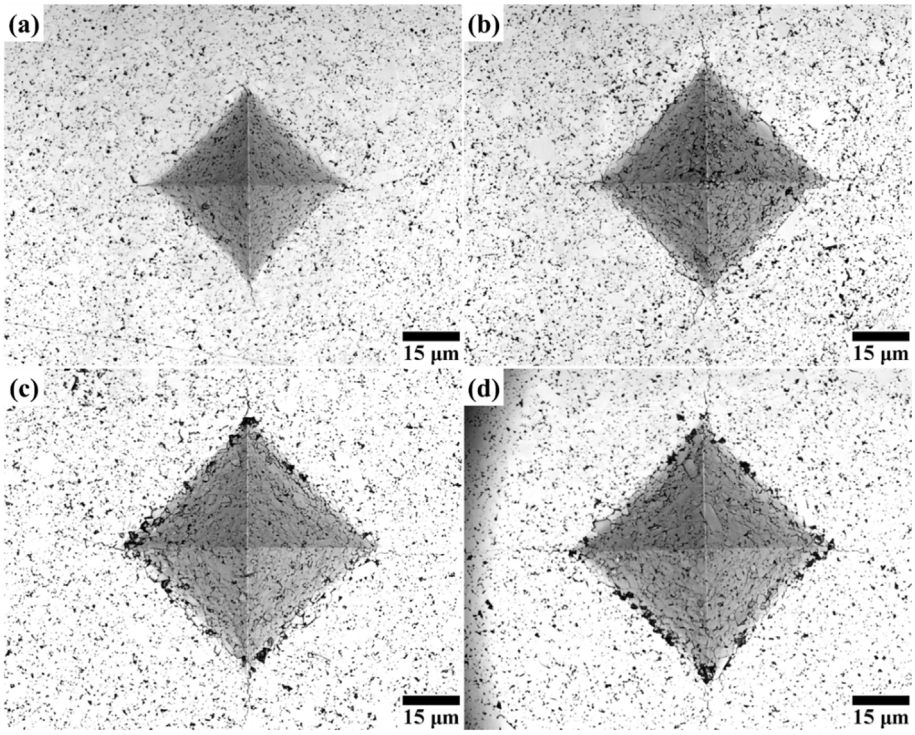

Fig. 4. LSCM micrographs of indentation imprints performed under applied load of 24.5 N on (a) non-corroded sample, and corroded specimens with different exposure times: (b) 1D, (c) 3D and (d) 7D.

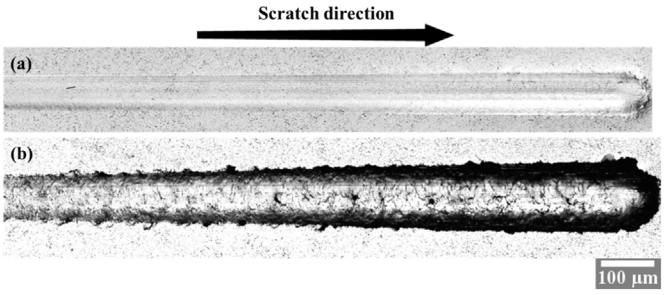

Fig. 5. LSCM micrographs of two scratch tracks performed on (a) non-corroded and (b) corroded (7D) samples, with increasing load ranging from 35 N to 60 N.

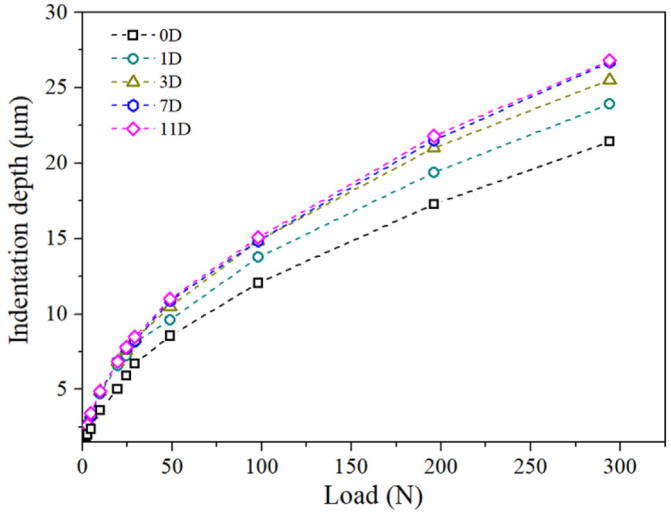

Fig. 6. Indentation depth as a function of applied load for uncorroded and corroded (for different exposure times) specimens.

are measured for 1D and 3D corroded conditions, depending on the imposed load. Such a trend is also evidenced when analyzing scratch hardness data, although here higher relative differences between pristine and corroded specimens are found. It would point out a higher sensitivity of irreversible deformation resistance of the hardmetal to corrosion-induced changes under the more complex loading state involved in sliding contact. In general, these experimental results highlight the lessening effect of corrosion on load-bearing capability of the hardmetal, as well as the dependence of the measured mechanical response on the ratio between indentation and/or scratch depth (and associated plastic zone) and thickness of the corroded layer, as it will be discussed below.

After being exposed to the 0.1 M HCl solution, the microstructure assemblage of the corroded zone becomes loose and porous due to the dissolution of the metallic phase [18,19,21]. Thus, the corrosion affected zone may be effectively described as a porous film adhered to a substrate consisting of the non-corroded hardmetal (Fig. 1). As a consequence, the contact response of the corroded samples becomes largely dependent on the thickness of the degrades layer, which is directly related to the exposure time. In order to understand this effect, a relative indentation depth (R) parameter, defined by the ratio between indentation depth and layer thickness, is recalled to account for the effect of coating thickness on measured mechanical properties [29–33]. In practice, it is assumed that substrate response does not affect the measured mechanical properties of the coating, as far as R is lower than 0.1 [34]. However, for a soft porous film on a hard substrate, it has been reported that such critical R value can even reach 0.3, because a higher capability of the porous film to confine plastic deformation within it [30]. The indentation depth (also measured by LSCM in this study) to layer thickness ratios for the different corroded samples and applied loads are included in Fig. 8. Slight deviation from average hardness value measured in the 7D and 11D cases should be attributed to indentation size effects, as widely reported in the literature [35,36]. On the other hand, hardness data gathered for 1D and 3D corroded specimens indicates an obvious “substrate effect” linked to the non-corroded hardmetal supporting the corroded layer. In this regard, higher

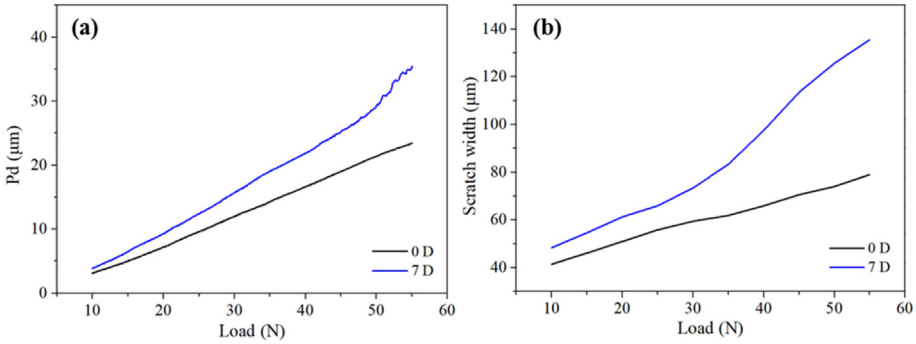

Fig. 7. Scratch (a) penetration depth (Pd) and (b) width as a function of applied load for non-corroded and 7-day corroded specimens.

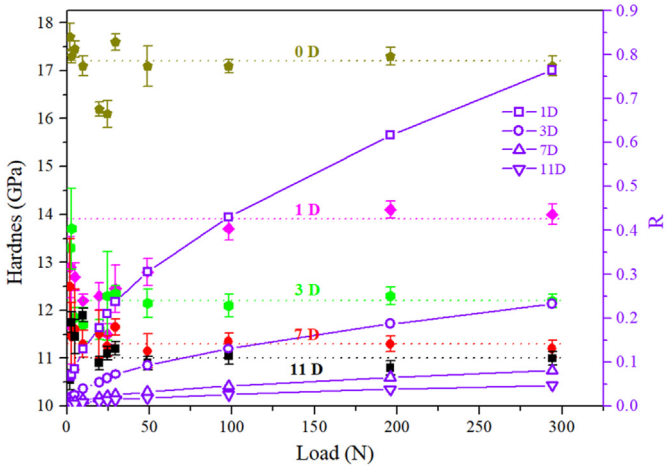

Fig. 8. Hardness and ratio between indentation depth and corroded layer thickness (R) as a function of applied load, for samples immersed in the corrosive solution during different times.

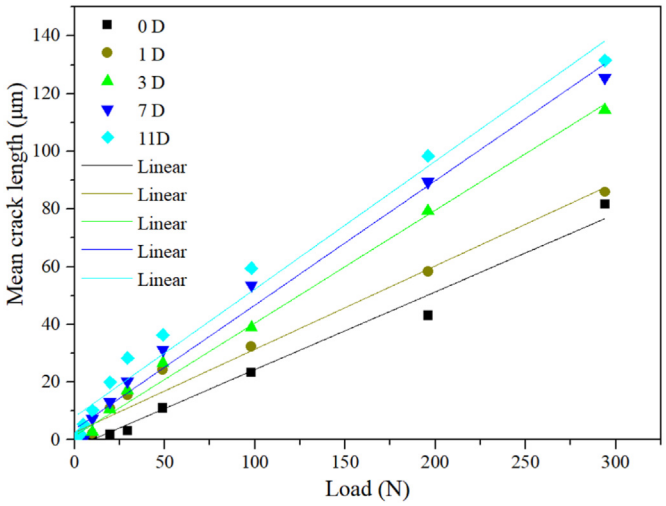

Fig. 9. Mean length of radial cracks, emanating from imprint corners, as a function of applied load for the pristine and corroded specimens investigated.

Table 1
Apparent scratch hardness data, measured under applied load of 50 N, for the different specimens studied. Corresponding Vickers hardness, measured under applied load of 49 N, are also listed for comparison purposes.

Condition	H_S (50 N) (GPa)	HV5(49 N) (GPa)
0D	23. 3 ± 0.5	17.1 ± 0.4
1D	10.5 ± 0.8	12.8 ± 0.3
3D	8.1 ± 0.8	12.2 ± 0.4
7D	8.1 ± 0.9	11.2 ± 0.3
11D	8.8 ± 0.9	10.9 ± 0.2

hardness values are measured as applied load increases or thickness of corroded layer decreases. Within the experimental scatter of the results, data measured for 1D and 3D exposed specimens would indicate relative indentation depths about 0.2–0.3 as critical for intrinsic assessment of the effective hardness of corroded layers, i.e. without being affected by the mechanical response of the substrate. This will support the idea of describing the corroded specimens as systems consisting of a porous ceramic layer on top of a very hard composite substrate.

Aiming to further document and analyze corrosion effects on mechanical integrity at the surface of the hardmetal studied, length of cracks emanating from imprint corners (Fig. 4) were measured for each tested condition. Determined mean values are plotted as a function of applied load in Fig. 9. A linear relationship was found in all the cases. The longer the exposure to the corrosive media, the higher the slope, pointing out a clear detrimental effect of corrosion on crack extension resistance (Fig. 10), i.e. on Palmqvist or indentation toughness [26,37]. Nevertheless, it should be underlined that relevance of lessening effects

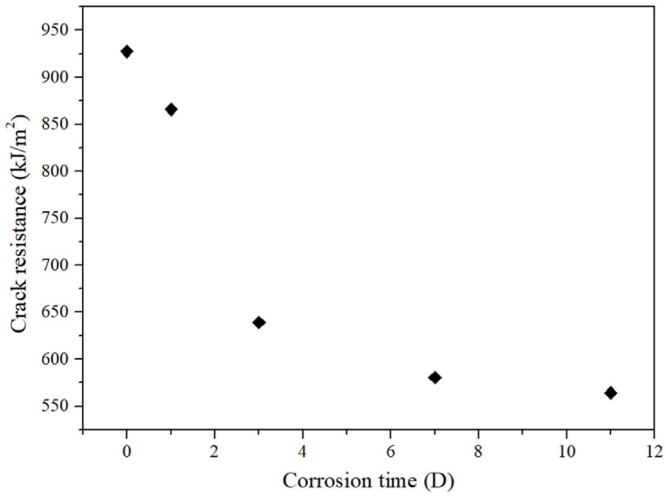

Fig. 10. Crack resistance as a function of immersion time for the different specimens studied.

on crack extension resistance decays over the first 3 days of immersion, and tends to stabilize for longer times (7 and 11 days).

Resistance against cracking phenomena of hardmetals is closely related to the energy expended in the constrained plastic stretching of Co binder ligament as cracks extend [38–40]. The higher the volume fraction of the binder phase, the more pronounced is the toughening due to ductile ligament reinforcements, as well as the corresponding

crack growth (R-curve) resistance [41,42]. Once corroded, there is a loose and porous WC skeleton left. Hence, effective removal of the ductile metallic phase implies that the referred toughening effect is no longer operative; and thus, energy required for subcritical crack propagation is lowered. As the corrosion time (corrosion front depth) increases, value of crack extension resistance decreased from 928 to 564 kJ/m^2. The transition from sharp changes at relatively short times into a rather stable lessening rate of crack extension resistance must be linked to the effective influence of the uncorroded substrate on the surface cracking phenomena discerned. As it was discussed above when analysing hardness data, substrate effects on the mechanical response of the material are expected to vanish gradually as the ratio between indentation depth and thickness of the corroded layer gets lower, i.e. as exposure time to corrosive media gets longer.

3.3. Corrosion effects on damage scenario induced during indentation and scratch tests

Similar to the findings reported on mechanical response, i.e. Vickers and scratch hardness as well as crack extension resistance; corrosion effects on damage induced under applied load are also extreme. It is clearly illustrated by comparing developed damage in non-corroded and corroded samples. In the case of pyramidal indentation (Fig. 11), opposite to the sharp and shallow cracks discerned in the non-corroded hardmetal, damage at the subsurface of the corroded conditions evolves from defined cracks close to the surface into branched ones as they growth into the bulk. Similarly, comb-like crack propagating paths underneath the scratch tracks are completely different for uncorroded and corroded conditions (Fig. 12). Systematic inspection - by controlling the distance between the scratch end and the edge - allows to discern that as the indenter gets closer to the edge, damaged zone changes from a well-defined cracking system for the uncorroded condition into a multiple-cracking scenario confined within the porous-like degraded layer for the corroded conditions. In agreement with previous studies on sintered steels exhibiting a relative large intrinsic porosity [43], cracks fork off within the corrosion layer aiming to follow easy paths of interconnected pores (Figs. 11b–1, 11c-2 and 12b). As a result, small-scale branching, interconnection and lateral crack growth parallel to the surface are evidenced, pointing out a potential development of macro-spalling like failures.

The above described damage scenarios at the subsurface of corroded hardmetals subjected to either indentation or scratch are linked to the effectiveness of a small length-scale interaction between cracks and the cavities within the binderless WC skeleton [44]. In this regard, effective pores - left after binder has been leached away - act not only as an assemblage of many small stress concentrators but also as crack precursors [45]. Hence, as load is applied and main cracks propagate

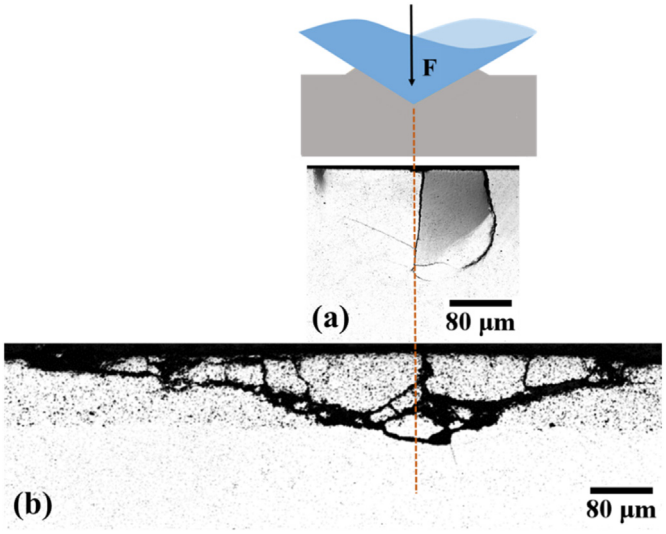

Fig. 12. Subsurface cracking scenario induced by scratching in (a) non-corroded and (b) corroded samples.

downwards, additional microstructurally short cracks nucleate at the referred pores and then propagate steadily out of them. From a mechanic viewpoint, the microcracking phenomena taking place in front of main fissures translates into crack wake shielding from the applied stress intensity factor [46]. It induces a decrease of the effective crack tip stress intensity factor, yielding as a result multiple branched cracks arrested at lower depths or following lateral-like paths parallel to the surface [47]. This would explain that uncorroded condition show fewer but shallower and deeper cracks than the corroded conditions (Figs. 11 and 12).

4. Conclusions

A systematic investigation of corrosion-induced changes on both load-bearing capability and damage scenario of a WC-Co hardmetal grade has been conducted. The study attempted to focus on indentation and scratch testing conditions yielding damage scenarios whose depths were similar to length scale of uniform and relatively thick (from 10s to 100s of microns) corroded layers. The following conclusions may be drawn:

(1) The corroded cemented carbide studied exhibits a lower load-bearing capability and crack extension resistance than the pristine one. These relative corrosion-induced lessening effects decreases as

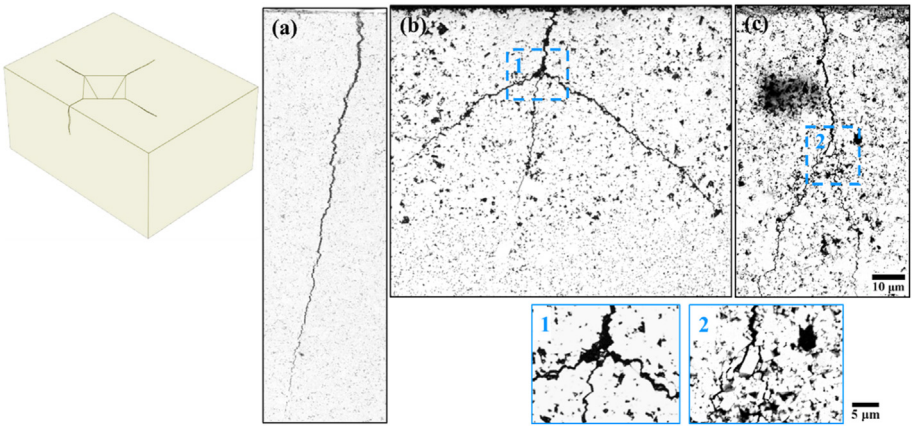

Fig. 11. Cross-section view of cracking phenomena resulting from pyramidal indentation under an applied load of 294 N for specimens previously exposed to corrosion media during different times: (a) pristine, (b) 3 days, and (c) 11 days.

exposure time increases, and no differences are discerned after 7 days of immersion. This trend is evidenced for both indentation and scratch tests, although a higher sensitivity of irreversible deformation resistance to microstructural changes introduced by corrosion is observed under sliding contact conditions. Vickers hardness of significantly corroded specimens decreases down to 11–12 GPa, i.e. about 60% the reference one determined for the uncorroded samples. From a mechanical viewpoint, such value may then be taken as the effective load-bearing capability of the unsupported WC skeleton.

(2) The contact response of the corroded hardmetals is largely dependent on the thickness of the degraded layer, which is directly related to the exposure time. In this regard, the corroded specimens may be described as systems consisting of a porous ceramic layer on top of a very hard composite substrate. Within this context, relative indentation depths lower than 0.2–0.3 of corroded layer thickness are determined as required testing conditions for effective assessment of the intrinsic hardness of corroded layers, i.e. without being affected by the mechanical response of the substrate.

(3) Significant corrosion effects on contact response are also evidenced in the damage scenario resulting, at both surface and subsurface levels, after indentation and scratch tests of the hardmetal studied. Independent of testing conditions, damaged zone changes from well-defined cracking systems for the uncorroded condition into multiple branched fissures confined within the porous-like degraded layers for the corroded ones. Cracks within the binderless and porous carbide network are discerned to get arrested at lower depths or following lateral-like paths parallel to the surface. Such scenario should be linked to the effectiveness of a small length-scale interaction between cracks and the cavities within the binderless WC skeleton, yielding as a final result the development of macro-spalling like failures at the edges of both indentation imprints and scratch tracks.

Declaration of competing interest

The authors declare no conflict of interest.

Acknowledgements

This work was financially supported by the collaborative Industry-University program between Hyperion Materials & Technologies and Universitat Politècnica de Catalunya, and partly funded by the Spanish Ministerio de Economía y Competividad through Grant MAT2015-70780-C4-3-P (MINECO/FEDER). Y. F. Zheng acknowledges the Ph.D. scholarship received from China Scholarship Council.

References

[1] E. Jiménez-Piqué, M. Turon-Vinas, H. Chen, T. Trifonov, J. Fair, E. Tarrés, L. Llanes, Focused ion beam tomography of WC-Co cemented carbides, Int. J. Refract. Metals Hard Mater. 67 (2017) 9–17, https://doi.org/10.1016/j.ijrmhm.2017.04.007.

[2] H.E. Exner, Physical and chemical nature of cemented carbides, Int. Mater. Rev. 4 (1979) 1149–1173, https://doi.org/10.1179/095066079790136363.

[3] J. Garcia, V.C. Cipres, A. Blomqvist, B. Kaplan, Cemented carbide microstructures: a review, Int. J. Refract. Metals Hard Mater. 80 (2018) 40–68, https://doi.org/10.1016/j.ijrmhm.2018.12.004.

[4] L. Prakash, 1.02 - Fundamentals and general applications of hardmetals, in: V.K. Sarin, D. Mari, L. Llanes (Eds.), Comprehensive Hard Materials, Elsevier, Oxford, 2014, pp. 29–90.

[5] V.A. Pugsley, G. Korn, S. Luyckx, H.G. Sockel, W. Heinrich, M. Wolf, H. Feld, R. Schulte, The influence of a corrosive wood-cutting environment on the mechanical properties of hardmetal tools, Int. J. Refract. Metals Hard Mater. 19 (2001) 311–318, https://doi.org/10.1016/S0263-4368(01)00059-2.

[6] U. Beste, T. Hartzell, H. Engqvist, N. Axén, Surface damage on cemented carbide rock-drill buttons, Wear 249 (2001) 324–329, https://doi.org/10.1016/S0043-1648(01)00553-1.

[7] R. Lu, L. Minarro, Y.-Y. Su, R.M. Shemenski, Failure mechanism of cemented tungsten carbide dies in wet drawing process of steel cord filament, Int. J. Refract. Metals Hard Mater. 26 (2008) 589–600, https://doi.org/10.1016/j.ijrmhm.2008.01.009.

[8] B. Bozzini, B. Busson, G.P. De Gaudenzi, C. Humbert, C. Mele, S. Tedeschi, A. Tadjeddine, Corrosion of cemented carbide grades in petrochemical slurries. Part I-Electrochemical adsorption of CN^-, SCN^- and MBT: a study based on in situ SFG, Int. J. Refract. Metals Hard Mater. 60 (2016) 37–51, https://doi.org/10.1016/j.ijrmhm.2016.06.010.

[9] A.M. Human, H.E. Exner, The relationship between electrochemical behaviour and in-service corrosion of WC based cemented carbides, Int. J. Refract. Metals Hard Mater. 15 (1997) 65–71, https://doi.org/10.1016/S0263-4368(96)00014-5.

[10] U.B.H. Engqvist, N. Axen, The influence of PH on sliding wear of WC-based materials, Int. J. Refract. Metals Hard Mater. 18 (2000) 103–109 https://doi.org/10.1016/S0263-4368(00)00007-X.

[11] S. Hochstrasser, Y. Mueller, C. Latkoczy, S. Virtanen, P. Schmutz, Analytical characterization of the corrosion mechanisms of WC–Co by electrochemical methods and inductively coupled plasma mass spectroscopy, Corros. Sci. 49 (2007) 2002–2020, https://doi.org/10.1016/j.corsci.2006.08.022.

[12] C.H. Yi, H.Y. Fan, J. Xiong, Z.X. Guo, H.S. Chen, Effect of WC content on the microstructures and corrosion behavior of Ti(C, N)-based cermets, Ceram. Int. 39 (2013) 503–509, https://doi.org/10.1016/j.ceramint.2012.06.055.

[13] W.B. Qiu, Y. Liu, J.W. Ye, H.J. Fan, Y.C. Qiu, Effects of (Ti,Ta,Nb,W)(C,N) on the microstructure, mechanical properties and corrosion behaviors of WC-Co cemented carbides, Ceram. Int. 43 (2017) 2918–2926, https://doi.org/10.1016/j.ceramint.2016.09.124.

[14] Q. Mao, Q.Q. Yang, W.H. Xiong, S.T. Li, L.J. Ruan, Corrosion behavior of Ni_3Al-bonded TiC-based cermets in H_2SO_4 and NaOH solutions, Ceram. Int. 44 (2018) 13303–13312, https://doi.org/10.1016/j.ceramint.2018.04.161.

[15] W.J. Tomlinson, I.D. Molyneux, Corrosion, erosion-corrosion, and the flexural strength of WC-Co hardmetals, J. Mater. Sci. 26 (1991) 1605–1608, https://doi.org/10.1007/BF00544670.

[16] A.J. Gant, M.G. Gee, A.T. May, The evaluation of tribo-corrosion synergy for WC-Co hardmetals in low stress abrasion, Wear 256 (2004) 500–516, https://doi.org/10.1016/j.wear.2003.04.001.

[17] V.A. Pugsley, H.-G. Sockel, Corrosion fatigue of cemented carbide cutting tool materials, Mater. Sci. Eng. A 366 (2004) 87–95, https://doi.org/10.1016/j.msea.2003.08.057.

[18] A.J. Gant, M.G. Gee, D.D. Gohil, H.G. Jones, L.P. Orkney, Use of FIB/SEM to assess the tribo-corrosion of WC/Co hardmetals in model single point abrasion experiments, Tribol. Int. 68 (2013) 56–66, https://doi.org/10.1016/j.triboint.2012.11.008.

[19] J.M. Tarragó, G. Fargas, L. Isern, S. Dorvlo, E. Tarres, C.M. Müller, E. Jimenez-Piqué, L. Llanes, Microstructural influence on tolerance to corrosion-induced damage in hardmetals, Mater. Design 111 (2016) 36–43, https://doi.org/10.1016/j.matdes.2016.08.066.

[20] W. Tang, L. Zhang, Y. Chen, H. Zhang, L. Zhou, Corrosion and strength degradation behaviors of binderless WC material and WC-Co hardmetal in alkaline solution: a comperative investigation, Int. J. Refract. Metals Hard Mater. 68 (2017) 1–8, https://doi.org/10.1016/j.ijrmhm.2017.06.003.

[21] Y.F. Zheng, G. Fargas, E. Armelin, O. Lavigne, L. Llanes, Corrosion-induced damage and residual strength of WC-Co, Ni cemented carbides: influence of microstructure and corrosion medium, Metals 9 (2019) 1018, https://doi.org/10.3390/met9091018.

[22] M.G. Gee, Model scratch corrosion studies for WC/Co hardmetals, Wear 268 (2010) 1170–1177, https://doi.org/10.1016/j.wear.2010.01.004.

[23] M.G. Gee, L. Nimishakavi, Model single point abrasion experiments on WC/Co hardmetals, Int. J. Refract. Metals Hard Mater. 29 (2011) 1–9, https://doi.org/10.1016/j.ijrmhm.2010.04.009.

[24] Y.F. Zheng, G. Fargas, H. Besharatloo, M. Serra, J.J. Roa, E. Armelin, L. Llanes, Assessment of corrosion-induced changes on the mechanical integrity of cemented carbides at small length scales, Int. J. Refract. Metals Hard Mater. 84 (2019) 105033, https://doi.org/10.1016/j.ijrmhm.2019.105033.

[25] ASTM G 171-03, Standard test method for scratch hardness of materials using a diamond stylus, ASTM International Standards, USA, 2017.

[26] H.E. Exner, The influence of sample preparation on Palmqvist method for toughness testing of cemented carbides, Trans TMS AIME 245 (1969) 677–683.

[27] E. Tarres, G. Ramírez, Y. Gaillard, E. Jiménez-Piqué, L. Llanes, Contact fatigue behavior of PVD-coated hardmetals, Int. J. Refract. Metals Hard Mater. 27 (2009) 323–331, https://doi.org/10.1016/j.ijrmhm.2008.05.003.

[28] J. Yang, F. García Marro, T. Trifonov, M. Odén, M.P. Johansson-Jõesaar, L. Llanes, Contact damage resistance of TiN-coated hardmetals: beneficial effects associated with substrate grinding, Surf. Coat. Technol. 275 (2015) 133–141, https://doi.org/10.1016/j.surfcoat.2015.05.028.

[29] X. Cai, H. Bangert, Hardness measurements of thin films-determining the critical ratio of depth to thickness using FEM, Thin Solid Films 264 (1995) 59–71, https://doi.org/10.1016/0040-6090(95)06569-5.

[30] C. Gamonpilas, E.P. Busso, On the effect of substrate properties on the indentation behaviour of coated systems, Mater. Sci. Eng. A 380 (2004) 52–61 doi:j.msea.2004.04.038.

[31] N. Panich, Y. Sun, Effect of penetration depth on indentation response of soft coatings on hard substrates: a finite element analysis, Surf. Coat. Technol. 182 (2004) 342–350, https://doi.org/10.1016/j.surfcoat.2003.07.002.

[32] R. Bartalin, A. Vaccari, V. Micheli, G. Gottardi, R. Pandiyan, A. Collini, P. Lori, G. Coser, N. Laidani, Critical relative indentation depth in carbon based thin films, Prog. Nat. Sci.-Mater. 24 (2014) 287–290, https://doi.org/10.1016/j.pnsc.2014.05.002.

[33] A.S. Kaygorodov, A.S. Mamaev, Substrate influence on the mechanical properties of TiC/a-C coatings, Mater. Phys. Mech. 30 (2017) 35–39.

[34] K. Tunvisut, N.P. O'Dowd, E.P. Busso, Use of scaling functions to determine mechanical properties of thin coatings from microindentation tests, Int. J. Solid Struct. 38 (2001) 335–351, https://doi.org/10.1016/S0020-7683(00)00017-2.
[35] P.J. Burnett, D.S. Rickerby, Assessment of coating hardness, Surf. Eng. 3 (1987) 69–76, https://doi.org/10.1179/sur.1987.3.1.69.
[36] A. Thomas, Microhardness measurement as a quality control technique for thin, hard coatings, Surf. Eng. 3 (1987) 117–122, https://doi.org/10.1179/sur.1987.3.2.117.
[37] D.K. Shetty, I.G. Wright, P.N. Mincer, A.H. Clauer, Indentation fracture of WC-Co cermets, J. Mater. Sci. 20 (1985) 1873–1882, https://doi.org/10.1007/BF00555296.
[38] L.S. Sigl, H.E. Exner, Experimental study of the mechanics of fracture in WC–Co alloys, Metall. Mater. Trans. 18 (1987) 1299–1308, https://doi.org/10.1007/BF02647199.
[39] L.S. Sigl, H.F. Fischmeister, On the fracture toughness of cemented carbides, Acta Metall. 36 (1988) 887–897, https://doi.org/10.1016/0001-6160(88)90143-5.
[40] J.M. Tarragó, E. Jiménez-Piqué, L. Schneider, D. Casellas, Y. Torres, L. Llanes, FIB/FESEM experimental and analytical assessment of R-curve behavior of WC-Co cemented carbides, Mater. Sci. Eng. A 645 (2015) 142–149, https://doi.org/10.1016/j.msea.2015.07.090.
[41] O. Raddatz, G.A. Schneider, N. Claussen, Modelling of R-curve behaviour in ceramic/metal composites, Acta Mater. 46 (1998) 6381–6395, https://doi.org/10.1016/S1359-6454(98)00317-6.
[42] J.M. Tarragó, D. Coureaux, Y. Torres, D. Casellas, I. Al-Dawery, L. Schneider, L. Llanes, Microstructural effects on the R-curve behavior of WC-Co cemented carbides, Mater. Design 97 (2016) 492–501, https://doi.org/10.1016/j.matdes.2016.02.115.
[43] S. Carabajar, C. Verdu, A. Hamel, R. Fougeres, Fatigue behaviour of a nickel alloyed sintered steel, Mater. Sci. Eng. A 257 (1998) 225–234, https://doi.org/10.1016/S0921-5093(98)00846-6.
[44] R.W. Rice, The porosity dependence of physical properties of materials: A summary review, Key Eng. Mater. 115 (1996) 1–20 https://doi.org/10.4028/www.scientific.net/KEM.115.1.
[45] J. Holmes, R.A. Queeney, Fatigue crack initiation in a porous steel, Powder Metall. 28 (1985) 231–235, https://doi.org/10.1179/pom.1985.28.4.231.
[46] Y.B. Ke, B. Cotterell, Y.W. Mai, The fracture resistance of sintered steel, Mater. Sci. Eng. A 117 (1989) 149–156, https://doi.org/10.1016/0921-5093(89)90096-8.
[47] B. Cotterell, S.Q. He, Y.W. Mai, Fatigue of sintered steel, Acta Mater. 42 (1994) 99–104, https://doi.org/10.1016/0956-7151(94)90051-5.

7.4 Article IV

Corrosion-induced changes on Hertzian contact damage in cemented carbides

Yafeng Zheng, Gemma Fargas, Olivier Lavigne, Erica Roitero, Luis Llanes.

In this study, the influence of corrosion on the mechanical response and damage induced under Hertzian indentation is assessed for three cemented carbides with metallic binders of different chemical nature. Corrosion is introduced in a controlled way, before subsequent spherical indentation testing, by immersing specimens in a stirred acidic medium. Results reveal quite strong corrosion effects on indentation stress-strain response and contact damage scenario. Such detrimental influence is found to be dependent on both the ratio between indentation depth and thickness of the corroded layer as well as chemical nature of the binder. In this regard, critical loads for emergence and evolution of specific damage events - ring and radial cracks, and even specimen failure - are proposed as figures of merit for material selection under the combined action of corrosion and contact loads. Within this context, the hardmetal grade with Co-base binder and addition of Cr is found to be the best option, among the three cemented carbides studied in this investigation. It points out the consideration of the synergic interaction between corrosion resistance and hardness/toughness correlation for microstructural design optimization of hardmetals under service-like conditions. These statements are supported by the relevant corrosion-induced changes also observed, by means of advanced characterization techniques, in terms of deformation/failure micromechanisms at both surface and subsurface levels.

Article IV

Corrosion-induced changes on Hertzian contact damage in cemented carbides

Y.F. Zheng

G. Fargas

O. Lavigne

E. Roitero

L. Llanes

Int. J. Refract. Met. Hard Mater. 92 (2020) 105334

International Journal of Refractory Metals & Hard Materials 92 (2020) 105334

Contents lists available at ScienceDirect

International Journal of Refractory Metals & Hard Materials

journal homepage: www.elsevier.com/locate/IJRMHM

Corrosion-induced changes on Hertzian contact damage in cemented carbides

Y.F. Zheng[a,b,*], G. Fargas[a,b], O. Lavigne[c], E. Roitero[a,b], L. Llanes[a,b]

[a] CIEFMA, Department of Materials Science and Engineering, Universitat Politècnica de Catalunya, Campus Diagonal Besòs-EEBE, Barcelona 08019, Spain
[b] Barcelona Research Centre in Multiscale Science and Engineering, Universitat Politècnica de Catalunya, Campus Diagonal Besòs-EEBE, Barcelona 08019, Spain
[c] Hyperion Materials and Technologies, Martorelles 08107, Spain

ARTICLE INFO

Keywords:
Corrosion
Hertzian indentation technique
Contact damage
Load-bearing capability
Cemented carbides

ABSTRACT

In this study, the influence of corrosion on the mechanical response and damage induced under Hertzian indentation is assessed for three cemented carbides with metallic binders of different chemical nature. Corrosion degradation is introduced in a controlled way, before subsequent spherical indentation testing, by immersing specimens in a stirred acidic medium. Results reveal quite strong corrosion effects on indentation stress-strain response and contact damage scenario. Such detrimental influence is found to be dependent on both the ratio between indentation depth and thickness of the corroded layer as well as chemical nature of the binder. In this regard, critical loads for emergence and evolution of specific damage events (i.e. ring and radial cracks, and even specimen failure) are proposed as figures of merit for material selection under the combined action of corrosion and contact loads. Within this context, the hardmetal grade with Co-base binder and addition of Cr is found to be the best option, among the three cemented carbides studied in this investigation. It points out the consideration of the synergic interaction between corrosion resistance and hardness/toughness correlation for microstructural design optimization of hardmetals under service-like conditions. These statements are supported by the relevant corrosion-induced changes also observed, by means of advanced characterization techniques, in terms of deformation/failure micromechanisms at both surface and subsurface levels.

1. Introduction

Cemented carbides are a group of powder metallurgical liquid-phase sintered composite materials consisting of brittle refractory carbides of the transition metals (e.g. WC, TiC, TaC) embedded in a metallic matrix [1]. The intrinsic ceramic-metal composite nature of these materials, in practice commonly referred to as hardmetals, together with optimized microstructural assemblages yield outstanding combinations of high hardness and strength together with excellent wear resistance [2–4]. This makes cemented carbides forefront materials in several engineering and tooling applications, such as metal cutting and forming, mining bits, rock drilling, mechanical seals, structural components and wear parts [5].

Many of the above applications frequently expose cemented carbides to harsh working conditions that involve corrosive aqueous media together with contact loads, impacts and fatigue, abrasion and/or erosion, etc. [5]. In those cases, defects resulting from environmental-assisted degradation (e.g. leaching and removal of metallic binder, microcracks and/or loosening/dislodging of carbides, among others) are often identified as main reasons for the shortened service life of hardmetal tools and components, e.g. Refs. [6–9].

The corrosion behavior of WC-base cemented carbides has been extensively investigated in recent decades, mainly focusing on the influence of several extrinsic and intrinsic factors, such as surface state, corrosive medium, microstructural assemblage and binder chemical nature (e.g. Refs. [10–24]). In these studies, several interesting findings have been documented. First, metallic binders are preferentially attacked in acidic and neutral environments, while ceramic phase is the one corroded in alkaline solution. Second, corrosion damage induced by acidic media is more pronounced than that resulting from exposure to neutral and basic ones. Third, larger dissolution of the binder phase in acid solution eventually results in the formation of a W-base oxide layer and a region depleted in Co, different from the scenario found when the cemented carbides are exposed to neutral and basic solutions.

Regarding industrial applications involving both corrosion and contact loading of hardmetal tools, components and wear parts (e.g. oil

* Corresponding author at: CIEFMA, Department of Materials Science and Engineering, Universitat Politècnica de Catalunya, Campus Diagonal Besòs-EEBE, Barcelona 08019, Spain.
E-mail address: yafeng.zheng@upc.edu (Y.F. Zheng).

https://doi.org/10.1016/j.ijrmhm.2020.105334
Received 15 May 2020; Received in revised form 20 July 2020; Accepted 20 July 2020
Available online 24 July 2020
0263-4368/

and gas extraction industry as well as underground/surface mining and rock drilling), several works have attempted to replicate – at the laboratory level – similar service-like conditions. Among them, the detrimental corrosion-related effects on tribological response and effective wear resistance of cemented carbides have aroused the greatest concern, mainly addressing microstructure-performance correlation from macroscopic and microscopic perspectives, e.g. Refs. [25–30]. A quite interesting outcome from these studies is the detailed understanding acquired on the damage mechanisms at the micro- and nanometric dimensions: cracking, fragmentation and easy removal of WC grains under (sliding) contact, directly associated with the mechanically unsupported, contiguous and binderless/porous carbide network left after exposure to corrosive media of the studied hardmetals. However, similar information linking corrosion-induced damage and contact mechanical response at relatively higher length scales is quite limited [31,32]. To fill this lack of knowledge, the present study aims to evaluate the influence of corrosion-induced changes on the contact damage response of cemented carbides, by implementing spherical indentation tests.

Following the experimental methodology and analysis procedure introduced and extensively developed by Lawn's group for studying ceramic materials using spherical indentation (see. Ref. [33] for a detailed review), the use of testing protocols based on Hertzian theory has proven to be quite successful on the assessment of mechanical response and damage induced under contact loading in both nude and coated cemented carbides [34–44]. In these studies, indentation has been conducted using spheres with curvature radii in the millimeter length scale. Thus, concentrated stresses are delivered over a small area of specimen surface such that typical “blunt” in-service conditions are simulated, indentation stress-strain curves may be attained, and damage evolution associated with increasing load can be examined. However, all the above studies have limited their scope to testing of pristine or virgin hardmetals. Hence, information on how the damage induced by corrosion may affect contact response for cemented carbides is completely lacking. Within the above framework, it is the aim of this investigation to determine and analyze the changes observed in the indentation stress-strain response as well as in surface/subsurface damage scenarios of hardmetals, after exposing them to an acidic media for different times. In doing so, addition of chromium and/or substitution of cobalt by nickel within the chemical nature of the metallic binder are invoked as experimental variables. Besides the mechanical study based on Hertzian indentation testing, the research is complemented with the combined use of advanced characterization techniques for assessment of surface and subsurface features.

2. Materials and experimental procedures

Three different medium-grained (between 1.3 and 1.5 μm in size) WC-base cemented carbides were investigated, and the corresponding microstructures are illustrated in Fig. 1. They were a set of experimental hardmetal grades supplied by Hyperion Materials and Technologies. Main microstructural and basic mechanical parameters, including binder content ($\%_{wt.}$) and addition (or not) of Cr_3C_2, mean grain size (d_{WC}), hardness (*HV30*) and Palmqvist indentation toughness (K_{Ic}) are detailed in Table 1. Mean size of WC grains was measured following the linear intercept method, using images acquired by means of Field Emission Scanning Electron Microscopy (FESEM). Hardness and indentation toughness were measured using a Vickers diamond pyramidal indentation and applying a load of 294 N. At least ten indentations were carried out for each grade, on diamond polished surfaces. Palmqvist indentation toughness (K_{Ic}) was evaluated using Shetty et al.'s Eq. [45].

Different levels of corrosion damage were introduced in a controlled way through simple immersion of specimens in stirred 0.1 M HCl solution at room temperature. In doing so, a constant volume of solution (250 ml) was employed for each condition, and stirring was conducted by using a magnetic rod with a rotation speed of 300 rpm. Samples exposed to acidic medium during 72, 168 and 264 h were used for determining the corrosion behavior of the investigated hardmetal grades. It was done by measuring the average corrosion front depth, out of cross-sectional views, using laser scanning confocal microscopy (LSCM). Furthermore, the interaction between corrosion damage and microstructure was inspected by means of Focused Ion Beam (FIB) and FESEM.

Assessment of the mechanical contact response by means of spherical indentation, in uncorroded and corroded specimens, was the main experimental activity in this study. Hertzian tests were conducted in a servo-hydraulic testing machine by using hardmetal indenters with a curvature radius (R) of 2.5 mm. Monotonic loading was conducted following a trapezoidal waveform, at a loading rate of 30 N s^{-1} and applying the full test force during 20 s. Applied loads ranged from 500 to 4000 N. At least three indentations were made at each load level. After mechanical testing, the contact radius (a) and residual indentation depth were measured, by means of LCSM, from the remnant impressions at each given load (P) after unloading. LSCM was also employed, under Nomarski illumination, for discerning surface damage produced by Hertzian contacts. Furthermore, critical loads for typical damage scenarios discerned in uncorroded and corroded specimen surfaces were determined in such inspection. Additionally, a high magnification inspection and analysis of damage features was carried out by means of FESEM.

Subsurface evolution of the indentation damage, with increasing corrosion time and applied load, was examined by conducting specific tests on “clamped-interface” specimens. The procedure followed for this examination is schematically outlined in Fig. 2. It includes five sequential stages [33,37,40,42,46–50]. First, pristine and corroded specimens were transversally cut to obtain different halves corresponding to each specific condition. Second, these two half-surfaces were set up together (into a mold of bakelite with the original top surfaces facing each other), and then ground and polished. Third, this mold was mechanically broken and the two halves were clamped again (this time into another mold of bakelite with the newly polished surfaces set up face-to-face). Fourth, uncorroded and corroded specimens were indented symmetrically across the surface trace on the interface. Fifth, once more time the two parts were mechanically separated, and polished cross-sections of corresponding half-surfaces were finally examined using LSCM and FESEM.

3. Results and discussion

3.1. Influence of microstructural phase assemblage on corrosion resistance

Fig. 3 shows cross-sectional micrographs for the three hardmetal grades studied, after exposure to the acidic solution during 72, 168 and 264 h, respectively. They reveal significant microstructural changes uniformly distributed at the surface and subsurface regions. As expected, longer immersion times yield more relevant changes as well as deeper corrosion fronts. Fig. 4 shows the measured values for the thickness of the degraded layer as a function of corrosion time. A linear relationship between corrosion front depth and time is discerned for the three cemented carbides studied. From the experimental data gathered, it is clear that Cr-containing grades (6CoCrM and 6NiCrM) are more resistant to the acidic medium than the Cr-free grade (6CoM). The corrosion rate of the latter ($\approx$ 1.7 μm/h) is about four times higher than those exhibited by the other two cemented carbides ($\approx$ 0.4 μm/h). Such a finding is in complete agreement with previous works by different research groups [11,13,14,16,17,21,23,32,51]. On the other hand, replacing most of the Co with Ni within the binder does not seem to improve corrosion resistance. This finding may be described as somehow unexpected, because it has been systematically reported that higher nickel content in the metallic binder yields superior performance, in terms of electrochemical figures of merit as well as less degradation depth under similar testing conditions (e.g. Refs.

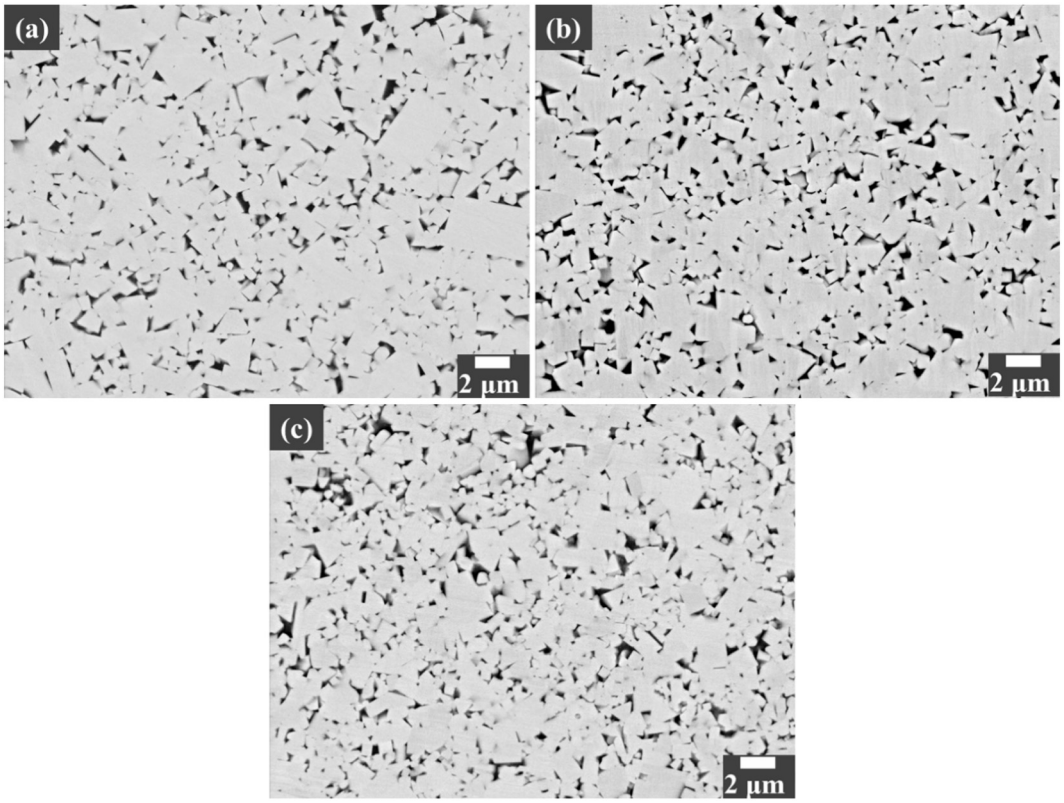

Fig. 1. FESEM micrographs of investigated cemented carbide grades:(a) 6CoM, (b) 6CoCrM, and (c) 6NiCrM.

Table 1
Microstructural and basic mechanical parameters for cemented carbides studied.

Specimen code	*wt%* binder	Addition of Cr_3C_2	d_{WC} (μm)	*HV30* (GPa)	K_{Ic} ($MPa_*m^{1/2}$)
6CoM	6Co	No	1.5 ± 0.2	16.0 ± 0.2	11.1 ± 0.2
6CoCrM	6Co	Yes*	1.4 ± 0.2	15.9 ± 0.1	11.0 ± 0.3
6NiCrM	5.5Ni-0.5Co	Yes*	1.3 ± 0.2	15.1 ± 0.1	10.0 ± 0.3

* Samples 6CoCrM and 6NiCrM contain a similar small amount of Cr_3C_2 (i.e. < 0.5%wt.)

[10,12,13,18]). Possible reasons for the results here attained could be ascribed to the relatively low binder content of the hardmetal grades and/or the relatively long corrosion times under consideration. However, evaluation and analysis of these single-side corrosion issues are beyond the scope of this study.

Detailed FIB/FESEM inspection of the cross-sections points out that discerned changes are mainly the result of a preferential attack of the metallic binder phases, which leads to porous/binderless WC skeletons throughout the affected layer. Very interesting, in the case of the Cr-containing hardmetal grades, part of the binder phase still remained undissolved near the surface of the specimen even after long exposure to 0.1 M HCl solution (264 h), as shown in Fig. 5b and c. Meanwhile,

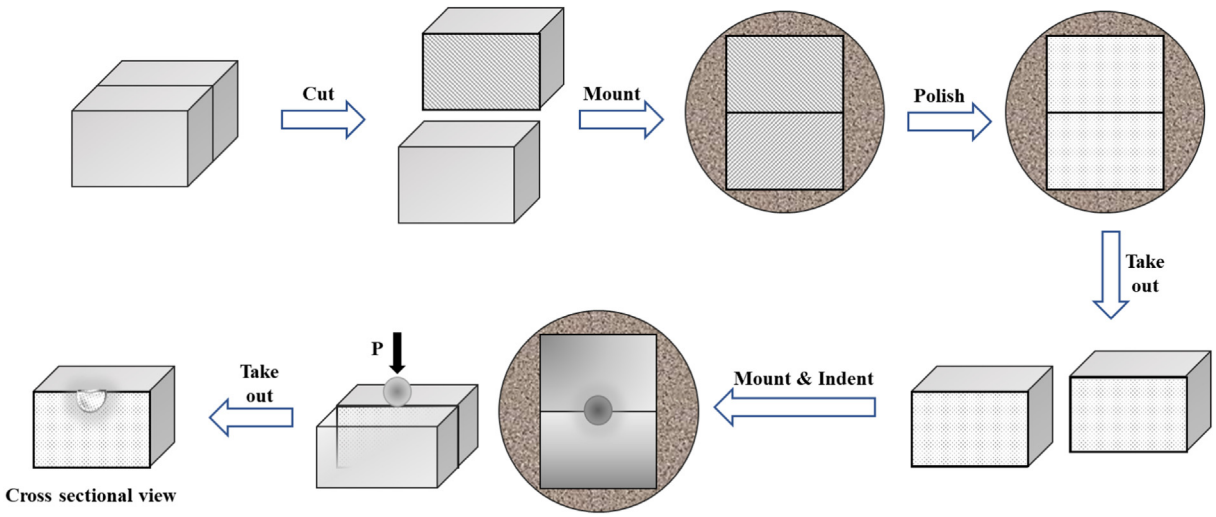

Fig. 2. Schematic representation of the bonding interface technique (BIT) procedure followed for sample preparation, in order to inspect and analyze the subsurface (cross-section) damage induced under Hertzian contact stresses.

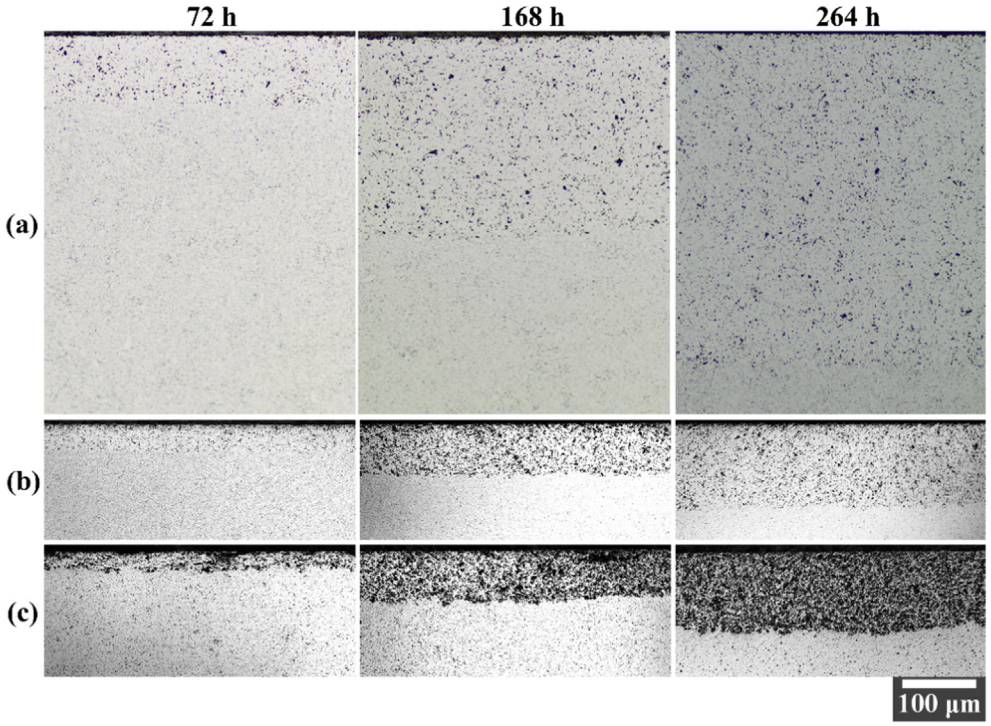

Fig. 3. Microstructural changes and induced degradation, after immersion in 0.1 M HCl solution (for 72, 168 and 264 h), discerned in cross-section images of (a) 6CoM, (b) 6CoCrM, and (c) 6NiCrM samples.

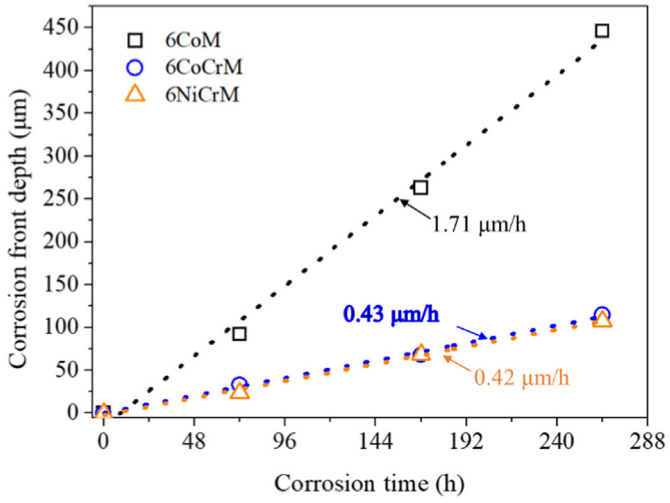

Fig. 4. Corrosion front depth as a function of exposure time, and corresponding degradation rates (slope) for the investigated hardmetal grades.

binder phase in the Cr-free grade is totally dissolved under similar testing conditions, leading to a completely binderless carbide skeleton (Fig. 5a). It may be rationalized by the fact that during sintering process of 6CoCrM and 6NiCrM hardmetal grades, chromium dissolves into the binder, leading to formation of a passivating binder-based chromium oxide layer which strongly inhibits the dissolution of the binder in acidic media [17,52].

3.2. Corrosion effects on the mechanical response under contact loading

Fig. 6 shows the residual indentation depth as a function of applied load for all the conditions studied. As expected, independent of hardmetal grade as well as pristine/corroded condition, the irreversible deformation gets more pronounced as indentation load increases. On the other hand, clear corrosion effects are discerned in terms of larger residual indentation depths of the materials previously exposed to the acidic medium.

Regarding experimental data analysis, it should be pointed out that data from Hertzian tests are usually presented in terms of contact pressure or indentation stress (p_0) as well as the resulting indentation strain (ε), e.g. Refs. [33,53]. Such approach was also implemented in this study. In doing so, p_0 and ε were calculated as $P/\pi a^2$ and a/R, respectively. Fig. 7 shows the corresponding indentation stress-strain (p_0-ε) curves measured for uncorroded and corroded specimens. Experimental data shown in Figs. 6 and 7 are limited to contact strains higher than 10%, as circumferential edges surrounding impressions were hard to define accurately for applied indentation loads below 1500 N. Within such stress-strain range, the mechanical response assessed for the hardmetals studied is similar to those reported in previous studies, and must be linked to quasi-plastic deformation phenomena [35–37,40]. An “apparent strain hardening” behavior is discerned in all the curves. Furthermore, a detrimental effect of corrosion on the load bearing capability of the three cemented carbides is evidenced, and it becomes more pronounced as exposure time is longer. However, such lessening effect – as given by lower relative differences between curves of uncorroded and corroded conditions – is less pronounced for 6CoCrM and 6NiCrM hardmetals, as it could be expected from their higher corrosion resistance as compared to the one exhibited by the Cr-free grade (6CoM).

Indentation stress-strain response seems to significantly depend on the depth of the corrosion affected zone. From a physical viewpoint, the degraded load-bearing capability evidenced must be attributed to the generation of porous/binderless corroded layers after corrosive exposure [28–31], as shown in Fig. 5. In this regard, based on recent findings reported by the authors for sharp indentation and scratch testing of corroded hardmetals [31], the degraded layer is not expected to play a significant role in the plastic yielding onset until its thickness reaches a certain value. Within this context, considering the overlapping of indentation stress-strain curves in Fig. 7b and c, it may be stated that corroded layers resulting from exposure to 72 h for 6NiCrM

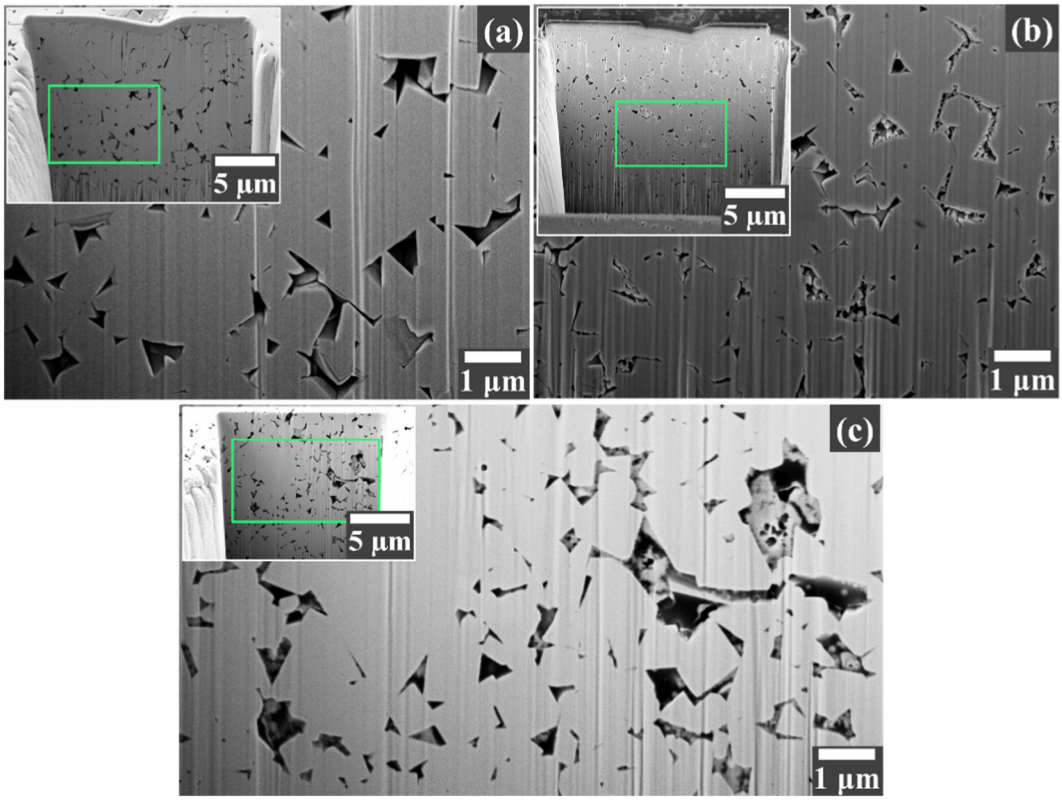

Fig. 5. FIB micrographs showing corrosion damage-microstructure interactions for (a) 6CoM, (b) 6CoCrM and (c) 6NiCrM samples immersed in 0.1 M HCl solution for 264 h.

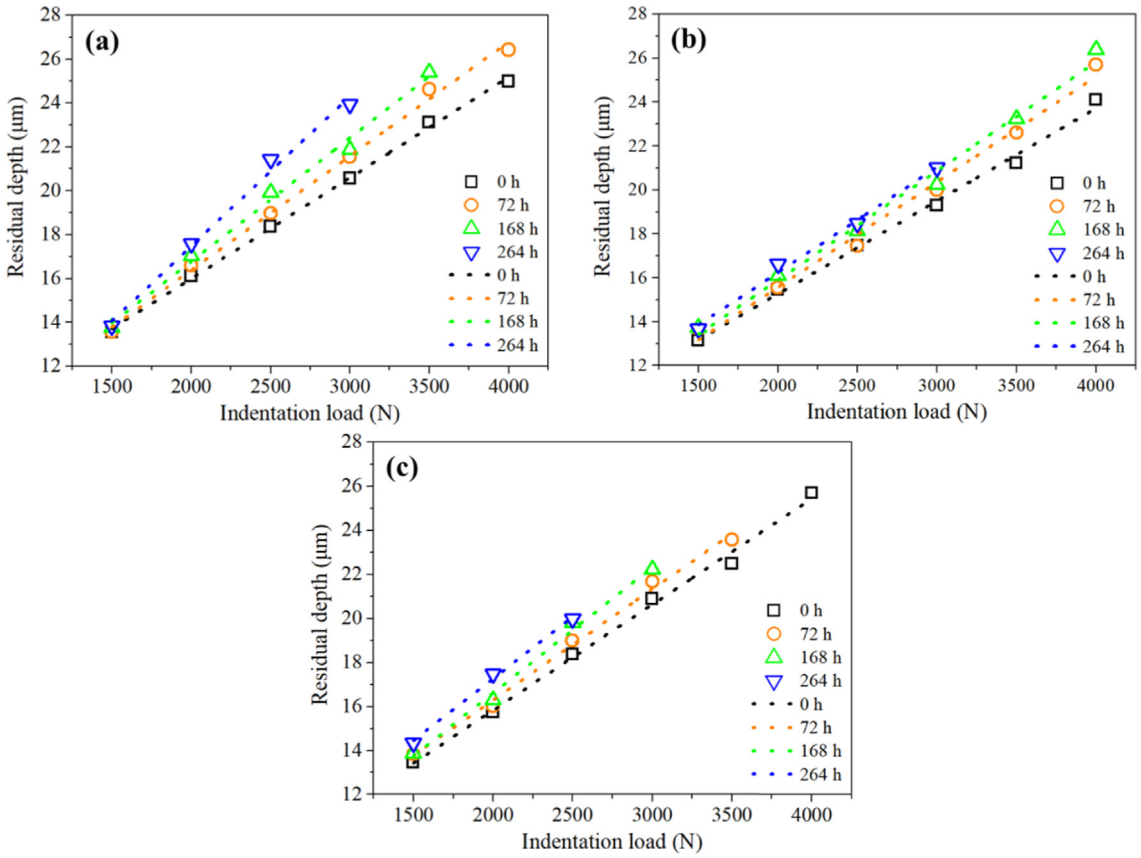

Fig. 6. Residual depth as a function of applied indentation load for uncorroded and corroded specimens for the three hardmetal grades studied: (a) 6CoM, (b) 6CoCrM, and (c) 6NiCrM.

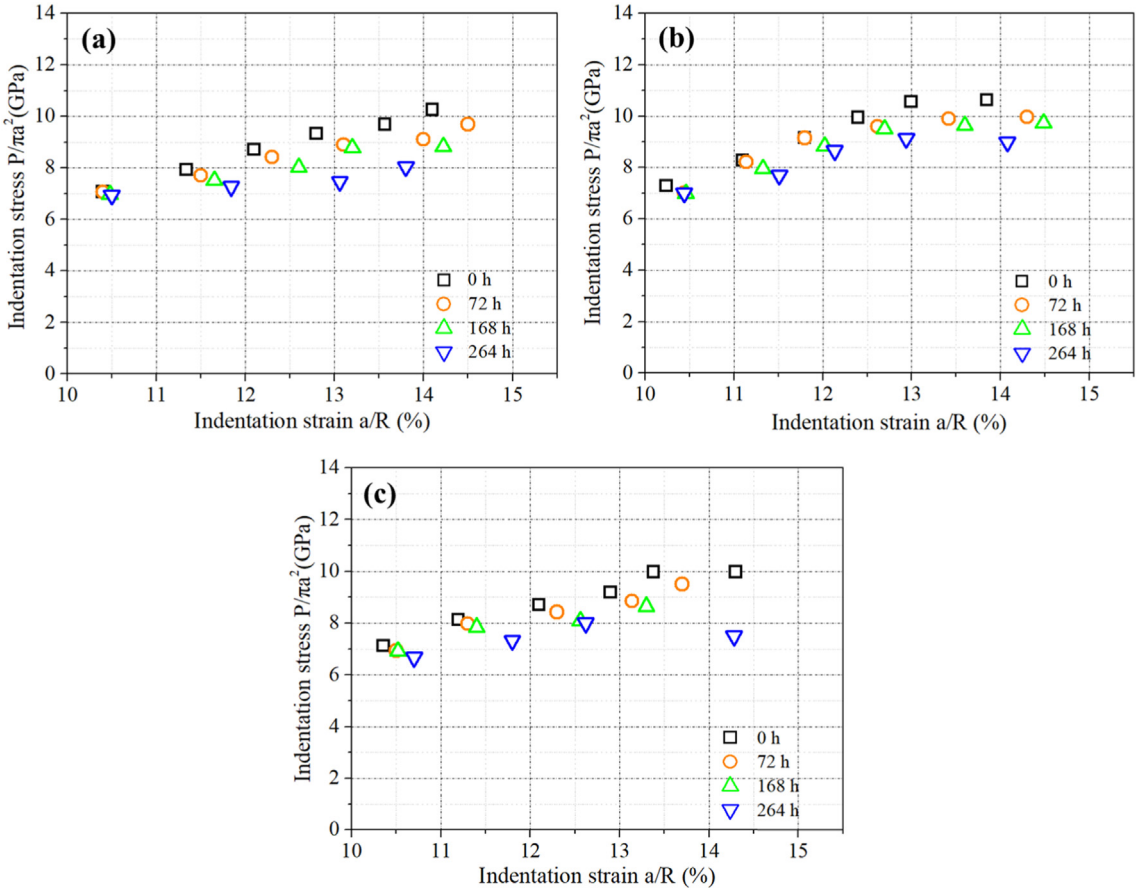

Fig. 7. Hertzian indentation stress-strain curves of (a) 6CoM, (b) 6CoCrM and (c) 6NiCrM hardmetal grades, as a function of corrosion time.

and 6CoCrM grades are thin enough, such that whole quasi-plastic deformation is still controlled by the uncorroded substrate. Such experimental finding is sustained by the very low ratio between layer thickness (about 25 μm) and indenter radius (2.5 mm), which would lead to maximum shear stresses placed within the base material [54,55]. On the other hand, as the thickness of the corrosion layer increases (from tens to hundreds of microns), the quasi-plastic deformation tends to be confined within the corroded layer. This is pointed out as the main reason for rationalizing the higher relative discrepancies among indentation stress-strain curves of pristine and corroded specimens, as corrosion time gets longer. For the extreme degradation condition (i.e. after exposure to acidic media for 264 h), indentation stress decay – measured on the basis of plateau values reached in the curves - is maximum for 6CoM (about 23%), intermediate for 6NiCrM (20%), and minimum for 6CoCrM (13%).

3.3. Corrosion effects on the evolution of surface damage induced by spherical indentation

The evolution of surface damage, from inelastic deformation to fracture, was assessed by means of an extensive and detailed visual inspection using LSCM. In agreement with previous studies [34–36,39,40], contact damage in pristine hardmetals was found to evolve, once residual imprints were already evidenced, from an initial partial ring crack which developed into a full ring crack as the indentation load increases (Fig. 8). Within this context, at load levels (higher than 2250 N) well-above the plastic yielding onset of the investigated hardmetal grades, the residual tensile radial stresses and strains at the regions close to the impression contour become large enough for inducing circumferential cracks at the surface of the tested specimens. Theoretical analysis of the residual surface stress distribution produced in a flat surface by a spherical indenter [56] points out that these residual stresses develop as the result of the superposition of elastic unloading stresses onto the stress at maximum load when the specimen has deformed plastically. Furthermore, it is stated that they move beyond the contact radius, so cracks would be expected to appear at $a/R > 1$. However, this was not discerned in this study, as ring cracks were found to nucleate just at the contour of the indentation imprint. Although reason for such discrepancy is unclear, it may be related to the undefined elastic-to-plastic transition within the mechanical response exhibited by cemented carbides [34–37,39], which could finally affect the effective residual stress state existing in the vicinity of the residual imprints. As it is extensively reported in the literature, irreversible deformation induced under contact loading in these materials – as well as in other “tough” ceramics - is not driven by conventional plastic deformation mechanisms, i.e. slip by dislocation movement. Instead, in those materials such transition is associated with quasi-plasticity phenomena, where internal shear-driven defects or faults with friction at sliding interfaces (e.g. microcracks) are commonly recalled for rationalizing it [35,36,39,40]. The fact that such discrepancy between theoretical analysis and experimental evidence is even more noticeable for corroded specimens (as it may be seen in Fig. 9) will support such hypothesis. In these degraded samples, binder is leached out at both surface and subsurface levels, yielding an effectively porous layer which enhances then the “quasi-plasticity” component in the contact damage response of the material under consideration [50]. Finally, and still analyzing the behavior of uncorroded specimens, it must be highlighted that under the experimental load conditions investigated (up to 4000 N) radial cracks outside the imprint, as an additional damage characteristic, were not observed in any of the hardmetal grades tested.

For the corroded cemented carbides, besides the similar evolution

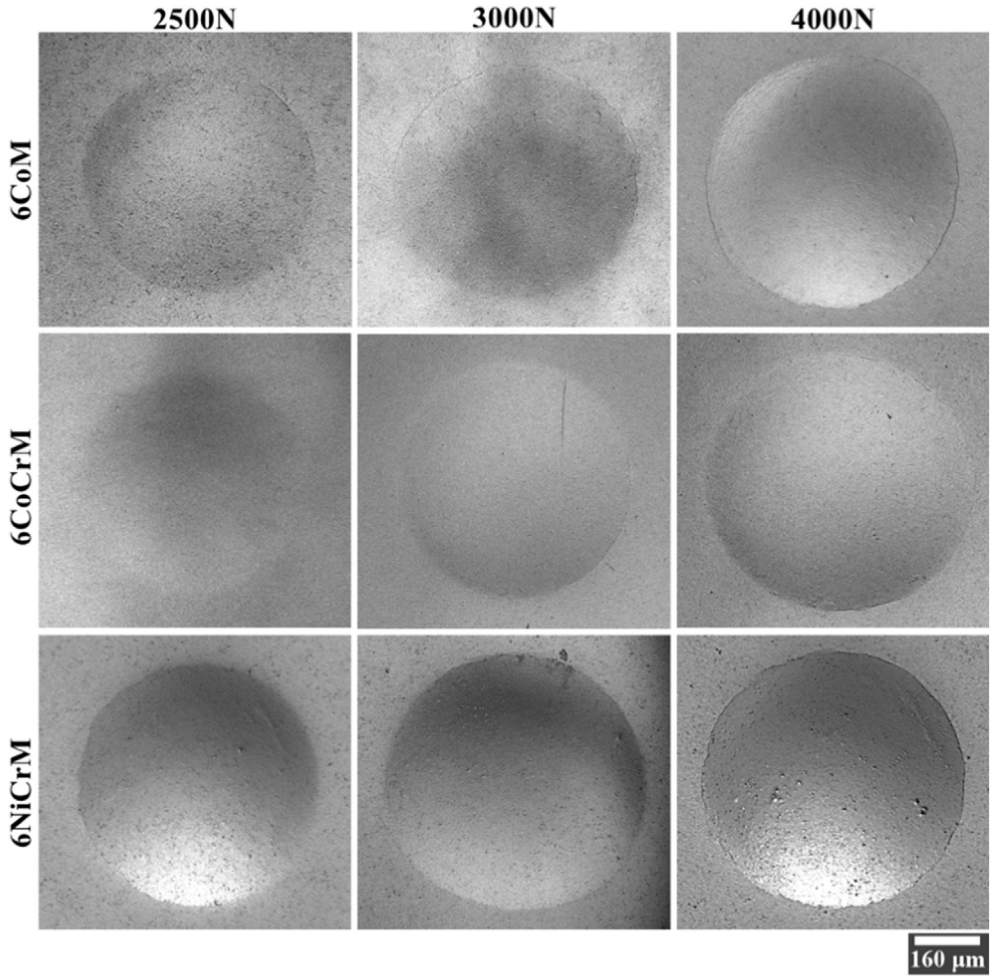

Fig. 8. Pristine (uncorroded) cemented carbides: damage features induced by spherical indentation under different applied loads (2500, 3000 and 4000 N).

discerned in terms of ring cracks, radial fissures and even specimen breakage were evidenced as additional damage features/scenarios under loading conditions evaluated in this study. Furthermore, critical loads for producing (partial/full) ring and radial cracks decrease as the corrosion time gets longer (Fig. 9). As reported in the literature [57], the critical load for emergence of ring cracks and the fracture toughness of the material are quadratically related. For cemented carbides, this means that such critical load level should be closely linked to microstructural parameters defining their toughening capability, i.e. volume fraction of the binder phase and/or carbide grain size. After exposure to acidic media, microstructural assemblage is degraded. Effective removal of the ductile metallic phase yields a loose and porous WC skeleton. Hence, the well-established toughening mechanism, based on ligament reinforcement mechanism [58–61], is no longer operative at the surface (and subsurface) level for corroded cemented carbides. Accordingly, the energy required for crack emergence and extension is lowered. On the other hand, as it was discussed above, the load-bearing capability of the studied hardmetal grades significantly depends on the thickness of the corroded layer. For relatively short exposure times (e.g. 72 h), corroded layers are rather thin, and the whole plastic deformation is mainly linked to the uncorroded hardmetal beneath it, which then effectively acts as a supporting substrate. As immersion time rises, the imposed deformation is shared by a thicker degraded layer and the uncorroded substrate. Finally, after 264 h immersion, deformation gets finally confined in the corroded layer; and thus, deformation and damage scenarios observed are those intrinsically related to the mechanical response of the binderless WC skeletons. Considering the loose and porous WC networks left after the binder is leached away, the shear stress during the unloading may be more likely to cause the initiation of radial cracks in the edge of the plastic zone. In this regard, residual porosity - after binder has been removed - acts not only as an assemblage of many small stress concentrators but also as crack precursors [62]. Indeed, such porous-like nature of the degraded layer must also be responsible for the interesting observation that initiation of these radial cracks is found to be located within the contact zone (Fig. 9), instead of outside it – as a simple extension outwards of the previously developed ring cracks, as it could be expected. Within this context, porosity is speculated to play a critical role not only by affecting the effective redistribution of the resulting residual stresses and strains after unloading (as recalled above), but also by introducing changes in the quasi-plastic damage scenario, i.e. local compaction and structural breakdown, followed by possible intrusion of material into the binderless cavities or growth and coalescence of interpore cracks [50]. In general, for ceramic materials, the formation of radial cracks heralds the end of the service life of engineering components [36]. Thus, it may be stated that premature failure will appear during the service of hardmetal tools and components involving corrosion and impact loading conditions simultaneously.

The information experimentally gathered and discussed above is summarized in Fig. 10. Representative images of identified damage events (symbols) in uncorroded and corroded specimens are also included in such a figure. For all the uncorroded specimens damage evolution is quite similar. As applied load is increased within the range of 2000–4000 N, incipient cracks emerge, propagate and coalesce, yielding full ring fissures at a load level of 3500 N in the three cases. Minor differences are observed in terms of resistance to generation of

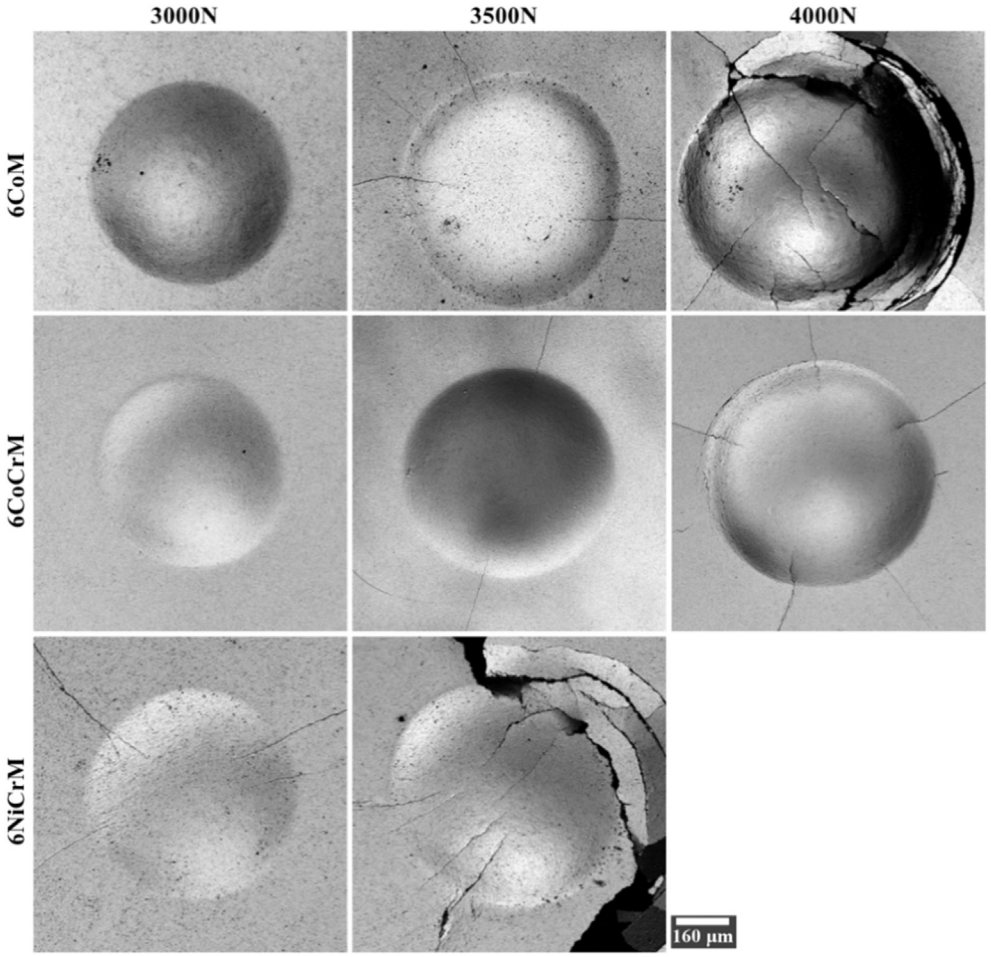

Fig. 9. Corroded (after 168 h immersion) cemented carbides: damage features induced by spherical indentation under different applied loads (3000, 3500 and 4000 N).

the incipient cracks. In this regard, Co-base grades show a slightly better behavior, possibly affiliated to their higher hardness-toughness (Table 1) correlation, as compared to the one exhibited by the 6NiCrM grade. Nevertheless, it is worth noting that partial/full ring cracks in 6CoM and 6NiCrM grades are somehow more visible than those observed in 6CoCrM, under the same loading condition (Fig. 8). Concerning the specimens previously exposed to acidic media and then tested, Fig. 10 clearly points out the lessening effects of corrosion on the resistance to nucleation and development of contact damage. This is quite clear in terms of both lower critical loads for the emergence of incipient cracks, and more severe damage evolution scenarios, in agreement with works published recently [31,32]. Regarding the former, it can be directly attributed to binder removal and the consequent loss of the main (intrinsic) toughening mechanism in the materials under consideration, as discussed above. The latter is supported by the observation of radial cracking and even specimen breakage as the applied load rises (Fig. 9), phenomena only discerned in pristine cemented carbides under much higher load levels ($> 20{,}000$ N, using a rigid indenter of 5.08 mm in radius) [36].

Following the above ideas, the load levels required for discerning the distinct damage events previously documented and discussed (i.e. incipient ring crack, full ring crack, radial crack, specimen breakage) are here proposed as merit figures for material selection under service-like conditions involving both corrosion and contact loads. Within this context, the results of this work indicate the 6CoCrM hardmetal grade as the best option among the three cemented carbides studied. Direct comparison with 6CoM points out that addition of chromium is a key factor, as it is helpful not only in refining the microstructure but also in improving the corrosion resistance (Table 1 and Fig. 4). On the other hand, analysis of the responses exhibited by 6CoCrM and 6NiCrM grades allows to assess the relevant and compromising influence of chemical nature of the binder. In this regard, even though replacement of Co with Ni seems to yield a less pronounced microstructural degradation, at least at the microstructural length scale (Fig. 5), due to exposure to acidic medium, it is clear that contact mechanical response of corroded 6NiCrM specimens is lower than the one exhibited by similarly degraded 6CoCrM specimens (Figs. 9 and 10). This is particularly true when referring to damage events taken place at relatively higher load levels, such as emergence of radial fissures and specimen breakage. These relative differences in contact damage response should also be intrinsically related to higher hardness-toughness correlations exhibited by WC-Co systems, as compared to WC-Ni ones, as commented before.

In order to further understand corrosion effects on surface deformation and damage mechanisms for the hardmetal grades studied, a detailed inspection at heavily deformed zones was carried out by means of FESEM. Fig. 11 shows images corresponding to residual imprints after indenting uncorroded and corroded 6NiCrM specimens to a load level of 3500 N. Concerning the uncorroded condition, a well-developed full ring crack is discerned, due to tensile radial stresses and strains existing in the vicinity of the residual imprints [63]. Fig. 11a-1 shows that the crack path mainly transverses the two-phase microstructure, following binder regions – close to binder/carbide interfaces – and/or WC grain boundaries. The indented zone shows a slightly damaged scenario involving several plastically deformed WC grains marked by blue arrows (evidenced by the slip lines on their surfaces)

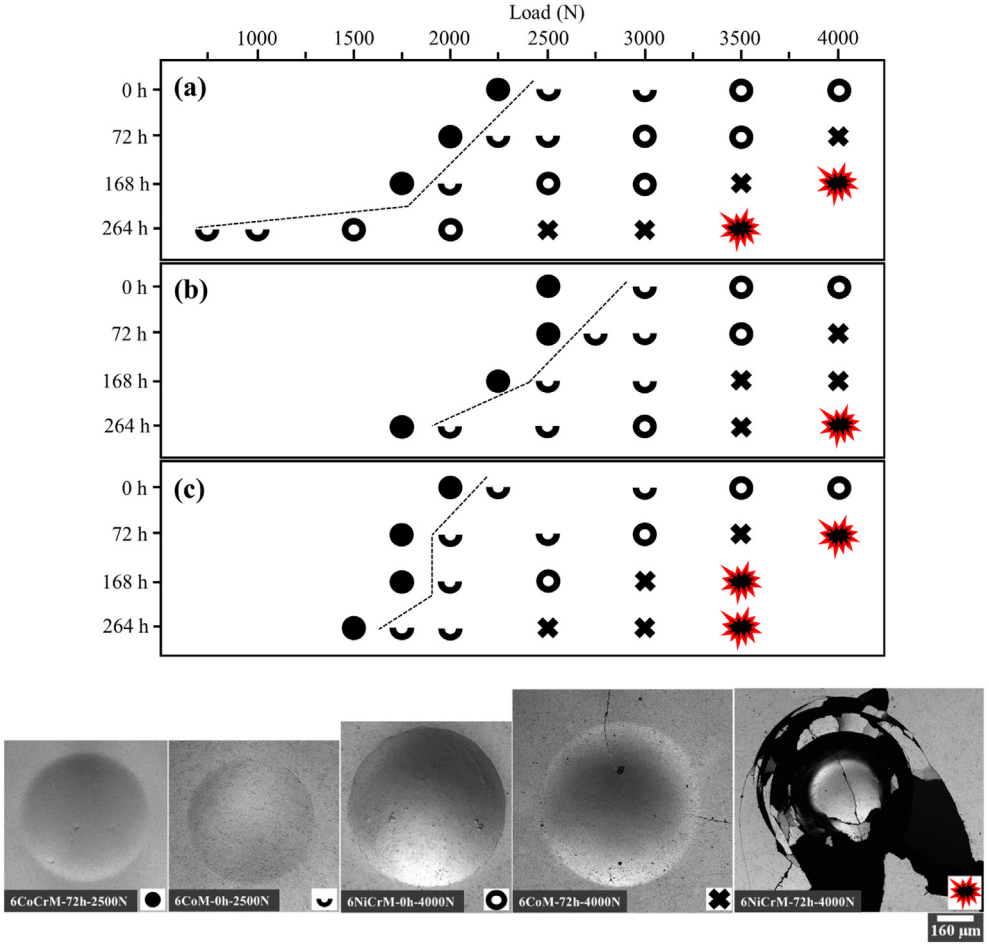

Fig. 10. Damage evolution diagram for (a) 6CoM, (b) 6CoCrM, and (c) 6NiCrM samples as a function of indentation load and corrosion time. Main damage features ascribed to each symbol (no cracks, partial ring crack, full ring crack, radial crack, and specimen breakage) are shown within the legend, including images of representative events.

and some edge broken particles marked by red arrows (Fig. 11a-2). Under effective compression loading, plastic deformation occurs preferentially in the binder phase. Meanwhile, the WC carbide starts to deform when the motion of dislocations in the binder phase is hindered due to work hardening [64–67]. For the corroded specimen, under similar loading conditions (Fig. 11b-1), in the vicinity of the residual impression a radial crack (yellow arrows) intersects a ring crack (light blue arrows). Meanwhile, due to the dissolution of the binder phase, radial crack appears as well-developed, accompanied by significant WC grain removal in the crack propagation path (Fig. 11b-2). In this regard, radial cracks seem to initiate within the contact zone, and then spread out from underneath the residual impression and propagate outwards, away from the impression contour. This observation is consistent with previous studies regarding spherical indentation test performed on pristine hardmetal at a quite high load level [36]. On the other hand, the damage scenario near the residual impression center is significantly different from the one evidenced in the uncorroded specimen. As it may be seen in Fig. 11b-3, besides plastic deformation many WC particles exhibit cracks and are even fragmented. Moreover, micrometric cavities are often evidenced, as a result of carbides dislodged during the contact load test. Hence, required accommodation of the imposed irreversible deformation results in deformation of single WC grains, particle cracking and fragmentation, as well as small-scale local collapse of the unsupported (binderless and porous) carbide network [30].

3.4. Subsurface damage scenario: Inspection of indented "clamped-interface" specimens

Microstructural changes induced at the subsurface level were assessed by preparing and indenting "clamped-interface" specimens. Fig. 12 shows FESEM images of indentation damage scenarios at a low load level (750 N), for both non-corroded and corroded conditions. For the pristine hardmetal, a conventional crack-microstructure interaction, involving fissures extending throughout metallic binder regions is evidenced (Fig. 12a) [58–60]. On the other hand, for the corroded specimens, the damage scenario is dominated by carbides overlapping over each other, as well as grains pulled-out in the heavily damaged zone (Fig. 12b). This is directly related to the poor subsurface integrity associated with the porous-like and binderless corroded layer, which is not able to provide sufficient load-bearing capability. Furthermore, angles of cone-like cracks are less acute and defined in the deformed zone of the corroded condition. In ceramic materials, such a trend has been found as R-curve (crack growth resistance) behavior gets less pronounced [68]. Hence, considering that R-curve behavior is directly related to ductile ligament reinforcement behind the crack tip in pristine hardmetals (e.g. Refs. [60,61]), above experimental findings should be attributed to the absence of toughening mechanisms related to the binder in the degraded layer [68].

Fig. 13 shows images corresponding to the subsurface damage scenario at a relatively high load level (1500 N) for both non-corroded and corroded conditions. For the pristine specimen, the deformed zone is mainly composed of WC grains with a large density of slip bands

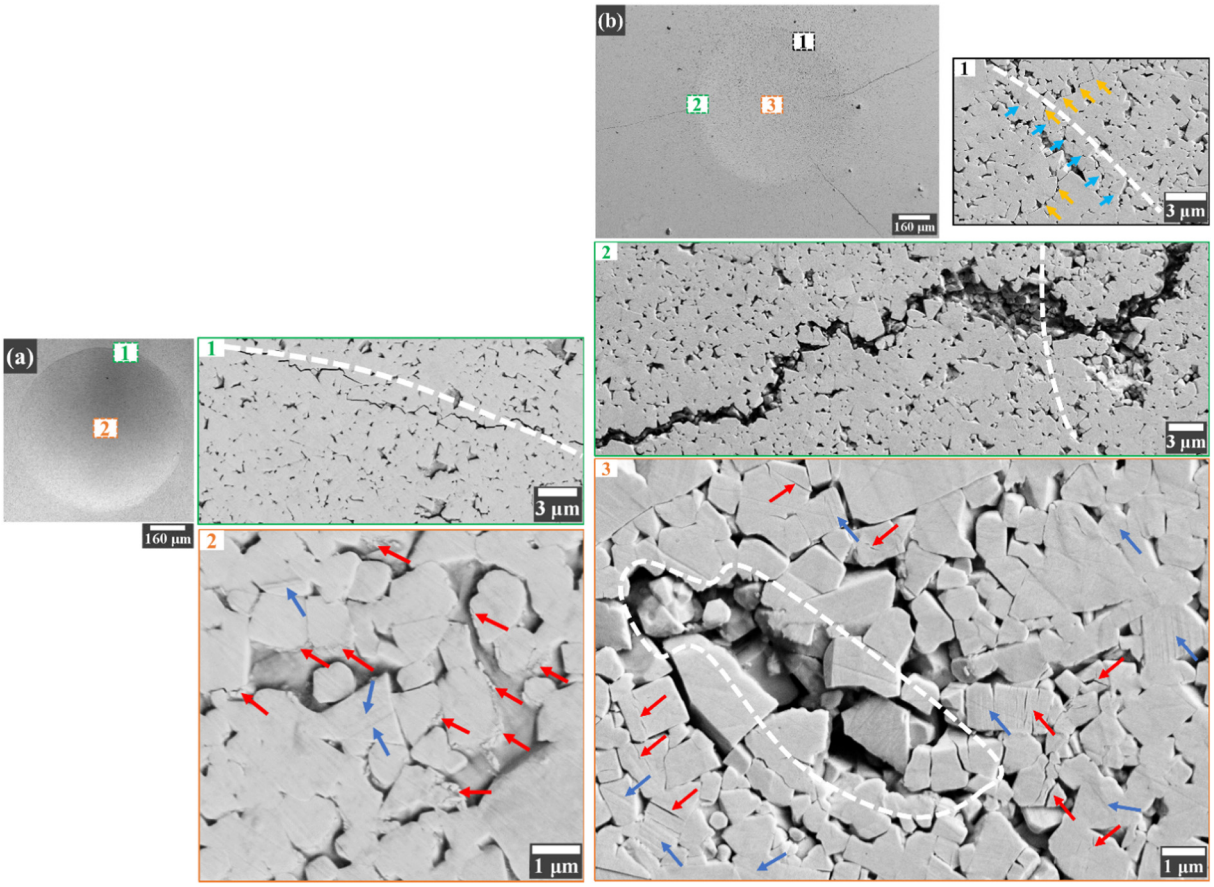

Fig. 11. FESEM images of indented areas (residual imprints) for 6NiCrM specimens under applied load of 3500 N: (a) uncorroded and (b) corroded (72 h).

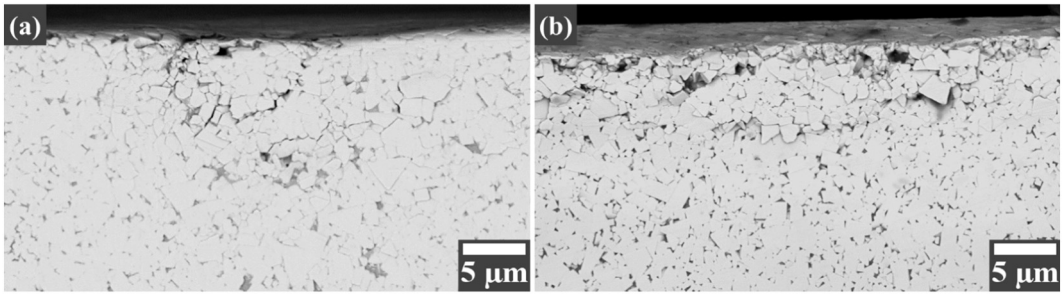

Fig. 12. Hertzian indentation damage discerned on the side view of indentation of one of the two halves of the bonded specimens in: (a) non-corroded 6NiCrM at load of 750 N, and (b) corroded 6CoCrM (72 h of corrosion) at load of 500 N.

(Fig. 13a-1). Although it cannot be ascertained from the shown micrograph, it may be speculated that plastic deformation of binder phase also plays a key role in this process [36,39,67]. Concerning the corroded specimen, the damage scenario is dominated by microcracks in the degraded layer, i.e. quite different from that found in the virgin material (Fig. 13b-1). In this regard, due to the removal of the ductile metallic phase, microcracks are more likely to initiate and propagate. It may be rationalized by considering the direct consequences of the binder being leached out. On one hand, leached binder leaves effective pores which may act as stress concentrators and crack precursors within binderless WC skeleton. On the other one, lack of binder implies that toughening mechanisms associated with ductile ligament reinforcement are now completely absent; and thus, energy required for subcritical crack propagation is effectively much lower than for the pristine condition [30–32]. Hence, induced microcracks may lead to catastrophic failure of the specimen as they propagate, interact and finally coalesce to form long cracks [31–33,50,69,70]. However, it is interesting to highlight that there is not any cracking feature in the region below the interface between the uncorroded and corroded zone (Fig. 13b-2). It indirectly sustains the large load-bearing and toughening capability of the cemented carbides (pristine condition) investigated, through energy absorption by quite effective deformation mechanisms of their two constitutive phases: the binder metallic phase and the ceramic WC grains.

Finally, when comparing the deformation and fracture scenarios obtained from BIT (Figs. 12 and 13) with that from the integral (bulk) specimen discussed above, it is clear that the former is more severe than the latter regarding emergence of microcracks at each specific loading condition. This is consistent with previous studies reported in the literature [42,48]. In the clamped specimens, the centerline of the indentation is at the artificial interface between the two halves, which cannot support the indenter as effectively as in a real bulk material. Thus, the interface edges are more prone to collapse, leading to a corresponding shift of the maximum stress field away from the bonded-

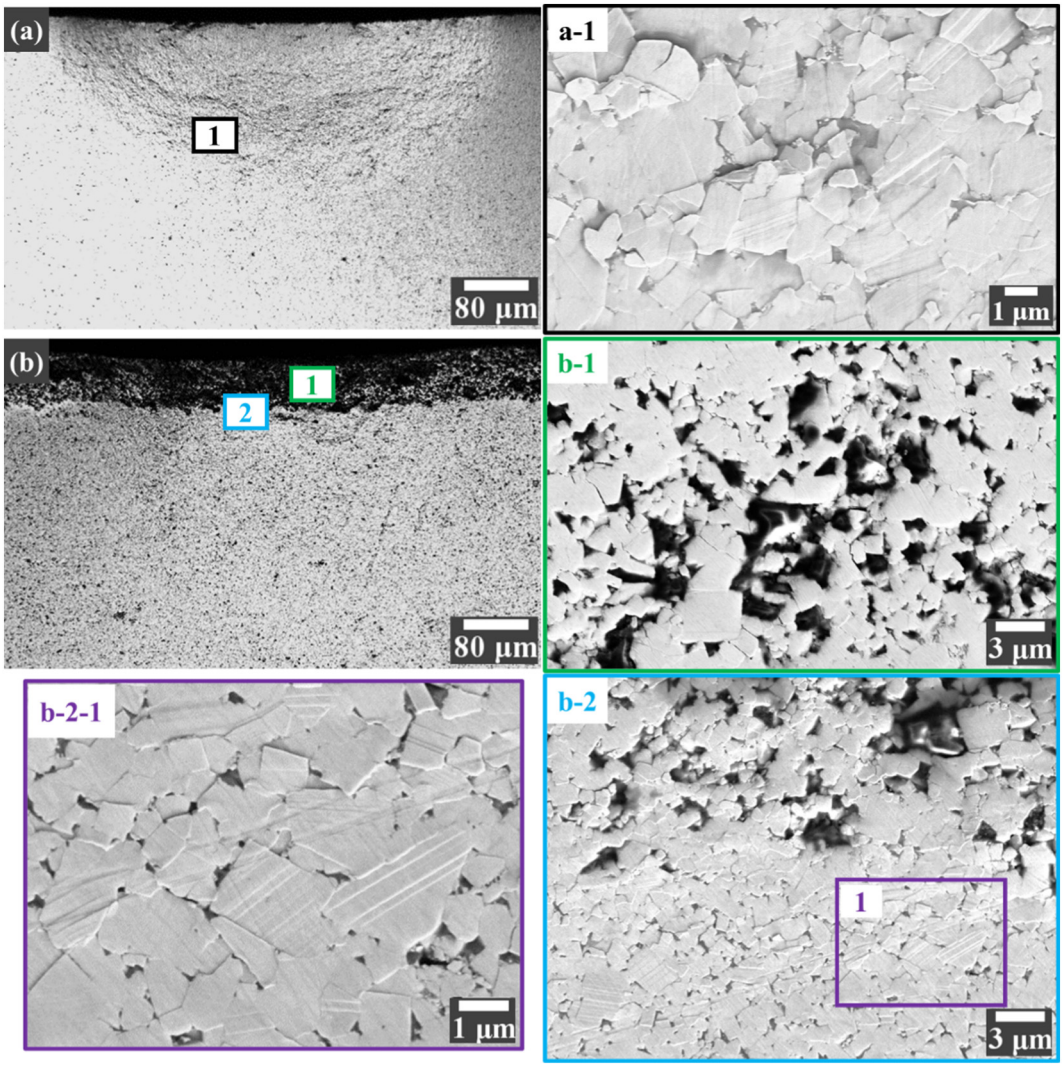

Fig. 13. 6NiCrM "clamped-interface" specimens indented at a load level of 1500 N: micrographs of subsurface damage for (a) uncorroded, and (b) corroded (168 h) conditions. The FESEM images are the enlarged views of the corresponding square areas, where black, green, light blue, and purple represent the damage scenario in the severely deformed area of the uncorroded sample, the corroded area, the area near the corrosion front, and the uncorroded area below the corrosion front, respectively. (For interpretation of the references to colour in this figure legend, the reader is referred to the web version of this article.)

interface. In this sense, since the interface edge is unsupported by the gap over its whole length, the weaker grain boundaries and friction would have a more pronounced effect than within the bulk of the material [42,48].

4. Conclusions

The influence of corrosion on mechanical response and damage scenario under Hertzian indentation for cemented carbides with binders of different chemical nature has been investigated. From the experimental findings and corresponding analysis, the following conclusions may be drawn:

1) Corroded cemented carbides exhibit a lower load-bearing capability than pristine ones. This is reflected by an increased indentation depth at a given applied load, i.e. a lower stress-strain response. In general, corrosion-induced lessening effects are found to depend on the ratio between indentation depth and thickness of the corroded layer; and thus, on the effective substrate-like role played by the underneath non-corroded hardmetal. In this regard, as exposure time to acid medium gets longer, the resulting and continuously thicker corroded layer gradually substitutes the uncorroded substrate as main responsible for controlling the quasi-plastic deformation induced by the indentation. As a consequence of the higher intrinsic corrosion resistance of hardmetal grades containing Cr (6CoCrM and 6NiCrM), as compared to the the Cr-free grade (6CoM), such detrimental effects are more pronounced in the latter than in the former.
2) The detrimental influence of corrosion is particularly evidenced in terms of contact damage: lower critical loads for the emergence of incipient cracks, and more severe evolution scenarios at the surface level. Considering these parameters as figures of merit for material selection, the hardmetal grade 6CoCrM is then proposed as the best option, as compared to the other two cemented carbides studied, for applications involving corrosion and contact loads. Such a finding points out the synergic and compromising effect of corrosion resistance linked to Cr addition and higher hardness-toughness correlation affiliated to Co (within the context of WC-Co systems, as compared to WC-Ni ones) for achieving an optimized performance under service-like conditions.
3) Significant corrosion effects on contact response are also evidenced at the subsurface level, in terms of deformation/damage micromechanisms. In this regard, the deformation-shared scenario commonly evidenced in pristine hardmetals is found to change into one

dominated by microcracks, emerging and evolving from cavities within the porous/binderless WC skeletons left after corrosion. At relatively high loads and independent of chemical nature of the binder, it finally yields radial fissures and even specimen failure under spherical indentation testing.

Declaration of Competing Interest

The authors declare no conflict of interest.

Acknowledgements

This work was financially supported by the collaborative Industry-University program between Hyperion Materials & Technologies and Universitat Politècnica de Catalunya, and partly funded by the Spanish Ministerio de Economía y Competitividad, and Ciencia e Innovación, through Grants MAT2015-70780-C4-3-P (MINECO/FEDER) and PID2019-106631GB-C41, respectively. Y.F. Zheng acknowledges the Ph.D. scholarship received from China Scholarship Council (No. 201706890018, Beijing, China).

References

[1] H.E. Exner, Physical and chemical nature of cemented carbides, Int. Met. Rev. 24 (1979) 149–173, https://doi.org/10.1179/imtr.1979.24.1.149.
[2] B. Roebuck, E.A. Almond, Deformation and fracture processes and the physical metallurgy of WC–Co hardmetals, Int. Mater. Rev. 33 (1988) 90–112, https://doi.org/10.1179/imr.1988.33.1.90.
[3] E. Jiménez-Piqué, M. Turon-Vinas, H. Chen, T. Trifonov, J. Fair, E. Tarrés, L. Llanes, Focused ion beam tomography of WC-Co cemented carbides, Int. J. Refract. Met. Hard Mater. 67 (2017) 9–17, https://doi.org/10.1016/j.ijrmhm.2017.04.007.
[4] J. García, V. Collado Ciprés, A. Blomqvist, B. Kaplan, Cemented carbide microstructures: a review, Int. J. Refract. Met. Hard Mater. 80 (2019) 40–68, https://doi.org/10.1016/j.ijrmhm.2018.12.004.
[5] L. Prakash, Fundamentals and general applications of hardmetals, in: V.K. Sarin, D. Mari, L. Llanes (Eds.), Comprehensive Hard Materials, Volume 1 - Hardmetals, Elsevier, Oxford (UK, 2014, pp. 29–90, , https://doi.org/10.1016/B978-0-08-096527-7.00002-7.
[6] V.A. Pugsley, G. Korn, S. Luyckx, H.G. Sockel, W. Heinrich, M. Wolf, H. Feld, R. Schulte, The influence of a corrosive wood-cutting environment on the mechanical properties of hardmetal tools, Int. J. Refract. Met. Hard Mater. 19 (2001) 311–318, https://doi.org/10.1016/S0263-4368(01)00059-2.
[7] R. Lu, L. Minarro, Y.-Y. Su, R.M. Shemenski, Failure mechanism of cemented tungsten carbide dies in wet drawing process of steel cord filament, Int. J. Refract. Met. Hard Mater. 26 (2008) 589–600, https://doi.org/10.1016/j.ijrmhm.2008.01.009.
[8] P.K. Katiyar, P.K. Singh, R. Singh, A.I. Kumar, Modes of failure of cemented tungsten carbide tool bits (WC/Co): a study of wear parts, Int. J. Refract. Met. Hard Mater. 54 (2016) 27–38, https://doi.org/10.1016/j.ijrmhm.2015.06.018.
[9] H.G. Jones, S.M. Norgren, M. Kritikos, K.P. Mingard, M.G. Gee, Examination of wear damage to rock-mining hardmetal drill bits, Int. J. Refract. Met. Hard Mater. 66 (2017) 1–10, https://doi.org/10.1016/j.ijrmhm.2017.01.013 0263-4368.
[10] W.J. Tomlinson, C.R. Linzell, Anodic polarization and corrosion of cemented carbides with cobalt and nickel binders, J. Mater. Sci. 23 (1988) 914–918, https://doi.org/10.1007/BF01153988.
[11] W.J. Tomlinson, N.J. Ayerst, Anodic polarization and corrosion of WC–Co hard metals containing small amounts of Cr_3C_2 and/or VC, J. Mater. Sci. 24 (1989) 2348–2352, https://doi.org/10.1007/BF01174495.
[12] A.M. Human, H.E. Exner, The relationship between electrochemical behaviour and in-service corrosion of WC based cemented carbides, Int. J. Refract. Met. Hard Mater. 15 (1997) 65–71, https://doi.org/10.1016/S0263-4368(96)00014-5.
[13] B. Bozzini, G.P. De Gaudenzi, M. Serra, A. Fanigliulo, F. Bogani, Corrosion behaviour of WC-Co based hardmetal in neutral chloride and acid sulphate media, Mater. Corros 53 (2002) 328–334, https://doi.org/10.1002/1521-4176(200205)53:5<328::AID-MACO328>3.0.CO;2-G.
[14] S. Sutthiruangwong, G. Mori, Corrosion properties of Co-based cemented carbides in acidic solutions, Int. J. Refract. Met. Hard Mater. 21 (2003) 135–145, https://doi.org/10.1016/S0263-4368(03)00027-1.
[15] B. Bozzini, G.P. De Gaudenzi, A. Fanigliulo, C. Mele, Electrochemical oxidation of WC in acidic sulphate solution, Corros. Sci. 46 (2004) 453–469, https://doi.org/10.1016/S0010-938X(03)00146-X.
[16] S. Sutthiruangwong, G. Mori, Influence of refractory metal carbide addition on corrosion properties of cemented carbides, Mater. Manuf. Process. 20 (2005) 47–56, https://doi.org/10.1081/AMP-200041607.
[17] S. Sutthiruangwong, G. Mori, R. Kösters, Passivity and pseudopassivity of cemented carbides, Int. J. Refract. Met. Hard Mater. 23 (2005) 129–136, https://doi.org/10.1016/j.ijrmhm.2004.11.006.
[18] C.F. Barbatti, F. Sket, J. Garcia, A. Pyzalla, Influence of binder metal and surface treatment on the corrosion resistance of (W,Ti)C-based hardmetals, Surf. Coat. Tech. 201 (2006) 3314–3327, https://doi.org/10.1016/j.surfcoat.2006.07.135.
[19] S. Hochstrasser, Y. Mueller, C. Latkoczy, S. Virtanen, P. Schmutz, Analytical characterization of the corrosion mechanisms of WC–Co by electrochemical methods and inductively coupled plasma mass spectroscopy, Corros. Sci. 49 (2007) 2002–2020, https://doi.org/10.1016/j.corsci.2006.08.022.
[20] F.J.J. Kellner, H. Hildebrand, S. Virtanen, Effect of WC grain size on the corrosion behaviour of WC-Co based hardmetals in alkaline solutions, Int. J. Refract. Met. Hard Mater. 27 (2009) 806–812, https://doi.org/10.1016/j.ijrmhm.2009.02.004.
[21] Ž. Alar, V. Alar, T. Aleksandrov Fabijanić, Electrochemical corrosion behavior of near-nano and nanostructured WC-Co cemented carbides, Metals 7 (2017) 69, https://doi.org/10.3390/met7030069.
[22] W. Tang, L. Zhang, Y. Chen, H. Zhang, L. Zhou, Corrosion and strength degradation behaviors of binderless WC material and WC-Co hardmetal in alkaline solution: a comperative investigation, Int. J. Refract. Met. Hard Mater. 68 (2017) 1–8, https://doi.org/10.1016/j.ijrmhm.2017.06.003.
[23] Y.F. Zheng, G. Fargas, E. Armelin, O. Lavigne, L. Llanes, Corrosion-induced damage and residual strength of WC-Co,Ni cemented carbides: influence of microstructure and corrosion medium, Metals 9 (2019) 1018, https://doi.org/10.3390/met9091018.
[24] A.M. Ferro Rocha, A.C. Bastos, J.P. Cardoso, F. Rodrigues, C.M. Fernandes, E. Soares, J. Sacramento, A.M.R. Senos, M.G.S. Ferreira, Corrosion behaviour of WC hardmetals with nickel-based binders, Corros. Sci. 147 (2019) 384–393, https://doi.org/10.1016/j.corsci.2018.11.015.
[25] U.B.H. Engqvist, N. Axen, The influence of pH on sliding wear of WC-based materials, Int. J. Refract. Met. Hard Mater. 18 (2000) 103–109, https://doi.org/10.1016/S0263-4368(00)00007-X.
[26] A.J. Gant, M.G. Gee, A.T. May, Microabrasion of WC-Co hardmetals in corrosive media, Wear 256 (2004) 954–962, https://doi.org/10.1016/j.wear.2003.09.003.
[27] M.R. Thakare, J.A. Wharton, R.J.K. Wood, C. Menger, Investigation of micro-scale abrasion–corrosion of WC-based sintered hardmetal and sprayed coating using in situ electrochemical current-noise measurements, Wear 267 (2009) 1967–1977, https://doi.org/10.1016/j.wear.2009.06.006.
[28] M.G. Gee, Model scratch corrosion studies for WC/Co hardmetals, Wear 268 (2010) 1170–1177, https://doi.org/10.1016/j.wear.2010.01.004.
[29] A.J. Gant, M.G. Gee, D.D. Gohil, H.G. Jones, L.P. Orkney, Use of FIB/SEM to assess the tribo-corrosion of WC/Co hardmetals in model single point abrasion experiments, Tribol. Int. 68 (2013) 56–66, https://doi.org/10.1016/j.triboint.2012.11.008.
[30] Y.F. Zheng, G. Fargas, H. Besharatloo, M. Serra, J.J. Roa, E. Armelin, O. Lavigne, L. Llanes, Assessment of corrosion-induced changes on the mechanical integrity of cemented carbides at small length scales, Int. J. Refract. Met. Hard Mater. 84 (2019) 105033, , https://doi.org/10.1016/j.ijrmhm.2019.105033.
[31] Y.F. Zheng, G. Fargas, O. Lavigne, L. Llanes, Indentation and scratch testing of a WC-6%wtCo cemented carbide: corrosion effects on load-bearing capability and induced damage, Ceram. Int. 46 (2020) 17591–17598, https://doi.org/10.1016/j.ceramint.2020.04.059.
[32] J.J. Roa, S. Simison, J. Grasso, M. Arcidiacono, L. Escalada, F. Soldera, J. García, A.D. Sosa, Cyclic contact fatigue of cemented carbides under dry and wet conditions: Correlation between microstructure, damage and electrochemical behavior, Int. J. Refract. Met. Hard Mater. 92 (2020) 105279, , https://doi.org/10.1016/j.ijrmhm.2020.105279.
[33] B.R. Lawn, Indentation of ceramics with spheres: a century after Hertz, J. Am. Ceram. Soc. 81 (1998) 1977–1994 https://doi.org/10.1111/j.1151-2916.1998.tb02580.x.
[34] E. Tarrés, Y. Torres, M. Anglada, L. Llanes, Daño por contacto hertziano en carburos cementados WC–Co: influencia de la microestructura y de los parámetros de contacto, Anales de Mecánica de la Fractura 22 (2005) 300–305 (in Spanish).
[35] H.B. Zhang, Z.Z. Fang, J.D. Belnap, Quasi-plastic deformation of WC-Co composites loaded with a spherical indenter, Metall. Mater. Trans. A 38 (2007) 552–561, https://doi.org/10.1007/s11661-006-9036-y.
[36] H.B. Zhang, Z.Z. Fang, Characterization of quasi-plastic deformation of WC-Co composite using Hertzian indentation technique, Int. J. Refract. Met. Hard Mater. 26 (2008) 106–114, https://doi.org/10.1016/j.ijrmhm.2007.02.002.
[37] E. Tarrés, G. Ramírez, Y. Gaillard, E. Jiménez-Piqué, L. Llanes, Contact fatigue behavior of PVD-coated hardmetals, Int. J. Refract. Met. Hard Mater. 27 (2009) 323–331, https://doi.org/10.1016/j.ijrmhm.2008.05.003.
[38] L. Llanes, E. Tarrés, G. Ramírez, C.A. Botero, E. Jiménez-Piqué, Fatigue susceptibility under contact loading of hardmetals coated with ceramic films, Procedia Eng. 2 (2010) 299–308, https://doi.org/10.1016/j.proeng.2010.03.033.
[39] H.B. Zhang, Q. Lu, L. Zhang, Z.Z. Fang, Dependence of microcrack number density on microstructural parameters during plastic deformation of WC-Co composite, Int. J. Refract. Met. Hard Mater. 28 (2010) 434–440, https://doi.org/10.1016/j.ijrmhm.2010.01.005.
[40] A. Góez, D. Coureaux, A. Ingebrand, B. Reig, E. Tarrés, A. Mestra, A. Mateo, E. Jiménez-Piqué, L. Llanes, Contact damage and residual strength in hardmetals, Int. J. Refract. Met. Hard Mater. 30 (2012) 121–127, https://doi.org/10.1016/j.ijrmhm.2011.07.013.
[41] R.B. Collier, K.P. Plucknett, Spherical indentation damage in TiC-Ni_3Al composites, Int. J. Refract. Met. Hard Mater. 30 (2012) 188–195, https://doi.org/10.1016/j.ijrmhm.2011.08.008.
[42] J. Yang, F. García Marro, T. Trifonov, M. Odén, M.P. Johansson-Jõesaar, L. Llanes, Contact damage resistance of TiN-coated hardmetals: beneficial effects associated with substrate grinding, Surf. Coat. Tech. 275 (2015) 133–141, https://doi.org/10.1016/j.surfcoat.2015.05.028.
[43] C. Jin, K.P. Plucknett, Hertzian indentation response in TiC-316L stainless steel

cermets, Int. J. Refract. Met. Hard Mater. 71 (2018) 172–182, https://doi.org/10.1016/j.ijrmhm.2017.11.044.
[44] I. El Azhari, J. García, F. Soldera, S. Suarez, E. Jiménez-Piqué, F. Mücklich, L. Llanes, Contact damage investigation of CVD carbonitride hard coatings deposited on cemented carbides, Int. J. Refract. Met. Hard Mater. 86 (2020) 105050, , https://doi.org/10.1016/j.ijrmhm.2019.105050.
[45] D.K. Shetty, I.G. Wright, P.N. Mincer, A.H. Clauer, Indentation fracture of WC-Co cermets, J. Mater. Sci. 20 (1985) 1873–1882, https://doi.org/10.1007/BF00555296.
[46] F. Guiberteau, N.P. Padture, B.R. Lawn, Effect of grain size on Hertzian contact damage in alumina, J. Am. Ceram. Soc. 77 (1994) 1825–1831, https://doi.org/10.1111/j.1151-2916.1994.tb07057.x.
[47] H. Cai, M.A. Stevens Kalceff, B.R. Lawn, Deformation and fracture of mica-containing glass ceramics in Hertzian contacts, J. Mater. Res. 9 (1994) 762–770, https://doi.org/10.1557/JMR.1994.0762.
[48] H. Helbawi, L. Zhang, I. Zarudi, Difference in subsurface damage in indented specimens with and without bonding layer, Int. J. Mech. Sci. 43 (2001) 1107–1121, https://doi.org/10.1016/S0020-7403(00)00032-1.
[49] P. Miranda, A. Pajares, F. Guiberteau, Y. Deng, B.R. Lawn, Designing damage-resistant brittle-coating structures: I. bilayer, Acta Mater. 51 (2003) 4347–4356, https://doi.org/10.1016/S1359-6454(03)00290-8.
[50] B.A. Latella, B.H. O'Connor, N.P. Padture, B.R. Lawn, Hertzian contact damage in porous alumina ceramics, J. Am. Ceram. Soc 80 (2005) 1027–1031, https://doi.org/10.1111/j.1151-2916.1997.tb02940.x.
[51] J.M. Tarragó, G. Fargas, L. Isern, S. Dorvlo, E. Tarres, C.M. Müller, E. Jimenez-Piqué, L. Llanes, Microstructural influence on tolerance to corrosion-induced damage in hardmetals, Mater. Design 111 (2016) 36–43, https://doi.org/10.1016/j.matdes.2016.08.066.
[52] J.E. Cho, S.Y. Hwang, K.Y. Kim, Corrosion behavior of thermal sprayed WC cermet coatings having various metallic binders in strong acidic environment, Surf. Coat. Tech. 200 (2006) 2653–2662, https://doi.org/10.1016/j.surfcoat.2004.10.142.
[53] A.C. Fischer-Cripps, B.R. Lawn, Indentation stress-strain curves for "quasi-ductile" ceramics, Acta Mater. 44 (1996) 519–527, https://doi.org/10.1016/1359-6454(95)00204-9.
[54] O. Knotek, B. Bosserhoff, A. Schrey, T. Leyendecker, O. Lemmer, S. Esser, A new technique for testing the impact load of thin films: the coating impact test, Surf. Coat. Tech. 54 (1992) 102–107, https://doi.org/10.1016/S0257-8972(09)90035-4.
[55] R. Bantle, A. Matthews, Investigation into the impact wear behaviour of ceramic coatings, Surf. Coat. Tech. 74 (1995) 857–868, https://doi.org/10.1016/0257-8972(95)08314-6.
[56] K.L. Johnson, An experimental determination of the contact stresses between plastically deformed cylinders and spheres, Engineering Plasticity, Cambridge University Press, Cambridge, 1968, pp. 341–361.
[57] F.C. Frank, B. Lawn, On the theory of Hertzian fracture, P. Roy. Soc. A-Math. Phy. 299 (1967) 291–306, https://doi.org/10.1098/rspa.1967.0137.
[58] L.S. Sigl, H.E. Exner, Experimental study of the mechanics of fracture in WC-Co alloys, Metall. Trans. A (1987) 1299–1308, https://doi.org/10.1007/BF02647199 18A.
[59] L.S. Sigl, H.F. Fischmeister, On the fracture toughness of cemented carbides, Acta Metall. 36 (1988) 887–897, https://doi.org/10.1016/0001-6160(88)90143-5.
[60] J.M. Tarragó, E. Jiménez-Piqué, L. Schneider, D. Casellas, Y. Torres, L. Llanes, FIB/FESEM experimental and analytical assessment of R-curve behavior of WC–Co cemented carbides, Mater. Sci. Eng. A 645 (2015) 142–149, https://doi.org/10.1016/j.msea.2015.07.090.
[61] J.M. Tarragó, D. Coureaux, Y. Torres, D. Casellas, I. Al-Daweri, L. Schneider, L. Llanes, Microstructural effects on the R-curve behavior of WC-Co cemented carbides, Mater. Design 975 (2016) 492–501, https://doi.org/10.1016/j.matdes.2016.02.115.
[62] J. Holmes, R.A. Queeney, Fatigue crack initiation in a porous steel, Powder Metall. 28 (1985) 231–235, https://doi.org/10.1179/pom.1985.28.4.231.
[63] D.F. Diao, K. Kato, K. Hokkirigawa, Fracture mechanisms of ceramic coatings in indentation, J. Tribol. 116 (1994) 860–869, https://doi.org/10.1115/1.2927346.
[64] V.K. Sarin, T. Johannesson, On the deformation of WC–Co cemented carbides, Met. Sci. 9 (1975) 472–476, https://doi.org/10.1179/030634575790444531.
[65] C.H. Vasel, A.D. Krawitz, E.F. Drake, E.A. Kenik, Binder deformation in WC-(Co, Ni) cemented carbide composites, Metall. Trans. A 16 (1985) 2309–2317, https://doi.org/10.1007/BF02670431.
[66] G. Erling, S. Kursawe, S. Luyckx, H.G. Sockel, Stable and unstable fracture surface features in WC-Co, J. Mater. Sci. Lett. 19 (2000) 437–438, https://doi.org/10.1023/A:1006755208450.
[67] X. Liu, J. Zhang, C. Hou, H. Wang, X. Song, Z. Nie, Mechanisms of WC plastic deformation in cemented carbide, Mater. Design 150 (2018) 154–164, https://doi.org/10.1016/j.matdes.2018.04.025.
[68] E. Jiménez-Piqué, L. Llanes, M. Anglada, Resistance to contact deformation and damage of hard ceramics, in: V.K. Sarin, D. Mari, L. Llanes (Eds.), Comprehensive Hard Materials, Volume 2 - Ceramics, Elsevier, Oxford (UK), 2014, pp. 367–383, , https://doi.org/10.1016/B978-0-08-096527-7.00032-5.
[69] N. Azeggagh, L. Joly-Pottuz, D. Nélias, J. Chevalier, M. Omori, T. Hashida, Hertzian contact damage in silicon nitride ceramics with different porosity contents, J. Eur. Ceram. Soc. 35 (2015) 2269–2276, https://doi.org/10.1016/j.jeurceramsoc.2015.01.031.
[70] Z. Chen, X. Wang, A. Atkinson, N. Brandon, Spherical indentation of porous ceramics: cracking and toughness, J. Eur. Ceram. Soc. 36 (2016) 3473–3480, https://doi.org/10.1016/j.jeurceramsoc.2016.05.010.

8. Results and conclusions

8.1. Summary of the results and discussion

This Ph.D. thesis is devoted to investigate the influence of corrosion on the mechanical response and damage of cemented carbides at different length scales, including changes in microstructural integrity, residual strength, small-scale mechanical integrity, load-bearing capability, Hertzian indentation strain-stress behavior and corresponding damage scenarios. It has been structured in four main sections, and the main findings are summarized as follows:

8.1.1 Corrosion-induced damage and residual strength of cemented carbides: influence of microstructure and corrosion medium

The corrosion-induced damage and the corresponding residual strength (damage tolerance) behavior of four microstructurally different cemented carbides exposed to three distinct corrosion media were studied. In doing so, besides the mechanical response referred, electrochemical parameters were measured as well as corrosion damage scenario was documented and analyzed. Information gathered is expected to be useful for defining microstructural design guidelines on the basis of damage tolerance as a function of type of corrosive medium.

As reported in **Article I**, the corrosion rates in acidic solution were higher for all studied cemented carbides grades compared to neutral and alkaline ones. Coarse-grained cobalt grade, 10CoC, displayed in each solution the highest values, while 9NiF showed the best corrosion resistance. The presence of small amount of chromium in 10CoUF grade together with the ultrafine microstructure proved to be more effective than the presence of 2%wt. of nickel in a coarse-grained cobalt grade, 10CoNiC. For all studied grades and solutions, the corrosion rates decreased with increasing immersion time.

Taking residual strength of corroded samples into consideration, each studied corrosive medium induced relatively different strength losses, most likely related to significant differences in the size and geometry of corrosion-induced damage acting as critical flaws for fracture. HCl solution was found to be the most aggressive medium. The highest strength loss, 60% approximately, was observed for 10CoC. Meanwhile, for neutral and alkaline solutions, retained strength was at least 80% in the worst-case scenario.

A detailed inspection of fractured surfaces, conducted by means of FESEM, revealed clear differences between the corrosion-induced damage as a function of the pH solution. Regarding carbide grain size in the neutral and alkaline solutions, the ultrafine-sized studied grade was much more affected by corrosion-induced damage than the coarser ones. Sharp corrosion pits were formed in ultrafine-sized cemented carbides as immersion time increases, which have a much more pronounced stress

rising effect. Consequently, higher strength loss was measured for the ultrafine grade.

Regarding micromechanisms, a detailed inspection of transversal cut micrographs permitted to evidence that dissolution of metallic binder in acidic and neutral solutions takes place in the core of binder pools rather than at the binder/carbide interface. Meanwhile, in alkaline solutions WC-Co cemented carbides showed a different behavior compared to acidic or neutral solutions. Exhaustive observations pointed out that at low time exposures in 0.1M NaOH, the corrosion of the WC grains was discerned to start at the binder/WC interface which led to the formation of microcracks and their growth inside WC grains at increasing dwell time.

8.1.2 Corrosion-induced changes on the mechanical integrity of cemented carbides at small length scales

Nanoindentation and nanoscratch testing, complemented with combined use of FESEM and FIB, were implemented for assessing and analyzing surface/subsurface and mechanical integrity changes induced by exposure to an acidic media of a hardmetal grade.

Results reported in **Article II** showed that small-scale mechanical properties of the studied grade were pronouncedly degraded due to the corrosion-induced damage. Young's modulus of 679 GPa and hardness of 24 GPa measured for the virgin condition were found to decrease to much lower values for the corroded condition, i.e. 464 GPa

and 15 GPa respectively. Deformation and damage scenarios were also observed to change dramatically when comparing virgin and corroded specimens. Regarding the former, both hard and soft phases exhibited effective deformation compatibility between them, with very few fracture features (cracks) localized in WC grains. Meanwhile, dissolution of the metallic binder yielded as a remnant microstructure, i.e. a mechanically unsupported carbide skeleton, which then reduced significantly the load-bearing capability of the corroded cemented carbide.

From the nanoscratch tests, it was clearly discerned that failure-related events, i.e. spallation, cracking, etc., were much more pronounced in the corroded specimen. Virgin specimen exhibited a higher scratch resistance response, as concluded from the narrower and shallower tracks. This also applied to damage tolerance, as related to spallation and local chipping degree. On the other hand, damage emerged earlier in the corroded specimen, as compared to the non-corroded one in terms of applied load. Here changes were evidenced in terms of absence of compatible plastic deformation between both phases (intrinsic to the toughening capability of the now removed binder) as well as localized microfracture within contiguous carbide grains. FIB/FESEM inspection revealed that for non-corroded and corroded surfaces, two-phase built-up material could be seen on the edge of the scratch track for the non-corroded surface. In contrast, edge tracks for the corroded specimens were characterized for large clumps of removed (and previously fragmented) carbide grains. It supported the fact that effective mechanical integrity of the remaining WC skeleton was significantly decreased,

yielding then easy removal of loose grains even by light abrasion.

8.1.3 Corrosion effect on the load-bearing capability and induced damage of cemented carbides

The nanomechanical study referred in the previous section was extended to higher length scales (from 10s to 100s of microns in depth) by exposing the hardmetal studied to longer corrosion times and by using pyramidal indentation and sliding contact (microscratch), under applied loads ranging from 5 to 300 N, as discriminative testing techniques. The former implied the existence of uniform and rather thick corrosion-affected layers, whereas the latter yielded damage scenarios whose depths were similar to the length scale of the degraded surface layers. Under these conditions, well-developed cracking systems were induced; and thus, changes on the crack-microstructure interaction as a function of corrosion extension could be studied.

Results reported in **Article III** indicated that damage scenarios got more pronounced, regarding discerned failure-related events such as chipping or spallation for the corroded conditions. Moreover, Vickers hardness was found to decrease from 17-18 GPa for the uncorroded material to 11–12 GPa for corroded conditions corresponding to exposure times of 7- and 11- days. The latter then represents the effective load-bearing capability of the unsupported WC skeleton. This statement was sustained by the fact that variable and intermediate hardness values were measured for corroded conditions resulting after exposure times of 1- and 3- days, depending on the imposed

load. Such a trend was also evidenced when analyzing scratch hardness data, although here higher relative differences between pristine and corroded specimens were found. It would point out a higher sensitivity of irreversible deformation resistance of the hardmetal to corrosion-induced changes under the more complex loading state involved in sliding contact.

Aiming to further document and analyze corrosion effects on mechanical integrity at the surface of the hardmetal studied, length of cracks emanating from imprint corners were measured for each tested condition. It was found that the longer the exposure to the corrosive media, the higher the slope, pointing out a clear detrimental effect of corrosion on crack extension resistance. Nevertheless, it should be underlined that relevance of lessening effects on crack extension resistance decayed over the first 3 days of immersion, and tended to stabilize for longer times (7 and 11 days).

Furthermore, corrosion effects on damage scenario induced during indentation and scratch tests were analyzed focusing on crack-microstructure interaction. In the case of pyramidal indentation, opposite to the sharp and shallow cracks discerned in the non-corroded hardmetal, damage at the subsurface of the corroded conditions evolved from defined cracks close to the surface into branched ones as they grew into the bulk. Similarly, comb-like crack propagating paths underneath the scratch tracks were completely different for uncorroded and corroded conditions. Systematic inspection – by controlling the distance between the scratch end and the edge – allowed to discern

that as the indenter got closer to the edge, damaged zone changed from a well-defined cracking system for the uncorroded condition into a multiple-cracking scenario confined within the porous-like degraded layer for the corroded conditions.

8.1.4 Corrosion-induced changes on Hertzian contact damage in cemented carbides

Aiming to evaluate corrosion effects on the mechanical integrity of hardmetals at even higher length scales, closer to those involved under service-like conditions, spherical indentation was implemented to document and analyze the changes observed in the indentation stress-strain response after exposing different grades to an acidic media for different times. In doing so, addition of chromium and/or substitution of cobalt by nickel within the chemical nature of the metallic binder were invoked as experimental variables. Besides the mechanical study, the research was complemented with the combined use of advanced characterization techniques for assessment of surface and subsurface features.

Results reported in **Article IV** revealed that indentation stress-strain response seemed to significantly depend on the depth of the corrosion affected zone. From a physical viewpoint, the degraded load-bearing capability evidenced must be attributed to the generation of porous/binderless corroded layers after corrosive exposure. On the other hand, as the thickness of the corrosion layer increased (from tens to hundreds of microns), the quasi-plastic deformation tended to be confined within the corroded layer.

This was pointed out as the main reason for rationalizing the higher relative discrepancies among indentation stress-strain curves of pristine and corroded specimens, as corrosion time gets longer. For the highest aggressive corrosive condition (i.e. after exposure to acidic media for 264 h), indentation stress decay – measured on the basis of plateau values reached in the curves – was maximum for 6CoM (about 23%), intermediate for 6NiCrM (20%), and minimum for 6CoCrM (13%).

The evolution of surface damage, from inelastic deformation to fracture, was assessed by means of an extensive and detailed visual inspection using LSCM. Contact damage in pristine hardmetals was found to evolve, once residual imprints were already observed, from an initial partial ring crack which developed into a full ring crack as the indentation load increases. For the corroded cemented carbides, besides the similar evolution discerned in terms of ring cracks, radial fissures and even specimen breakage were evidenced as additional damage features/scenarios under loading conditions evaluated in this study. Furthermore, critical loads for producing (partial/full) ring and radial cracks decreasd as the corrosion time gets longer. Within this context, the results of this work indicate the 6CoCrM hardmetal grade as the best option among the three cemented carbides studied.

In order to further understand corrosion effects on surface deformation and damage mechanisms for the hardmetal grades studied, a detailed inspection at heavily deformed zones was carried out by means of FESEM. Concerning the uncorroded condition, a

well-developed full ring crack was discerned, due to tensile radial stresses and strains existing in the vicinity of the residual imprints. The crack path mainly transversed the two-phase microstructure, following binder regions – close to binder/carbide interfaces – and/or WC grain boundaries. The indented zone showed a slightly damaged scenario involving several plastically deformed WC grains and some edge broken particles. For the corroded specimen, under similar loading conditions, damage features were not only more pronounced but also included a new type: radial cracks. Due to the dissolution of the binder phase, these appear as well-developed fissures, accompanied by significant WC grain removal in the crack propagation path, which finally resulted – in some cases – in rupture of the tested specimens.

8.2 General conclusions

- Electrochemical and immersion tests revealed that nickel binder displays more noble corrosion potential and critical current density compared to cobalt grades in acidic and neutral solutions containing chlorides. In these conditions, the presence of small amounts of chromium improves more the corrosion resistance of the materials than mixing nickel and cobalt as a binder. No significant differences among studied grades were observed in alkaline solution.

- Corrosion damage resulted in strength degradation on the basis of stress rising effects associated with the formation of surface corrosion pits in acidic solution for all studied grades. In neutral and alkaline solutions, corrosion effects on residual strength are less pronounced. Under these conditions, the grade more affected by exposure to corrosion medium is the ultrafine one.

- In acidic solution, the binder was preferentially attacked. The binder dissolution started from the center of binder pools, independent of binder chemical nature, and spreads to the edges until binder phase was completely consumed. In alkaline solution, corrosion process was initially located at the binder/WC interface. As exposure time increased, corrosion evolved into microcracks which propagated inside the WC phase, yielding finally a fragmented-like scenario.

- Immersion testing in an acidic solution results in a significant degradation of surface/subsurface integrity of cemented carbides. In this regard, effective changes in microstructural assemblage of the material are discerned by FESEM/FIB inspection: from an interpenetrating two-phase network for the non-corroded composite to a contiguous and binderless (i.e. with cavities in regions where binder has been dissolved) carbide skeleton in the corroded material.

- Corrosion in acidic media is found to be quite detrimental for the mechanical integrity of the hardmetal alloy studied. Due to the lower load-bearing capability

of the referred mechanically unsupported carbide network existing in the corroded cemented carbide, their small-scale elastic modulus, hardness and sliding contact (scratch) resistance are significantly degraded, as compared to those exhibited by the non-corroded hardmetal.

- Deformation/fracture micromechanisms are also significantly affected by corrosion. As the metallic binder is leached out during exposure to the acidic solution, its well-established toughening capability in non-corroded hardmetals is also completely lost. Consequently, deformation induced by the imposed loads must be exclusively accommodated by the binderless and porous network of carbide phase. It is done through multiple cracking and fragmentation of individual grains. Furthermore, as re-embedment of them into the metallic phase (as it occurs for the non-corroded specimens) is no longer possible, it finally yields easy pull-out and removal of the hard phase in the corroded material.

- Corroded cemented carbides exhibit lower load-bearing capability and crack extension resistance than pristine ones. These relative corrosion-induced lessening effects decreases as exposure time increases, and no differences are discerned after 7 days of immersion. This trend is evidenced for both indentation and scratch tests, although a higher sensitivity of irreversible deformation resistance to microstructural changes introduced by corrosion is observed under sliding contact conditions. Vickers hardness of significantly corroded specimens decreases down to about 60% the reference one determined for uncorroded samples. From a

mechanical viewpoint, these measured values may then be taken as the effective load-bearing capability of the unsupported WC skeleton.

- The contact response of the corroded hardmetals is largely dependent on the thickness of the degraded layer, which is directly related to the exposure time. In this regard, the corroded specimens may be described as systems consisting of a porous ceramic layer on top of a very hard composite substrate. Within this context, relative indentation depths lower than 0.2–0.3 of corroded layer thickness are determined as required testing conditions for effective assessment of the intrinsic hardness of corroded layers, i.e. without being affected by the mechanical response of the substrate.

- Significant corrosion effects on contact response are also evidenced in the damage scenario resulting, at both surface and subsurface levels, after indentation and scratch tests of the hardmetal studied. Independent of testing conditions, damaged zone changes from well-defined cracking systems for the uncorroded condition into multiple branched fissures confined within the porous-like degraded layers for the corroded ones. Cracks within the binderless and porous carbide network are discerned to get arrested at lower depths or following lateral-like paths parallel to the surface. Such scenario should be linked to the effectiveness of a small length-scale interaction between cracks and the cavities within the binderless WC skeleton, yielding as a final result the development of macro-spalling like failures at the edges of both indentation imprints and scratch tracks.

- The degraded load-bearing capability after corrosion is also reflected by an increased indentation depth at a given applied load, i.e. a lower stress-strain response. In general, corrosion-induced lessening effects are found to depend on the ratio between indentation depth and thickness of the corroded layer; and thus, on the effective substrate-like role played by the underneath non-corroded hardmetal. In this regard, as exposure time to acid medium gets longer, the resulting and continuously thicker corroded layer gradually substitutes the uncorroded substrate as main responsible for controlling the quasi-plastic deformation induced by the indentation. As a consequence of the higher intrinsic corrosion resistance of hardmetal grades containing Cr (6CoCrM and 6NiCrM), as compared to the the Cr-free grade (6CoM), such detrimental effects are more pronounced in the latter than in the former.

- The detrimental influence of corrosion is particularly evidenced in terms of contact damage: lower critical loads for the emergence of incipient cracks, and more severe evolution scenarios at the surface level. Considering these parameters as figures of merit for material selection, the hardmetal grade 6CoCrM is then proposed as the best option, as compared to the other two cemented carbides studied, for applications involving corrosion and contact loads. Such a finding points out the synergic and compromising effect of corrosion resistance linked to Cr addition and higher hardness-toughness correlation affiliated to Co (within the context of WC-Co systems, as compared to WC-Ni ones) for achieving an optimized performance

under service-like conditions.

- Relevant corrosion effects on contact response are also discerned at the subsurface level, in terms of deformation/damage micromechanisms. In this regard, the deformation-shared scenario commonly evidenced in pristine hardmetals is found to change into one dominated by microcracks, emerging and evolving from cavities within the porous/binderless WC skeletons left after corrosion. At relatively high loads and independent of chemical nature of the binder, it finally yields radial fissures and even specimen failure under spherical indentation testing.

8.3 Impact and perspectives

The main outcome of this Ph.D. thesis is the in-depth knowledge attained about the effects of corrosion-induced damage on the mechanical integrity and load-bearing capability of cemented carbides with distinct microstructures at different length scales. The study as a whole permits to point out guidelines for microstructural design of these materials under combined consideration of corrosion and mechanical contact as service-like conditions. It includes the assessment of the evolution of microstructure-property-performance interrelations due to the degradation of the material under severe working conditions. Although this thesis represents a well-defined step in this direction, more extensive research should be conducted for covering additional service-like conditions. Within this context, future work should also include consideration of

synergistic effects among different damage mechanisms.

In this thesis relevant attention was paid to document and analyze the influence of corrosion damage induced by acidic solution on the mechanical contact response of cemented carbides. Results reported in **Article I** reveal that basic solution may cause detrimental damage in the WC phases, where the corrosion process was initially located at the binder/WC interface, and then evolved into the ceramic phase as the corrosion time increased. Therefore, future work should be recalled for exploring how this corrosion damage induced under basic media affects the mechanical contact response of cemented carbides.

Regarding extrinsic damage evaluated in this thesis, it was exclusively introduced by monotonic loading, as it was reported in **Articles II**, **III** and **IV**. Considering that some applications of hardmetal tools and components involve contact loads of cyclic nature, changes on the contact fatigue resistance induced by corrosion should also be proposed as future work.

Finally, the influence of different corrosive media on the damage tolerance behavior of cemented carbides was evaluated by the retained strength of corroded specimens (**Article I**). Considering service conditions involving the combined action of corrosion and impact loads (monotonic/cyclic), it would be meaningful to assess how such extrinsic damage affects the effective strength of cemented carbides. In this regard,

evaluation of residual strength of corroded and contact-damaged specimens may be proposed as a suitable approach for rationalizing the influence of microstructure on the damage tolerance behavior of cemented carbides.

References

[1] H.E. Exner, Physical and chemical nature of cemented carbides, Int. Met. Rev. (1979) 149–173.

[2] J. García, V.C. Ciprés, A. Blomqvist, B. Kaplan, Cemented carbide microstructures : a review, Int. J. Refract. Met. Hard Mater. 80 (2019) 40–68.

[3] L. Prakash, Fundamentals and general applications of hardmetals, in: V.K. Sarin, D. Mari, L. Llanes (Eds.), Compr. Hard Mater., Elsevier, 2014: pp. 29–90.

[4] V.A. Pugsley, G. Korn, S. Luyckx, H.G. Sockel, W. Heinrich, M. Wolf, H. Feld, R. Schulte, The influence of a corrosive wood-cutting environment on the mechanical properties of hardmetal tools, Int. J. Refract. Met. Hard Mater. 19 (2001) 311–318.

[5] V.A. Pugsley, H.G. Sockel, Corrosion fatigue of cemented carbide cutting tool materials, Mater. Sci. Eng. A 366 (2004) 87–95.

[6] R. Lu, L. Minarro, Y.-Y. Su, R.M. Shemenski, Failure mechanism of cemented tungsten carbide dies in wet drawing process of steel cord filament, Int. J. Refract. Met. Hard Mater. 26 (2008) 589–600.

[7] E.O. Cobo, R.A. Suárez Baldo, J.B. Bessone, Corrosion of chromium plated rotor in drilling fluid, Surf. Coat.Tech. 122 (1999) 39–43.

[8] B. Lu, Erosion-corrosion in oil and gas production, Res. Rev. Mater. Sci. Chem. 2 (2013) 19–60.

[9] W.J. Tomlinson, I.D. Molyneux, Corrosion, erosion-corrosion, and the flexural strength of WC-Co hardmetals, J. Mater. Sci. 26 (1991) 1605–1608.

[10] A.M. Human, H.E. Exner, The relationship between electrochemical behaviour and in-service corrosion of WC based cemented carbides, Int. J. Refract. Met. Hard Mater. 15 (1997) 65–71.

[11] H. Engqvist, U. Beste, N. Axen, The influence of pH on sliding wear of WC-based materials, Int. J. Refract. Met. Hard Mater. 18 (2000) 103–109.

[12] A.J. Gant, M.G. Gee, A.T. May, The evaluation of tribo-corrosion synergy for WC-Co hardmetals in low stress abrasion, Wear 256 (2004) 500–516.

[13] S. Hochstrasser(-Kurz), Y. Mueller, C. Latkoczy, S. Virtanen, P. Schmutz, Analytical characterization of the corrosion mechanisms of WC-Co by electrochemical methods and inductively coupled plasma mass spectroscopy, Corros. Sci. 49 (2007) 2002–2020.

[14] A.J. Gant, M.G. Gee, D.D. Gohil, H.G. Jones, L.P. Orkney, Use of FIB/SEM to assess the tribo-corrosion of WC/Co hardmetals in model single point abrasion experiments, Tribol. Int. 68 (2013) 56–66.

[15] C. Yi, H. Fan, J. Xiong, Z. Guo, G. Dong, W. Wan, H. Chen, Effect of WC content on the microstructures and corrosion behavior of Ti(C, N)-based cermets, Ceram. Int. 39 (2013) 503–509.

[16] J.M. Tarragó, G. Fargas, L. Isern, S. Dorvlo, E. Tarres, C.M. Müller, E. Jiménez-Piqué, L. Llanes, Microstructural influence on tolerance to corrosion-induced damage in hardmetals, Mater. Des. 111 (2016) 36–43.

[17] W. Tang, L. Zhang, Y. Chen, H. Zhang, L. Zhou, Corrosion and strength degradation behaviors of binderless WC material and WC-Co hardmetal in alkaline solution: a comparative investigation, Int. J. Refract. Met. Hard Mater. 68 (2017) 1–8.

[18] W. Qiu, Y. Liu, J. Ye, H. Fan, Y. Qiu, Effects of (Ti,Ta,Nb,W)(C,N) on the microstructure, mechanical properties and corrosion behaviors of WC-Co cemented carbides, Ceram. Int. 43 (2017) 2918–2926.

[19] Q. Mao, Q. Yang, W. Xiong, S. Li, M. Zhang, L. Ruan, Corrosion behavior of Ni_3Al-bonded TiC-based cermets in H_2SO_4 and NaOH solutions, Ceram. Int. 44 (2018) 13303–13312.

[20] E. Jiménez-Piqué, M. Turon-Vinas, H. Chen, T. Trifonov, J. Fair, E. Tarrés, L. Llanes, Focused ion beam tomography of WC-Co cemented carbides, Int. J. Refract. Met. Hard Mater. 67 (2017) 9–17.

[21] P.C. Angelo, R. Subramanian, Powder metallurgy: science, technology and applications, New Delhi: PHI learning Pvt. Ltd., 2008.

[22] H.M. Ortner, P. Ettmayer, H. Kolaska, The history of the technological progress of hardmetals, Int. J. Refract. Met. Hard Mater. 44 (2014) 148–159.

[23] K. Schröter, DRP 420.689: sintered hard metal alloy and procedure for its fabrication, US1549615 (1923).

[24] P. Ettmayer, H. Kolaska, H.M. Ortner, History of hardmetals, in: V.K. Sarin, D. Mari, L. Llanes (Eds.), Compr. Hard Mater., Elsevier, 2014: pp. 3-27.

[25] L.Y. Zhou, China's cemented carbide output increased by 11.59% year-on-year in 2018, accounting for 38% of global output, China Metall. News. (2019).

[26] W.D. Schubert, E. Lassner, W. Bohlke, Cemented carbides – a success story, ITIA Newsletter, June 2010

[27] P.K. Katiyar, P.K. Singh, R. Singh, A.L. Kumar, Modes of failure of cemented tungsten carbide tool bits (WC/Co): a study of wear parts, Int. J. Refract. Met. Hard Mater. 54 (2016) 27–38.

[28] A.F. Lisovsky, N. V Tkachenko, V. Kebko, Structure of a binding phase in re-alloyed WC-Co cemented carbides, Int. J. Refract. Met. Hard Mater. 10 (1991) 33–36.

[29] J.M. Tarragó, C. Ferrari, B. Reig, D. Coureaux, L. Schneider, L. Llanes, Mechanics and mechanisms of fatigue in a WC-Ni hardmetal and a comparative study with respect to WC-Co hardmetals, Int. J. Fatigue 70 (2015) 252–257.

[30] W. Midlands, Nickel in hardmetals, Int. J. Refract. Met. Hard Mater. 11 (1993) 137–149.

[31] G. Gille, J. Bredthauer, B. Gries, B. Mende, W. Heinrich, Advanced and new grades of WC and binder powder – their properties and application, Int. J. Refract. Met. Hard Mater. 18 (2000) 87–102.

[32] A.J. Gant, M.G. Gee, Abrasion of tungsten carbide hardmetals using hard counterfaces, Int. J. Refract. Met. Hard Mater. 24 (2006) 189–198.

[33] M.G. Gee, A.J. Gant, B. Roebuck, Wear mechanisms in abrasion and erosion of WC/Co and related hardmetals, Wear 263 (2007) 137–148.

[34] H.C. Lee, J. Gurland, Hardness and deformation of cemented tungsten carbide, Mater. Sci. Eng. 33 (1978) 125–133.

[35] J. Gurland, A structural approach to the yield strength of two-phase alloys with coarse microstructures, Mater. Sci. Eng. 40 (1979) 59–71.

[36] D.N. French, D.A. Thomas, Hardness anisotropy and slip in WC crystals, Trans. Met. Soc. AIME 233 (1965) 950–952.

[37] B. Roebuck, E.A. Almond, Deformation and fracture processes and the physical metallurgy of WC-Co hardmetals, Int. Mater. Rev. 33 (1988) 90–112.

[38] P. Ettmayer, Hardmetals and cermets, Annu. Rev. Mater. Sci. 19 (1989) 145–164.

[39] K. Jia, T.E. Fischer, B. Gallois, Microstructure, hardness and toughness of nanostructured and conventional WC-Co composites, Nanostruct. Mater. 10 (1998) 875–891.

[40] M.G. Gee, B. Roebuck, P. Lindahl, H.-O. Andren, Constituent phase nanoindentation of WC/Co and Ti(C,N) hard metals, Mater. Sci. Eng. A 209 (2002) 128–136.

[41] A. Michalski, D. Siemiaszko, Nanocrystalline cemented carbides sintered by the pulse plasma method, Int. J. Refract. Met. Hard Mater. 25 (2007) 153–158.

[42] Z.Z. Fang, X. Wang, T. Ryu, K.S. Hwang, H.Y. Sohn, Synthesis, sintering, and mechanical properties of nanocrystalline cemented tungsten carbide – a review, Int. J. Refract. Met. Hard Mater. 27 (2009) 288–299.

[43] A. Mukhopadhyay, B. Basu, Recent developments on WC-based bulk composites, J. Mater. Sci. 46 (2011) 571–589.

[44] A. Duszová, R. Halgaš, M. Bľanda, P. Hvizdoš, F. Lofaj, J. Dusza, J. Morgiel, Nanoindentation of WC-Co hardmetals, J. Eur. Ceram. Soc. 33 (2013) 2227–2232.

[45] J.J. Roa, E. Jiménez-Piqué, C. Verge, J.M. Tarragó, A. Mateo, J. Fair, L. Llanes, Intrinsic hardness of constitutive phases in WC-Co composites: nanoindentation testing, statistical analysis, WC crystal orientation effects and flow stress for the constrained metallic binder, J. Eur. Ceram. Soc. 35 (2015) 3419–3425.

[46] P. Kenny, The application of fracture mechanics to cemented tungsten carbides, Powder Metall. 14 (1971) 22–38.

[47] N. Ingelstrom and H. Nordberg, The fracture toughness of cemented tungsten carbides, Eng. Fract. Mech. 6 (1974) 597–607.

[48] R.A. Cutler, A.V. Virkar, The effect of binder thickness and residual stresses on the fracture toughness of cemented carbides, J. Mater. Sci. 20 (1985) 3557–3573.

[49] S.I. Cha, S.H. Hong, G.H. Ha, B.K. Kim, Mechanical properties of WC-10Co cemented carbides sintered from nanocrystalline spray conversion processed powders, Int. J. Refract. Met. Hard Mater. 19 (2001) 397–403.

[50] J.R. Pickens, J. Gurland, The fracture toughness of WC-Co alloys measured on single-edge notched beam specimens precracked by electron discharge machining, Mater. Sci. Eng. 33 (1978) 135–142.

[51] R.K. Viswanadham, T.S. Sun, E.F. Drake, J.A. Peck, Quantitative fractography of WC-Co cermets by Auger spectroscopy, J. Mater. Sci. 16 (1981) 1029–1038.

[52] D.K. Shetty, I.G. Wright, P.N. Mincer, A.H. Clauer, Indentation fracture of WC-Co cermets, J. Mater. Sci. 20 (1985) 1873–1882.

[53] L.S. Sigl, H.F. Fischmeister, On the fracture toughness of cemented carbides, Acta Metall. 36 (1988) 887–897.

[54] Y. Torres, D. Casellas, M. Anglada, L. Llanes, Fracture toughness evaluation of hardmetals: influence of testing procedure, Int. J. Refract. Met. Hard Mater. 19 (2001) 27–34.

[55] S. Sheikh, R. M'Saoubi, P. Flasar, M. Schwind, T. Persson, J. Yang, L. Llanes, Fracture toughness of cemented carbides: testing method and microstructural effects, Int. J. Refract. Met. Hard Mater. 49 (2015) 153–160.

[56] F. Sergejev, M. Antonov, Comparative study on indentation fracture toughness measurements of cemented carbides, Proc. Est. Acad. Sci. Eng. 12 (2006) 388–398.

[57] H.E. Exner, The influence of sample preparation on Palmqvists method for toughness testing of cemented carbides, Trans Met Soc AIME 245 (1969) 677–683.

[58] A.G. Evans, R.M. McMeeking, On the toughening of ceramics by strong reinforcements, Acta Metall. 34 (1986) 2435–2441.

[59] L.S. Sigl, P.A. Mataga, B.J. Dalgleish, R.M. McMeeking, A.G. Evans, On the toughness of brittle materials reinforced with a ductile phase, Acta Metall. 36 (1988) 945–953.

[60] J.M. Tarragó, E. Jiménez-Piqué, L. Schneider, D. Casellas, Y. Torres, L. Llanes, FIB/FESEM experimental and analytical assessment of R-curve behavior of WC-Co cemented carbides, Mater. Sci. Eng. A 645 (2015) 142–149.

[61] V.D. Krstic, On the fracture of brittle-matrix/ductile-particle composites, Philos. Mag. A 48 (1983) 695–708.

[62] L.S. Sigl, H.E. Exner, Experimental study of the mechanics of fracture in WC-Co alloys, Metall. Trans. A 18A (1987) 1299–1308.

[63] P.A. Mataga, Deformation of crack-bridging ductile reinforcements in toughened brittle materials, Acta Metall. 37 (1989) 3349–3359.

[64] Y. Torres, R. Bermejo, L. Llanes, M. Anglada, Influence of notch radius and R-curve behaviour on the fracture toughness evaluation of WC-Co cemented carbides, Eng. Fract. Mech. 75 (2008) 4422–4430.

[65] Y. Torres, J.M. Tarrago, D. Coureaux, E. Tarrés, B. Roebuck, P. Chan, M. James, B. Liang, M. Tillman, R.K. Viswanadham, K.P. Mingard, A. Mestra, L. Llanes, Fracture and fatigue of rock bit cemented carbides: mechanics and mechanisms of crack growth resistance under monotonic and cyclic loading, Int. J. Refract. Met. Hard Mater. 45 (2014) 179–188.

[66] J.M. Tarragó, D. Coureaux, Y. Torres, D. Casellas, I. Al-Dawery, L. Schneider, L. Llanes, Microstructural effects on the R-curve behavior of WC-Co cemented carbides, Mater. Des. 97 (2016) 492–501.

[67] G.R. Odette, B.L. Chao, J.W. Sheckherd, G.E. Lucas, Ductile phase toughening mechanisms in a TiAl-TiNb laminate composite, Acta Metall. Mater. 40 (1992) 2381–2389.

[68] J.M. Tarragó, E. Jiménez-Piqué, M. Turon-Vinas, L. Rivero, L. Llanes, I. Al-Dawery, L. Schneider, Fracture and fatigue behavior of cemented carbides: 3D FIB tomography of crack-microstructure interactions, Int. J. Powder Metall. 50 (2014) 1-10.

[69] A.V. Shatov, S.S. Ponomarev, S.A. Firstov, Fracture and strength of hardmetals at room temperature, in: V.K. Sarin, D. Mari, L. Llanes (Eds.), Compr. Hard Mater., Elsevier, 2014: pp. 301-343.

[70] E.A. Almond, B. Roebuck, Defect-initiated fracture and the bend strength of WC-Co hardmetals, Met. Sci. 11 (1977) 458–461.

[71] B. Roebuck, The tensile strength of hardmetals, J. Mater. Sci. 14 (1979) 2837–2844.

[72] E.A. Almond, Deformation characteristics and mechanical properties of hardmetals, in: Sci. Hard Mater., Springer, 1983: pp. 517–561.

[73] D.R. Moyle, E.R. Kimmel, Effect of coarse WC grains on transverse rupture strength of fine grain hardmetals, in: 12th Int. Plansee Semin., 1989: pp. 311–320.

[74] H.E. Exner, J. Gurland, A review of parameters influencing some mechanical properties of tungsten carbide-cobalt alloys, Powder Metall. 13 (1970) 13–31.

[75] B. Roebuck, Notched bend tests on WC-Co hardmetals, J. Mater. Sci. 23 (1988) 281–287.

[76] J. Dusza, Ľ. Parilák, J. Diblḱ, M. Šlesár, Elastic and plastic behaviour of WC-Co composites, Ceram. Int. 9 (1983) 144–146.

[77] C.H. Vasel, A.D. Krawitz, E.F. Drake, E.A. Kenik, Binder deformation in WC-(Co, Ni) cemented carbide composites, Metall. Trans. A 16A (1985) 2309–2317.

[78] D.J. Rowcliffe, V. Jayaram, M.K. Hibbs, R. Sinclair, Compressive deformation and fracture in WC materials, Mater. Sci. Eng. A 105 (1988) 299–303.

[79] L.I. Aleksandrova, V.P. Bondarenko, M.G. Loshak, Metallographic aspects of deformation and fracture of hard alloys under compression, Powder Metall. Met. Ceram. 44 (2005) 489–498.

[80] J. Larsen-Basse, Effect of composition, microstructure, and service conditions on the wear of cemented carbides, J. Met. 35 (1983) 35–42.

[81] L. Nøkleberg, T. Søntvedt, Erosion in choke valves-oil and gas industry applications, Wear 186–187 (1995) 401–412.

[82] J. Küpferle, A. Röttger, W. Theisen, Fatigue and surface spalling of cemented carbides under cyclic impact loading – evaluation of the mechanical properties with respect to microstructural processes, Wear 390–391 (2017) 33–40.

[83] K.S. Lee, S.K. Lee, B.R. Lawn, Contact damage and strength degradation in brittle/quasi-plastic silicon nitride bilayers, J. Am. Ceram. Soc. 81 (1998) 2394–2404.

[84] E. Jiménez-Piqué, L. Llanes, M. Anglada, Resistance to contact deformation and damage of hard ceramics, in: V.K. Sarin, L. Llanes, D. Mari (Eds.), Compr. Hard Mater., 2014: pp. 367–383.

[85] B.R. Lawn, Indentation of ceramics with spheres: a century after Hertz, J. Am. Ceram. Soc. 81 (1998) 1977–1994.

[86] E. Tarrés, Y. Torres, M. Anglada, L. Llanes, Daño por contacto hertziano en carburos cementados WC-Co: influencia de la microestructura y de los parámetros de contacto, Anales Mecánica de la Fractura 22 (2005) 300–305.

[87] H.B. Zhang, Z.Z. Fang, J.D. Belnap, Quasi-plastic deformation of WC-Co composites loaded with a spherical indenter, Metall. Mater. Trans. A 38 (2007) 552–561.

[88] H.B. Zhang, Z.Z. Fang, Characterization of quasi-plastic deformation of WC-Co composite using Hertzian indentation technique, Int. J. Refract. Met. Hard Mater. 26 (2008) 106–114.

[89] E. Tarrés, G. Ramírez, Y. Gaillard, E. Jiménez-Piqué, L. Llanes, Contact fatigue behavior of PVD-coated hardmetals, Int. J. Refract. Met. Hard Mater. 27 (2009) 323–331.

[90] L. Llanes, E. Tarrés, G. Ramírez, C.A. Botero, E. Jiménez-Piqué, Fatigue susceptibility under contact loading of hardmetals coated with ceramic films, Procedia Eng. 2 (2010) 299–308.

[91] H. Zhang, Q. Lu, L. Zhang, Z.Z. Fang, Dependence of microcrack number density on microstructural parameters during plastic deformation of WC-Co composite, Int. J. Refract. Met. Hard Mater. 28 (2010) 434–440.

[92] A. Góez, D. Coureaux, A. Ingebrand, B. Reig, E. Tarrés, A. Mestra, A. Mateo, E. Jiménez-Piqué, L. Llanes, Contact damage and residual strength in hardmetals, Int. J. Refract. Met. Hard Mater. 30 (2012) 121–127.

[93] R.B. Collier, K.P. Plucknett, Spherical indentation damage in TiC-Ni_3Al composites, Int. J. Refract. Met. Hard Mater. 30 (2012) 188–195.

[94] J. Yang, F. García Marro, T. Trifonov, M. Odén, M.P. Johansson-Jõesaar, L. Llanes, Contact damage resistance of TiN-coated hardmetals: beneficial effects associated with substrate grinding, Surf. Coat. Tech. 275 (2015) 133–141.

[95] C. Jin, K.P. Plucknett, Hertzian indentation response of TiC-316L stainless steel cermets, Int. J. Refract. Met. Hard Mater. 72 (2018) 172–182.

[96] I. El Azhari, J. García, F. Soldera, S. Suarez, E. Jiménez-Piqué, F. Mücklich, L. Llanes, Contact damage investigation of CVD carbonitride hard coatings deposited on cemented carbides, Int. J. Refract. Met. Hard Mater. 86 (2020) 105050.

[97] D.F. Diao, K. Kato, K. Hokkirigawa, Fracture mechanisms of ceramic coatings in indentation, J. Tribol. 116 (1994) 860–869.

[98] F.B. Abudaia, J.T. Evans, B.A. Shaw, Spherical indentation fatigue cracking, Mater. Sci. Eng. A 391 (2005) 181–187.

[99] B.R. Lawn, R. Wilshaw, Indentation fracture: principles and applications, J. Mater. Sci. 10 (1975) 1049–1081.

[100] F. Guiberteau, N.P. Padture, B.R. Lawn, Effect of grain size on Hertzian contact damage in alumina, J. Am. Ceram. Soc. 77 (1994) 1825–1831.

[101] H. Cai, S.M.A. Kalceff, B.R. Lawn, Deformation and fracture of mica-containing glass-ceramics in Hertzian contacts, J. Mater. Res. 9 (1994) 762–770.

[102] B.A. Latella, B.H. O'Connor, N.P. Padture, B.R. Lawn, Hertzian contact damage in porous alumina ceramics, J. Am. Ceram. Soc. 80 (1997) 1027–1031.

[103] H. Helbawi, L. Zhang, I. Zarudi, Difference in subsurface damage in indented specimens with and without bonding layer, Int. J. Mech. Sci. 43 (2001) 1107–1121.

[104] P. Miranda, A. Pajares, F. Guiberteau, Y. Deng, B.R. Lawn, Designing damage-resistant brittle-coating structures: I. bilayers, Acta Mater. 51 (2003) 4347–4356.

[105] K. Yang, G. Xian, H. Zhao, H. Fan, J. Wang, H. Wang, H. Du, Effect of Mo content on the structure and mechanical properties of TiAlMoN films deposited on WC-Co cemented carbide substrate by magnetron sputtering, Int. J. Refract. Met. Hard Mater. 52 (2015) 29–35.

[106] B.R. Lawn, S.M. Wiederhorn, H.H. Johnson, Strength degradation of brittle surfaces: blunt indenters, J. Am. Ceram. Soc. 58 (1975) 428–432.

[107] H. Cai, M.A. Stevens Kalceff, B.M. Hooks, B.R. Lawn, K. Chyung, Cyclic fatigue of a mica-containing glass-ceramic at Hertzian contacts, J. Mater. Res. 9 (1994) 2654–2661.

[108] B.R. Lawn, S.K. Lee, I.M. Peterson, S. Wuttiphan, Model of strength degradation from Hertzian contact damage in tough ceramics, J. Am. Ceram. Soc. 81 (1998) 1509–1520.

[109] I.M. Peterson, S. Wuttiphan, B.R. Lawn, K. Chyung, Role of microstructure on contact damage and strength degradation of micaceous glass-ceramics, Dent. Mater. 14 (1998) 80–89.

[110] Y.G. Jung, I.M. Peterson, A. Pajares, B.R. Lawn, Contact damage resistance and strength degradation of glass-infiltrated alumina and spinel ceramics, J. Dent. Res. 78 (1999) 804–814.

[111] S.K. Lee, B.R. Lawn, Role of microstructure in Hertzian contact damage in silicon nitride: II, strength degradation, J. Am. Ceram. Soc. 81 (2005) 997–1003.

[112] M.G. Gee, A.J. Gant, B. Roebuck, K.P. Mingard. Wear of hardmetals,, in: V.K. Sarin, D. Mari, L. Llanes (Eds.), Compr. Hard Mater., Elsevier, 2014: pp. 363–383.

[113] M.G. Gee, B. Roebuck, A. Gant, Abrasive wear testing with the ASTM B611 and modified ASTM G65 rotating wheel test systems, in: 16th Int. Plansee Semin. High Perform. PM Mater., Reutte, Austria, 2005: pp. 1235–1249.

[114] K. Jia, T.E. Fischer, Abrasion resistance of nanostructured and conventional cemented carbides, Wear 200 (1996) 206–214.

[115] H. Engqvist, S. Ederyd, N. Axén, S. Hogmark, Grooving wear of single-crystal tungsten carbide, Wear 230 (1999) 165–174.

[116] M.G. Gee, A.D. Gee, A cost effective test system for micro-tribology experiments, Wear 263 (2007) 1484–1491.

[117] B. Roebuck, A.J. Gant, M.G. Gee, Abrasion and toughness property maps for WC/Co hardmetals, Powder Metall. 50 (2007) 111–114.

[118] M.G. Gee, L. Nimishakavi, Model single point abrasion experiments on WC/Co hardmetals, Int. J. Refract. Met. Hard Mater. 29 (2011) 1–9.

[119] M.G. Gee, Model scratch corrosion studies for WC/Co hardmetals, Wear 268 (2010) 1170–1177.

[120] J. Heinrichs, M. Olsson, S. Jacobson, Surface degradation of cemented carbides in scratching contact with granite and diamond-the roles of microstructure and composition, Wear 342–343 (2015) 210–221.

[121] J. Heinrichs, M. Olsson, S. Jacobson, Initial deformation and wear of cemented carbides in rock drilling as examined by a sliding wear test, Int. J. Refract. Met. Hard Mater. 64 (2017) 7–13.

[122] H. Wang, M. Gee, Q. Qiu, H. Zhang, X. Liu, H. Nie, X. Song, Z. Nie, Grain size effect on wear resistance of WC-Co cemented carbides under different tribological conditions, J. Mater. Sci. Tech. 35 (2019) 2435–2446.

[123] Y. Ahn, N.G. Cho, S.H. Lee, D. Lee, Lateral crack in abrasive wear of brittle materials, JSME Int. J. 46 (2003) 140–144.

[124] H. Liao, B. Normand, C. Coddet, Influence of coating microstructure on the abrasive wear resistance of WC/Co cermet coatings, Surf. Coat. Tech. 124 (2000) 235–242.

[125] B. Bozzini, G.P. De Gaudenzi, M. Serra, A. Fanigliulo, F. Bogani, Corrosion behaviour of WC-Co based hardmetal in neutral chloride and acid sulphate media, Mater. Corros. 53 (2002) 328–334.

[126] Q. Zhang, Y. He, W. Wang, N. Lin, C. Wu, N. Li, Corrosion behavior of WC-Co hardmetals in the oil-in-water emulsions containing sulfate reducing Citrobacter sp., Corros. Sci. 94 (2015) 48–60.

[127] B. Bozzini, B. Busson, G.P. De Gaudenzi, C. Humbert, C. Mele, S. Tedeschi, A. Tadjeddine, Corrosion of cemented carbide grades in petrochemical slurries. Part I - electrochemical adsorption of CN^{-}, SCN^{-} and MBT: a study based on in situ SFG, Int. J. Refract. Met. Hard Mater. 60 (2016) 37–51.

[128] J.R. Davis, ASM specialty handbook: tool materials, Ohio: ASM international, 1995.

[129] S. Sutthiruangwong, G. Mori, Corrosion properties of Co-based cemented carbides in acidic solutions, Int. J. Refract. Met. Hard Mater. 21 (2003) 135–145.

[130] B. Bozzini, G.P. De Gaudenzi, A. Fanigliulo, C. Mele, Electrochemical oxidation of WC in acidic sulphate solution, Corros. Sci. 46 (2004) 453–469.

[131] D.S. Konadu, J. van der Merwe, J.H. Potgieter, S. Potgieter-Vermaak, C.N. Machio, The corrosion behaviour of WC-VC-Co hardmetals in acidic media, Corros. Sci. 52 (2010) 3118–3125.

[132] A.B. Oliveira, A.C. Bastos, C.M. Fernandes, C.M.S. Pinho, A.M.R. Senos, E. Soares, J. Sacramento, M.L. Zheludkevich, M.G.S. Ferreira, Corrosion behaviour of WC-10% AISI 304 cemented carbides, Corros. Sci. 100 (2015) 322–331.

[133] P.K. Katiyar, N.S. Randhawa, Corrosion behavior of WC-Co tool bits in simulated (concrete, soil, and mine) solutions with and without chloride additions, Int. J. Refract. Met. Hard Mater. 85 (2019) 105062.

[134] A.M.F. Rocha, A.C. Bastos, J.P. Cardoso, F. Rodrigues, C.M. Fernandes, E. Soares, J. Sacramento, A.M.R. Senos, M.G.S. Ferreira, Corrosion behaviour of WC hardmetals with nickel-based binders, Corros. Sci. 147 (2019) 384–393.

[135] S. Guo, R. Bao, S. Li, Y. Ye, E. Zhu, W. Wang, Y. Zhang, H. Chen, Y. Ye, The role of Y_2O_3, Cu, Mo and Mo_2C additives on optimizing the corrosion resistance of WC-6Co cemented carbide in HCl and NaOH solutions, J. Alloys Compd. 827 (2020) 154269.

[136] G. Fargas, C.M. Müller, D. Sosa, J. Tarragó, E. Tarrés, J. Fair, L. Llanes, Influence of the microstructure on corrosion induced damage of WC-Co cemented carbides, Powder Metall. 63 (2020) 174-179.

[137] A.M. Human, The corrosion of tungsten carbide based cemented carbides, Doctoral Thesis, Technical University of Darmstadt, Darmstadt (1994).

[138] N. Sacks, The wear and corrosive-wear response of tungsten carbide-cobalt hardmetals under woodcutting and three body abrasion conditions, Doctoral Thesis, Universität Erlangen-Nürnberg, Erlangen (2002).

[139] S. Sutthiruangwong, G. Mori, R. Kösters, Passivity and pseudopassivity of cemented carbides, Int. J. Refract. Met. Hard Mater. 23 (2005) 129–136.

[140] F.J.J. Kellner, H. Hildebrand, S. Virtanen, Effect of WC grain size on the corrosion behavior of WC-Co based hardmetals in alkaline solutions, Int. J. Refract. Met. Hard Mater. 27 (2009) 806–812.

[141] L. Zhang, Y. Chen, Q.L. Wan, T. Liu, J.F. Zhu, W. Tian, Electrochemical corrosion behaviors of straight WC-Co alloys: exclusive variation in grain sizes and aggressive media, Int. J. Refract. Met. Hard Mater. 57 (2016) 70–77.

[142] M. Pourbaix, Atlas of electrochemical equilibria in aqueous solutions, Houston: NACE International/Brussels: Cebelcor, 1966.

[143] M.R. Thakare, J.A. Wharton, R.J.K. Wood, C. Menger, Exposure effects of alkaline drilling fluid on the microscale abrasion-corrosion of WC-based hardmetals, Wear 263 (2007) 125–136.

[144] M.R. Thakare, J.A. Wharton, R.J.K. Wood, C. Menger, Exposure effects of strong alkaline conditions on the microscale abrasion-corrosion of D-gun sprayed WC-10Co-4Cr coating, Tribol. Int. 41 (2008) 629–639.

[145] U. Beste, S. Jacobson, A new view of the deterioration and wear of WC/Co cemented carbide rock drill buttons, Wear 264 (2008) 1129–1141.

[146] F.J.J. Kellner, M.S. Killian, G. Yang, E. Spiecker, S. Virtanen, TEM and ToF-SIMS studies on the corrosion behavior of vanadium and chromium containing WC-Co hard metals in alkaline solutions, Int. J. Refract. Met. Hard Mater. 29 (2011) 376–383.

[147] N. Lin, Y. He, C. Wu, S. Liu, X. Xiao, Y. Jiang, Influence of TiC additions on the corrosion behaviour of WC-Co hardmetals in alkaline solution, Int. J. Refract. Met. Hard Mater. 46 (2014) 52–57.

[148] W.A. Badawy, Electrochemical behaviour of cobalt in aqueous solutions of different pH, J. Appl. Electrochem. (2000) 693–704.

[149] E.J. Wentzel, C. Allen, The erosion-corrosion resistance of tungsten-carbide hard metals, Int. J. Refract. Met. Hard Mater. 15 (1997) 81–87.

[150] E.J.Wentzel, C.Allen, Erosion-corrosion resistance of tungsten carbide hard metals with different binder compositions, Wear 181–183 (1995) 63–69.

[151] T.A. Fabijanić, M. Kurtela, I. Škrinjarić, J. Pötschke, M. Mayer, Electrochemical corrosion resistance of Ni and Co bonded near-nano and nanostructured cemented carbides, Metals 10 (2020) 1–12.

[152] W.J. Tomlinson, C.R. Linzell, Anodic polarization and corrosion of cemented carbides with cobalt and nickel binders, J. Mater. Sci. 23 (1988) 914–918.

[153] H. Scholl, B. Hofman, A. Rauscher, Anodic polarization of cemented carbides of the type [(WC,M): M = Fe, Ni or Co] in sulphuric acid solution, Electrochim. Acta. 37 (1992) 447–452.

[154] J.E. Cho, S.Y. Hwang, K.Y. Kim, Corrosion behavior of thermal sprayed WC cermet coatings having various metallic binders in strong acidic environment, Surf. Coat. Tech. 200 (2006) 2653–2662.

[155] P.K. Katiyar, A comprehensive review on synergy effect between corrosion and wear of cemented tungsten carbide tool bits: a mechanistic approach, Int. J. Refract. Met. Hard Mater. 92 (2020) 105315.

[156] Z. Guo, J. Xiong, M. Yang, X. Song, C. Jiang, Effect of Mo_2C on the microstructure and properties of WC-TiC-Ni cemented carbide, Int. J. Refract. Met. Hard Mater. 26 (2008) 601–605.

[157] R.M. Genga, L.A. Cornish, G. Akdogan, Effect of Mo_2C additions on the properties of SPS manufactured WC-TiC-Ni cemented carbides, Int. J. Refract. Met. Hard Mater. 41 (2013) 12–21.

[158] W. Ji, B. Zou, Y. Liu, C. Huang, P. Guo, Frictional behavior and wear resistance performance of gradient cermet composite tool materials sliding against hard materials, Ceram. Int. 43 (2017) 7816–7826.

[159] W.J. Tomlinson, N.J. Ayerst, Anodic polarization and corrosion of WC-Co hardmetals containing small amounts of Cr_3C_2 and/or VC, J. Mater. Sci. 24 (1989) 2348–2352.

[160] A. Human, H.E. Exner, Electrochemical behaviour of tungsten-carbide hardmetals, Mater. Sci. Eng. A 209 (1996) 180–191.

[161] U. Beste, T. Hartzell, H. Engqvist, N. Axén, Surface damage on cemented carbide rock-drill buttons, Wear 249 (2001) 324–329.

[162] American Society for Testing and Materials. ASTM G65-00: standard test method for measuring abrasion using the dry sand/rubber wheel apparatus. West Conshohocken: ASTM; 2000.

[163] P.H. Shipway, S. Wirojanupatump, The role of lubrication and corrosion in abrasion of materials in aqueous environments, Tribol. Int. 35 (2002) 661–667.

[164] A.J. Gant, M.G. Gee, A.T. May, Microabrasion of WC-Co hardmetals in corrosive media, Wear 256 (2004) 954–962.

[165] P.H. Shipway, L. Howell, Microscale abrasion – corrosion behaviour of WC-Co hardmetals and HVOF sprayed coatings, Wear 258 (2005) 303–312.

[166] M.R. Thakare, J.A. Wharton, R.J.K. Wood, C. Menger, Investigation of micro-scale abrasion-corrosion of WC-based sintered hardmetal and sprayed coating using in situ electrochemical current-noise measurements, Wear 267 (2009) 1967–1977.

[167] M.G. Gee, K.P. Mingard, A.J. Gant, H.G. Jones, FIB/SEM determination of sub-surface damage caused by micro-tribology scratching of WC/Co hardmetal samples, in: M. De Graef, H. F. Poulsen, A. Lewis, J. Simmons, G, Spanos (Eds.), Proc. 1st Int. Conf. 3D Mater. Sci., Wiley, 2016: pp. 25–30.

[168] S. Ndlovu, K. Durst, M. Göken, Investigation of the sliding contact properties of WC-Co hard metals using nanoscratch testing, Wear 263 (2007) 1602–1609.

[169] H.Q. Sun, R. Irwan, H. Huang, G.W. Stachowiak, Surface characteristics and removal mechanism of cemented tungsten carbides in nanoscratching, Wear 268 (2010) 1400–1408.

[170] T. Csanádi, M. Novák, A. Naughton-Duszová, J. Dusza, Anisotropic nanoscratch resistance of WC grains in WC-Co composite, Int. J. Refract. Met. Hard Mater. 51 (2015) 188–191.

[171] J.J. Roa, S. Simison, J. Grasso, M. Arcidiacono, L. Escalada, F. Soldera, J. Garcia, A.D. Sosa, Cyclic contact fatigue of cemented carbides under dry and wet conditions: correlation between microstructure, damage and electrochemical behavior, Int. J. Refract. Met. Hard Mater. 92 (2020) 105279.

[172] J.M. Tarragó, D. Coureaux, Y. Torres, F. Wu, I. Al-Dawery, L. Llanes, Implementation of an effective time-saving two-stage methodology for microstructural characterization of cemented carbides, Int. J. Refract. Met. Hard Mater. 55 (2016) 80–86.

[173] J.M. Tarragó, J.J. Roa, V. Valle, J.M. Marshall, L. Llanes, Fracture and fatigue behavior of WC-Co and WC-CoNi cemented carbides, Int. J. Refract. Met. Hard Mater. 49 (2015) 184–191.

[174] J.M. Tarragó, S. Dorvlo, J. Esteve, L. Llanes, Influence of the microstructure on the thermal shock behavior of cemented carbides, Ceram. Int. 42 (2016) 12701–12708.

[175] H. Engqvist, U. Wiklund, Mapping of mechanical properties of WC-Co using nanoindentation, Tribol. Lett. 8 (2000) 147–152.

[176] M.G. Gee, R.J.K. Wood, J. Walker, J.C.P. Zun, Scratch testing of WC/Co hardmetals, Tribol. Int. 54 (2012) 77–86.

[177] W.C. Oliver, G.M. Pharr, An improved technique for determining hardness and elastic modulus using load and displacement sensing indentation experiments, J. Mater. Res. 7 (1992) 1564–1583.

[178] N. Barbakadze, S. Enders, S. Gorb, E. Arzt, Local mechanical properties of the head articulation cuticle in the beetle Pachnoda marginata (Coleoptera, Scarabaeidae), J. Exp. Biol. 209 (2006) 722–730.

[179] B. Bhushan, Nanomechanical characterization of solid surfaces and thin films, in: B. Bhushan (Ed.), Nanotribology and Nanomechanics, Springer, 2017: pp. 177–251.

[180] R.D. Dukino, M. V. Swain, Comparative measurement of indentation fracture toughness with Berkovich and Vickers indenters, J. Am. Ceram. Soc. 75 (1992) 3299–3304.

[181] H. Li, R.C. Bradt, The effect of indentation-induced cracking on the apparent microhardness, J. Mater. Sci. 31 (1996) 1065–1070.

[182] G.D. Quinn, P. Green, K. Xu, Cracking and the indentation size effect for Knoop hardness of glasses, J. Am. Ceram. Soc. 86 (2003) 441–448.

[183] J. Wade, S. Ghosh, P. Claydon, H. Wu, Contact damage of silicon carbide ceramics with different grain structures measured by Hertzian and Vickers indentation, J. Eur. Ceram. Soc. 35 (2015) 1725–1736.

[184] K. Fan, J.Y. Pastor, J. Ruiz-Hervias, J. Gurauskis, C. Baudin, Determination of mechanical properties of Al_2O_3/Y-TZP ceramic composites: influence of testing method and residual stresses, Ceram. Int. 42 (2016) 18700–18710.

[185] M.G. Gee, Low load multiple scratch tests of ceramics and hard metals, Wear 250–251 (2001) 264–281.

[186] K.P. Mingard, M.G. Gee, EBSD examination of worn WC/Co hardmetal surfaces, Wear 263 (2007) 643–652.

[187] M. Gee, K. Mingard, B. Roebuck, Application of EBSD to the evaluation of plastic deformation in the mechanical testing of WC/Co hardmetal, Int. J. Refract. Met. Hard Mater. 27 (2009) 300–312.

[188] A. Nisar, K. Balani, Role of interfaces on multi-length scale wear mechanics of TaC-based composites, Adv. Eng. Mater. 19 (2017) 1–10.

[189] American Society for Testing and Materials. ASTM G171: standard test method for scratch hardness of materials using a diamond stylus. West Conshohocken: ASTM; 2017.

[190] G. Sundararajan, M. Roy, Hardness testing, in: G. Sundararajan, M. Roy (Eds.), Encycl. Mater. Sci. Technol., Elsevier, Oxford, 2001: pp. 3728–3736.

[191] A.C. Fischer-Cripps, B.R. Lawn, Indentation stress-strain curves for “quasi-ductile” ceramics, Acta Mater. 44 (1996) 519–527.

[192] B.M. Gadella, T. Van Haeften, K. Van Bavel, J.A. Valentijn, Multi-photon excitation microscopy for advanced biomedical imaging, Vet. Sci. Tomorrow. (2003).

[193] J.I. Goldstein, D.E. Newbury, J.R. Michael, N.W.M. Ritchie, J.H.J. Scott, D.C. Joy, Scanning electron microscopy and X-ray microanalysis, Springer, 2017.

[194] P.R. Munroe, The application of focused ion beam microscopy in the material sciences, Mater. Charact. 60 (2009) 2–13.

[195] R. Wirth, Focused ion beam (FIB) combined with SEM and TEM: advanced analytical tools for studies of chemical composition, microstructure and crystal structure in geomaterials on a nanometre scale, Chem. Geol. 261 (2009) 217–229.

[196] A. Rigort, J.M. Plitzko, Cryo-focused-ion-beam applications in structural biology, Arch. Biochem. Biophys. 581 (2015) 122–130.